THE UNIVERSITY *of* EDINBURGH

Development of Software for Reliability Based Design of Steel Framed Structures in Fire

Shaun Devaney

Doctor of Philosophy

The University of Edinburgh

2014

Declaration

The research which is detailed in this thesis has been completed solely by Shaun Devaney at the University of Edinburgh under the supervision of Professor Asif Usmani and Doctor Stephen Welch. Where other sources are used, full references are given. The work detailed in this thesis has not been submitted for any other degree or professional qualification.

_____

Shaun Devaney

The University of Edinburgh, 2015

Abstract

Fire in building structures represents a risk both to life and property that cannot be fully eliminated. It is the aim of fire safety engineering to reduce this risk to an acceptable level through the application of scientific and engineering principles to evaluate the risk posed by fire and to determine the optimal set of protective measures. This is increasingly being achieved through performance-based design methods. Performance-based design sets out performance requirements, typically related to life safety and control of property losses, and the designer is free to choose the most suitable approach to meet these requirements. Accurate performance-based design requires the evaluation of the risks to a structure through the evaluation of the range of hazards that may occur and the resulting structural responses.

The purpose of this research is to develop simplified methodologies for the reliability based design of steel framed structures in fire. These methodologies are incorporated into a software package, FireLab, which is intended to act as a tool for practicing engineers to aid in learning and applying performance-based design. FireLab is a Matlab based program that incorporates a number of different models for analysing the response of structural elements exposed to fire. It includes both deterministic and probabilistic analysis procedures.

A range of simple fire models are presented for modelling compartment fires. A set of heat transfer processes are discussed for calculating the temperature distribution within common structural elements exposed to fire. A variety of structural models are discussed which may be used to model the effects of fire on a structure. An analytical model for the analysis of composite beams has been implemented in the software program. Interfaces between the software and 2 separate third party programs have also been created to allow for the analysis of composite beams using the finite element method. Analytical methods for the analysis of composite slabs under thermo-mechanical load have been implemented in the software. These methods account for the additional load carrying capacity that slabs have in fire due to the positive effects of tensile membrane action. A numerical analysis method for the vertical stability of structures subjected to multi-floor fires has been implemented using the direct stiffness method. This method

uses an elastic 2nd order solution in order to check the stability of a column under the fire induced horizontal loads from sagging floors. These models of potential failure scenarios provide the basis for the probabilistic analysis methods.

A variety of methods for reliability analysis are evaluated based on ease of use, accuracy and efficiency. A selection of these methods has been implemented in the software program. A selection of sample cases are examined in order to illustrate the procedures and to evaluate the important input variables. These methods provide the probability of failure of a structure under specific loads. The probability of failure is a useful parameter in comparing the level of safety between various design options. A more comprehensive framework is developed for the evaluation of the probable costs due to fire associated with a given design. This framework is based on an existing framework from earthquake engineering. It involves calculating the statistical spread of both the magnitude and likelihood of occurrence of fire and the resulting structural responses. The damage that occurs from the structural response may be then estimated. Finally, given the likely level of damage that will occur it is possible to estimate the cost of the damage either in terms of monetary cost of repair or downtime due to repair works. This method is applied to a variety of design options for a typical office building in order to illustrate the application of the framework.

Lay Summary

It is impossible to eliminate the risk of fire in buildings. Fire represents a risk to life safety, property and business operations. It is the responsibility of structural engineers to ensure that buildings will perform adequately in the event of a fire occurring. Current practice in structural engineering involves the use of prescriptive rules to protect a building in the event of a fire. These rules typically state how each element of a building is to be constructed. They are derived from experience and are based on what has worked in the past. As a result, the prescriptive method is unsuitable for pioneering structures, new construction materials or innovative construction methods as past experience is of little relevance.

Performance based design offers an alternative to the traditional prescriptive design. Performance based design standards are composed of rules that define the required performance of a structure. By framing the standards in this manner the design team is free to adopt the most effective solution to any given design problem. This encourages innovation and efficiency within the construction industry. The use of performance based methods for structural fire design has grown significantly in the past few decades. Performance based design is now the standard approach in the design of large or complex structures. There are a number of disadvantages associated with performance based design. Performance based design is a complex and difficult procedure that requires advanced knowledge and training. It typically stops short of quantifying the risk posed by fire.

It is the aim of this thesis to develop simplified methods that allow designers to carry out reliability based design of steel framed structures in fire. Reliability based design goes beyond basic performance based design in an attempt to quantify the level of safety inherent in a design. It involves the probabilistic evaluation of the range of loads that may affect the structure during its design life and the range of structural responses that occur as a result of the loads. This approach can allow the designer to calculate the probability of failure of a structure over its lifetime. The probability of failure is an important parameter that allows for the comparison of competing design options. This thesis presents methods for the probabilistic design of structures subject to fire. A

method for the calculation of the likelihood of fire induced costs, based on an existing method from earthquake engineering, is also presented.

The work in this thesis covers the analysis of steel-concrete composite beams, composite slabs and multi-storey columns. A software program has been created containing a variety of fire, heat transfer and structural models. This program was designed to provide a simplified method for conducting reliability based design in order to encourage the widespread use of these methods by practicing engineers.

Acknowledgements

I would like to acknowledge the help and support I received from my supervisors, Asif Usmani and Stephen Welch, throughout my PhD. In particular I would like to thank Asif. His knowledge of engineering and enthusiasm for research has been a fantastic help. I would like to thank Prof. C.S. Manohar of the Indian Institute of Science (I.I.Sc.), Bangalore for hosting me at the I.I.Sc. and for introducing me to some of the more complex areas of structural reliability. The financial support of the UK-India Research Initiative (UKIERI) made it possible for me to visit the I.I.Sc. and their support is gratefully acknowledged. I would like to thank David Lange for his advice and the many discussions which greatly aided my understanding of performance-based design.

I also owe a tremendous debt of gratitude to Caroline and my family. They have been a constant source of support and encouragement throughout my PhD.

This research was funded by an EPSRC-Tata Steel case award, and their support is gratefully acknowledged.

Publications

The following papers have been produced as a result of this research:

Journal papers:

Lange, D., Devaney, S. and Usmani, A. (2014), An application of the PEER performance based earthquake engineering framework to structures in fire, *Engineering Structures*, vol. 66, pp. 100-115.

Conference papers:

Lange, D., Devaney, S., & Usmani, A. S. (2012). Applying the PEER Performance Based Earthquake Engineering Methodology to Structures in Fire. in M. Fontana, A. Frangini, & M. Knobloch (Eds.), In *Proceedings of the 7th International Conference on Structures in Fire* (pp. 21–30). Zurich: ETH Zurich.

Devaney, S., Lange, D., Usmani, A., & Manohar, C. S. (2012). Development of a performance-based structural fire engineering framework for implementation as a software design tool. in *Proceedings of the 6th International Asranet Conference*. Croydon.

Devaney, S., Lange, D., Usmani, A. S., & Manohar, C. S. (2012). Adapting the PEER Methodology to Account for the Fire Hazard in Built Structures. in J. G. Teng, J. G. Dai, S. S. Law, Y. Xia, & S. Y. Zhu (Eds.), *Proceedings of the First International Conference on Performance-based and Life-cycle Structural Engineering* (pp. 441–447). Hong Kong: Hong Kong Polytechnic University.

Devaney, S., Kazaeinejad, P., & Usmani, A. S. (2013). A Practical Approach to Large Deflections of Thermomechanically Loaded Rectangular Plates. in W. J. McCarter, O. Laghrouche, & G. Walker (Eds.), *Proceedings of the Infrastructure and Environment Scotland 1st Postgraduate Conference* (pp. 133–137). Edinburgh: Heriot-Watt University.

Devaney, S., Usmani, A., Manohar, C.S., (2014). Software FireLab for Probabilistic Analysis of Steel-Framed Structures in Fire, in G.-Q. Li, V. Kodur, S.-C. Jiang, J. Jiang, S.-W. Chen & G.-B. Lou, *Proceedings of the 8th International Conference on Structures in Fire* (pp. 919-926). Shanghai, Tongji University Press.

Devaney, S., Usmani, A., & Manohar, C. S. (2014). Software FireLab for Probabilistic Analysis of Structures in Fire, in *International Conference on Safety & Reliability of Ships, Offshore & Subsea Structures*, Glasgow, Asranet.

Table of Contents

Table of Figures

Table of Tables

Nomenclature

Roman

A	Area of cross section
A_{fi}	Floor area of the fire compartment
A_m	Surface area of the member per unit length
A_s	Cross sectional area of the rebar
B	Breadth of the beam/slab
C	Required confidence level in the result of a Monte Carlo simulation
$Coll$	Collapse occurrence
D	Flexural stiffness of the plate
DSi	Damage state i
E	Young's modulus of elasticity
E_{ref}	Reference value of Young's modulus of elasticity
E_s	Young's modulus of steel
E_2	Modulus of hardening of steel
F	Airy stress function
$\boldsymbol{F}$	Vector of joint force components
F_i	Continuous and increasing distribution functions
F_j^{-1}	Inverse of the j-ith cumulative distribution function
$F.O.$	Occurrence of a fire event
F_T	Thermal force
F_x	Resultant axial force
F_{xi}	Axial force acting on element at node i
F_{yi}	Transverse force acting on element at node i
$G(\hat{x})$	Limit state function
H_C	Height of the compartment
H	Horizontal loads acting on column
I	Second moment of area
$I[\ ]$	Indicator function
$\boldsymbol{J}$	Jacobian matrix
$\boldsymbol{K_{el}}$	System elastic stiffness matrix

$\boldsymbol{K_g}$	System geometric stiffness matrix
$\boldsymbol{K_{tot}}$	System stiffness matrix
L_e	Losses due to earthquake
L_f	Losses due to fire
L	Length of the beam/slab
M	Moment
$M_{Re,T}$	Temperature-dependent moment resistance of the member
M_T	Thermal moment
M_x	Resultant axial moment
M_{zi}	Moment acting on the element at node i
M^T	Thermal moment
N	Number of scenarios examined
N_{int}	Number of intervals in each variable range
N^T	Thermal force
NC	Non collapse
P	Axial force
$\boldsymbol{P}$	Vector of nodal force components
$\boldsymbol{P_{corr}}$	Correlation matrix
$\boldsymbol{P_f}$	Vector of forces acting at unrestrained degrees of freedom
$\boldsymbol{P_r}$	Vector of forces acting at restrained degrees of freedom
$P_{Re,T}$	Temperature-dependent axial resistance of the member
$\boldsymbol{P^F}$	Vector of fixed-end forces
$\boldsymbol{P^F_f}$	Vector of fixed end forces acting on unrestrained degrees of freedom
$\boldsymbol{P^F_r}$	Vector of fixed end forces acting on restrained degrees of freedom
$\dot{Q}$	Heat release rate
$\dot{Q}''$	Heat release rate per unit area
$R(X>x)$	Annual rate of exceeding a given value of the variable x
T	Temperature of the gas
$\boldsymbol{T}$	Transformation matrix
T_D	Design life of a building in years
T_a	Ambient temperature
T_{ff}	Temperature of the far-field
T_m	Maximum temperature above the ambient temperature in the BFD curve
T_{peak}	Peak gas temperature

T_{sce}	Force in the rebar across the central crack
T_{sx}	Force in the x-direction across the diagonal crack
T_{sy}	Force in the y-direction across the diagonal crack
T_u	Ultimate force of the rebar
T_y	Yield force of the rebar
$T_{,z}$	Thermal gradient
T_∞	Ambient temperature
T_1	Temperature on the unexposed face of the member
T_2	Temperature on the exposed face of the member
U_c	Deflection of slab
U_{cf}	Deflection at failure
U_i	Standardised form of variable *i*, with a mean of zero and a standard deviation of one
V	Vertical load on column
V_m	Volume of the member per unit length
V_n	Volume of rebar number n
X_i	Value of the variable
a	Length of the slab
b	Width of the slab
c_a	Specific heat of steel
c_c	Specific heat of concrete
c_p	Specific heat of the fire protection material
c_s	Specific heat of steel
d	Depth of the member
d_c	Depth of concrete layer
d_p	Depth of fire protection material
$f_{\boldsymbol{x}}(\boldsymbol{x})$	Joint probability density function
f_y	Yield stress of steel
h	Thickness of the section
$\dot{h}_{net,c}$	Net convective heat flux
$\dot{h}_{net,d}$	Net design value of heat flux from the fire acting on the member
$\dot{h}_{net,r}$	Net radiative heat flux

$h_v(\ )$	Importance-sampling probability density function
$\boldsymbol{k}$	Element stiffness matrix
$\boldsymbol{k_{el}}$	Elastic element stiffness matrix
$\boldsymbol{k_g}$	Geometric element stiffness matrix
$\boldsymbol{k_{el,global}}$	Elastic element stiffness matrix in global coordinates
$\boldsymbol{k_{g,global}}$	Geometric element stiffness matrix in global coordinates
k_p	Pyrolysis coefficient
k_{sh}	Correction factor for the shadow effect
l	Width of the slab
l_f	Specific value of loss due to fire
n	Number of variables
$n_{ff,max}$	Number of potential fire floors considered
p	Transverse load acting on a member
p_f	Probability of failure
$p_1, p_2, .. p_4$	Parameters affecting the rate of occurrence of structurally significant fires
q	Uniformly distributed load
q_f	Fuel load density
$\dot{q}_b$	Rate of heat storage in the gas volume
$\dot{q}_c$	Rate of heat release due to combustion
$\dot{q}_l$	Rate of heat loss due to replacement of hot gases by cold gases
$\dot{q}_r$	Rate of heat loss by radiation through openings
$\dot{q}_w$	Rate of heat loss through the walls, ceiling and floor
r	Radius of the fire plume
r_{ff}	Radius of the far-field
r_{fi}	Annual rate of occurrence of a structurally significant fire
$r_{fi,ff}$	Annual rate of occurrence of a floor being affected by fire within the considered region
r_n	Annual rate of occurrence
r_{nf}	Radius of the near-field
s_c	Shape constant in BFD curve
t	Time
t_b	Burning time in travelling fire methodology
t_{crit}	Critical time at which the greatest number of floors are exposed to fire

t_m	Time at which T_m occurs in the BFD curve definition
t^*	Parameter based on the time from ignition
v	Deflection
w	Vertical deflection of the plate/slab
w_{lim}	Limiting deflection
w_n	Total deflection
w_T	Thermal deflection
x	Horizontal coordinate
$x_j^{(i)}$	i-th Latin hypercube sample of the j-ith variable
y	Lever arm from the neutral axis
y_i	Coordinates of point i on the limit state surface
z	Distance from middle surface

Greek

$\boldsymbol{\Delta}$	Vector of nodal displacements
$\boldsymbol{\Delta_f}$	Vector of unrestrained nodal displacements
$\boldsymbol{\Delta_r}$	Vector of restrained nodal displacements
ΔT	Temperature change
ΔT_r	Temperature change in the rebar
Δt	Time interval
$\Delta\theta_{a,t}$	Temperature change in the steel
Π_{ext}	External work
Π_{int}	Internal work
$\Phi( )$	Standard normal cumulative distribution function
α	Coefficient of thermal expansion
α_c	Coefficient of heat transfer by convection
$\alpha_{c,2}$	Coefficient of heat transfer by convection on the unexposed side of the member
α_s	Coefficient of thermal expansion of steel
β	Reliability (or ‘safety’) index
δ	Deflection
ε_c	Surface emissivity of concrete
ε_f	Emissivity of the fire

ε_{lim}	Limiting strain
ε_m	Surface emissivity of the member
$\varepsilon_{mechanical}$	Mechanical strain in a member
ε_{sct}	Strain due to the difference in thermal expansion between the steel rebar and the surrounding concrete
$\varepsilon_{thermal}$	Thermal strain in a member
ε_{total}	Total strain in a member
ε_{wm}	Mechanical strain in the rebar
ε_{wT}	Mechanical strain in the rebar due to thermal deflection
ε_x	Strain in the *x*-direction
ε_{xm}	Membrane strain in the *x*-direction
η	Factor defining the distance from the end of the slab to the central crack
$\theta_{a,t}$	Steel temperature
θ_{amb}	Ambient temperature
$\theta_{c,i}$	Concrete temperature, in layer *i*
θ_g	Gas temperature in the fire compartment
θ_m	Member surface temperature
θ_r	Effective radiation temperature of the fire environment
θ_s	Member temperature
λ_c	Thermal conductivity of the concrete
λ_p	Thermal conductivity of the fire protection material
λ_x	Mean annual frequency of exceedance curve for the variable *x*
μ_{Xi}	Mean value of the variable X_i
μ_z	Mean value of the response
ν	Poisson's ratio
ρ_a	Unit mass of steel
ρ_c	Unit mass of concrete
ρ_{ij}	Correlation coefficient between variables *i* and *j*
ρ_s	Unit mass of steel
ρ_p	Unit mass of the fire protection material
σ	Stephan Boltzmann constant
σ_b	Bond strength
σ_{Xi}	Standard deviation of the variable X_i
σ_x	Stress in the *x*-direction

σ_{sec}	Stress in the section
σ_z	Standard deviation of the response
$\sigma(\varepsilon)$	Stress-strain curve
φ	Configuration factor
φ_n	n-dimensional normal density function
φ_2	Bivariate normal density function

Abbreviations

ALARP	As Low As Reasonably Practicable
BS	British Standard
CFD	Computational Fluid Dynamics
CIB	Conseil International de Batiment
C.o.V.	Coefficient of Variation
DM	Damage Measure
DV	Decision Variable
EC	EuroCode
EDP	Engineering Demand Parameter
FEMA	Federal Emergency Management Agency
FORM	First-Order Reliability Method
FOSM	First-Order Second-Moment method
IM	Intensity Measure
JCSS	Joint Committee on Structural Safety
LHS	Latin hypercube sampling
NASA	National Aeronautics and Space Administration
OpenSees	Open System for Earthquake Engineering Simulation
PBEE	Performance-Based Earthquake Engineering
PBSFE	Performance-Based Structural Fire Design
PEER	Pacific Earthquake Engineering Research
SCI	Steel Construction Institute
SFPE	Society of Fire Protection Engineers
SORM	Second-Order Reliability Method
UK	United Kingdom
USA	United States of America

Chapter 1: Introduction

1.1 Background to the Project

The process of structural engineering involves calculating the loads which will act on the structure throughout its life and the resistance of the structure to these loads. Only when it has been proven that the resistance of the structure is greater than the applied loads is the structure deemed acceptable. This process is used when considering dead loads, imposed loads and wind loads, but the process is not generally applied to fire loads.

Current design for fire, in accordance with the Building Regulations, involves the determination of a single member's resistance to collapse, resistance to fire penetration and resistance to the transfer of excessive heat. It has been proven that this method inadequately captures the real behaviour of a structure and that better methods are required. In recent years finite element models have successfully been used to model the behaviour of a structure exposed to fire [1]. But the use of finite element models has many disadvantages. Finite element analysis is a time-consuming process which must be carried out by highly skilled people and because of this it is not commonly used.

This project involves the analysis and design of steel framed composite structures in fire. This project focuses on the application of analytical equations combined with probabilistic analysis to produce a software package for undertaking structural fire engineering [2]–[4]. Probabilistic design is an alternative approach to "safety factor" design which enables the engineer to analyse each project individually and to produce a tailored design. Large fires are a rare occurrence in buildings and they result in widely varied effects when they do occur. It is because of these reasons that probabilistic design is suited to structural fire design [5].

The design of steel framed structures in fire is an area of significant on-going research. Many of the recent advances in the area of structural fire engineering have come from the full-scale Cardington frame fire tests [6]. These tests allowed engineers to scientifically examine the behaviour of steel framed structures under fire conditions. Some of the realisations from these tests include the appreciation of the importance of alternative load transfer mechanisms within the frame, the importance of the realistic

temperature distributions within the structural members and the importance of member end connection details in terms of the restraint they provide to thermally induced deformation of the member. Despite the importance of these findings they remain underused in the design of structures.

Previous work in this area has been carried out by the University of Edinburgh, among others, some of which led to the development of analytical methods for determining the deflection and stress/strain distributions in composite floor systems under fire loading [3]. These methods were developed from the Cardington test results and have been checked against numerical models to confirm their accuracy. Separate methods for the calculation of the membrane capacity of floor slabs in fire have been developed by Bailey [4] and Omer et al. [7]. These methods and others will be studied and they will be used in this project.

1.2 Research Aims

It is impossible to rule out the threat of fire in buildings and it is important that fire safety engineering is used to ensure that the risk posed by fire is reduced to an acceptable level. It is therefore the aim of this project to develop a software program for use by practicing engineers to undertake reliability based design of steel framed structures in fire.

- Adapt and apply the Pacific Earthquake Engineering Research (PEER) center's – Performance-Based Earthquake Engineering (PBEE) method to performance-based structural fire engineering [8]. The novel elements of this work include the identification of suitable intensity measures and the development of fragility functions to describe the relationship between the structural response to a fire and the resulting damage.
- Apply probabilistic procedures to existing analytical methods for analysing structural members in fire, such as composite beams and composite slabs.
- Produce Matlab scripts that perform structural analysis of members subjected to fire.
- Produce Matlab scripts that perform reliability analysis of structural elements in fire.

1.3 Outline of Thesis Chapters

Chapter 1

Introduction

A brief discussion of the research aims and the background to the project is given, along with an overview of the research undertaken.

Chapter 2

Uncertainties in Structural Fire Engineering

An overview of structural fire engineering is presented, including the models required to analyse a structural fire engineering problem. A range of fire models, heat transfer models and structural analysis models are examined. Sources of uncertainty in the inputs that govern the behaviour of each model are discussed. Suitable probability distribution functions and distribution parameters are provided for the important inputs.

Chapter 3

Performance-Based Engineering

A literature review of the development and application of performance-based engineering is presented. The performance-based approach is compared to the prescriptive approach and the relative advantages of each are discussed. The development of performance-based earthquake engineering is analysed and its effects on the development of performance-based structural fire engineering is discussed.

Chapter 4

Methods of Probabilistic Analysis

A variety of methods of probabilistic analysis suitable for use in the analysis of structural fire engineering problems are examined. The advantages and disadvantages of each approach are reviewed and the approaches are applied to example problems in structural

fire engineering. Sensitivity analysis is used to predict the input parameters associated with the highest level of uncertainty.

Chapter 5

The PEER-PBEE Framework and its Application to Structural Fire Engineering

The development of the Pacific Earthquake Engineering Research (PEER) center's approach to performance-based earthquake engineering (PBEE) is presented. This framework represents the state of the art in performance-based methods. It allows for designers to base their design decisions upon factors such as repair cost or risk of fatalities. The framework is adapted to structural fire engineering. Suitable intensity measures and engineering demand parameters are identified for use in the framework. Fragility functions are developed to describe the damage done to a structure, given the response of the structure to a set of loads. Example applications of the framework to a variety of cases are provided.

Chapter 6

Development of Software FireLab for the Probabilistic Design of Structures Subjected to Fire

The development of FireLab, a software package for the analysis of steel-framed structures subjected to fire, is presented. The reasons behind the development of the program are discussed. The range of application of the program and the models it uses are discussed. The results of the validation process for the models built in to FireLab are discussed in this chapter. A set of example applications of FireLab is provided.

Chapter 7

Conclusions and Future Work

A general discussion of the research carried out is provided which summarises the results and conclusions of the work. Suggestions for possible areas of future work are provided.

Chapter 2: Uncertainties in Structural Fire Engineering

2.1 Preamble

This chapter deals with structural fire engineering, the types of models that are required, the model variables and the uncertainties associated with the input variables. The deterministic analysis of a structure, or structural member, under fire load requires three analysis models: a fire model, a heat transfer model and a structural analysis model. Various fire models for modelling a fully developed compartment fire are examined for use in performance-based structural fire engineering. The governing variables are identified and probability distributions are assigned to these variables.

Suitable heat transfer models are identified for both concrete and steel members. Heat transfer analysis is required in order to account for the effects of temperature dependent material properties and it facilitates the inclusion of the effects of thermal expansion of the structure in the structural analysis. Temperature dependent material models, based on the Eurocode (EC) models, are outlined for use in the structural analysis with the results of the heat transfer analysis.

Structural analysis models are described for the analysis of various sub-structure components within a steel framed building. The models apply to concrete-steel composite beams, composite slabs and vertical stability of a multi-storey building under multiple floor fires. Probability distributions are assigned to the geometrical and material inputs that introduce large amounts of uncertainty into the analysis.

2.2 Fire Modelling

Accurately describing the load is the first stage of any performance-based engineering assessment. Therefore it is vital that both the behaviour of the fire and its effects on the structure are accurately modelled. In this work the main fire load under consideration is a fully developed compartment fire. Other types of fire such as smouldering fires or localised fires are not considered. Typical compartment fires begin with a growth phase as the fire spreads from its point of origin, which is associated with low temperatures

across most of the compartment. As the fire spreads, a smoke layer begins to form underneath the ceiling and the temperature in the compartment starts to rise, shown in Figure 2.1. Assuming there is sufficient ventilation and sufficient fuel, the fire transitions into a fully developed fire where all of the combustible items in the room begin burning. This transition process is known as flashover. After flashover the fire enters its fully developed phase and soon reaches its peak temperature. As the available fuel is consumed the temperature begins to decrease and the fire enters the decay phase. The main random variables associated with the different stages of the fire curve are listed below in Table 2.1.

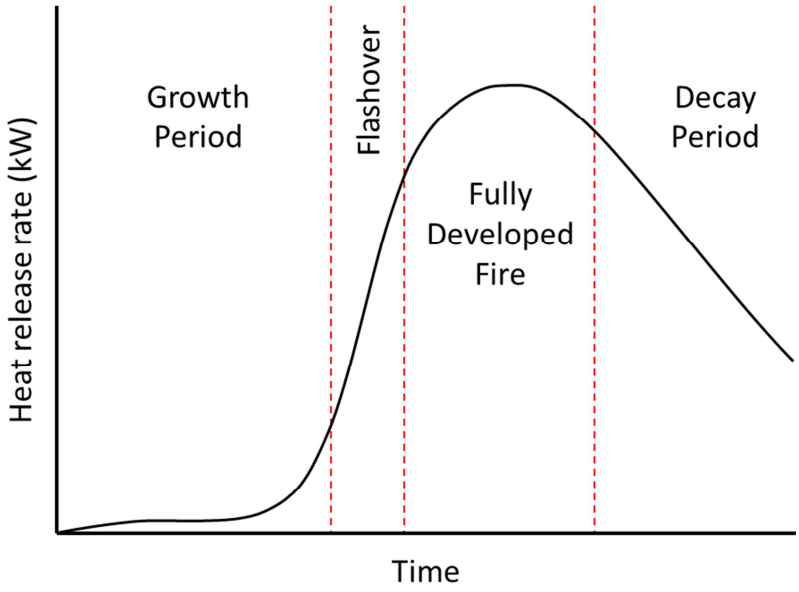

Figure 2.1: Development of a well-ventilated compartment fire (adapted from [9]).

Table 2.1: Variables influencing the various stages in the development of a compartment fire.

Stage of Development	Associated Variables
Growth Period	Nature of the first item to catch fire Spatial distribution of the fuel
Flashover	Fuel Ventilation Compartment geometry
Fully Developed Stage	Fuel Ventilation
Decay Period	Ventilation

No single variable can fully describe the fires effect on a structure but some of the key features of a fire are:

- The initial heating rate as the fire develops
- The peak temperature of the fire
- The duration of the fire
- The rate of cooling as the fire decays

A fire model must capture all four of the above points if it is to accurately represent a real fire. In large compartments it is not reasonable to assume that a fire will be uniform throughout the whole compartment. In this case it is more likely that the fire will move through the compartment, spreading to areas with untouched fuel and dying out in areas where the fuel has been consumed [10]. Spatial effects will also lead to increasingly complex behaviour in large compartments. The geometry of the enclosure has a significant effect on the behaviour of fire in large spaces [9].

2.2.1 Variables affecting fire development

The occurrence, development and spread of fire in a building are all complex processes that depend on many different factors. The occurrence of fire within a building is

dependent on factors such as the contents of the building, the type of building, the size of the building, the presence of active fire protection measures and the location of the building. This section explores the uncertainty associated with these factors. The calculation of the rate of fire occurrence within a building is discussed in more detail in section 2.4.2.

Fire development is a complex phenomenon that is dependent on fuel load, ventilation conditions and the thermal properties of the compartment boundaries. The amount of fuel load and the area of ventilation together determine whether a fire is ventilation controlled or fuel controlled. A ventilation controlled fire is one which is not receiving sufficient oxygen to burn all of the available fuel while a fuel controlled fire is one which is receiving more oxygen than is required to burn the fuel. Determining if the fire is ventilation controlled or fuel controlled is important as it affects the development of the fire. The type of fuel within the compartment affects the rate of fire spread within the compartment and the magnitude of the heat flux from the fire [11]. Common assumptions in modelling compartment fires are that the fuel is cellulosic and evenly distributed across the compartment. The Eurocode uses a Gumbel (Extreme value type I) distribution to describe the range of fuel loads that are likely to occur in a building [12]. The Gumbel distribution was chosen based on fuel load surveys of various building types [13], [14]. The form of the Gumbel distribution is defined by two parameters, the mode and the shape factor. The mode defines the value of fuel load that is most likely to occur and the shape factor defines the spread of the distribution [15]. These values may be calculated from the Eurocodes and from the background document to the Eurocodes [12], [13], e.g. for an office the mode is 363.29MJ/m^2 and the shape factor is 98.24. Other occupancy types, such as warehouses, may be better described by a lognormal distribution. This is necessary when there is a large spread in the distribution of fuel load values (i.e. a high standard deviation) in order to avoid the occurrence of negative values. A comparison of various options for fuel load distributions, each with the same mean and variance, is shown in Figure 2.2.

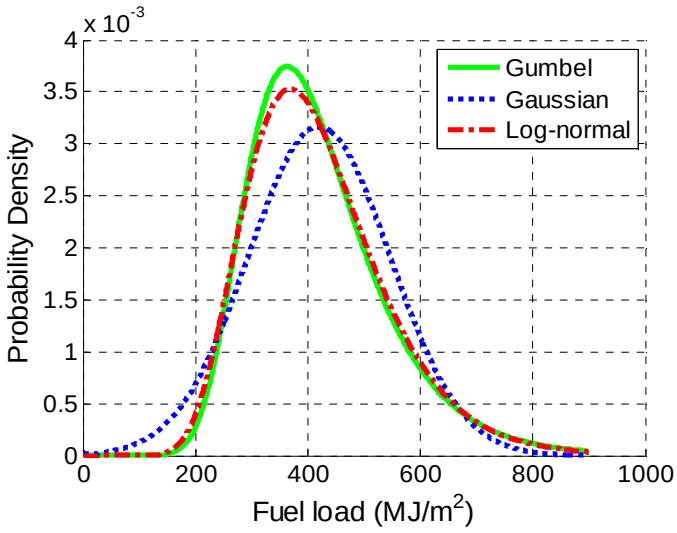

Figure 2.2: Comparison of various fuel load distributions.

The ventilation conditions are equally important in determining the behaviour of the fire. Fire behaviour is heavily dependent on the size of the ventilation openings, the location of the ventilation openings and the presence of air flows within the compartment [16]. Currently basic fire models do not account for air flows induced by the location of the openings. Neither do they account for the location of the openings, except in some instances where openings in the walls are distinguished from openings in the ceiling. In practice it is impossible to predict the size of the openings. This is a difficult problem as it cannot be known if doors or windows will be open or shut when a fire starts, neither can it be known if any windows will be broken by the fire and if so which windows will be broken. This is a significant problem in the deterministic analysis of a fire as the amount of ventilation controls the development of the fire and it is difficult to estimate the level of ventilation that represents the worst case. The truncated lognormal distribution has been chosen to describe the variation of the area of ventilation, in accordance with the JCSS model code, Part II [17]. A truncated distribution is used as it allows an upper bound to set equal to the maximum possible area of ventilation. The maximum possible area of ventilation may be taken as the sum of the areas of all of the doors, windows and openings.

The thermal properties of the boundaries of the fire enclosure also play an important role in controlling the development of the fire. Highly insulated compartments retain much of the heat generated by a fire, leading to shorter times to flashover and higher peak

temperatures. When considering the heat loss through the compartment boundaries two variables are important, the thermal inertia and the thickness of the enclosure boundary. The thermal inertia of the enclosure boundaries is dependent upon three material properties; thermal conductivity, density and specific heat capacity. These properties can vary greatly from one compartment to another depending on the construction methods and construction materials used. However there is little variation in the thermal inertia of a boundary, given a specific type of construction. Neither is there much variation in the thickness of the boundary, given the specific type of construction. For this reason, probability distributions have not been assigned to the boundary variables.

2.2.2 Fire models

Mathematical models for predicting fire temperatures are widely used in structural fire engineering for the purpose of defining the fire load placed on the structure. These models range from simple, nominal temperature-time curves through to computationally demanding computational fluid dynamics models. The simplest model in widespread use is the standard temperature-time curve. The idea of a standard international temperature-time curve was first proposed at an international conference in 1910, but no agreement was reached at the time. However international influences can clearly be seen when the various standard curves are compared. The Eurocode standard curve and the ASTM E119 curve, for example, are practically identical [12], [18] as shown in Figure 2.3. The standard temperature-time curve in use today in the UK was first published in 1932 and is defined in both BS 476-Part 20 and BS EN 1991-1-2:2002 as [19]:

$$T = 345log_{10}(8t + 1) + 20 \quad (2.1)$$

where T is the mean gas temperature in the furnace (in °C) and t is the time (in minutes) up to a maximum of 360 minutes.

The standard fire curve is intended to represent the worst case fire and is based on what furnaces of the period could produce, but it does not realistically represent the development of a fire and it cannot be said to represent every possible fire. The standard curve is still in widespread use in structural fire engineering. This is partly because of the ease of application of the curve to different scenarios and because the curve is used as the basis of fire resistance testing of construction products. A major drawback in the use

of the standard curve in performance-based engineering is that it does not accurately capture the behaviour of the fire. The standard temperature-time curve does not account for variation in the fuel load, ventilation or compartment size. In addition to these points, the standard curve does not include a cooling phase. In terms of uncertainty analysis, the standard temperature-time curve can be said to have a very high degree of model uncertainty as it is unable to accurately predict the development of a fire.

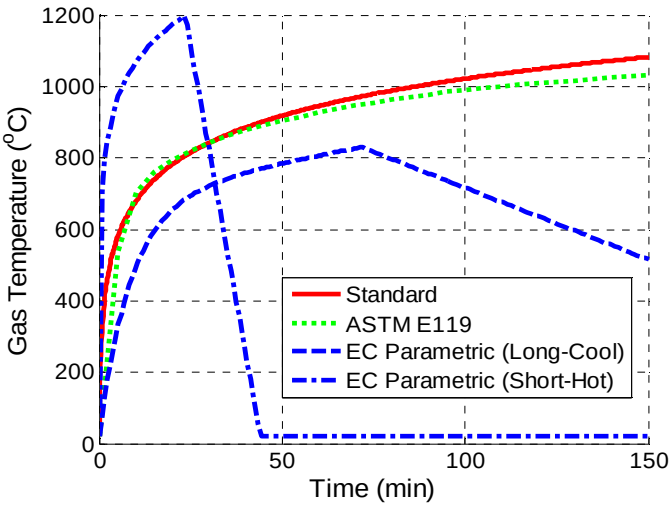

Figure 2.3: Comparison of commonly used fire curves.

Efforts to overcome the problems associated with the standard curve have resulted in the development of other methods, including various types of gas temperature-time curves such as the Joint Committee on Structural Safety (JCSS) temperature-time curve, the Swedish code curves, the Eurocode parametric curve and the BFD curve [12], [17], [20].

The JCSS gas temperature-time curve is based on the Eurocode standard temperature-time curve. It is similar to the standard temperature-time curve except that the duration of the fire is a variable, calculated based on compartment geometry, fuel load and ventilation openings. The JCSS curve suffers from two of the same problems as the standard curve, the rate of heating does not vary and there is no cooling phase included. The JCSS curve therefore is also associated with a high degree of model uncertainty, even though it is a more accurate model than the standard temperature-time curve.

The Swedish curves were created by Pettersson et al. [21] as a method for easily predicting the temperature-time history of a fire in a given compartment. The gas temperature is calculated through solving the following heat balance equation:

$$\dot{q}_c = \dot{q}_l + \dot{q}_w + \dot{q}_r + \dot{q}_b \quad (2.2)$$

where $\dot{q}_c$ is the rate of heat release due to combustion, $\dot{q}_l$ is the rate of heat loss due to replacement of hot gases by cold ones, $\dot{q}_w$ is the rate of heat loss through the walls, ceiling and floor, $\dot{q}_r$ is the rate of heat loss by radiation through the openings and $\dot{q}_b$ is the rate of heat storage in the gas volume.

One of the major assumptions of Pettersson's method is that the temperature is assumed to be uniform throughout the compartment, i.e. a one-zone model. The Pettersson method therefore is not suitable for large compartments or for localised fires. The solution of the above equation for the compartment temperature is an involved process and therefore Pettersson presented calculated temperature-time histories for a range of ventilation conditions and fuel loads.

The Eurocode parametric temperature-time curve, shown above in Figure 2.3, is a model of a fully developed compartment fire. It is based on Pettersson's earlier work and as such it relies on the assumption that the temperature is uniform throughout the compartment. The parametric fire is commonly used in the UK and the equation for the heating phase is given below in Equation (2.3) [12].

$$\Theta_g = 20 + 1325(1 - 0.324e^{-0.2t*} - 0.204e^{-1.7t*} - 0.472e^{-19t*}) \quad (2.3)$$

where θ_g is the gas temperature in the fire compartment and t* is a parameter based on the time from ignition, the boundary conditions of the compartment and the opening factor.

The parametric fire is based on cellulosic fuels and is divided into two parts. It consists of a logarithmic heating phase followed by a linear cooling phase. The curve accounts for the differences in fuel load, ventilation, compartment geometry and compartment linings [12]. The Eurocode parametric curve represents a large improvement over the standard curve but it also has its limitations. The use of a fire curve requires the assumption that the compartment temperature does not vary across the compartment. The linear cooling phase does not accurately capture the behaviour of real fires. In

addition to these disadvantages the following limits are placed upon the use of the parametric curve in the Eurocode [12]:

- The fire compartment must have a floor area of less than 500m^2.
- The maximum compartment height is 4m.
- There can be no openings in the roof.

Although the first two limits are lifted in the UK National Annex, the parametric curve is likely to be overly conservative in these cases [22], [23]. The parametric curve is suitable for use in stochastic analysis methods, such as the Monte Carlo method, as it is quick to run and can account for variations in the compartment that may affect a fire's behaviour.

The BFD curve is produced by a single equation which models both the heating and the cooling phase of the fire as a log-normal curve [20], [24], [25]. The basic equation is given as:

$$T = T_m e^{-z} + T_a \tag{2.4}$$

where

$$z = \frac{(\log(t) - \log(t_m))^2}{s_c} \tag{2.5}$$

where T is the gas temperature, T_m is the maximum temperature above the ambient temperature, T_a is the ambient temperature, t_m is the time at which T_m occurs and s_c is the shape constant for the curve.

While the above equation only requires three inputs (maximum temperature, time to maximum temperature and the shape constant), various other factors must be considered in the derivation of these inputs. Different methods of determining the maximum temperature of a post-flashover fire are well documented and include methods from Babrauskas, Law and the Swedish Curves [26], [27]. The determination of the time at which the maximum temperature occurs is more difficult as a "design fire" must first be chosen, based on the expected fire growth. The shape factor is easily derived as it is linearly dependent on the pyrolysis coefficient, k_p. The pyrolysis coefficient is a factor which is based on the rate of burning of the fuel and the size and shape of the ventilation openings [20]. It is important to note that the relationship between the shape factor and the pyrolysis coefficient varies, depending on whether the compartment is insulated or

non-insulated. The BFD curve appears to provide a reliable method for estimating gas temperature, but is not widely used.

Pettersson's method, the Eurocode parametric curve and the BFD curve all represent a significant reduction in model uncertainty, in comparison with either the standard temperature-time curve or the JCSS curve. This is due to the fact they are able to produce reasonable predictions of the development of a fire. The model uncertainty associated with each type of fire model was not quantified in this work.

A more in-depth option for capturing the behaviour of the fire is to use a multiple zone model. Using this method the compartment is split into zones which represent the areas of different fire behaviour. The gas temperature is found by solving the heat and mass balance equations for the system in each zone. In a one-zone model, the fire is assumed to exhibit uniformity at every point in the compartment, including temperature, density, internal energy and pressure of the gas. One-zone models take into account the transfer of mass between the fire and the gas in the compartment. The main drawback of one-zone models is that they require the assumption that the physical properties of the gas are uniform throughout the zone.

In a typical multiple zone model the compartment is split into two zones; an upper zone and a lower zone, Figure 2.4. The upper zone is where the hot smoke and gases gather and the lower zone is where cold air is drawn in to feed the fire. A number of sub models are required for the calculation of the gas temperature. A combustion model is required to calculate the heat produced by the fire, based on the fuel load and oxygen concentration in the compartment. A vent model is required to calculate the heat and mass transfer through the compartment openings. An air entrainment model is required to calculate the mass transfer between the layers. A heat transfer model, typically a one-dimensional finite element or finite difference solution, is required to calculate the heat loss through the compartment boundaries. The use of zone models is well established and computer packages based on these concepts are widely available. CFast is a free package for modelling a two-zone fire and Ozone is a free package that employs either a one or two-zone model depending on the fire conditions [28]–[30]. Two-zone models are a more accurate representation of a fire than a one-zone model, particularly during the earlier stages of the fire. This increase in accuracy means that two-zone models have a

reduced level of model uncertainty in comparison to one-zone models and methods based on one-zone models.

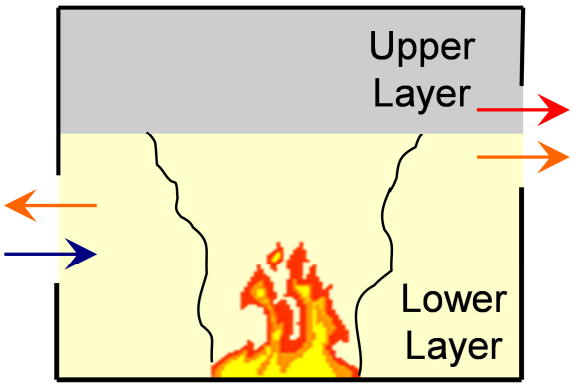

Figure 2.4: Example of a typical two zone model.

The most advanced analysis option for the determination of fire behaviour in a compartment is to use a field model. Field models are three dimensional models of the compartment that allow for the solution of the mass, momentum and energy equations at discrete points in space. Field models are the most accurate type of fire model and therefore have the lowest level of model uncertainty associated with them. Field models are typically solved using computer packages based on computational fluid dynamics (CFD). Widely used CFD packages for fire modelling include FDS and FireFOAM [31], [32]. Using this method the range of fire behaviour can be modelled by changing variables such as the size of openings or the fuel load. The disadvantages of field models are that they are inherently complex and computationally expensive. When creating the model it is important to ensure that the mesh size used is small enough to accurately capture the fire behaviour, but using smaller mesh sizes can lead to much longer computation times for the model. There is much on-going research into producing better CFD models.

While CFD is capable of predicting fire growth and fire spread in large compartments, analytical models for travelling fires have been developed as a simplified tool for structural fire design. A recent method for modelling travelling fires was developed by Rein et al. [33] and extended by Stern-Gottfried et al. [34]. This method assumes that the temperature field at any given time can be classed as “near-field” or “far-field”. The near-field is subject to a near infinite range of variation in size, shape and travel path

through any given compartment. In order to simplify the problem, the model proposed by Stern-Gottfried et al. considers only a single type of near-field. They propose treating the fire as uniform across the width of the compartment and assuming that it travels in one direction only, down the length of the compartment. The near field temperature is equal to the peak temperature and represents the heart of the fire where flames are directly heating the structure. The size of the floor area that the near-field covers and the speed at which it travels through the compartment may vary. A range of near-field sizes must be checked by the designer to find the worst case fire. The local burning time spent by the near-field over a point may be calculated from:

$$t_b = \frac{q_f}{\dot{Q}''} \tag{2.6}$$

where t_b is the burning time (s), q_f is the fuel load density (MJ/m^2) and $\dot{Q}''$ is the heat release rate per unit area (kW/m^2).

The temperature of the near-field is set at 1200°C, based on a conservative estimate of the typical peak temperature achieved in office fires [9]. The far-field represents both the area ahead of the fire that is being heated by the hot gases and the area behind the fire where all of the combustible materials have been consumed. The temperature of the far-field layer is based on the correlations presented by Alpert [35], [36] which were derived from fire tests. Alpert's original correlation relates the peak gas temperature to the radial distance from the centre of the fire plume:

$$T_{peak} - T_\infty = 5.38 \frac{\left(\dot{Q}/r\right)^{2/3}}{H_C} \tag{2.7}$$

where T_{peak} is the peak temperature of the gases, T_∞ is the ambient temperature, H_C is the height of the compartment, $\dot{Q}$ is the heat release rate and r is the radius of the fire plume.

This correlation is based on results from axisymmetric plume tests of radius r. In order to apply this equation to a rectangular fire, the radius of a circle with an equivalent area is calculated. The relationship was further simplified by Stern-Gottfried et al. [37] by using a fourth-power average to calculate a single representative value for the far-field gas temperature.

$$T_{ff} = \frac{\left[\int_{r_{nf}}^{r_{ff}} {T_{peak}}^4 dr\right]^{1/4}}{\left(r_{ff} - r_{nf}\right)^{1/4}} \tag{2.8}$$

where T_{ff} is the temperature of the far-field, T_{peak} is the peak temperature of the gases, r_{ff} is the radius of the far-field, r_{nf} is the radius of the near-field.

2.3 Heat Transfer Analysis

Heat transfer analysis is a complex, yet essential part of any analysis of the effects of fire on a structure. Heat transfer analysis considers the three basic mechanisms of heat transfer (conduction, convection and radiation) to calculate the temperature distribution within a structural member [9]. Depending on the situation, one of the mechanisms may dominate the behaviour of the system. For example, heat transfer within a solid may be accurately modelled by considering conduction only. In typical engineering analyses the heat gains and heat losses are assumed to be dominated by convective and radiative heat fluxes only within the gaseous phase, and the heat transfer within the solid is due to conduction. When considering heat transfer within a member it is important to consider both the geometry of the member and the thermal inertia of the member's constitutive materials. The geometry of the member affects both the section factor and the configuration factor. The section factor is the ratio of the heated perimeter of a cross section to its cross sectional area. The greater the heated perimeter, relative to the area, the greater is the capacity for heat absorption. The configuration factor affects the magnitude of the net radiative heat flux. It accounts for the positioning of the member relative to the fire and to its distance from the fire. It is an important factor in determining the incident heat flux upon the surface of the member. Thermal inertia is a measure of the heat stored by a material and is defined as the square root of the product of three material properties; thermal conductivity, density and specific heat capacity.

There are considerable levels of parameter uncertainty involved in heat transfer analysis. For example, the coefficient of heat transfer by convection and the surface emissivity of a structural member both show considerable variance. In contrast to this, there is relatively little model uncertainty involved in heat transfer analysis and it is not considered further in this thesis. Both the lumped capacitance and the finite difference

approaches to heat transfer presented in the following sections are accurate and robust methods.

The Eurocodes specify the thermal actions as the sum of the net convective heat flux and the net radiative heat flux. These heat fluxes are determined from the equations given below [12]:

$$\dot{h}_{net,c} = \alpha_c(\Theta_g - \Theta_m) \tag{2.9}$$

where $\dot{h}_{net,c}$ is the net convective heat flux (W/m^2), α_c is the coefficient of heat transfer by convection (W/m^{2}K), θ_g is the gas temperature in the vicinity of the fire exposed member (°C) and θ_m is the surface temperature of the member (°C).

$$\dot{h}_{net,r} = \Phi\varepsilon_m\varepsilon_f\sigma[(\Theta_r + 273)^4 - (\Theta_m + 273)^4] \tag{2.10}$$

where $\dot{h}_{net,r}$ is the net radiative heat flux (W/m^2), Φ is the configuration factor (conservatively taken as 1), ε_m is the surface emissivity of the member, ε_f is the emissivity of the fire, σ is the Stephan Boltzmann constant (= 5.67x10^{-8} W/m^{2}K^4) and θ_r is the effective radiation temperature of the fire environment (°C).

Steel sections, in general, are easily heated as they have both a high thermal inertia and a high section factor. The reason that steel members tend to have a high section factor is that steel members are typically very thin for economy. A lumped capacitance approach is therefore highly suitable for typical steel members [38]. The lumped capacitance method is a step by step approach that assumes that there is a uniform temperature throughout the member.

For an unprotected steel section, the temperature rise is calculated from:

$$\Delta\theta_{a,t} = k_{sh}\frac{A_m/V_m}{c_a\rho_a}\dot{h}_{net,d}\Delta t \tag{2.11}$$

where

$$k_{sh} = \frac{[A_m/V_m]_b}{[A_m/V_m]} \tag{2.12}$$

where $\Delta\theta_{a,t}$ is the change in component temperature over a single time step, k_{sh} is the correction factor for the shadow effect, A_m/V_m is the section factor for unprotected steel members (1/m), A_m is the surface area of the member per unit length (m^2/m), V_m is the volume of the member per unit length (m^3/m), $[A_m/V_m]_b$ is the box value of the section

factor, c_a is the specific heat of steel (J/kgK), $\dot{h}_{net,d}$ is the net design value of heat flux from the fire acting on the member, Δt is the time interval (sec) and ρ_a is the unit mass of steel (kg/m^3). The box value of the section factor of a steel member is equal to the section factor of a rectangle that encloses the cross section of the steel member.

The procedure for calculating the temperature of protected steel sections is similar to that of unprotected sections except that the net heat flux acting on the section is not required as it is assumed that the outer layer of insulation is at the same temperature as the surrounding gases. The temperature change in a steel section during a given time step may be calculated from [38]:

$$\Delta\theta_{a,t} = \frac{A_p}{V_m} \cdot \frac{\lambda_p}{d_p \rho_s c_s} \cdot \frac{\rho_s c_s}{\rho_s c_s + \left[\left(A_p/V_m\right) d_p \rho_p c_p/2\right]} \cdot \left(\theta_g - \theta_{a,t}\right) . \Delta t \qquad (2.13)$$

where $\Delta\theta_{a,t}$ is the change in component temperature over a single time step, A_p/V_m is the section factor for a steel member insulated by fire protection material, λ_p is the thermal conductivity of the fire protection material (W/mK), d_p is the depth of the fire protection material (m), ρ_s is the unit mass of the steel (kg/m^3), c_s is the specific heat of steel (J/kgK), ρ_p is the unit mass of the fire protection material (kg/m^3), c_p is the specific heat of the fire protection material (J/kgK), θ_g temperature of the fire (°C), $\theta_{a,t}$ is the temperature of the steel (°C) and Δt is the time step (seconds). The above procedure is only applicable for non-reactive fire protection materials such as sprayed mineral fibre, vermiculite plaster, gypsum plaster, mineral wool, etc.

Heat transfer through a thermally thick section, such as a concrete slab, cannot be analysed using the lumped capacitance assumption due to the large thermal gradients that occur through the section. Due to the complexity of the problem, the temperature distribution within concrete slabs is best found using numerical methods. A finite difference formulation is particularly useful when considering a slab subject to a compartment fire as the problem may be reduced to one dimension by treating the slab as an infinite plate [9]. This simplification requires the assumption that the temperature varies only through the depth of the slab and not across the face of the slab. The net heat flux applied to the exposed surface of the slab is the sum of the net convective heat flux and the net radiative heat flux. The heat loss from the unexposed surface of the slab is based on convective losses. The heat loss due to radiation is accounted for by the use of a modified coefficient of heat transfer, in accordance with Eurocode 1 [12]. To

determine the temperature distribution within the member the slab is divided into several horizontal strips, with conduction occurring between each strip. The finite difference equations for analysing a concrete slab heated on one side are set out below.

Equation for the layer of the slab adjacent to the exposed surface:

$$\theta_{c,1}(t+\Delta t) = \theta_{c,1}(t) + \left\{\frac{\alpha_c \Delta t\left[\theta_g(t+\Delta t) - \theta_{c,1}(t)\right]}{\rho_c c_c d_c}\right\} + \left\{\frac{\varepsilon_c \sigma \Delta t}{\rho_c c_c d_c}\left[\left(\theta_g(t+\Delta t)+273\right)^4 - \left(\theta_{c,1}(t)+273\right)^4\right]\right\} - \left\{\frac{\lambda_c \Delta t}{\rho_c c_c {d_c}^2}\left[\theta_{c,1}(t) - \theta_{c,2}(t)\right]\right\} \quad (2.14)$$

Equation for the intermediate layers:

$$\theta_{c,i}(t+\Delta t) = \theta_{c,i}(t) + \left\{\frac{\lambda_c \Delta t}{\rho_c c_c {d_c}^2}\left[\theta_{c,i-1}(t) - 2\theta_{c,i}(t) + \theta_{c,i+1}(t)\right]\right\} \quad (2.15)$$

Equation for the layer adjacent to the unexposed surface:

$$\theta_{c,n}(t+\Delta t) = \theta_{c,n}(t) + \left\{\frac{\lambda_c \Delta t}{\rho_c c_c {d_c}^2}\left[\theta_{c,n-1}(t) - \theta_{c,n}(t)\right]\right\} - \left\{\frac{\alpha_{c,2} \Delta t\left[\theta_{c,n}(t) - \theta_{amb}\right]}{\rho_c c_c d_c}\right\} \quad (2.16)$$

where $\theta_{c,i}(t)$ is the temperature of layer i of the concrete slab at time t, α_c is the coefficient of heat transfer by convection, Δt is the time step, θ_g is the gas temperature, ρ_c is the density of concrete, c_c is the specific heat of concrete, d_c is the depth of a layer of the slab, ε_c is the emissivity of the concrete slab, σ is the Stephan Boltzmann constant, λ_c is the conductivity of concrete, $\alpha_{c,2}$ is the coefficient of heat transfer by convection on the unexposed side of the member (including radiation effects) and θ_{amb} is the ambient temperature above the slab.

2.4 Structural Analysis

Structural analysis involves the evaluation of the various responses of a structure to different combinations of loads to ensure that the structure will safely withstand these loads. Modern design is based on the concept of limit states. Under limit state design the performance requirements are split into ultimate limit states and serviceability limit states. Ultimate limit states relate to the possible collapse mechanisms of the structure whereas serviceability limit states relate to the usability and durability of the structure. The performance of the structure is evaluated separately under each limit state. Historically structural analysis has not been used to evaluate the response of structures under fire loading, instead designers have relied either on design tables or the use of critical temperatures [39]. The critical temperature method features in the Eurocodes for both steel structures and composite structures. It involves calculating a limiting temperature that the structure cannot exceed based on the type of structural member and the degree of utilization of the member.

Design tables are available that provide the minimum dimensions which must be specified in order to achieve a specific resistance time when subjected to the standard fire. The furnace test used to determine resistance against collapse is flawed as it only considers one temperature-time curve and it does not use realistic boundary constraints. For example, in a beam test the beam is simply supported and therefore the test cannot accurately capture the behaviour of the beam as part of a larger structure. The effects of end restraints have long been accounted for in other areas of structural engineering. Moment redistribution is commonly applied to continuous beams to account for the effects of their continuity, or lack of it, over each individual span [40]. Likewise, examination of the behaviour of a beam in fire must account for the end restraints. Steel frames with a composite concrete deck slab provide certain advantages and also some constraints when subjected to fire loading. The better than expected behaviour of this kind of construction was first noticed after the 1990 Broadgate fire, in London [41]. In this event a partially constructed steel concrete composite building, with partially completed fire protection, suffered a large fire but did not suffer serious structural damage (the cost of structural frame repair was a small fraction of the overall repair cost). The better than expected behaviour of the Broadgate building led to six full-scale fire tests on an 8 storey frame at the BRE Large Building Test Facility at Cardington [6], [42] built specifically for this purpose, and carried out in collaboration by BRE and

British Steel (now Tata Steel). These tests led to a much more comprehensive understanding of the response of steel frame composite structures to fire and produced fresh insights leading to the development of the first generation performance-based engineering methods for fire resistance design of structures [43].

In recent decades the understanding of the fundamentals of structural behaviour under fire has greatly increased due to the large amount of research carried out in the field. Prior to the Cardington tests the behaviour of a structure in fire was thought to be dominated by the degradation of the construction materials and the effects of thermal expansion and thermal deformation were under-appreciated [2]. For example steel loses half of its strength at less than 600°C and concrete starts to degrade rapidly after 300°C [44], [45]. Analysis of the tests highlighted certain aspects of structural behaviour as being of paramount importance. It was found that structural members that were restrained against thermal expansion were subject to very high stresses, even at relatively low temperatures. The total strain in a heated member is equal to the sum of the mechanical strain and the thermal strain, as shown in equation (2.17) [2].

$$\varepsilon_{total} = \varepsilon_{thermal} + \varepsilon_{mechanical} \tag{2.17}$$

If the member is prevented from expanding, the total strain is zero and the mechanical strain is equal to the negative of the thermal strain. If a member is effectively restrained then it may experience significant stresses due to thermal strains. The thermal gradient has also been shown to have a large effect on the behaviour of structural members. Thermally thin members, such as steel sections, tend to have relatively low thermal gradients as the heat is rapidly transferred through the depth of the cross-section. Concrete members on the other hand may experience large thermal gradients as concrete has a low thermal conductivity. The thermal gradient across the depth of a section is obtained from (assuming a linear thermal gradient, which is almost never the case in a concrete member):

$$T_{,z} = \frac{T_2 - T_1}{d} \tag{2.18}$$

where $T_{,z}$ is the thermal gradient, T_2 is the temperature on the exposed face of the member, T_1 is the temperature on the unexposed face of the member and d is the depth of the member. Slabs and walls in particular tend to have large thermal gradients, as only one face of the member is exposed to the heat source. Thermal gradients through a

member result in thermal bowing of the member as the hotter portion of the member expands more than the cooler portion. The stress distribution resulting from thermal bowing is highly dependent on the member restraints.

Simply supported members do not experience any stresses due to thermal bowing as the beam ends are free to rotate to form the “bow” shape and the roller support accommodates the overall shortening of the member due to the new shape. Pinned-end members (with ends free to rotate but restrained against lateral translation) experience bending stresses due to the P-δ effect when subjected to thermal gradients. The P-δ effect refers to the moment that is generated when a purely axial load is offset from the centreline of a structural element. For both simply supported and pinned-end members, large thermal gradients lead to large deflections. In the case of a member with fully fixed end restraints a thermal gradient does not cause any deformation. The rotational restraint prevents deflection and instead a constant bending moment is induced along the length of the beam.

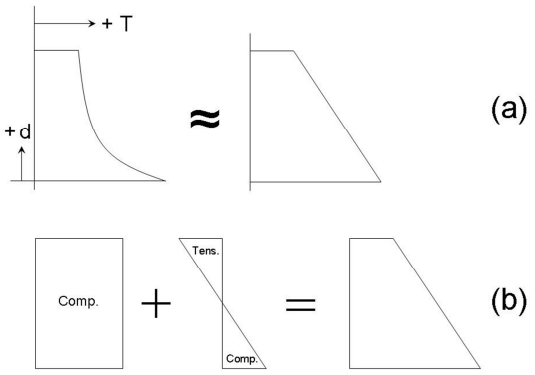

Figure 2.5: (a) Typical temperature distribution compared to an idealised temperature distribution and (b) the related expansion induced stress and thermal bowing induced stress combined into the overall stress state.

A typical temperature distribution is shown above in Figure 2.5. In such a case, where the member is subject to both thermal expansion and thermal bowing the behaviour of the member may vary considerably depending on the restraint conditions. For example,

where one mechanism dominates the behaviour then the effects of the weaker mechanism may be negligible. If the thermal expansion and the contraction due to thermal bowing are of equal magnitude then they cancel out any axial force which may arise due to the member restraints. This can only occur if the outwards movement of the ends of the beam caused by thermal expansion is equal to the pull in of the ends of the beam caused by thermal bowing.

2.4.1 Variables affecting structural response

The prediction of structural response to fire loading is a difficult problem that is dependent upon many different factors. The range of factors affecting the response can be split into three basic groups: material variables, geometric variables and loading variables. The fire itself will obviously have a large effect on the structural response and the variables related to the definition of the fire have been discussed earlier in section 2.2.1.

Loading variables

The mechanical loading acting upon a structure consists of two parts; the permanent load due to the self-weight of the structure and the imposed load due to the furniture and occupants in the structure. A stochastic description of these two variables is given in Table 2.2.

Table 2.2: Stochastic definition of loading variables.

	Characteristic (or nominal) value at ambient	Units	Varies with temperature	Distribution type	Mean (distribution parameter 1)	Coefficient of Variation (distribution parameter 2)
Permanent load	/	kN/m^2	No	Gaussian‡2	/	0.1 ‡1
Imposed load (office)	3‡2	kN/m^2	No	Gumbel‡2	1.8	0.35 ‡1

‡1 [46]; ‡2 [47]

Material variables

Three structural materials that are widely used in composite construction are structural steel, reinforcing steel and concrete.

Structural steel in the UK is typically one of two grades, s355 and s275. These grades denote the yield strength of the steel. Under the Eurocodes steel may be modelled as an elastic-plastic material [48]. This requires three parameters to fully define the material stress-strain curve; the Young's modulus, the yield stress and the ultimate strain. The stress-strain curve of steel varies with increasing temperature. As the temperature is increased both the Young's modulus and the yield stress are decreased as shown in Figure 2.6.

The reduction factors shown are derived from tensile tests under transient heating tests [49], [50]. In transient-state tests the test specimen is subjected to a constant load before being exposed to an increasing temperature [51]. The temperature and strain values are recorded during the test under a constant stress. The strain rate in transient-state tests is influenced by the rate of heating. The Eurocode values are valid for heating rate between 2 and 50°C/min [44]. Steady-state tests may also be used to measure the stress-strain

relationship of steel under elevated temperatures. Steady-state tests involve heating the specimen to a constant temperature before carrying out a tensile test. This approach was widely used in the past due to its simplicity, however it is now less used due to improvements in testing apparatus [52]. Also, transient state tests provide a better representation of the typical fire scenario. Kirby and Preston showed that the level of reduction in material properties under elevated temperatures varies with variation of the heating rate [52]. This introduces a source of uncertainty into the material parameters. The dispersion of the test results is largest at lower temperatures and is greatly reduced at temperatures over 700°C. The Eurocode reduction factors shown below ignore the contribution that strain hardening makes to the yield stress of the steel.

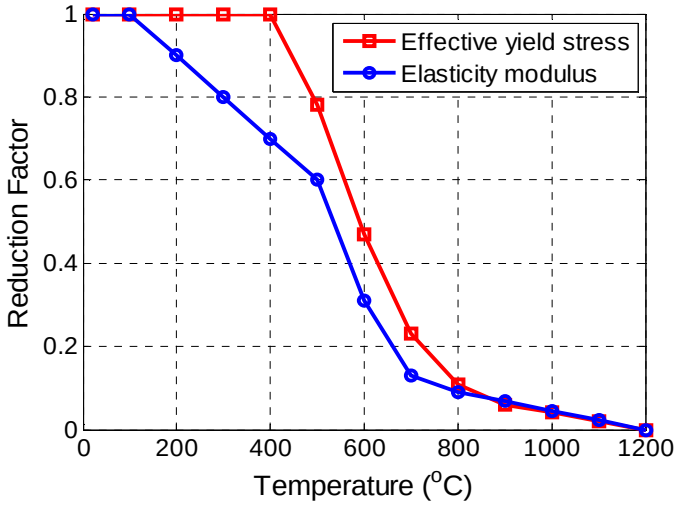

Figure 2.6: Reduction factors for the yield stress and the Young's modulus of hot-rolled steel, as shown in BS EN 1993-1-2.

Work by Byfield and Nethercot showed that the geometric variability of steel members is relatively low and does not have much effect on the capacity of the member [53], [54]. The study showed that the inherent variation in the material properties has a greater influence on the safety index of structural steelwork, compared to the geometry variation. Distribution parameters for the properties of steel are given below in Table 2.3. The ultimate strain of structural steel, shown in the table below, is assumed to be temperature independent as per Eurocode 3 [44].

Table 2.3: List of material properties for structural steel.

	Characteristic (or nominal) value at ambient	Units	Varies with temperature	Distribution type	Mean (distribution parameter 1)	Coefficient of Variation (distribution parameter 2)
Young's modulus of elasticity	210‡1	GPa	Yes	Lognormal‡2	210	0.03 ‡2
Poisson's ratio	0.3‡1	/	No	Lognormal‡2	0.3	0.03 ‡2
Yield stress	275 or 355‡1,‡5	MPa	Yes	Lognormal‡2	309.3 or 399.2	0.07‡2,‡4
Ultimate strain	0.20‡3	/	No	Lognormal‡2	0.20	0.06 ‡2
Coefficient of thermal expansion	$12x10^{-6}$ ‡1	/°C	Yes	None	/	/
Density	7850‡3	kg/m^3	No	Gaussian	7850	< 0.01‡6
Thermal Conductivity	53.334‡3	W/mK	Yes	None	/	/
Specific heat	439.8‡3	J/kgK	Yes	None	/	/

‡1 [55]; ‡2 [56]; ‡3 [44]; ‡4 [53]; ‡5 [57]; ‡6[17]

Concrete is a highly variable composite material, composed of aggregate, sand, cement, water and chemical additives [58]. In general, concrete offers good fire resistance. It is a non-combustible material and it does not emit toxic fumes. Both the strength and stiffness of concrete are reduced by exposure to high temperatures. This occurs due to

chemical and physical changes in the structure of the material. At approximately 100°C concrete begins to suffer the loss of physically bound water in the aggregate and the cement matrix. At 120°C the gypsum in the cement begins to decompose and the chemically bound water is lost. These processes weaken concrete to the point that it is generally not considered as structurally useful past 550°C. Eurocode 2 provides reduction factors for calculating the reduction in the compressive strength and the corresponding strain. These factors are shown below in Figure 2.7. The reduction in the compressive strength of concrete at elevated temperatures is subject to a significant level of uncertainty. The magnitude of the reduction in compressive strength is affected by factors such as heating rate, loading rate, type of aggregate, specimen size, curing conditions and the use of admixtures [59], [60]. The stress-strain relationship for concrete under elevated temperatures may be measured using either transient or steady-state tests. The difference in test methods accounts for a portion of the uncertainty in the stress-strain results for heated concrete. As with structural steel, transient tests are now most commonly used as they best reflect the loading imposed upon structures by fire.

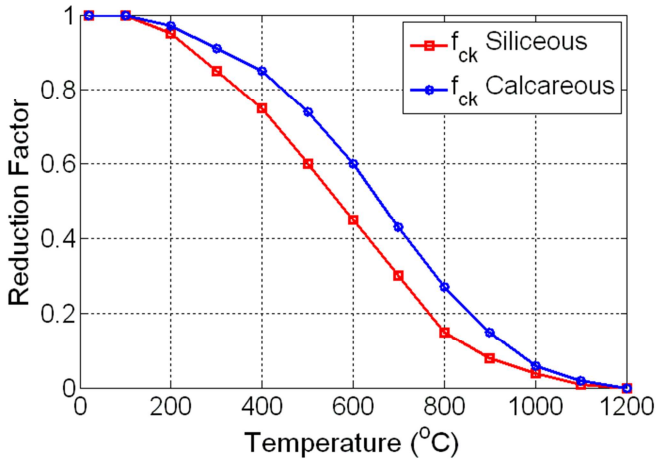

Figure 2.7: Reduction factors for the compressive strength of concrete.

The thermal properties of concrete, such as thermal conductivity, are required for conducting heat transfer analysis. These thermal properties are provided in the Eurocodes and the typical ambient values are listed below in Table 2.4 [45].

Table 2.4: List of material properties for normal concrete.

	Characteristic value at ambient	Units	Varies with temperature	Distribution type	Mean (distribution parameter 1)	Coefficient of Variation (distribution parameter 2)
Young's modulus of elasticity, E_{cm}	29 – 37 ‡1	GPa	Yes	Lognormal ‡2,‡3	29 - 37 ‡1	0.15 ‡3
Poisson's ratio	0.2 ‡1	/	No	None	/	/
Compressive cylinder strength, $f_{ck,cy}$	15 – 50‡1	MPa	Yes	Lognormal‡4	20.1 – 66.9	0.06 ‡3 – 0.17‡4
Ultimate compressive strain, ε_{cu}	0.0035 ‡1	/	No	None	/	/
Coefficient of thermal expansion	$10x10^{-6}$‡1	/°C	Yes	None	/	/
Density	~ 2440‡5	kg/m^3	No	Gaussian	~ 2440	0.04 – 0.08‡7
Thermal Conductivity	1.95 –1.33 ‡6	W/mK	Yes	None	/	/
Specific heat	900‡6	J/kgK	Yes	None	/	/

‡1[61]; ‡2 [56]; ‡3 [62]; ‡4 [63]; ‡5 [47]; ‡6[45]; ‡7 [17]

Reinforcing steel is a common construction material, widely used in both steel framed and concrete framed buildings. It is available in the form of hot rolled steel bars or as cold worked reinforcement meshes. Cold worked steel and hot rolled steel exhibit different stress-strain behaviour, both at ambient temperatures and at elevated temperatures, due to their method of production. The reduction in Young's modulus and effective yield stress with increasing temperatures, as described in Eurocode 2, is shown below in Figure 2.8 for both types of reinforcing steel. Probabilistic definitions of the material properties for reinforcing steel are given below in Table 2.5.

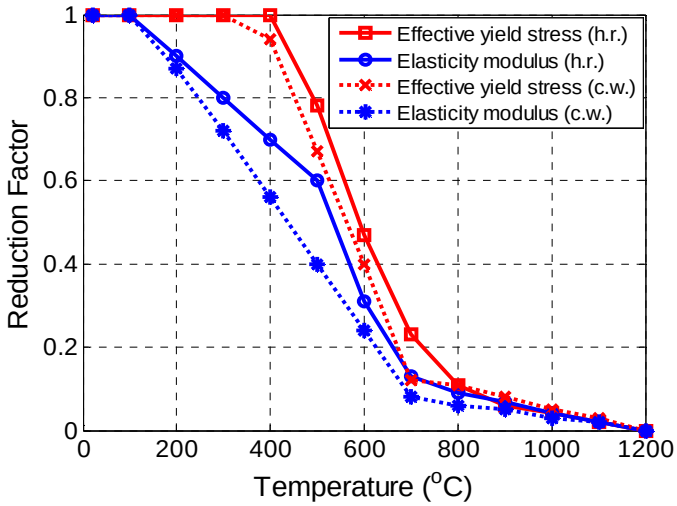

Figure 2.8: Reduction factors for the yield stress and Young's modulus of hot rolled rebar and cold worked rebar.

Table 2.5: List of material properties for reinforcing steel.

	Characteristic value at ambient	Units	Varies with temperature	Distribution type	Mean (distribution parameter 1)	Coefficient of Variation (distribution parameter 2)
Young's modulus of elasticity	200‡1	GPa	Yes	Lognormal‡2	200	0.03 ‡2,‡3
Poisson's ratio	0.3‡2	/	No	Lognormal‡2	0.3	0.03 ‡2,‡3
Yield stress	400 – 600‡1,‡6	MPa	Yes	Lognormal‡2	449.8 – 674.8	0.07 ‡2,‡3,‡5
Ultimate strain, ε_{uk}	0.025 (10% quantile value) ‡1	/	No	Lognormal	0.027	0.06 ‡2,‡3,‡5
Coefficient of thermal expansion	$12x10^{-6}$ ‡2	/°C	Yes	None	/	/
Density	7850‡1	kg/m^3	No	Gaussian	7850	< 0.01 ‡7
Thermal Conductivity	53.334‡4	W/mK	Yes	None	/	/
Specific heat	439.8‡4	J/kgK	Yes	None	/	/

‡1 [64]; ‡2 [55]; ‡3 [56]; ‡4[44] ; ‡5 [65]; ‡6 [61]; ‡7 [17]

2.4.2 Structural analysis models

Steel-concrete composite beams are commonly used in multi-storey buildings, particularly in office buildings. Composite structures typically consist of a steel skeleton, composed of columns and beams, combined with cast in-situ concrete slabs (Figure 2.9). The in-situ concrete slabs are supported during construction by permanent, sheet metal formwork. The concrete and steel members are connected by shear studs. Shear studs are welded at regular intervals to the upper flange of a beam and are required to distribute the shear forces and to ensure that the elements act as one composite member.

Figure 2.9: Illustration of a typical steel-concrete composite member [66].

Composite structures efficiently carry loads by taking advantage of the different strengths of construction materials. In a composite beam the bending stress causes tension in the steel beam and compression in the concrete slab. In this way less steel is required, making the structure more economical and the concrete is kept in compression as it is weak in tension.

Composite beams are required to meet bending and shear ultimate limit states and the deflection serviceability limit state at ambient temperatures. The requirements for composite beams subjected to fire are different in that the beam must maintain its load bearing capability but serviceability limits are not considered. The behaviour of a

composite beam changes at very high temperatures, with catenary action replacing bending action as the dominant load transfer mechanism. Because of this change in load transfer mechanism different methods of structural analysis are usually required, as discussed in the following sections.

Analytical methods for the analysis of composite beams

Several methods have been previously published for the analysis of composite beams at elevated temperatures [67]–[70]. A simplified approach was put forward by Usmani based on the "Method of Slices" [67], [71]. The composite beam to be analysed is split into horizontal slices based on the geometry of the cross section, as shown in Figure 2.10.

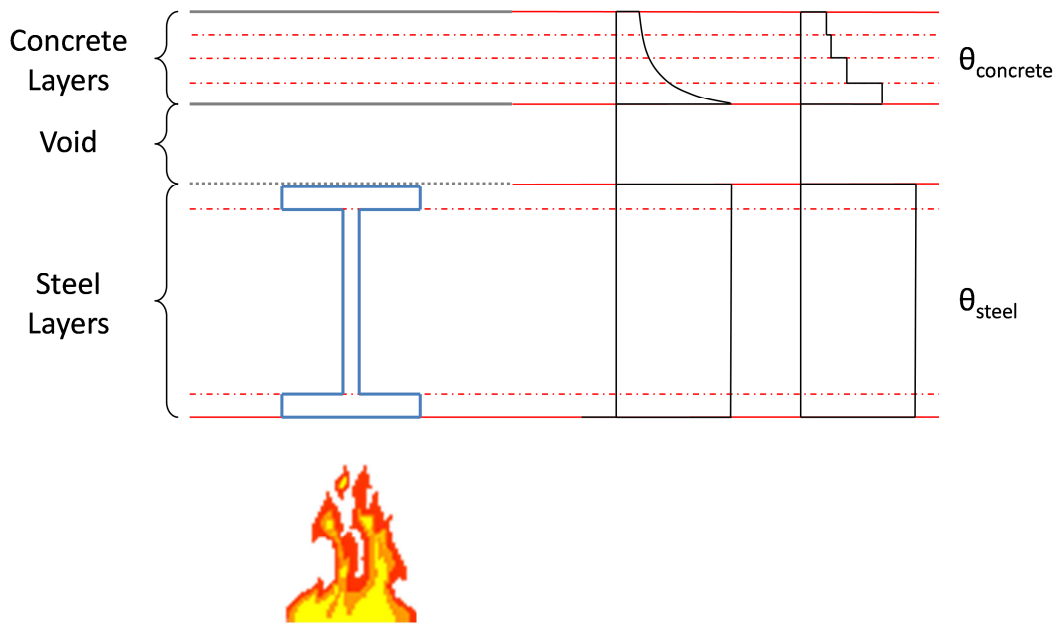

Figure 2.10: Cross-section of a heated steel-concrete composite, showing the associated actual and simplified temperature distributions.

The magnitude of the temperature rise ΔT and the thermal gradient $T_{,z}$ in each slice are found by conducting a heat transfer analysis. This allows the material properties of each slice to be calculated, accounting for the material degradation due to high temperatures.

The cross sectional width of each slice is modified in relation to a reference value of Young's modulus of elasticity, E_{ref}. This allows the beam to be treated as homogeneous.

The stresses in the section are calculated from an expanded version of the basic equation for beams subject to combined bending and axial loads, shown in Equation (2.19).

$$\sigma_{sec} = \frac{P}{A} + \frac{My}{I} \tag{2.19}$$

where σ_{sec} is the stress in the section (MPa), P is the axial force in the section (N), A is the cross sectional area of the section (mm^2), M is the moment acting on the section (Nmm), y is the lever arm from the neutral axis (mm) and I is the second moment of area (mm^4). The first term in Equation (2.19) above is the stress due to axial force acting on the member and the second term is the bending stress due to bending moments acting on the member.

The axial force in the equation above is generated by the boundary conditions restricting the translation of the ends of the beam due to thermal expansion and thermal bowing. The moment term in the equation above is dependent on three elements: the moment due to the applied load, the moment due to the thermal gradient and the moment due to the P-δ effect caused by thermal expansion. The advantages of this method are that it can calculate the stress/strain distribution through the depth of the cross section and the deflection of the cross section. The disadvantage of this method is that it is only applicable to beams at relatively low temperatures, i.e. less than 700°C. Also, this method does not account for the effects of other load transfer mechanisms such as compressive arch action or catenary membrane action. The limitations of this method result in a large level of model uncertainty being associated with this method. Due to the limitations of this method, it is best suited either to insulated members or uninsulated members exposed to cool fires.

Cameron proposed a method for analysing composite beams based on catenary action alone as the sole load carrying mechanism [68]. While this method is not suitable for use at ambient temperatures, it is a valid assumption for beams in fully developed fires. As catenary action is taken as the load transfer mechanism, the stress in the beam is calculated from the strain in the reinforcing bars and in the steel beam. As with the previously described method, not accounting for other load transfer mechanisms such as bending action or compressive arch action leads to model uncertainty. The level of

model uncertainty varies depending on the nature of the beam; very hot, slender beams will transfer loads almost entirely by catenary action whereas a stiffer, cooler beam will transfer relatively little of the load by catenary action.

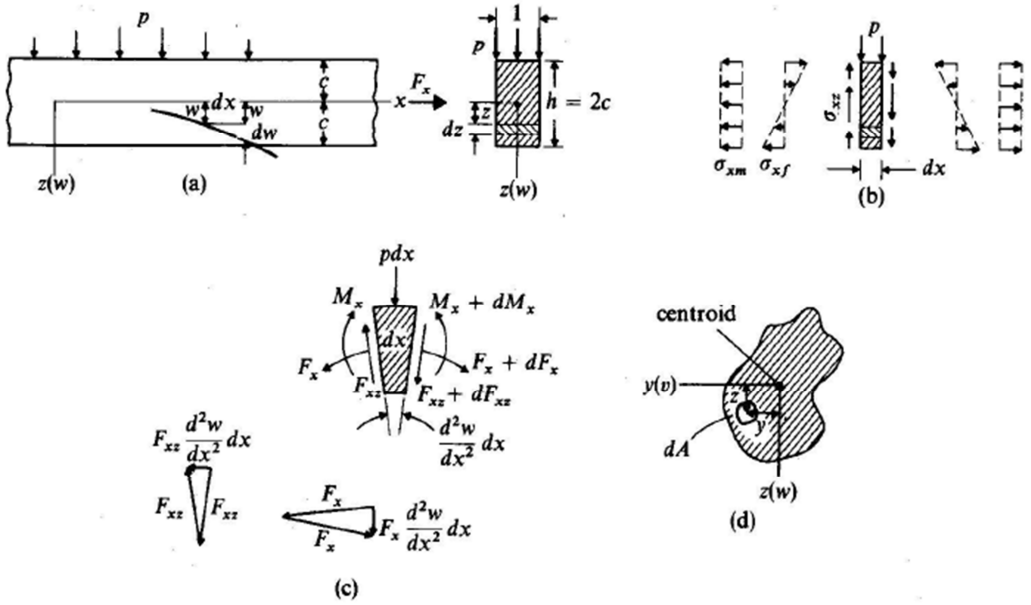

Figure 2.11: Geometry and internal forces of a deflected beam [72].

The main assumptions of the method include:

- uniform strain along the length of the beam
- the deflected beam is in the shape of sine curve
- uniform temperature distribution along the length of the beam
- lateral restraints to the ends of the beam
- the beam is prismatic

Cameron's method is split into two stages, firstly the thermal deflection is calculated and then the additional load induced deflection is calculated.

According to the Euler-Bernoulli classical beam theory, the strain at any point in a beam can be represented by:

$$\varepsilon_x = \varepsilon_{xm} - z\left(d^2w/dx^2\right) - \alpha\Delta T \tag{2.20 a}$$

$$\sigma_x = E\varepsilon_{xm} - Ez\left(d^2w/dx^2\right) - E\alpha\Delta T \tag{2.20 b}$$

where ε_x is the strain in the x-direction, ε_{xm} is the membrane strain, z is the distance from the middle surface, α is the coefficient of thermal expansion of the material and ΔT is the rise in temperature. The stress at any point in a beam can be derived by multiplying Equation (2.20 a) by the Young's modulus of the material E. The geometry and internal stresses/strains in a beam are shown above in Figure 2.11.

The stress resultants acting on the beam can then be calculated by integration of Equation (2.20 a) through the depth of the beam. This gives the resultant force and bending moment as:

$$F_x = \int_{-h/2}^{h/2} \sigma_x \, dz = EA\varepsilon_{xm} - N^T \tag{2.21 a}$$

$$M_x = \int_{-h/2}^{h/2} \sigma_x z \, dz = -EI\left(d^2w/dx^2\right) - M^T \tag{2.21 b}$$

where the thermal force N^T and the thermal moment M^T are expressed as:

$$N^T = E\alpha \int_{-h/2}^{h/2} \Delta T \, dz \tag{2.22 a}$$

$$M^T = E\alpha \int_{-h/2}^{h/2} \Delta T z \, dz \tag{2.22 b}$$

Incorporating Equations (2.22 a) and (2.22 b) into the governing equation of equilibrium for a beam gives:

$$EI\left(d^4w/dx^4\right) = p + d^2M^T/dx^2 + EA\varepsilon_{xm}\left(d^2w/dx^2\right) - N^T\left(d^2w/dx^2\right) \qquad (2.23)$$

where E is the Young's modulus of the material, I is the second moment of area of the beam, p is the transverse load acting on the beam and A is the cross sectional area of the beam. In order to solve this governing differential equation, the thermal moment and deflection terms are represented by the first term of a single Fourier sine series. The governing equation can then be reduced to a cubic equation in terms of thermal deflection w_T:

$$w_T^3 + \left\{\left(\frac{4I}{A}\right) - \left(\frac{4N^TL^2}{\pi^2EA}\right)\right\}w_T + \left\{\frac{16M^TL^2}{\pi^3EA}\right\} = 0 \qquad (2.24)$$

The above equation may be solved to calculate the thermal deflection. The total deflection of the beam due to both the transverse mechanical and thermal loads is then calculated using the virtual work principle. The deflection of the beam is increased in increments and the load required to induce the increased deflection is then calculated. The deflection is increased until the calculated load is equal to the applied load. The internal work done is defined as the integral of the area under the stress-strain curve multiplied by the volume of each steel element:

$$\Pi_{int} = \sum_{n=1}^{no.\ rebars}\left[V_n\int_{\varepsilon_{wT}}^{\varepsilon_{wn}}\sigma(\varepsilon)d\varepsilon\right] \qquad (2.25)$$

where Π_{int} is the internal work, V_n is the volume of the rebar, ε_{wn} is the mechanical strain in the rebar at a deflection of w_n, ε_{wT} is the mechanical strain in the rebar due to the thermal deflection and $\sigma(\varepsilon)$ is the stress-strain curve of the rebar.

The external work is calculated from the movement of the transverse load due to the incremental increase in deflection. It may be defined as:

$$\Pi_{ext} = \frac{qLB(w_n - w_T)}{\pi} \qquad (2.26)$$

where Π_{ext} is the external work done, q is the uniformly distributed load, L is the length of the beam, B is the width of the concrete beam, w_n is the total deflection of the slab and w_T is the thermal deflection of the slab.

The load increment p is then found from:

$$p = \frac{\Pi_{int}\pi}{\mathrm{LB}(w_n - w_T)} \tag{2.27}$$

As Cameron's method assumes that the loads acting on the beam are transferred solely by catenary action, it is best suited to slender heated members. Stiff or well-insulated members may retain significant bending capacity which is not accounted for in Cameron's method.

Finite element methods for the analysis of composite beams

The finite element method allows for accurate solutions to the problems of modelling heat transfer through a composite beam and modelling the structural response of a composite beam. Two finite element programs have been examined as part of this work; OpenSees and Abaqus. OpenSees (Open System for Earthquake Engineering Simulation) is an open source software framework that was primarily developed for simulating the response of structural systems to seismic action [73]. OpenSees has been adapted to the analysis of structures in fire by researchers at the University of Edinburgh [74]. Abaqus is a powerful commercial software program capable of both heat transfer analysis and thermomechanical analysis [75]. Both finite element programs are highly accurate and have little model uncertainty associated with them.

A geometrically and materially nonlinear static analysis was conducted using OpenSees. A two-dimensional composite beam model was created in OpenSees using displacement-based elements connected by rigid links (Figure 2.12). Displacement-based elements are capable of capturing the spread of plasticity along the length of an element which allows for the accurate representation of nonlinear material behaviour. The temperature data was input directly into the input file as the heat transfer analysis option within OpenSees is currently under development. The boundary conditions are variable and may be considered as simply supported, pinned, fully fixed or a translational spring may be implemented. The length of the beam is split into ten elements and the cross sections of the steel beam and the concrete slab are divided into twelve fibres and nine fibres respectively. Fibres are also used to represent each of the steel reinforcing bars individually. Each fibre stores information on material properties, cross-sectional area

and location. The material models included within the OpenSees program were used to assign material properties to the concrete, structural steel and the reinforcing steel. Each of these material models are based upon the temperature dependent uniaxial material models in Eurocodes 2 and 3 [44], [45]. A transverse, uniformly distributed load is applied to the surface of the concrete. Load control is used to capture the nonlinear behaviour of the section. The beam is analysed over a number of time steps, each with a different temperature distribution, in order to analyse how the behaviour of the beam varies with the fire. Outputs include deflection at the nodes and stress/strain values in the elements.

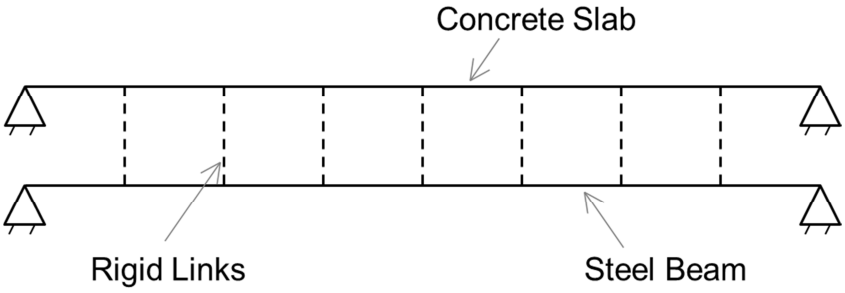

Figure 2.12: OpenSees model of a composite beam.

Two separate models were created for the analysis of composite beams using the Abaqus package. The first model is a two-dimensional model of the cross-section of the beam for conducting transient heat transfer analysis. The slab cross-section is taken as a rectangle with a single trapezoidal rib centred above the steel beam. The beam is assumed to be a doubly-symmetric I-beam. The I-beam may be specified as encased in fire protection or as unprotected, as shown below in Figure 2.13. Convective heat gain and heat loss are modelled using surface film conditions. A surface film condition is applied to the underside of the slab and around the perimeter of the beam (except for above the upper flange) to model for convective heat gain from the fire. A separate surface film condition is applied to the top of the slab in order to account for convective heat loss. The convective heat transfer coefficients were taken from the Eurocodes [12]. The radiative heat transfer from the fire to the structure was modelled using a surface radiation interaction. The surface radiation interaction was applied to the same surfaces as the surface film condition. The material emissivity of 0.7 was taken from the Eurocodes [12]. The heat transfer between the steel beam and the bottom of the concrete slab was

modelled using a surface to surface contact with a conductivity equivalent to the conductivity of steel.

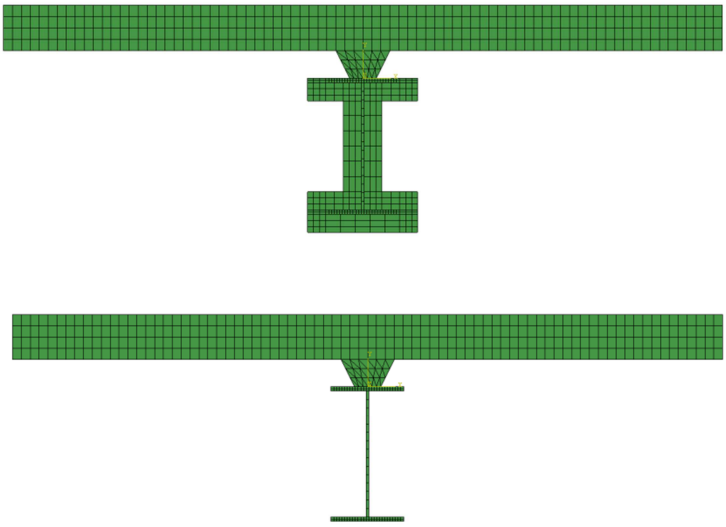

Figure 2.13: Meshed model of the composite beam cross-section with fire protection applied to the beam and with no fire protection applied.

Where fire protection is applied to the beam, the surface of the steel beam is tied to the inner surface of the fire protection. This effectively assumes perfect conduction between the two surfaces and maintains matching temperatures on both surfaces. The model is meshed with a mixture of 3-node triangular and 4-node quadrilateral heat transfer elements.

A separate model was created for the thermomechanical analysis. The model uses 2-node linear beam elements to model the steel beam and 4-node doubly curved shell elements for the concrete slab, as shown in Figure 2.14. Any strengthening effects from the fire protection are neglected due to the very low stiffness of typical fire protection materials. The beam and the slab are joined by rigid beam-type connectors to ensure composite behaviour between the two structural members. Beam-type connectors restrain both the relative displacement and relative rotation between the connected nodes. The steel

reinforcing bars are modelled using a rebar layer within the shell element. The rebar is represented as a smeared layer, of a constant thickness, across the width of the slab.

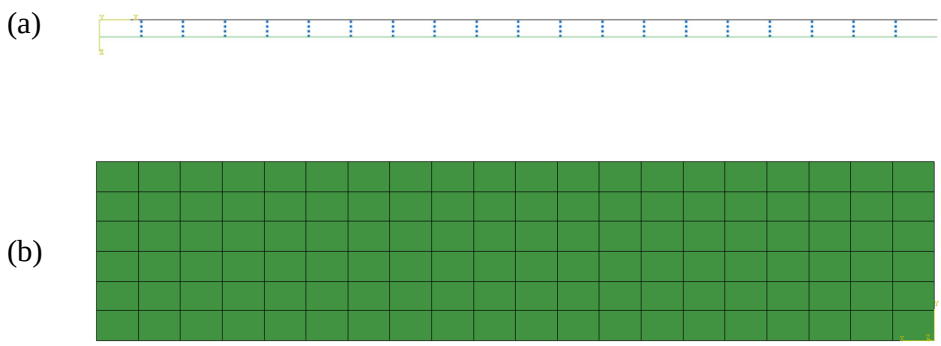

Figure 2.14: (a) Elevation and (b) plan view of an Abaqus model of a composite beam.

The uniformly distributed load acting on the slab is applied as a pressure on to the shell elements. The elevated temperatures are applied as separate predefined fields for the beam and the slab. The beam is assigned a uniform temperature increase based on the heat transfer analysis results. The slab is assigned different temperatures, taken from the heat transfer analysis, at five points through the depth of the shell.

Restraints are applied around the perimeter of the slab and at the ends of the beam. The ends of the beam and slab may be assigned different boundary conditions such as simply supported or fully fixed. The sides of the concrete slab are restrained from moving perpendicular to the span of the beam and from rotating around the same axis. These restraints were applied in order to account for the effect of the adjacent structure.

Both the OpenSees and Abaqus models described above have been incorporated into the software tool FireLab, discussed in Chapter 6. These finite element models provide a more accurate method for analysing composite beams, compared with the analytical methods. They allow the designer to fully capture both bending action and catenary action within the beam.

Analytical methods for the analysis of composite slabs

Reinforced concrete slabs typically exhibit large reserves of strength when subjected to elevated temperatures, beyond the level of strength predicted by yield line analysis. This is partly due to the fact that slabs must meet strict deflection limits at ambient temperatures, in addition to the ultimate limit states. As temperatures increase, the primary load carrying mechanisms change from bending/shear action to tensile membrane action (Figure 2.15). Tensile membrane action occurs in slabs which are subject to large deflections. In reinforced concrete slabs, the tensile forces are carried primarily by the steel reinforcement. The following section presents three different analytical methods for the analysis of heated slabs. Each method is broadly similar in terms of accuracy and each carries approximately the same level of model uncertainty. No attempt has been made to quantify the model uncertainty associated with each approach and this uncertainty is not considered further in this work.

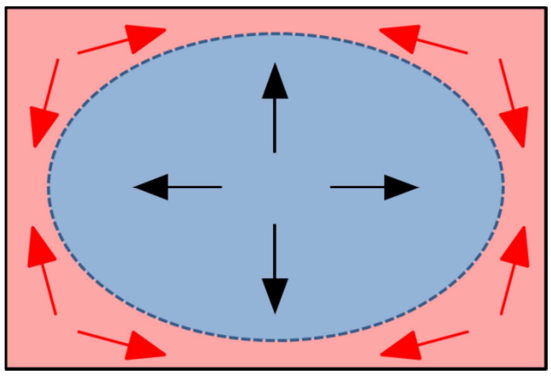

Figure 2.15: Plan view of slab showing the central tensile region, surrounded by a compressive ring.

The tests at Cardington confirmed the beneficial effects of tensile membrane action and led to the development of a variety of new methods for the analysis of reinforced concrete slabs subjected to elevated temperatures. Bailey developed a method based on a modified yield line method for the plastic analysis of slabs at ambient temperatures [4], [76], [77]. Bailey's method is applicable to two-way spanning, rectilinear, reinforced concrete slabs with vertical supports along the edges. The yield line method requires the identification of all probable crack patterns that may form when the slab is heavily

loaded. Each section of the slab (as defined by the crack pattern) is treated as a rigid segment. The energy necessary for the slab segments to rotate around these cracks is compared to the energy necessary for the load to move a given distance to determine the load capacity of the slab [78]. But yield line cracks do not necessarily form in thin, heated slabs and therefore the rotation of the slab cannot be measured. The Bailey method is capable of producing reliable results but is based on a number of assumptions.

- The slab segments are treated as rigid, planar sections and the effects of thermal curvature on the shape of the section are ignored.
- The edges of the slab are assumed to be simply supported. This is based on the assumption that the rebar which crosses the boundary of the slab will rupture due to the large hogging moments. Although rupture of rebars was observed at the Cardington tests, but it is not known at what point it occurred during the tests, specifically whether it was during the heating or the cooling phase, furthermore it was found to be concentrated around columns, which suggests the latter.
- Failure of the slab is taken as the formation of a full depth crack across the width at the midspan (Figure 2.16), however this assumption is really only valid for simply supported slabs and therefore this sort of failure was not observed in any of the Cardington tests, where the slab boundaries were generally restrained from lateral translation.

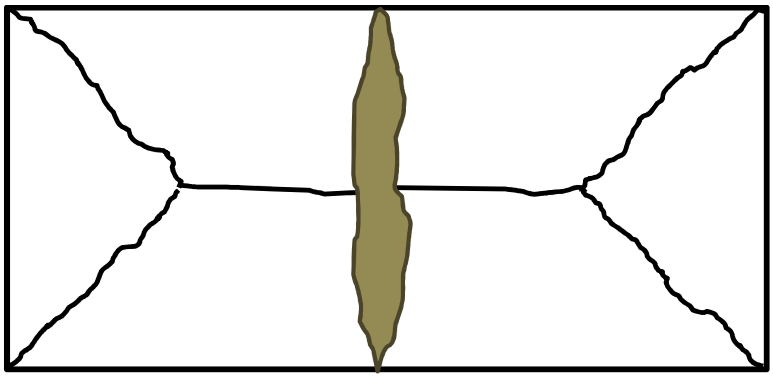

Figure 2.16: Failure mode considered by the Bailey method [4].

The first step of the Bailey method is to calculate the maximum deflection of the slab based on Equation (2.28) [79]. The first term of Equation (2.28) accounts for the thermal

deflection and the second term accounts for the mechanical deflection, assuming the slab has a parabolic deflected shape. It conservatively assumes that the rebar will fail at half of the average yield strain in order to avoid the complex calculation of localised stresses near crack locations.

$$v = \frac{\alpha(T_2 - T_1)l^2}{19.2h} + \sqrt{\left(\frac{0.5f_y}{E}\right)_{Reinf't_{20°C}} \frac{3L^2}{8}} \tag{2.28}$$

but

$$v < \frac{\alpha(T_2 - T_1)l^2}{19.2h} + \frac{l}{30} \tag{2.29}$$

where v is the deflection, T_1 is the temperature of the top of the slab, T_2 is the temperature of the underside of the slab, l is the width of the slab, h is the depth of the slab, f_y is the yield stress of the reinforcement, E is the Young's modulus of the reinforcement and L is the length of the slab. The capacity of the slab is then determined using yield line analysis before applying an enhancement factor to account for the increased capacity due to tensile membrane action.

A yield line approach was similarly adopted by Omer, Izzuddin, Elghazouli as the basis of their method for the analysis of lightly reinforced concrete slabs in fire [7], [80]. This method is based on earlier work by Izzuddin on the failure of lightly reinforced concrete beams in fire [70]. The failure criterion employed by the model is based on the strain concentrations at the yield line cracks. The crack width which the reinforcement must span is calculated at three locations; across the central span, along the x-direction across the diagonal span and along the y-direction across the diagonal span. In the simplified model, the crack width is calculated as the sum of three components; the crack width due to vertical deflection, the crack width due to thermal curvature and the contraction of the crack width due to thermal expansion. The force in the steel reinforcement is then calculated at the three locations considering the crack width, the yield stress of the rebar and the bond stress. Using the principal of virtual work, the external work is then compared to the internal work to derive the relationship between load and deflection, as given in Equation (2.30).

$$q = \frac{24U_c}{3 - 2\eta}\left(T_{sce}\frac{1 - 2\eta}{b^2} + T_{sy}\frac{\eta}{b^2} + T_{sx}\frac{1}{4\eta a^2}\right) \tag{2.30}$$

where q is the uniformly distributed load, U_c is the deflection, η is a factor defining the distance from the end of the slab to the central crack, T_{sce} is the force in the rebar across the central crack, b is the width of the slab, T_{sy} is the force in the y-direction across the diagonal crack, T_{sx} is the force in the x-direction across the diagonal crack and a is the length of the slab. By replacing T_{sce} in the above equation with the ultimate force of the reinforcement it is possible to calculate the failure deflection of the slab, Equation (2.31).

$$U_{cf} = \sqrt{\frac{\left(T_u - T_y\right)^2 b}{2A_s E_2 \sigma_b} + \frac{b^2}{2}\alpha_c \Delta T_r - \varepsilon_{sct}\frac{b^2}{4} - \frac{\kappa^2 b^4}{192}} \tag{2.31}$$

where U_{cf} is the deflection at failure, T_u is the ultimate force of the rebar, T_y is the yield force of the rebar, A_s is the cross sectional area of the rebar, E_2 is the modulus of hardening of steel (assuming a rigid hardening material model), σ_b is the bond strength, α_c is the coefficient of thermal expansion of concrete, ΔT_r is the temperature rise in the rebar, ε_{sct} is the strain due to the difference in thermal expansion between the steel rebar and the surrounding concrete. The Izzuddin method is a simple method for analysing lightly reinforced concrete slabs in fire, however it does have a number of disadvantages. It is reliant on the bond strength between the rebar and the concrete and on the strain-hardening modulus of the steel reinforcement. These properties are not commonly used in design and they are difficult to quantify. Yield line behaviour is assumed, which may not apply to a slab subject to an intense fire.

An analytical method for the analysis of heated slabs, based on elasticity theory, was developed by Usmani and Cameron [3], [81], [82]. This method is an extension of their method for the analysis of beams. The method allows for normal transverse loads to be applied to the slab to account for dead and imposed loads. The method involves several simplifying assumptions:

- the plate is laterally restrained against translation but free to rotate along all edges
- the plate has a rectilinear shape in plan
- the temperature is evenly distributed over the slab and varies only through the depth of the slab
- the development of localised strains is not accounted for
- failure of the slab is defined as rupture of the steel reinforcement

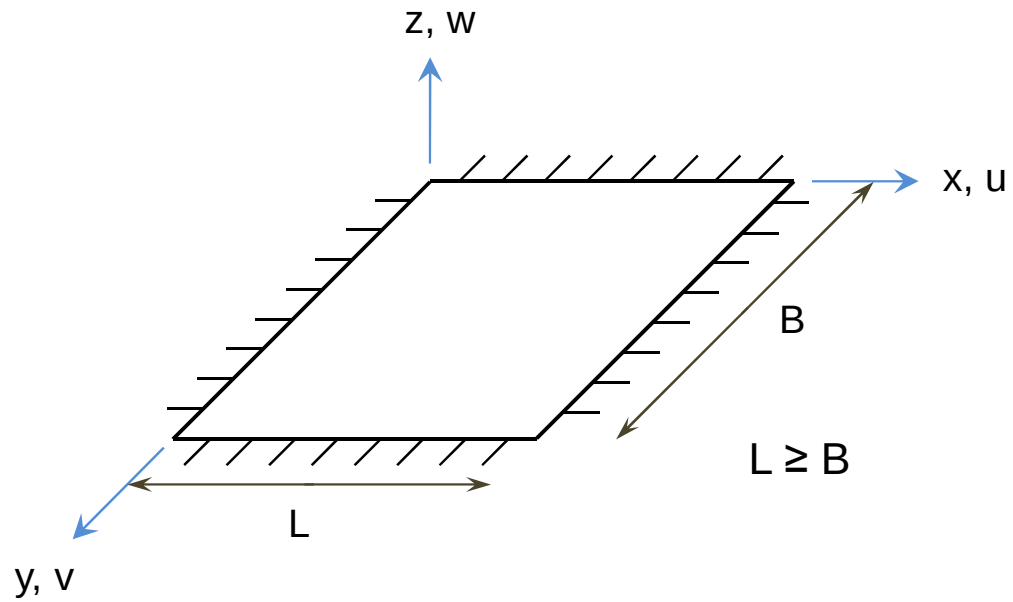

Figure 2.17: Slab geometry (adapted from Usmani and Cameron [3]).

Firstly the non-linear strain-displacement relations are expressed considering membrane strains, bending strains and thermal expansion strains. The equations for the stress components are found from classical plate theory. Integrating the equations for the stress components gives the stress resultants, N^T and M^T. In order to simplify the solution of the problem, the membrane stress resultants are described in terms of an Airy stress function *F(x,y)*. Differentiating the non-linear strain-displacement relations twice and summing the results yields the equation for compatibility for a plate. Using Hooke's law to describe the strains in terms of the stress resultants and substituting into the compatibility equation yields the membrane equilibrium equation including temperature effects:

$$D\left(\frac{\partial^4 w}{\partial x^4}+2\frac{\partial^4 4}{\partial x^2 y^2}+\frac{\partial^4 w}{\partial y^4}\right)-h\left(\frac{\partial^2 F}{\partial y^2}\frac{\partial^2 w}{\partial x^2}+\frac{\partial^2 F}{\partial x^2}\frac{\partial^2 w}{\partial y^2}-2\frac{\partial^2 F}{\partial x \partial y}\frac{\partial^2 w}{\partial x \partial y}\right) + \frac{1}{1-\upsilon}\left(\frac{\partial^2 M^T}{\partial x^2}+\frac{\partial^2 M^T}{\partial y^2}\right)=0 \tag{2.32}$$

where

$$D=\frac{Eh^3}{12(1-\upsilon^2)} \tag{2.33}$$

where D is the flexural stiffness of the plate, w is the vertical deflection of the plate, h is the depth of the plate, F is the Airy stress function, v is Poisson's ratio, M^T is the thermal moment and E is the Young's modulus. If the slab is assumed to be pinned along the edges and double Fourier series are used to represent the thermal deflection of the slab and the thermal moment, then the governing differential equation given above in Equation (2.32) can be solved to produce a cubic equation with respect to the thermal deflection, Equation (2.34).

$$\frac{3}{4}\left\{(3-\nu^2)\left(1+\frac{L^4}{B^4}\right)+4\nu\frac{L^2}{B^2}\right\}\left(\frac{w_T}{h}\right)^3 + \left\{\left(1+\frac{L^2}{B^2}\right)^2-12\frac{L^2(1+\nu)N^T}{\pi^2Eh^3}\left(1+\frac{L^2}{B^2}\right)\right\}\left(\frac{w_T}{h}\right) - 192\frac{L^2(1+\nu)M^T}{\pi^4Eh^4}\left(1+\frac{L^2}{B^2}\right)=0 \tag{2.34}$$

where N^T and M^T are given by Equations (2.22 a) and (2.22 b).

The cubic equation given above is solved in order to calculate the thermal deflection. The virtual work principle is then used to calculate the total deflection of the slab due to both the mechanical and thermal loads. Starting with the thermal deflection, the deflection is increased incrementally until the calculated load is equal to the applied uniformly distributed load. The internal work done is defined as the integral of the area under the stress-strain curve multiplied by the volume of each steel element, as in the beam solution:

$$\Pi_{int} = \sum_{n=1}^{no.\ rebars}\left[V_n\int_{\varepsilon_{wT}}^{\varepsilon_{wn}}\sigma(\varepsilon)d\varepsilon\right] \tag{2.35}$$

where Π_{int} is the internal work, V_n is the volume of the rebar, ε_{wn} is the mechanical strain in the rebar at a deflection of w_n, ε_{wT} is the mechanical strain in the rebar at a deflection of w_T and $\sigma(\varepsilon)$ is the stress-strain curve of the rebar.

The external work is calculated from the displacement of the mechanical loads due to the increase in deflection. It may be defined as:

$$\Pi_{ext} = \left(q_{n-1}+\frac{\Delta q}{2}\right)\Delta w\frac{4LB}{\pi^2} \tag{2.36}$$

where Π_{ext} is the external work done, q is the uniformly distributed load, w is the deflection, L is the length of the slab and B is the width of the slab.

The load increment p is then found from:

$$p = 2\frac{\Delta\Pi_{int}\pi^2}{\Delta w 4LB} - 2q_{n-1} \quad (2.37)$$

Analysis of multi-storey stability

Steel columns are highly susceptible to collapse due to fire loads and can lead to the collapse of a significant proportion of a building. Column failure may occur directly due to weakening of the column material and horizontal deformations resulting in P-δ type destabilising forces. Indirect effects such as lateral "push" or "pull" forces due to the thermal bowing and membrane action in floors may also lead to failure [83]–[85]. For these reasons fire protection is typically applied to all steel columns [86]. The behaviour of steel columns subject to fire within a single storey has been widely investigated [87]–[91]. In addition to these studies, there has also been research into the probabilistic performance of columns in fire. Zhang et al. studied the reduction in reliability of steel columns spanning a single storey over their design life due to aging of the intumescent fire protection [92]. Nigro et al. applied the probabilistic approach to the assessment of multi-storey steel framed car parks, however they did not consider the occurrence of multiple floor fires [93]. There are many available methods for determining the failure limit of single storey steel columns in fire, either analytically or numerically [44], [90], [94]. Bailey reviewed the Cardington fire tests to examine the effect of a fire in one fire compartment on a continuous column in a multi-storey frame [95]. Bailey showed that the instability may occur in a continuous column, mainly due to the expansion of connecting beams causing a P-δ effect in the column.

The fire induced loads on a column may be magnified if the fire spreads vertically to affect a column over multiple floors. This load case has not been traditionally considered by designers as it is assumed that compartmentation will prevent fire from spreading. This assumption is routinely used despite the well-known occurrence of multi-storey fires such as the Windsor Tower in Madrid, the Interstate Bank building in Los Angeles, the TVCC building in Beijing, the World Trade Centre towers in New York, etc. [96]–

[98]. Multi-storey stability under vertically spreading fires has been examined by researchers at the University of Edinburgh over the past number of years [83]–[85], [99]–[101]. This work was initiated after the collapse of the World Trade Center towers highlighted the need to consider the effects of multiple floor fires on a structure [102]. It has been shown by Usmani et al. that vertical instability in a structure occurs due to two different mechanisms: the weak floor collapse mechanism and the strong floor collapse mechanism (Figure 2.18) [84]. These mechanisms are based on a global analysis of the structure and they do not account for local effects such as connection failure or shear stud failure. Due to a lack of experimental data on the behaviour of full scale steel frame structures subject to multiple floor fires it is difficult to quantify the uncertainty associated with models which attempt to capture the behaviour of these structures. The model uncertainty associated with these models is not considered further in this work.

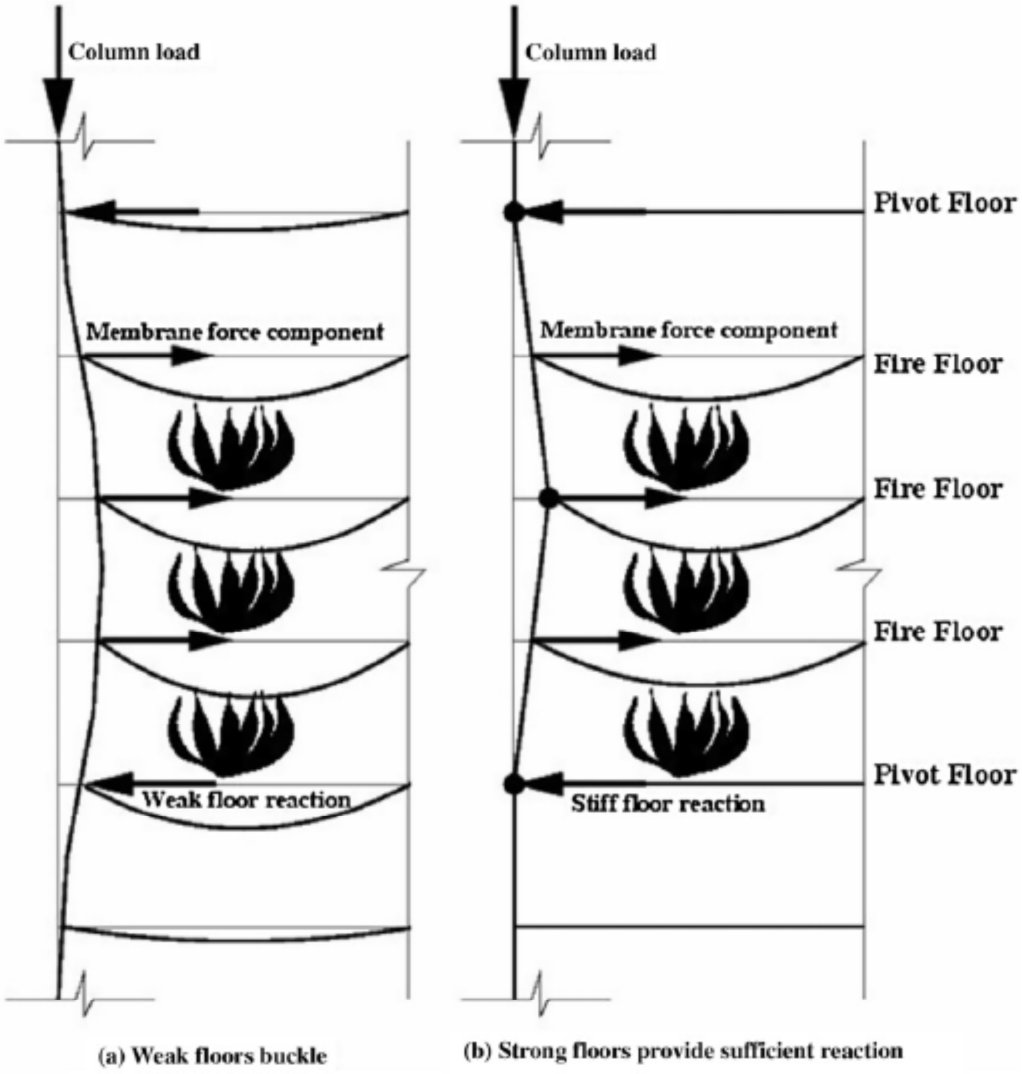

Figure 2.18: Possible collapse mechanisms for tall buildings under multiple floor fires [85].

Weak floor collapse occurs due to failure of the unheated floor beam below the fire affected floors. As the fire spreads vertically and attacks a number of consecutive floor beams, these beams weaken and begin to carry the load through catenary action. These loads act in unison to pull the column inwards and create a large compressive axial force in the unheated floor below the lowermost fire floor. The beam under axial compression and also subjected to P-δ moments may then fail either by yielding or buckling, but in typical structures flexural failure occurs rather than buckling. This kind of failure however occurs when the flexural capacity of the floor is low, and was found to be unlikely for most real floor systems [84]. Following the initial failure of the first

unheated floor, the inward force from the fire affected floors is transferred downwards to the next beam, and so on, leading to the progressive collapse of the whole building. Alternatively, if the beam below the fire floors is sufficiently strong to withstand the axial compression then failure may occur through the strong floor collapse mechanism. Strong floor collapse occurs when the horizontal forces from the fire affected floors create plastic hinges in the column. For example, if there are fires on three floors (as in Figure 2.18) then there will be three inward acting forces counteracted by two outward acting forces either side of the fire floors. The floors above and below the fire floors are termed “pivot floors” as it is where the column is subjected to large bending moments because of the “pull-in” forces imposed by the sagging fire floors. Eventually, the first plastic hinge forms at the lowest pivot floor under a combination of the axial load in the column and the bending moments from the fire floors and two further plastic hinges follow in quick succession in the middle and then the upper most pivot floor leading to a plastic collapse mechanism.

The first step of analysing the effects of a multiple floor fire is to establish a model for vertical fire spread and fire development within each horizontal compartment. Vertical fire spread may occur due to a number of factors:

- External spread at the façade due to:
    - window breakage
    - lack of an effective fire barrier between the floor slab and the wall cladding
    - combustion of the insulation core within the wall cladding panels
- Internal spread due to:
    - the presence of ducts and openings for mechanical and electrical services
    - large openings in the floor plate for atria or balconies
    - compartment failure due to the formation of cracks
    - compartment failure due to thermal conduction through the compartment boundaries

Vertical fire spread is an inherently non-deterministic phenomenon due to the uncertainties involved in the ignition and development of a fire within a compartment and the many different avenues of possible fire spread. Despite the difficulties involved

in determining fire spread, it is necessary to estimate the probability of fire spread, the limit of vertical fire spread and the rate of vertical fire spread.

The probability of fire spread may be calculated using fault tree analysis, where fire spread by each separate route is given a probability of occurrence. The total probability of fire spread is then given by the sum of the probabilities of each separate route of fire spread. The difficulty in this method lies in defining the probability of fire spread by each route. There is insufficient data to define the likelihood of spread either from experimental tests or from historical occurrences and so the probabilities must be estimated based on expert judgement. An alternative to using fault tree analysis is to calculate the probability of fire spread from historical fire statistics. Unfortunately these statistics are not widely available. Statistics from the Home Office for 1988 give the number of fires by occupancy type and a description of the extent of fire spread [103]. The statistics show the number of fires confined to the initial area, the number of fires that spread beyond the initial area but remained confined to the initial floor, fires that spread beyond both the initial area and initial floor and fires that spread beyond the building. The upper bound for the occurrence of vertical fire spread is given as the sum of the probability of fire spread beyond the fire floor but confined to the building and the probability of fire spread beyond the building, shown in Table 2.6. Note that the data given in Table 2.6 are expressed as percentages and are a subset of the data given in the Home Office report, rounded to a single decimal place. Due to this fact, the collated numbers may not agree exactly with the given data. The first column in Table 2.6 below, labelled Total, refers to the probability of fire spread across all of the occupancy types.

Table 2.6: Probability of fire spread, derived from Home Office statistics (expressed as percentages) [103].

	Total	Dwellings	Industrial	Shops	Hotels	Education	Other
Beyond initial area	9.0	7.6	9.1	13.5	6.8	14.2	10.9
Confined to initial floor	3.7	3.5	3.6	5.0	2.0	7.1	3.8
Beyond initial floor, but confined to building	4.0	4.0	4.4	7.2	4.7	5.9	3.9
Beyond building	1.3	0.2	1.2	1.2	0.1	1.2	3.3
Upper bound for vertical spread	5.3	4.1	5.6	8.4	4.8	7.1	7.2

The Department for Communities and Local Government publishes more recent, albeit limited statistics and they give the average probability of a fire spreading beyond the room of ignition in non-dwelling type buildings (as recorded in 2010-2012) as 26% [104]. This measure includes cases of both vertical and/or horizontal spread.

There are no statistical records of the extent of vertical fire spread and therefore the limits must be estimated based on expert judgement. While the total number of floors damaged by fire is an important parameter in estimating the damage costs, it is not always necessary in order to calculate the critical load case for the structure.

The rate of fire spread is especially important as it enables the calculation of the number of concurrent floor fires at any given time following ignition. If the rate of fire spread is low, then the number of floors on fire at any given point in time will also be low. The instance where the greatest number of floors are exposed to fire is the critical load case and may be referred to as the critical time, t_{crit} [84].

Once critical load case is established, the temperature-time curves for the structure are calculated (Figure 2.19). The temperature-time curves shown in Figure 2.19 below are

based on the Eurocode parametric temperature-time curve and use an assumed value to account for the time taken for fire spread between floors.

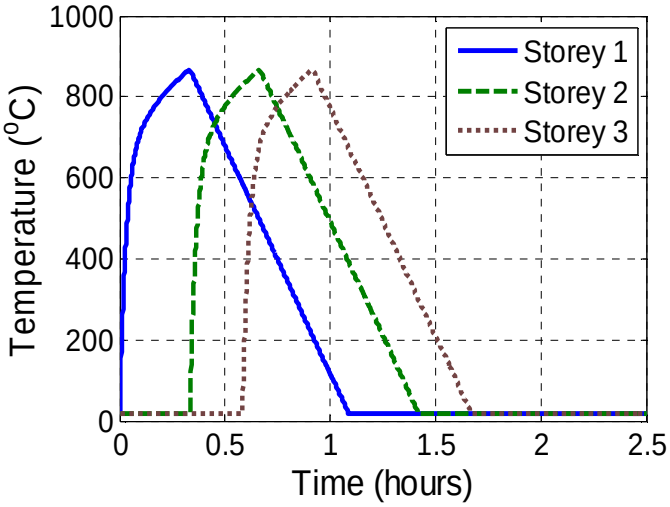

Figure 2.19: Temperature-time histories for fires on three separate floors.

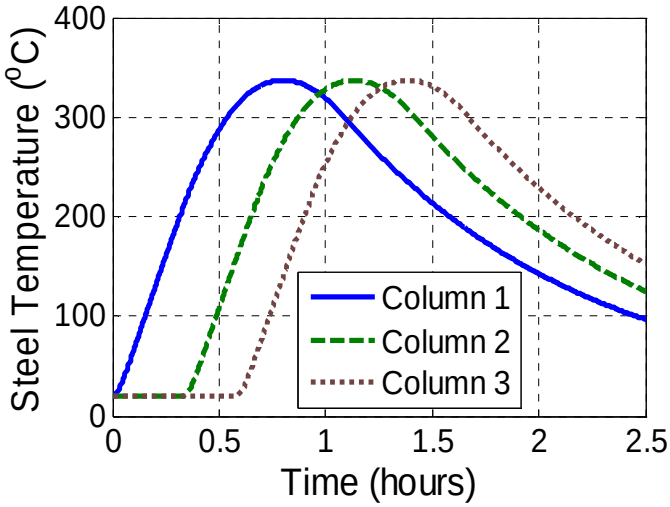

Figure 2.20: Temperature-time histories for the steel columns on three separate floors.

A series of heat transfer analyses are carried out on the column at each storey level, using the temperature data obtained from the fire models. This can be done using simple

lumped capacitance methods as described previously in section 2.3. Given the temperature histories of the columns (Figure 2.20), it is possible to determine the required temperature-dependent material properties for steel at each time step. Figure 2.21 shows a simplified structural model for examining the effects of the temperature and mechanical loads on the stability of the column. The model is composed of six floors at an indeterminate level within the structure of a tall building. The vertical load *V* represents the axial load in the column from the building above the modelled zone. The horizontal loads *H* represent the loads from the fire affected beams acting under catenary action.

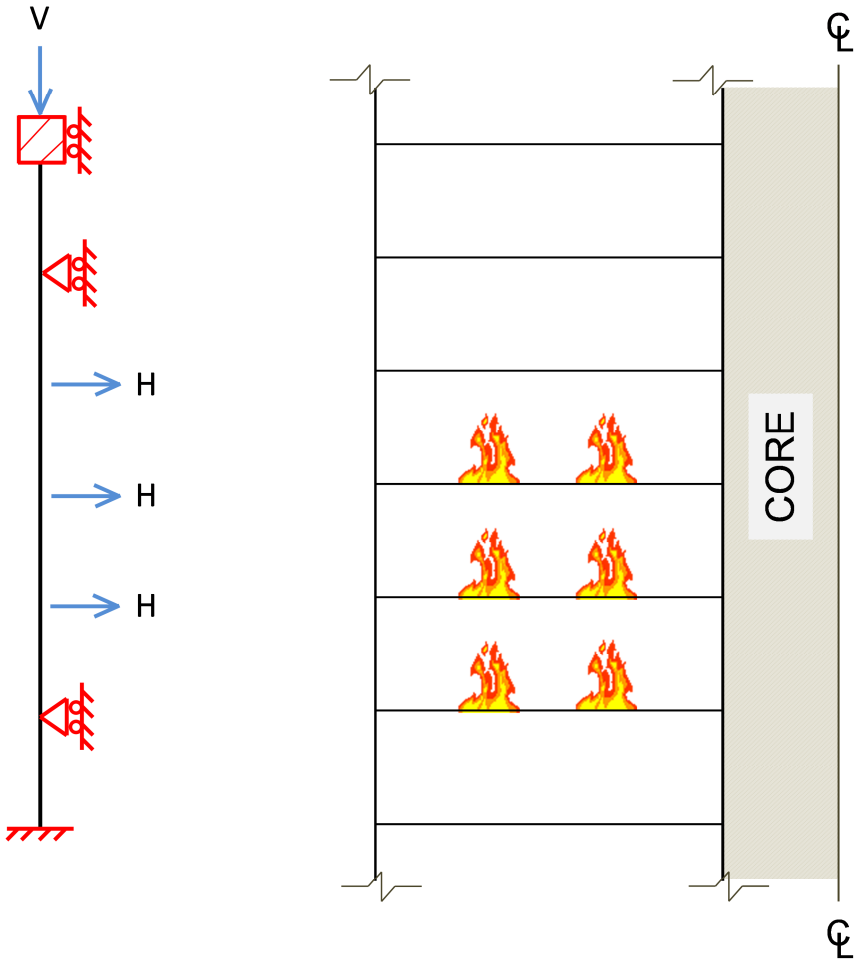

(a) (b)

Figure 2.21: (a) Structural model of a multi-storey column under vertical and horizontal loads, (b) Elevation sketch of a typical tall building under multiple floor fires.

The horizontal loads significantly lower the capacity of the column by imposing additional moments and inducing a progressively worsening *P-δ* effect. These 2nd order effects must be captured by the structural analysis model in order to accurately capture the response of the structure. In order to simplify the problem, the composite beam model based on "the method of slices" described in section 2.4.2 is used to calculate the "design pull-in force", *H*. The beam is modelled as simply supported, with an axial spring at the free end to account for the restraint provided by the column. Using this

model, the horizontal force from each slab can be found for each time step in the analysis.

The direct stiffness method offers a suitable approach to analysing multi-storey columns under multiple floor fires. The direct stiffness method is:

- computationally efficient
- accurate
- suitably adaptable to account for a varying number of fire floors
- able to account for the geometric nonlinearity of the structural response

The direct stiffness method is a matrix based structural analysis procedure. Comprehensive descriptions of matrix structural analysis have been presented by McGuire et al. and by Weaver and Gere [105], [106]. The following section presents the derivation of the equations required for the analysis of a multi-storey column using the direct stiffness method. These equations have been implemented in Matlab and are used in Chapters 5 and 6 of this thesis [107].

Following the direct stiffness method, the structure to be analysed is split into idealised elements (or members). A set of equations is formed for each member relating the displacements of each degree of freedom to the applied loads, based on the material and geometric properties of the member. These member matrices are then compiled into a system matrix equation which describes the behaviour of the entire structure. This system matrix equation is given as:

$$\{\boldsymbol{P}\} = [\boldsymbol{K_{tot}}]\{\boldsymbol{\Delta}\} + \{\boldsymbol{P^F}\} \tag{2.38}$$

where $\boldsymbol{P}$ is the vector of nodal force components, $\boldsymbol{K_{tot}}$ is the system stiffness matrix, $\boldsymbol{\Delta}$ is the vector of nodal displacements and $\boldsymbol{P^F}$ is the vector of fixed-end forces caused by loads applied between nodes. In order to build this system of equations it is necessary to first consider each element individually. The same governing equations are applied to an individual member as shown in Equation (2.39) below.

$$\begin{Bmatrix} F_{x1} \\ F_{y1} \\ M_{z1} \\ F_{x2} \\ F_{y2} \\ M_{z2} \end{Bmatrix} = [\boldsymbol{k}] \begin{Bmatrix} u_1 \\ v_1 \\ \theta_{z1} \\ u_2 \\ v_2 \\ \theta_{z2} \end{Bmatrix} \tag{2.39}$$

where $\boldsymbol{F}$ is the vector of joint force components, $\boldsymbol{k}$ is the element stiffness matrix and $\boldsymbol{\Delta}$ is the vector of nodal displacements. In a geometrically nonlinear analysis the element stiffness matrix $\boldsymbol{k}$ is composed of two components; an elastic element stiffness matrix $\boldsymbol{k_{el}}$ and a geometric element stiffness matrix $\boldsymbol{k_g}$. The degrees of freedom considered in a frame element are shown below in Figure 2.22.

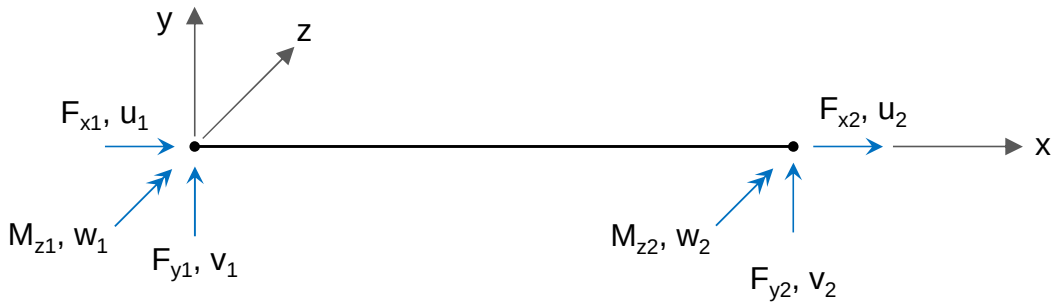

Figure 2.22: Frame element.

If a unit displacement is applied along one of the degrees of freedom and the other degrees of freedom are restrained then the resulting force is equal in value to the elastic stiffness coefficient. The elastic stiffness matrix of a frame element, shown in Equation (2.40), is composed of the elastic stiffness coefficient for each degree of freedom.

$$[\boldsymbol{k_{el}}] = \begin{bmatrix} \frac{EA}{L} & 0 & 0 & \frac{-EA}{L} & 0 & 0 \\ & \frac{12EI}{L^3} & \frac{6EI}{L^2} & 0 & -\frac{12EI}{L^3} & \frac{6EI}{L^2} \\ & & \frac{4EI}{L} & 0 & -\frac{6EI}{L^2} & \frac{2EI}{L} \\ & & & \frac{EA}{L} & 0 & 0 \\ & Sym. & & & \frac{12EI}{L^3} & -\frac{6EI}{L^2} \\ & & & & & \frac{4EI}{L} \end{bmatrix} \tag{2.40}$$

The geometric element stiffness matrix, shown below in Equation (2.41), accounts for the change in stiffness that occurs due to the displacement of an element.

$$[\boldsymbol{k_g}] = \begin{bmatrix} \frac{F_{x2}}{L} & 0 & 0 & \frac{-F_{x2}}{L} & 0 & 0 \\ & \frac{6F_{x2}}{5L} & \frac{F_{x2}}{10} & 0 & -\frac{6F_{x2}}{5L} & \frac{F_{x2}}{10} \\ & & \frac{2F_{x2}L}{15} & 0 & -\frac{F_{x2}}{10} & -\frac{F_{x2}L}{30} \\ & & & 1 & 0 & 0 \\ & Sym. & & & \frac{6F_{x2}}{5L} & -\frac{F_{x2}}{10} \\ & & & & & \frac{2F_{x2}L}{15} \end{bmatrix} \tag{2.41}$$

Element stiffness matrices are derived in a local coordinate system, with the x-axis aligned to the length of the element. Before these matrices can be combined they are first expressed in a global coordinate system using a transformation matrix.

$$[\boldsymbol{T}] = \begin{bmatrix} cos(\theta) & sin(\theta) & 0 & 0 & 0 & 0 \\ -sin(\theta) & cos(\theta) & 0 & 0 & 0 & 0 \\ 0 & 0 & 1 & 0 & 0 & 0 \\ 0 & 0 & 0 & cos(\theta) & sin(\theta) & 0 \\ 0 & 0 & 0 & -sin(\theta) & cos(\theta) & 0 \\ 0 & 0 & 0 & 0 & 0 & 1 \end{bmatrix} \quad (2.42)$$

The global element stiffness matrices are calculated according to Equation (2.43 a) and (2.43 b).

$$[\boldsymbol{k}_{el,global}] = [\boldsymbol{T}]'[\boldsymbol{k}_{el}][\boldsymbol{T}] \quad (2.43\ a)$$

$$[\boldsymbol{k}_{g,global}] = [\boldsymbol{T}]'[\boldsymbol{k}_{g}][\boldsymbol{T}] \quad (2.43\ b)$$

Once the stiffness matrices are expressed in global coordinates they are combined into the assembled elastic stiffness matrix and assembled geometric stiffness matrix. The assembled matrices are then summed to yield the assembled total stiffness matrix.

$$\boldsymbol{K_{tot}} = \boldsymbol{K_{el}} + \boldsymbol{K_g} \quad (2.44)$$

In order to simplify the solution to the matrix equation that defines the behaviour of the structure, shown in Equation (2.38) above, the matrices are re-arranged according to the support conditions. This yields Equation (2.45), shown below.

$$\begin{Bmatrix} \boldsymbol{P_f} \\ \boldsymbol{P_r} \end{Bmatrix} = \begin{bmatrix} \boldsymbol{K_{ff}} & \boldsymbol{K_{fr}} \\ \boldsymbol{K_{rf}} & \boldsymbol{K_{rr}} \end{bmatrix} \begin{Bmatrix} \boldsymbol{\Delta_f} \\ \boldsymbol{\Delta_r} \end{Bmatrix} + \begin{Bmatrix} \boldsymbol{P_f^F} \\ \boldsymbol{P_r^F} \end{Bmatrix} \quad (2.45)$$

where the subscript *f* refers to a free degree of freedom and *r* refers to a restrained degree of freedom. The fixed end forces are caused both by forces applied to the member in between nodes and by forces arising from thermal expansion of the member. There are no applied forces in between the nodes considered in this case. Thermal moments are not considered as the heat transfer procedure assumes a uniform temperature across the depth of the column section. The fixed end force vector $\boldsymbol{P^F}$ for a single element is given as:

$$\{\boldsymbol{P^F}\} = \begin{Bmatrix} F_{T,x1} \\ F_{T,y1} \\ M_{T,z1} \\ F_{T,x2} \\ F_{T,y2} \\ M_{T,z2} \end{Bmatrix} + \begin{Bmatrix} F_{x1}^F \\ F_{y1}^F \\ F_{z1}^F \\ F_{x2}^F \\ F_{y2}^F \\ F_{z2}^F \end{Bmatrix} \tag{2.46}$$

where:

$$F_{T,x1} = -F_{T,x2} = E_s A \alpha_s (\theta_s - \theta_{ambient}) \tag{2.47}$$

$$F_{T,y} = 0 \tag{2.48}$$

$$M_{T,z} = 0 \tag{2.49}$$

$$F^F = 0 \tag{2.50}$$

where F_T is the thermal force in an element, M_T is the thermal moment in an element, F^F is the force due to loads applied to the element, E_s is the Young's modulus of steel, A is the area of the element, α_s is the coefficient of thermal expansion of steel, θ_s is the temperature of the column and $\theta_{ambient}$ is the ambient temperature.

The simplest solution to the above system of equations in Equation (2.45) is a first-order solution. Equation (2.45) may be simplified, given that $\boldsymbol{\Delta_r}$ is equal to 0.

$$\{\boldsymbol{P_f}\} = [\boldsymbol{K_{ff}}]\{\boldsymbol{\Delta_f}\} + \{\boldsymbol{P_f^F}\} \tag{2.51 a}$$

$$\{\boldsymbol{P_r}\} = [\boldsymbol{K_{rf}}]\{\boldsymbol{\Delta_f}\} + \{\boldsymbol{P_r^F}\} \tag{2.51 b}$$

The free displacements of the nodes can then be found from:

$$\{\boldsymbol{\Delta_f}\} = [\boldsymbol{K_{ff}}]^{-1}(\{\boldsymbol{P_f}\} - \{\boldsymbol{P_f^F}\}) \tag{2.52}$$

The reactions at the restrained degrees of freedom can be found by substituting the calculated displacements from Equation (2.52) into Equation (2.51 b) above.

A second-order elastic analysis requires an incremental solution. The basic approach is known as the Euler method, where the loads are applied incrementally, as defined in Equation (2.53).

$$\{dP\} = [K_{tot}]\{\mathbf{d\Delta}\} + \{dP^F\} \tag{2.53}$$

The global elastic member stiffness matrices must be re-evaluated with each iteration due to the changing orientation and the global geometric member stiffness matrices must be re-evaluated due to the changing force and orientation. The system of equations is then solved as before. This procedure is followed until the full load is applied to the structure.

Once the reaction forces and displacements at each node are determined, the axial force and bending moment acting at any point of the structure may be calculated. The combined axial and bending loads are checked against the Eurocode limits for failure of a section, as illustrated in Figure 2.23. If the section is plastic or compact (class 1 or 2 respectively), then the Eurocode allows for the effect of low axial force to be ignored. The effects of the axial force cannot be ignored in semi-compact or slender sections and the Eurocode states that the applied stress due to bending and axial forces must be less than the design yield stress [48]. If the section fails the check then the structure is deemed to have failed by a strong floor collapse. If the section passes then a weak floor check is carried out.

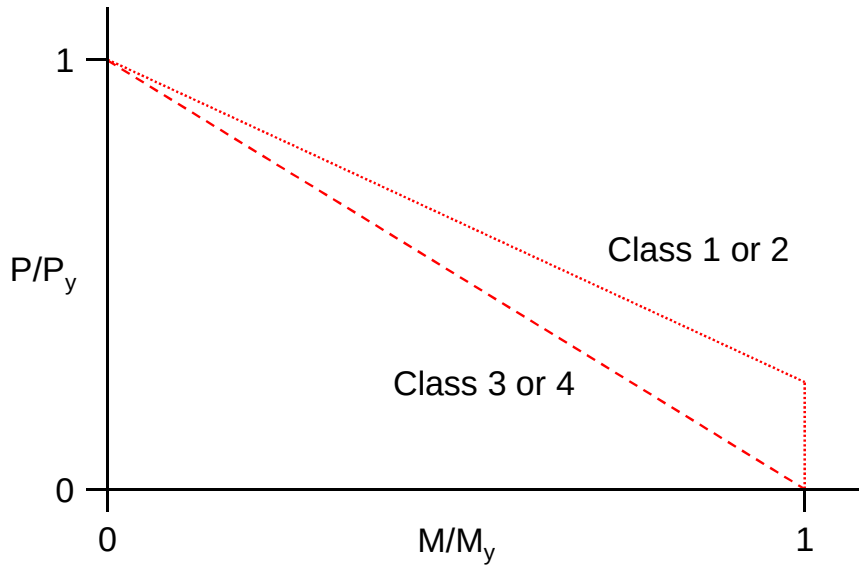

Figure 2.23: Eurocode failure envelopes for steel sections under combined bending and axial force.

The weak floor check is carried out on the composite beam supporting the lowest fire floor. Due to the insulating nature of concrete slabs and the buoyancy of hot gases it is assumed that the composite beam is unaffected by the fire. The composite beam is subject to large compressive axial forces from the column and transverse loading from the dead and imposed load on the floor, as shown in Figure 2.24. The axial force creates a *P*-δ effect which requires a second order analysis.

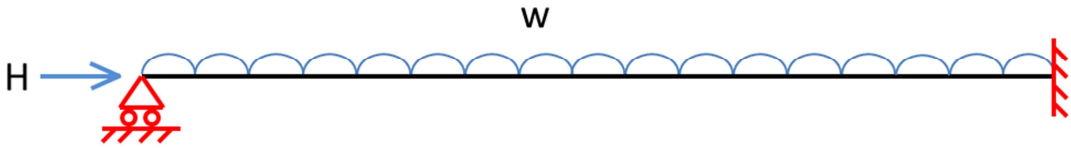

Figure 2.24: Structural model of a composite beam.

A geometrically nonlinear analysis is carried out using the direct stiffness method to determine the distribution of bending moments along the beam. The material properties of the concrete slab vary through the depth of the slab due to the variation in temperature. Therefore, the composite beam is split into horizontal slices and the area of each slice is modified based on a modular ratio so that the beam may be treated as a beam of homogenous material. For the direct stiffness analysis the length of the beam is divided into 5 elements and the load is incremented over 10 steps. These values were chosen as a compromise between accuracy and computational speed.

The moment capacity of the composite beam is calculated in accordance with the Eurocode guidance for ambient temperature design [108], [109]. The weak floor check is then carried out by checking that the stress due to the maximum applied bending and axial forces does not exceed the design yield stress.

2.5 Summary

An overview has been given of the three stages involved in a structural fire engineering analysis; fire modelling, heat transfer analysis and structural analysis. The behaviour of fires in compartments was outlined. The importance of fuel load and ventilation in the development of a fire was highlighted and stochastic definitions were presented for these two variables. A variety of fire models were presented including the standard EC temperature-time curve, the parametric EC temperature-time curve, the JCSS temperature-time curve and a travelling fire model for large compartments. A range of methods were presented for conducting heat transfer analysis. A method of calculating the net heat flux, based on the sum of the radiative and convective heat fluxes, acting on the structure was described. A lumped capacitance method for conducting heat transfer in thermally thin members, such as steel sections, was presented. A one-dimensional finite difference approximation for conducting heat transfer through thermally thick members, such as concrete slabs, was described.

Suitable temperature dependent material properties are listed for concrete, structural steel and reinforcing steel. Stochastic definitions are provided for the important material properties. A range of structural analysis models have been examined; including analytical composite beam models, finite element based composite beam models and analytical slab models. A direct stiffness based model was developed for the analysis of the stability of a tall building subject to multiple floor fires. Structural failure due to the occurrence of weak floor collapse or strong floor collapse is examined.

Chapter 3: Performance-Based Engineering

3.1 Preamble

This chapter outlines the development and application of performance-based engineering. Historically building codes have set out a list of requirements that must be met during the design and construction of a building. These requirements dictate the types of materials that may be used, how the building may be constructed, how large the building may be and the form of egress routes from the building. These types of building codes are known as prescriptive codes due to the nature of the prescriptive specifications they contain. Prescriptive codes are frequently based on empirical rules that have developed over many years or have been adopted to counter a specific risk following a large disaster.

The main advantages of prescriptive codes are that they are simple for designers to apply and easy for the regulatory authorities to check. In comparison with prescriptive regulations, performance-based regulations introduce an additional level of complexity into the design process. The advantages and disadvantages of both systems are considered in this chapter. Performance-based engineering is based on the idea of designing to a set of identified performance objectives using engineering methods that are based on scientific principles. This method allows the designer flexibility in the choice of solutions to meet the performance objectives. Suitable performance objectives for performance-based design are considered in this chapter. The importance of defining the risks to the structure and calculating the reliability of the structure under loads for performance-based design is discussed. The application of performance-based design to structural fire engineering is also discussed in this chapter.

3.2 Overview of Performance-Based Engineering

3.2.1 Definition of performance-based engineering

Performance-based engineering (also referred to as performance-based design) was succinctly defined by Gibson [110] as:

"The performance approach is the practice of thinking and working in terms of ends rather than means. It is concerned with what a building or a building product is required to do and not with prescribing how it is to be constructed."

Performance-based engineering requires the establishment of structure-specific performance goals. These goals typically relate to the safety of the occupants, the serviceability of the structure and the level of protection required for the contents. Once these goals have been identified the designer may then choose any method to meet them. This is in contrast with the prescriptive approach which provides a list of specific obligations which must be abided by to ensure compliance with the building code. The prescriptive approach does not allow for consideration of any mitigating factors which may be present in a design and is frequently seen to be overly conservative [111]. In practice prescriptive design restricts the range of design options available to the design team and can lead to redundancy in the design. This in turn leads to uneconomical designs. Another drawback of the prescriptive approach is that it may not provide the required levels of safety if it is applied to unusual or innovative structures. A major advantage of the performance-based approach is the flexibility afforded in the design of the structure and the use of new or innovative materials or products. The performance-based approach can lead to large cost savings by increasing the efficiency of the structure.

Despite the obvious advantages of performance-based design, the prescriptive approach is still frequently used in practice. This may be attributed to several factors. The prescriptive approach is simple and straightforward to apply. The performance-based approach may not offer any benefits over the prescriptive approach for simpler, traditional types of building. The performance-based approach has a higher initial cost and involves a more in-depth design process. Problems may arise in defining performance goals acceptable to all stakeholders. Difficulty may also be presented by the possible overlaps in responsibility between various parties involved in the design team.

3.2.2 History and origins of performance-based engineering

Traditionally, building codes and standards have been written in a prescriptive format. Prescriptive standards specify rules that must be followed in order to guarantee a safe building. Prescriptive standards are still widely used as they provide a simple approach to design, are quick to apply and have been proven over time to be safe. Performance-based engineering on the other hand specifies performance criteria that must be met by the structure. This allows the design team to explore many more design options that can meet these criteria than possible under prescriptive regulations.

Modern performance-based code frameworks first appeared in the 1960's and 1970's. These early performance-based frameworks were concerned with designing for rare, extreme load cases such as earthquakes or fire [112]–[114]. The advantages of performance-based design over prescriptive design were outlined by the Conseil International de Batiment (CIB) in 1982 and performance-based design has continued to spread since then [110]. The field of earthquake engineering has been at the forefront of the development of performance-based engineering methods since the 1960's when Cornell proposed a method for the probabilistic assessment of earthquake loads, now known as probabilistic seismic hazard analysis [115]. Cornell's methods were incorporated into the model code, ATC-3-06 [112]. ATC-3-06 proposed that structures be designed to resist a single design earthquake with a return period of 475 years. It also introduced the use of inter-storey drift as a performance metric, where the design could be categorised based on the estimated level of drift that would result from the design earthquake occurring. The next advancement in earthquake engineering came from considering a set of performance levels, instead of a single performance level, as shown in Table 3.1 [116].

Table 3.1: Performance limit states as defined in the Vision 2000 report.

Fully Operational	Continuous service. Negligible structural and non-structural damage.
Operational	Most operations and functions can resume immediately. Structure safe for occupancy. Essential operations protected, non-essential operations disrupted. Repair required to restore some non-essential services. Minor damage.
Life Safe	Moderate damage, but the structure remains stable. Selected, important building systems, fittings or contents protected from damage. Life safety is generally assured. The building may need to be evacuated following earthquake. Repair possible, but not necessarily economically practical.
Near Collapse	Severe damage, but structural collapse is prevented. Repair generally not possible.

With the publication of the Vision 2000 report, it was recognised that structures were subject to a range of earthquake motions and that society is willing to accept more frequent occurrence of minor damage compared to major damage. The Vision 2000 report outlined a performance matrix based on a set of four design earthquakes and the four performance levels, Figure 3.1. This matrix defines the required performance of a building across a range of earthquakes, based on the importance of the building's function.

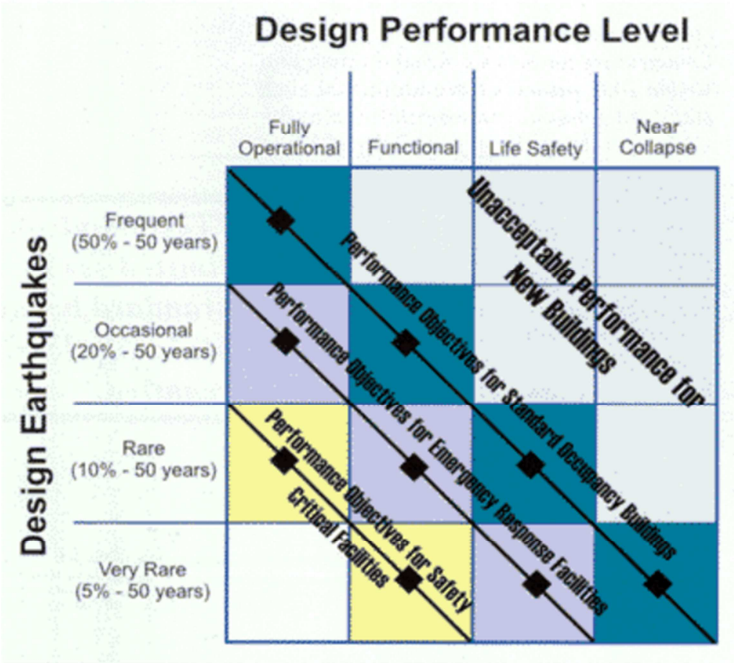

Figure 3.1: Vision 2000 performance objectives [117].

This methodology is still widely used today in earthquake engineering and similar approaches have been implemented by various design code bodies; the Los Angeles Tall Building Structural Design Council, the Structural Engineering Association of Northern California, the Pacific Earthquake Engineering Research Center and the Council of Tall Building and Urban Habitat [118]–[121]. A comprehensive evaluation and comparison of the requirements of these four guidelines is given by Gerges, Benuska and Kumabe [122]. Similar approaches have also been used in the areas of fire engineering and blast engineering [123].

The next advancement in performance-based earthquake engineering came from the Pacific Earthquake Engineering Research (PEER) center [124], [125]. They proposed a new framework to account for the effects of a range of possible earthquakes, instead of the previously used set of design earthquakes. The PEER framework also introduced new performance metrics; repair costs, downtime due to repair and fatalities. The PEER framework and its application to other areas of engineering are discussed in detail in Chapter 5. The PEER framework has been widely documented and is the focus of much on-going research, but is not yet widely used in practice.

3.2.3 Risk and reliability in performance-based engineering

Risk is a highly subjective concept that is based on both the magnitude and frequency of occurrence of a hazard. To a structural engineer, the notion of risk related to a project is often associated with structural collapse, whereas a developer would see the same risk in terms of monetary loss. It is not only the nature of the risk that may be perceived differently by different people but also the magnitude of the risk, e.g. air travel is often seen as high risk despite it being a safer form of travel than travelling by car.

In structural design, risk may be controlled either by removing/reducing the magnitude of the hazard or by reducing the frequency of occurrence of the hazard (i.e. increasing the reliability of the design). For example, the Eurocodes define the reliability class of a structure based on the consequence class which is based on the expected loss of human life and the economic, social and environmental consequences, Table 3.2 [126].

Table 3.2: Description of consequence classes from Eurocode 1990.

Consequences Class	Description	Examples of buildings and civil engineering works
CC3	**High** consequence for loss of human life, *or* economic, social or environmental consequences **very great**	Grandstands, public buildings where consequences of failure are high (e.g. a concert hall)
CC2	**Medium** consequence for loss of human life, economic, social or environmental consequences **considerable**	Residential and office buildings, public buildings where consequences of failure are medium (e.g. an office building)
CC1	**Low** consequence for loss of human life, *and* economic, social or environmental consequences **small or negligible**	Agricultural buildings where people do not normally enter (e.g. storage buildings), greenhouses

Performance-based engineering allows considerable freedom in selecting the form of the structure and the intensity of the design load cases and because of this it is important that the level of risk in the final design is evaluated. A risk analysis must consider three points [127]:

1. What can happen?
2. What is the likelihood of it occurring?
3. What are the consequences of it occurring?

Provided these questions are addressed, the risk may be evaluated either qualitatively or quantitatively. Qualitative risk analysis typically consists of identifying all possible risks and classifying them within a risk matrix based on the expected impact and frequency.

The scale for measuring impact and frequency can differ depending on the risk or the industry. A well-recognised, four level scale is given in the SFPE (Society of Fire Protection Engineers) Handbook of Fire Protection Engineering, shown in Table 3.3 and Table 3.4.

Table 3.3: Possible consequence ranking criteria [26].

Consequence Level	Impact on Populace	Impact on Property/Operations
High (*H*)	Immediate fatalities, acute injuries—immediately life threatening or permanently disabling	Damage > $XX million—building destroyed & surrounding property damaged
Moderate (*M*)	Serious injuries, permanent disabilities, hospitalization required	$YY < damage < $XX million—major equipment destroyed, minor impact on surroundings
Low (*L*)	Minor injuries, no permanent disabilities, no hospitalization	Damage < $YY—reparable damage to building, significant operational downtime, no impact on surroundings
Negligible (*N*)	Negligible injuries	Minor repairs to building required, minimal operational downtime

Table 3.4: Example frequency criteria used for probability ranking [26].

Acronym	Description	Frequency Level (median time to event)	Description
A	Anticipated, expected	$> 10^{-2}$/yr (<100 years)	Common incidents that may occur several times during the lifetime of the building.
U	Unlikely	$10^{-4} < f < 10^{-2}$/yr (100 to 10,000 years)	Events that are not anticipated to occur during the lifetime of the facility. Natural phenomena of this probability class include: UBC-level earthquake, 100-year flood, maximum wind gust, etc.
EU	Extremely unlikely	$10^{-6} < f < 10^{-4}$/yr (10,000 to 1 million years)	Events that will probably not occur during the life cycle of the building
BEU	Beyond extremely unlikely	$< 10^{-6}$/yr (> 1 million years)	All other accidents

These scales are combined to form the risk matrix shown in Figure 3.2. The advantages of qualitative risk analysis are that it is a flexible, easily applicable method. Qualitative risk analysis may be conducted by anyone who is familiar with the nature of the anticipated hazards and does not require any specialist knowledge of mathematics or probabilistic analysis. Qualitative risk analysis is also very easy to interpret as the greater risks are easily identified from their position in the risk matrix. A disadvantage of qualitative risk analysis is that the same risk may be classed differently by different people, as the classification depends on the experience and judgement of the person undertaking the risk assessment.

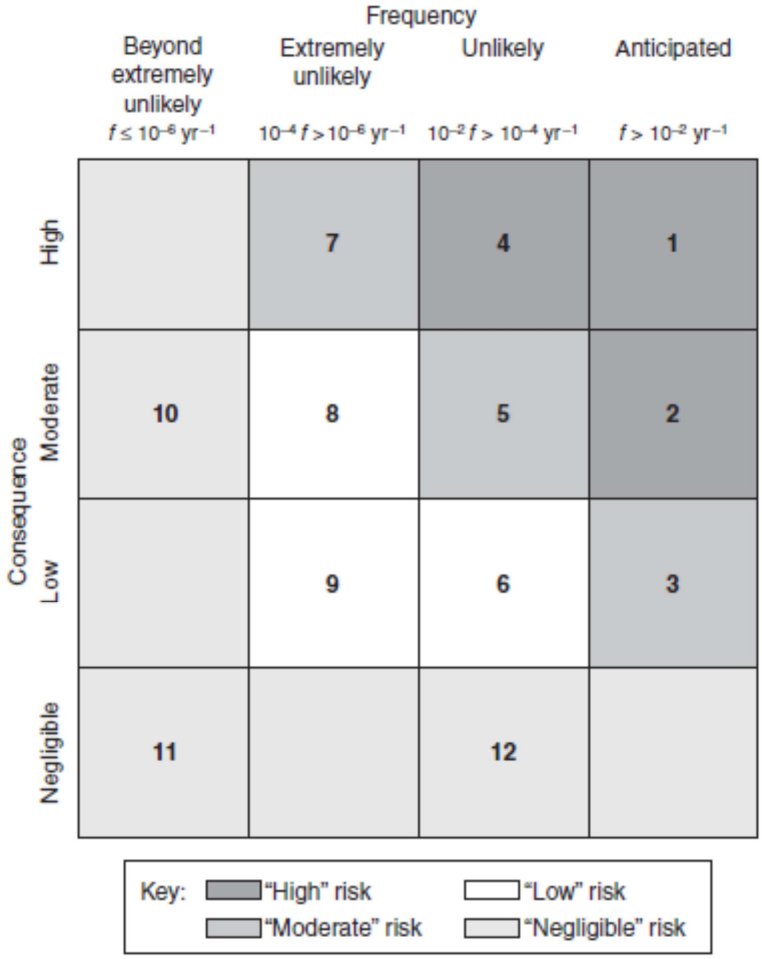

Figure 3.2: Example risk ranking matrix [26].

Quantitative risk analysis (also referred to as probabilistic risk analysis) is a systematic method of risk assessment where the risk is measured in terms of costs and associated frequencies [127]. It was first developed in the 1960's for the aerospace sector by NASA following a major accident in the Apollo program. Since then it has spread across the aerospace sector and is now also widely used across the aviation, nuclear and chemical process sectors.

The first step of quantitative risk analysis is the identification of all the possible hazards that may occur. The impact or magnitude of the identified hazards is then evaluated. Typically the impact of the hazard is measured in terms of the number of deaths that would result from the occurrence of the hazard. However, the impact may also be

measured in terms of downtime or financial loss due to business interruption and repair costs.

The likelihood of occurrence of an event may be estimated using fault tree analysis, event tree analysis or expert opinion. Fault tree analysis and event tree analysis both rely heavily on historical data for calculating the probability of occurrence of the various outcomes that may arise due to a hazard.

The results of a quantitative risk analysis may typically be presented in two forms, either as a single figure of expected loss or as a range of expected losses. In both cases the losses are associated with a likelihood of occurrence. If the results are given as a range of losses, then they may be graphically illustrated using a frequency-consequence curve (also known as an FN curves or Farmer curves when the consequence is in terms of expected fatalities), as shown in Figure 3.3 [128].

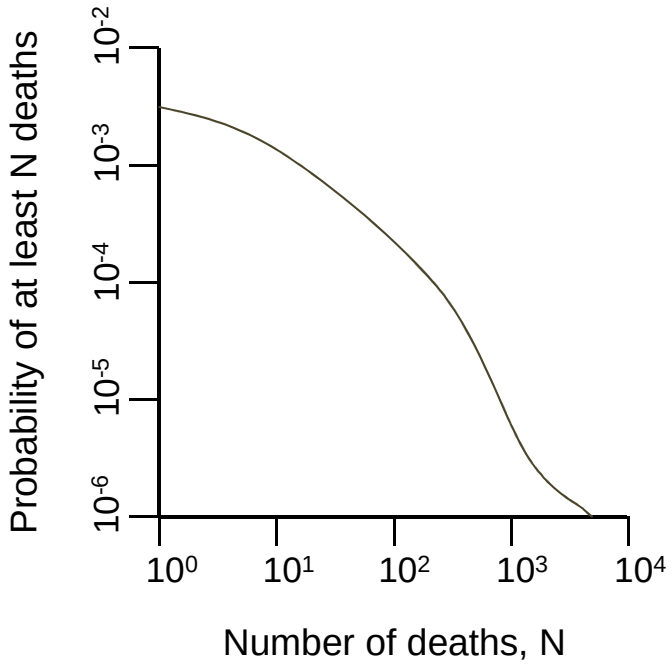

Figure 3.3: Typical frequency-consequence curve.

Frequency-consequence (fC) curves highlight the risk profile associated with a particular hazard. For example, it is possible to look at the curve and see if the risk is evenly spread across the range of possible events, dominated by high-impact, low-frequency events or

dominated by frequent, low-impact events. The ALARP (as low as reasonably practicable) principle is generally used when evaluating the acceptability of an fC curve. The ALARP principle defines three regions of risk; an acceptable region, an unacceptable region and a tolerable region where the risk must be minimised as much as is reasonably practical. One of the earliest examples of this procedure is shown in Figure 3.4. This criterion was developed for the Dutch Government, who were concerned with the threat posed by large industrial facilities to the general public.

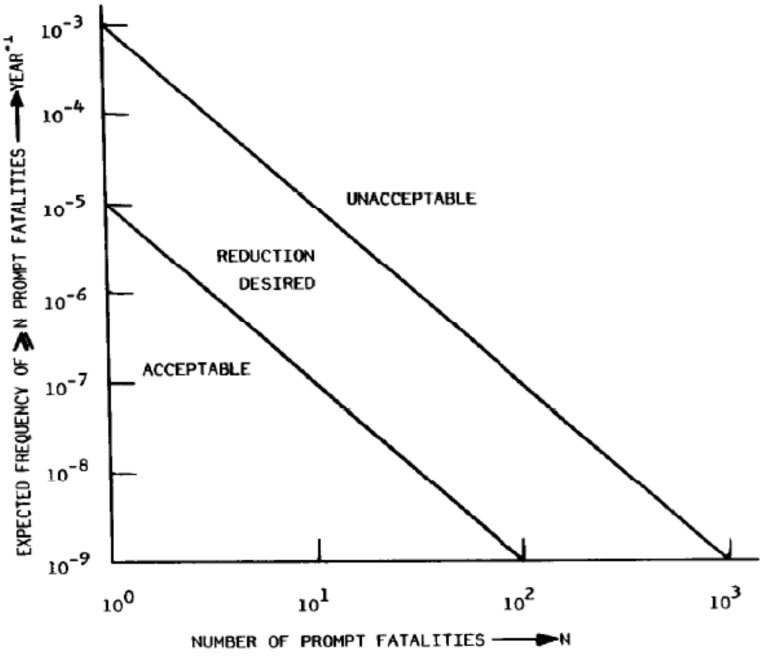

Figure 3.4: Dutch government criterion for group risk [129].

Shortly afterwards a similar set of criteria was developed in the UK. This set of criteria was originally developed for categorising the risk of transporting hazardous materials and is shown in Figure 3.5. The tolerability limits are by nature rather arbitrary. The limits were chosen for the sake of simplicity as straight lines on a log-log graph. It can be seen that the Dutch and the UK tolerability limits for high-impact incidents are quite different due to the fact that the Dutch chose to use a slope of -2 while the UK chose to use a slope of -1.

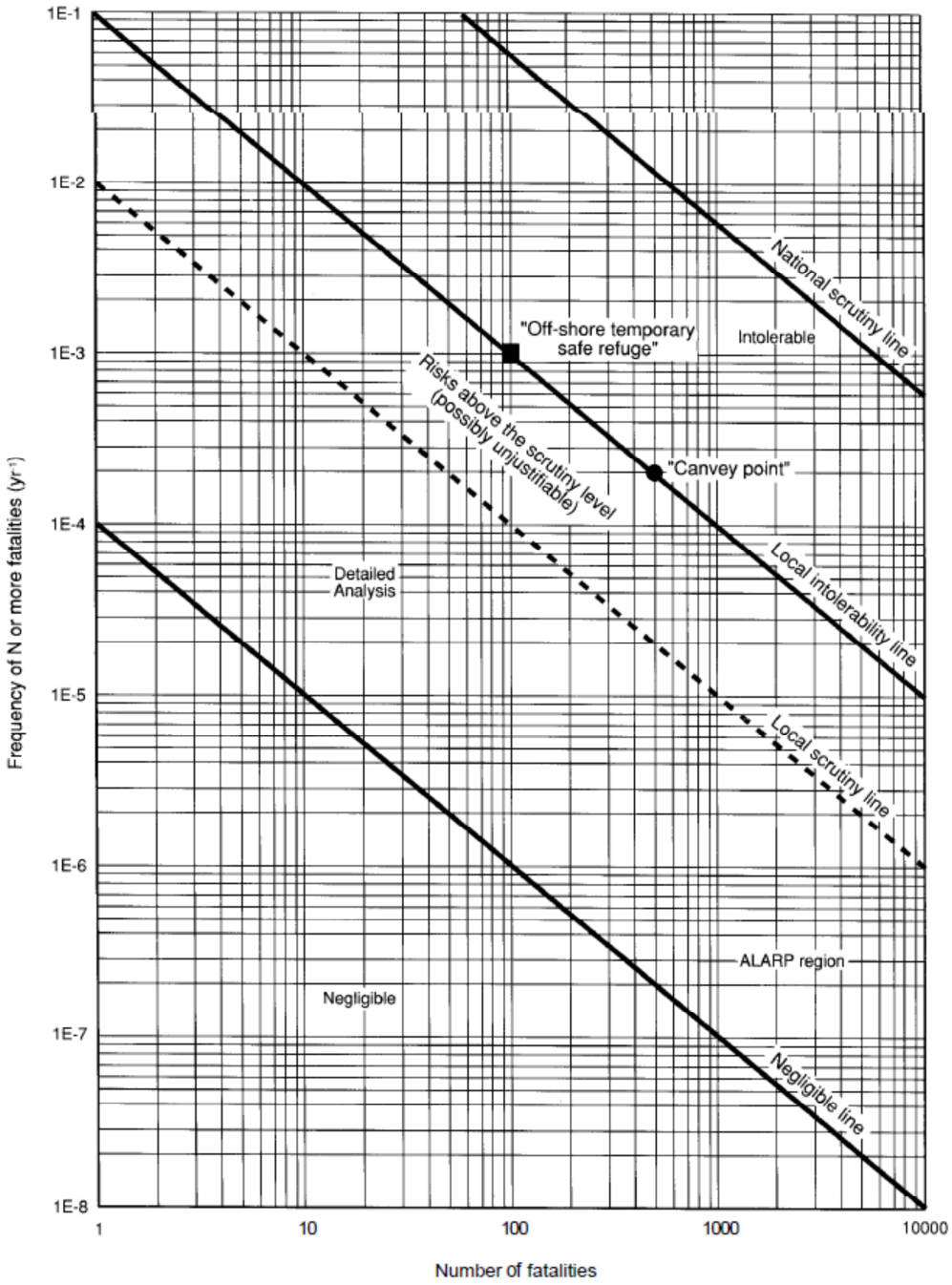

Figure 3.5: Risk criteria developed for major hazards of transport study [130].

3.3 Performance-Based Engineering of Structures in Fire

3.3.1 Development of performance-based structural fire engineering

Advances in fire design have typically been reactive measures, aimed at preventing the reoccurrence of some recent tragedy. For example, the first fire regulations introduced in the United Kingdom were brought in after the Great Fire of London in 1666 and were primarily aimed at limiting fire spread between buildings. These regulations covered the London area only and other areas all developed their own codes and standards. It was in this manner that prescriptive type fire codes developed, with more and more rules being added as different risks were identified. Throughout the 20th century lessons learned from the Second World War and from the introduction of new materials and construction methods were added to the codes [131]. This system became very complex and difficult to apply, with the Building Regulations running up to 307 pages, resulting in the need for a new approach to regulations. While the "Fire Precautions Act of 1971" allowed for the use of alternative solutions a lack of knowledge and a lack of suitably qualified designers prevented the application of performance-based solutions. The first step towards promoting performance-based design in the UK was "The Building Regulations 1985", which were introduced to cover England and Wales [132]. These regulations set out objectives (or performance requirements) which a structure must meet, without specifying how to meet these methods. A typical requirement from the regulations relating to external fire spread is shown below:

B4. – (1) The external walls of the building shall offer adequate resistance to the spread of fire over the walls and from one building to another, having regard for height, use and position of the building.

Approved Documents were published alongside the new regulations with technical specifications as examples of how the requirements could be met. A combination of the simple design process and a high probability of acceptance led designers to rely almost entirely on the Approved Documents. The Approved Documents are an example of fire safety engineering regulations. Fire safety engineering covers the entire fire safety package including, for example, fire development, fire spread, smoke movement, structural behaviour, evacuation procedures, etc. Structural fire engineering may therefore be viewed as a single topic within the broader discipline of fire safety

engineering. Fire safety engineering, in turn, represents one area within a performance based engineering framework.

The UK was not the first country to look at ways of improving the safety and efficiency of the building codes. The Nordic countries were amongst the earliest adopters of a performance-based approach to structural fire design, with alternative design methods allowed by the building code since 1967 [114]. A paper by Magnusson and Pettersson in 1981 established an early framework for conducting reliability based analysis of structures exposed to fire and listed the essential components of a performance-based design methodology [133]. Magnusson and Pettersson's method states that the load effect on the structure should not exceed the capacity of the structure for a specified exposure time. The uncertainty effects are accounted for in the model through the use of partial factors to increase the load effects and decrease the capacity. A performance-based approach was developed in the USA in the early 1970's by Nelson, though it was not widely used. Various other frameworks were put forward in the USA throughout the 1970's and 1980's with limited success [134]. The Conseil International du Bâtiment (CIB) attempted to harmonize European building standards with a report on the performance-based approach in 1982. This work was further promoted in 1986 with the publication of a model code (in the form of a design guide) which was intended to provoke international debate and further code development [14]. New Zealand produced a draft version of a performance-based code in 1984, but it was never adopted due to disagreement between various parties which arose due to a lack of consultation during the drafting process [135]. An international standard, ISO 6241, was published in 1984 by the International Organisation for Standardization which set out the general principles, outlined the process of performance-based design and stated the factors to be considered, such as outbreak of fire, spread of fire, etc.

Wakamatsu, from the Building Research Institute of Japan published the results of a six year research program into evaluating building fire safety in 1988 [136]. Wakamatsu describes the reasons for moving away from the prescriptive approach, the general performance objectives and the method of evaluating performance. The method defines 3 sub-systems; fire outbreak and spread, smoke control and evacuation and fire resistance. The method is based on the premise that the performance-based design achieves equivalency with a typical prescriptive design.

The 1990's saw a surge in the development and implementation of performance-based design codes, with New Zealand, Canada, Australia and the UK all publishing new performance-based codes [135], [137], [138]. Numerous papers were published at this time promoting these new approaches and presenting ways to improve upon the uptake of performance-based design [139], [140]. The development of better frameworks and tools has continued up to the present day [141]–[144]. Standards and codes for structural fire engineering have also advanced with the publication of the Eurocodes and BS 7974 [145].

The practical application of performance-based structural fire engineering has also grown and is now practiced by many consulting firms in the UK [146], [147]. Currently, these firms tend to adopt a qualitative approach to the assessment of the fire load. A condensed view of the relative advantages and disadvantages of performance-based fire codes is given below:

Advantages of performance-based fire codes

- Cost-effective
- Proven, uniform levels of safety across different building/occupancy types
- Lower risk to life/and property
- Flexibility of tailoring the solution to the specific problem based on sound scientific and engineering principles
- Eliminates technical barriers to trade
- Allows the harmonisation of international regulation systems
- Allows innovative design, materials and technologies

Disadvantages of performance-based fire codes

- Greater initial design costs
- More difficult/involved design process for the building professionals
- Difficult to set appropriate objectives, e.g. how much effort should be made to protect a human life?
- Difficult to validate new or different design models
- Lack of people qualified to deal with the calculation of uncertainty
- Gaps in the existing technical knowledge of the profession
- Higher level of education needed by designers

- Need for advanced analysis models

3.3.2 Current performance-based structural fire engineering methods

A proven design framework for structural fire engineering is shown in the form of a flowchart in Figure 3.6. This framework was developed by Institution of Structural Engineers as a guide for both practicing engineers and approving bodies who are involved in structural fire design [141]. Alternative frameworks include the “Rational fire safety engineering approach to fire resistance in buildings” by the CIB [148] and BS 7974 [145], although these frameworks also include non-structural considerations such as smoke spread.

The first stage of the design process is to determine the performance goals. The fundamental performance goal in structural engineering is life safety. Additional performance goals, such as property protection, may be considered depending upon the requirements of the client.

In England and Wales, the life safety performance goal is achieved through the specification of functional objectives in the Building Regulations [149]. The functional objectives which relate to the structural performance are:

- The building shall be designed and constructed so that in the event of fire its stability will be maintained for a reasonable period.
- To inhibit the spread of fire within the building it shall be divided with fire resisting construction to an extent appropriate to the size and intended use of the building.

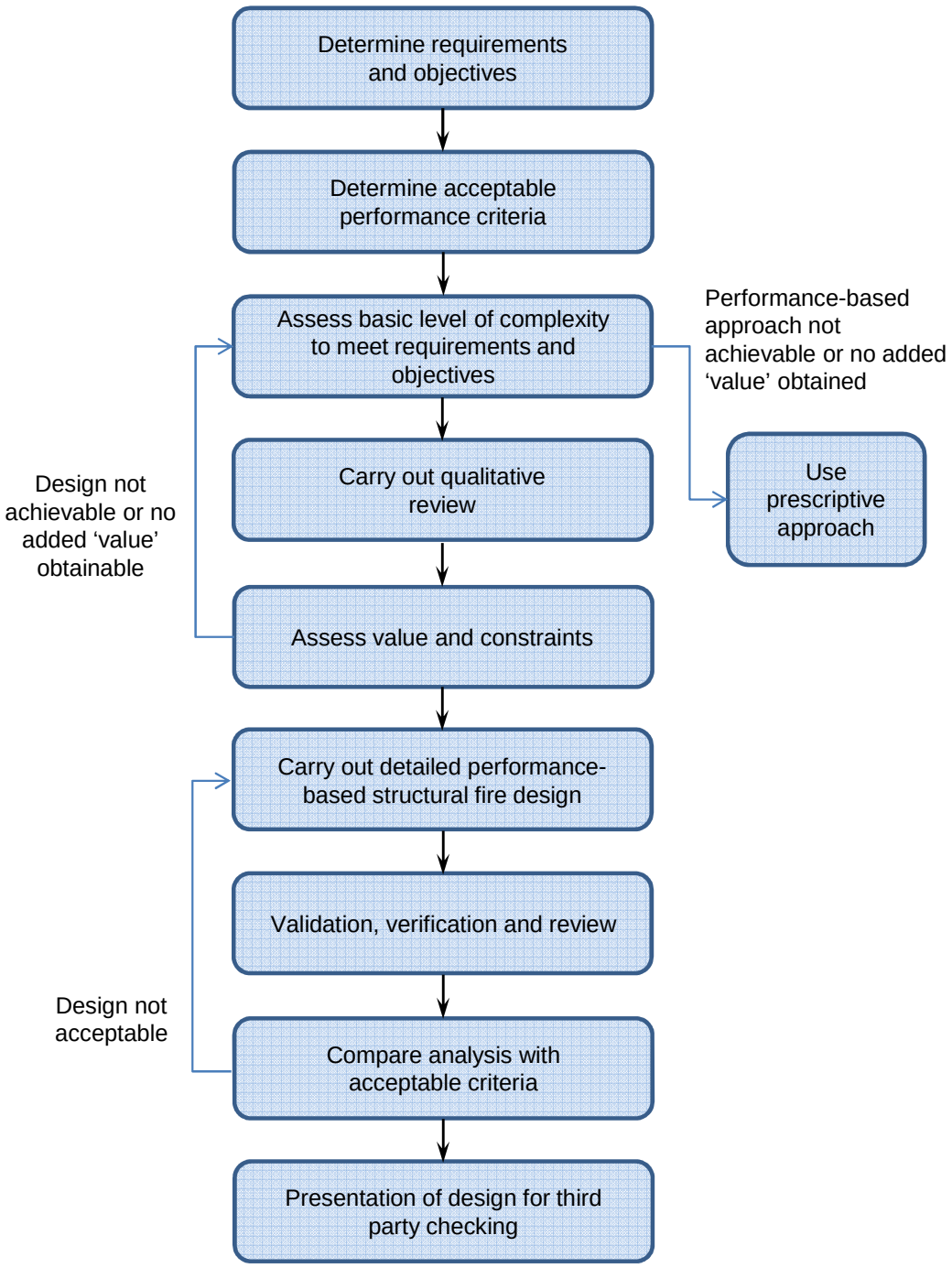

Figure 3.6: Design process for performance-based structural fire engineering [141].

The second stage is to determine acceptable performance criteria. The criteria may be deterministic, comparative or probabilistic. An example of deterministic criteria would

be a limiting deflection or limiting rate of deflection for beams within the structure. The comparative approach involves proving that the performance-based method offers an equivalent or greater level of safety than the prescriptive method. The probabilistic method involves the calculation of both the range of magnitude and frequency of the fire hazard, as discussed earlier in section 2.2.

The third stage is to assess the difficulty of the problem, the range of design options and the capabilities of the designer in order to determine the suitability of the performance-based approach.

The fourth stage is a qualitative review in order to develop an idea of how the structure will react to the fire load and to determine if the chosen models are suitable.

The fifth stage is to assess if there is a good reason for proceeding with performance-based design. Typical reasons are cost savings or increased reliability of the structure. It also involves the assessment of the chosen methodology to ensure that it can be carried out as planned.

The sixth stage is to carry out the structural fire design. This stage will involve fire modelling, heat transfer and structural analysis.

The seventh stage is a review of the results. The results should be sensible and should match up with the qualitative review. The inputs should be checked for accuracy. A sensitivity analysis should be carried out on important variables to check for weaknesses in the design.

The eighth stage is a check against the acceptability criteria. If the design does not meet these criteria then it must be revised.

The ninth stage is a check by a third party for errors in the input, the suitability of chosen models, modelling assumptions and interpretation of the results.

If the design passes the third party check then it is deemed to be suitable and the design may be communicated to the other members of the design team.

3.4 Summary

Performance-based engineering is a general engineering framework that allows designers to define the design objectives in accordance with the nature of the project and it then allows for the use of any solution that meets those design objectives. It is a procedure which is suited to rare, high impact loading events such as fire, earthquake or blast as it allows the designer to accurately account for both the magnitude and frequency of the load and it allows the designer to adapt the structure to minimise the effect of the load.

Performance-based structural fire engineering is typically based on the principles of qualitative risk analysis. The exact behaviour of a fire in a compartment cannot be modelled deterministically; therefore the designer chooses two or three design fires as a representation of the range of fires that could occur. These design fires are chosen based on the designers experience and knowledge. Suitable performance objectives for performance-based structural fire engineering are discussed. A current, best-practice framework for performance-based structural fire engineering has been presented.

Quantitative risk analysis allows the designer to evaluate the safety of a design. Other forms of performance-based engineering, such as earthquake engineering, wind engineering and fire safety engineering, incorporate quantitative risk analysis into the design process. However, structural fire engineering does not typically include a quantitative risk analysis. Chapter 3 presents an example of performance-based structural fire engineering framework based on quantitative risk analysis.

Chapter 4: Methods of Probabilistic Analysis

4.1 Preamble

This chapter discusses various methods of probabilistic analysis. Probabilistic analysis is required in order to explicitly account for the uncertainties involved in engineering problems. A probabilistic analysis calculates the probability of an event occurring and is typically used in engineering to determine the probability of exceeding a specific performance limit. Probabilistic analysis methods form the basis for the implementation of reliability analysis and quantitative risk assessment. This chapter looks at various methods for conducting probabilistic analysis such as crude Monte Carlo simulation, importance sampling, First-Order Reliability Method and subset simulation. The development of these methods and their relative advantages and disadvantages are examined.

The application of probabilistic analysis methods to structural fire engineering is examined. One-at-a-time sensitivity analyses are carried out in order to identify the important variables for both composite beams and composite slabs. The variables identified as important can be treated as stochastic variables, while the unimportant variables may be treated as deterministic variables in further probabilistic analysis.

A composite beam and a composite slab are analysed using the Monte Carlo approach with Latin hypercube sampling and the results are examined. Results from the analysis of a composite beam using the First-Order Reliability Method are also presented in this chapter.

4.2 Monte Carlo Simulation

Monte Carlo methods are a broad class of techniques involving repeated random sampling in order to simulate a sufficient number of artificial experiments and gather the numerical results. Monte Carlo methods were first developed by Metropolis and Ulam as a method for solving difficult differential equations in the field of physics [150] and are now used across a diverse range of areas including science, engineering and business.

Monte Carlo methods are useful where there is substantial uncertainty in either the input or output of a problem. A Monte Carlo simulation can be used to quantify the uncertainty associated with a problem, e.g. for calculating the probability of failure of a structure [15], [151].

In order to calculate the probability of failure of a structure, a limit state function $G(\hat{\boldsymbol{x}})$ must first be developed. If the structure fails in a simulation, $G(\hat{\boldsymbol{x}}) \leq 0$ otherwise $G(\hat{\boldsymbol{x}}) > 0$. In a crude Monte Carlo simulation $\hat{\boldsymbol{x}}$ is a vector of sample values of the inputs, randomly drawn from the probability distributions of each input variable. The process of creating a vector of sample inputs and evaluating the limit state function is repeated a large number of times. The probability of failure may then be evaluated by:

$$p_f = \frac{n(G(\hat{x}_i) \leq 0)}{N} \tag{4.1}$$

where p_f is the probability of failure, $n(G(\hat{\boldsymbol{x}}) \leq 0)$ is the number of trials which violated the limit state function and N is the total number of trials performed. The probability of failure calculated by Monte Carlo simulation is a random variable, due to the randomness in the inputs. The accuracy of the estimate of the probability of failure increases with an increase in the number of trials N. Increasing the number of trials also reduces the variance of the estimated probability of failure. The main disadvantage of the Monte Carlo method is its inefficiency in calculating small failure probabilities [152]. The number of trials required to generate an accurate answer is proportional to $1/p_f$. In the case of structural reliability calculations this is important as the probability failure is typically in the range of 10^{-5} to 10^{-7}.

It is not possible to calculate exactly how many trials are required in order to accurately calculate the probability of failure. This can result in too many runs being conducted, which is inefficient and time consuming, or too few runs, which will produce an inaccurate estimate of the probability of failure. A method for estimating the number of trials required for a given confidence level in the probability of failure was presented by Broding et al. [153] as:

$$N > \frac{-\ln(1 - C)}{p_f} \tag{4.2}$$

where C is the required confidence level. A drawback of this equation is that the probability of failure must be estimated before the Monte Carlo simulation is attempted.

A second method of evaluating the accuracy of a Monte Carlo simulation is to plot the estimate of the failure probability against the number of runs for several points within the simulation, as shown in Figure 4.1. The accuracy of the answer may then be evaluated by examining the convergence of the plotted line. This method is useful for analysing the results of a Monte Carlo simulation, but does not provide any information on the number of trials required prior to starting the simulation.

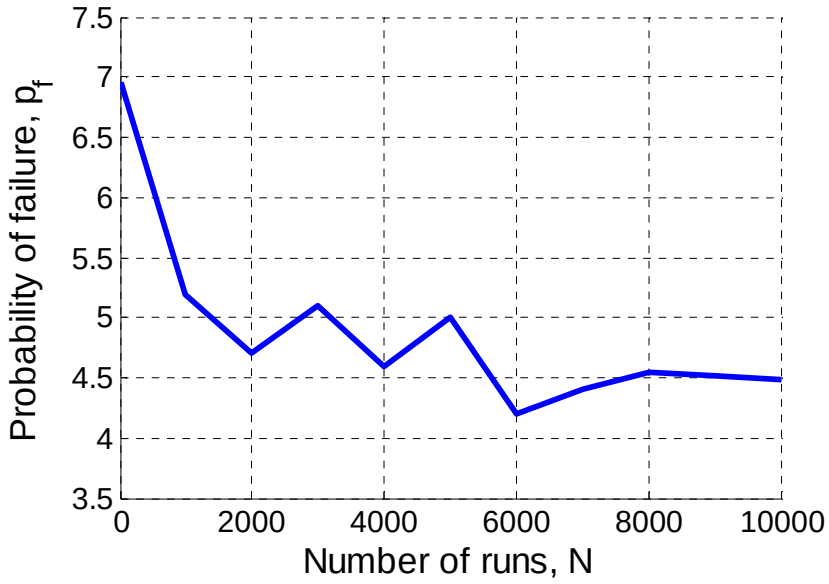

Figure 4.1: Example convergency plot of the results of a Monte Carlo simulation.

Monte Carlo simulation is a very useful method for estimating the reliability of a structure as it is robust, accurate and is able to account for highly variable limit state functions. These advantages ensure that Monte Carlo method is still widely used, despite the computational inefficiencies, e.g. the Monte Carlo method has previously been used to evaluate the performance of a simply supported steel beam in a fire [154].

4.2.1 Sampling methods

The simplest sampling approach for use in Monte Carlo simulation is pseudo-random sampling. This involves the generation of pseudo-random numbers using a random number generator. The process is referred to as pseudo-random sampling as it is not truly random and only a finite amount of distinct numbers can be generated. In this work, the

Mersenne Twister algorithm (as implemented in Matlab) has been used [107], [155]. This algorithm produces random numbers in the open interval (0,1). The disadvantage of random sampling is that the samples may end up clustered together, rather than evenly spread across the sample space. This reduces the rate of convergence of the Monte Carlo simulation.

Reduced variance sampling involves the use of techniques that improve the distribution of the samples throughout the sample space in order to reduce the variance of the results of the Monte Carlo simulation [156]. Typical examples of these techniques are stratified sampling and Latin hypercube sampling. Stratified sampling is a simple technique whereby the sampling space is divided up into a number of non-overlapping subgroups (or strata) of known probability. A given number of values are then randomly sampled from each subgroup.

Latin hypercube sampling (LHS) is a sampling procedure based on dividing each variables range into intervals of equal probability [157]. If two variables are considered, then the sample space takes the form of a rectangle divided by rows and columns. A Latin square is formed if a single sample is drawn from each row and each column. A Latin hypercube is formed when this same process is applied to a sample space of more than three dimensions. The samples are drawn randomly from within each interval.

The method for creating samples from a Latin hypercube is given as [156]:

$$x_j^{(i)} = F_j^{-1}\left(\frac{\pi_{ij} - 1 + \xi_{ij}}{N_{int}}\right) \tag{4.3}$$

where N_{int} is the number of intervals each variable range has been split into, n is the number of variables, $x_j^{(i)}$ is the i-th Latin hypercube sample of the j-th variable, F_j^{-1} is the inverse of the cumulative distribution function of the j-th variable, π_{ij} is drawn from an N_{int} x n matrix with independent random permutations of {1, 2,…, N_{int}} and ξ_{ij} is drawn from an N_{int} x n matrix of independent random numbers uniformly distributed on the closed interval [0,1]. In this work, the samples are shuffled using the “randperm” command in Matlab. The command “randperm” returns a vector containing a random permutation of integers drawn from a specified range. The “randperm” command is applied to each column of the N_{int} x n matrix from which π_{ij} is drawn. An example of LHS is given for two variables, one with a normal distribution and one with a Gumbel distribution, in Figure 4.2. Each variable range has been split into ten intervals and a

single sample has been selected randomly from each interval. Note that the outer edges of the square are marked at the points which correspond to $P(x_i \leq 0.001)$ and $P(x_i \leq 0.999)$. This is for illustrative purposes only and in practice the outer intervals stretch to infinity.

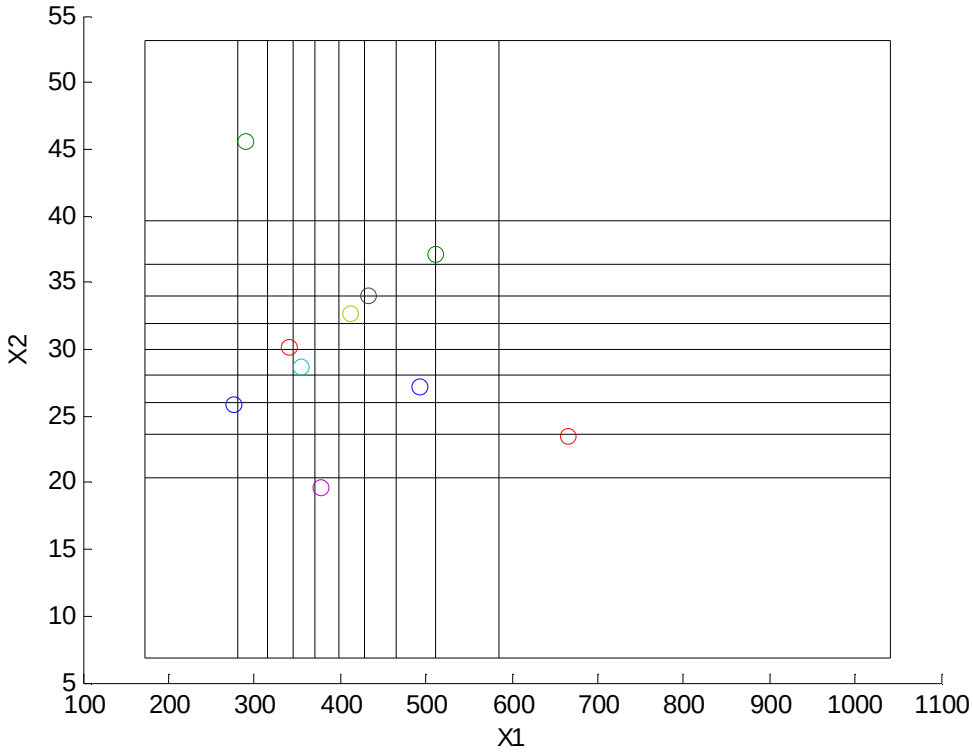

Figure 4.2: Grid of samples spaces, with samples shown.

4.2.2 Importance sampling

Importance sampling was developed to reduce the inefficiencies that are inherent in crude Monte Carlo simulations. It is based on the adaptation of the samples so that more samples lie in the region of most interest, i.e. the region adjacent to the limit state function [152], [158], [159].

The generalized form of a reliability problem may be written as:

$$p_f = P[G(\boldsymbol{X}) \leq 0] = \int \dots \int_{G(\boldsymbol{X}) \leq 0} f_{\boldsymbol{x}}(\boldsymbol{x}) d\boldsymbol{x} \tag{4.4}$$

where p_f is the probability of failure, $G(\boldsymbol{X})$ is the limit state function and $f_x(\boldsymbol{x})$ is the joint probability density function for the vector of variables $\boldsymbol{X}$.

This may be re-written as:

$$p_f = \int \dots \int I[G(\boldsymbol{x}) \leq 0] f_x(\boldsymbol{x}) d\boldsymbol{x} \tag{4.5}$$

where $I[\ ]$ is an indicator function which is equal to 1 if true and 0 if false. The purpose of the indicator function is to identify the integration domain. In importance sampling an additional parameter is introduced, the importance-sampling probability density function $h_v(\ )$. The multiple integral in Equation (4.5) can now be written as:

$$p_f = \int \dots \int I[G(\boldsymbol{x}) \leq 0] \frac{f_x(\boldsymbol{x})}{h_v(\boldsymbol{x})} h_v(\boldsymbol{x}) d\boldsymbol{x} \tag{4.6}$$

Derivation of the importance-sampling probability density function is notoriously difficult to carry out, particularly for complex problems with high-dimensions or extremely nonlinear failure functions [151], [158], [160]. If a good estimate is made for the importance-sampling probability density function then the variance in the result of the Monte Carlo simulation may be reduced by one or two orders of magnitude, however if a poor estimate is made then the variance of the result may be increased by a similar amount. These drawbacks mean that importance sampling is not suitable for complex structural fire engineering problems.

4.2.3 Subset simulation

Subset simulation is a Monte Carlo simulation based technique that may be used for calculating the probability of failure of a system [161]. It uses a Markov chain Monte Carlo simulation technique to calculate the probability of failure for a set of intermediate failure events. The probability of failure can then be calculated as the product of the conditional failure probabilities of each intermediate event. In this process, each intermediate failure event must be a subset of the preceding event. A second requirement of the process is that the Markov chain is assumed to be ergodic. Subset simulation is a robust, accurate method and it is less computationally demanding than crude Monte Carlo simulation [162], [163]. Subset simulation has previously been applied to fire

modelling in order to identify the probability of occurrence of various temperatures in a compartment [164]. Based on the inherent advantages of subset simulation in calculating small probabilities it is a promising method for future research into the probabilistic analysis of structural fire engineering problems.

4.2.4 Sensitivity analysis

A one-at-a-time sensitivity analysis was used in order to examine the relationship between the input and output variables and to identify the major sources of uncertainty in the model inputs. It also allowed for a simplification of the problem by identifying the inputs with limited uncertainty so that they may be treated as deterministic. Reducing the number of stochastic inputs to a problem helps to reduce the variance in the results of a Monte Carlo simulation and is a necessity for other probabilistic methods such as the first order reliability method, discussed in detail in section 4.3. The results of the one-at-a-time sensitivity analyses conducted in this section will be used later in sections 4.2.5, 4.3 and 5 to identify the major sources of uncertainty so that these inputs may be treated stochastically in the analyses.

The uncertainty in the output from the analysis of a steel-concrete composite beam subjected to both fire loading and a mechanical loading was examined using a one-at-a-time sensitivity analysis. A lumped capacitance approach was used to calculate the temperature distribution within the beam and the mechanical analysis of the beam was conducted using OpenSees [73]. Each of the inputs was increased and decreased in turn by five percent and the resulting variation in the output parameters from the nominal results was recorded. This method does not account for the level of variation that is expected to occur in practice, e.g. the fuel load will likely vary by much more than 5%, but the length of the compartment is highly unlikely to vary by as much as 5%. This method does not account for any correlation between the input variables (e.g. between the yield stress and ultimate strain of steel), nor does it account for model interactions where the variation of two inputs in unison produces a variation in the output far greater than the sum of the variation produced by varying the two inputs independently.

The fire was modelled using the parametric temperature-time curve from Eurocode 1 [12]. The resulting variation is shown in Figure 4.3. It can be seen that the fuel load is by

far the dominant source of uncertainty. It should be noted that the conditions for this analysis led to a fuel controlled fire; if the area of ventilation is reduced then it too becomes an important source of uncertainty. The compartment dimensions also lead to uncertainty in the peak temperature of the fire, however the dimensions are highly unlikely to vary by as much as 5% in practice. Therefore, it can be seen that the compartment dimensions do not contribute significantly to the problem uncertainty.

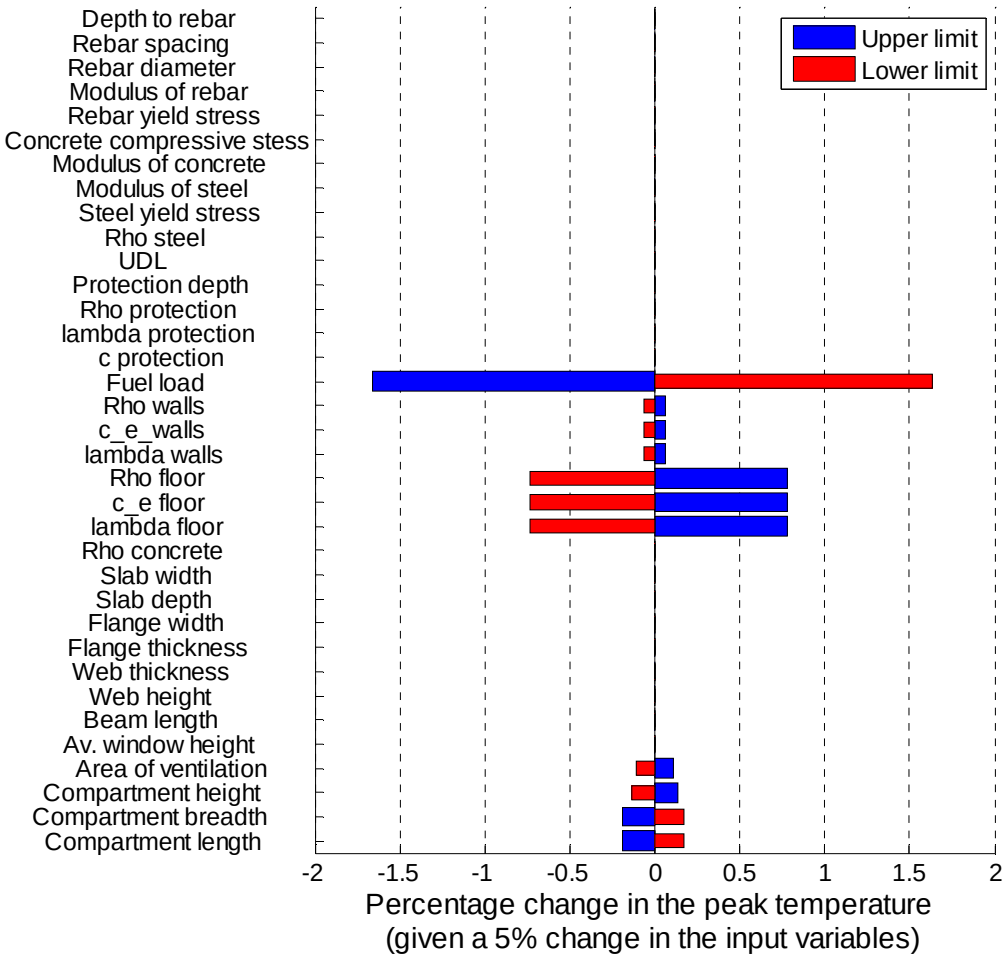

Figure 4.3: Sensitivity analysis of the inputs that affect the peak temperature in the compartment.

The structural response of the composite beam was modelled using an OpenSees model. The midspan deflection of the beam was chosen as the output to analyse, see Figure 4.4. Important variables that impact on the structural response of the beam include the length

of the beam, the web height, the depth of the fire protection, the material properties of the fire protection, the uniformly distributed load and the elasticity modulus of steel. The fuel load and area of ventilation are also important sources of uncertainty due to their variability. It is noted that certain variables exhibit a variation in the same direction for both the upper and lower limits. It is thought that this occurs as a result of a complex, nonlinear relationship between the input and the measured output.

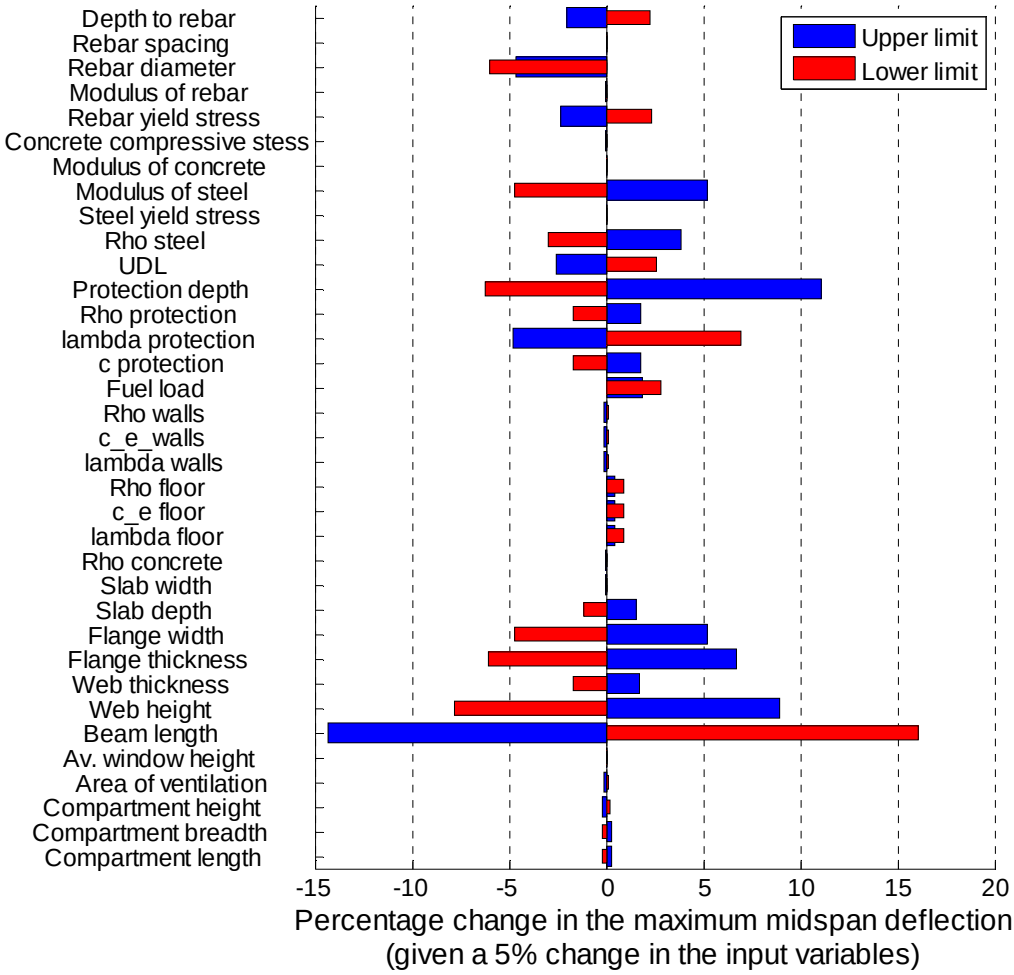

Figure 4.4: Sensitivity analysis of the inputs that affect the maximum midspan deflection of a composite beam.

The behaviour of a concrete slab was examined using the sensitivity analysis methodology. The slab is of a similar form of construction as the composite beam that was discussed above. The parametric temperature-time curve was used to model the fire.

The same compartment dimensions and construction was used as previously, but the area of ventilation was reduced and the fuel load was increased. This resulted in a hotter fire that was less controlled by the fuel load.

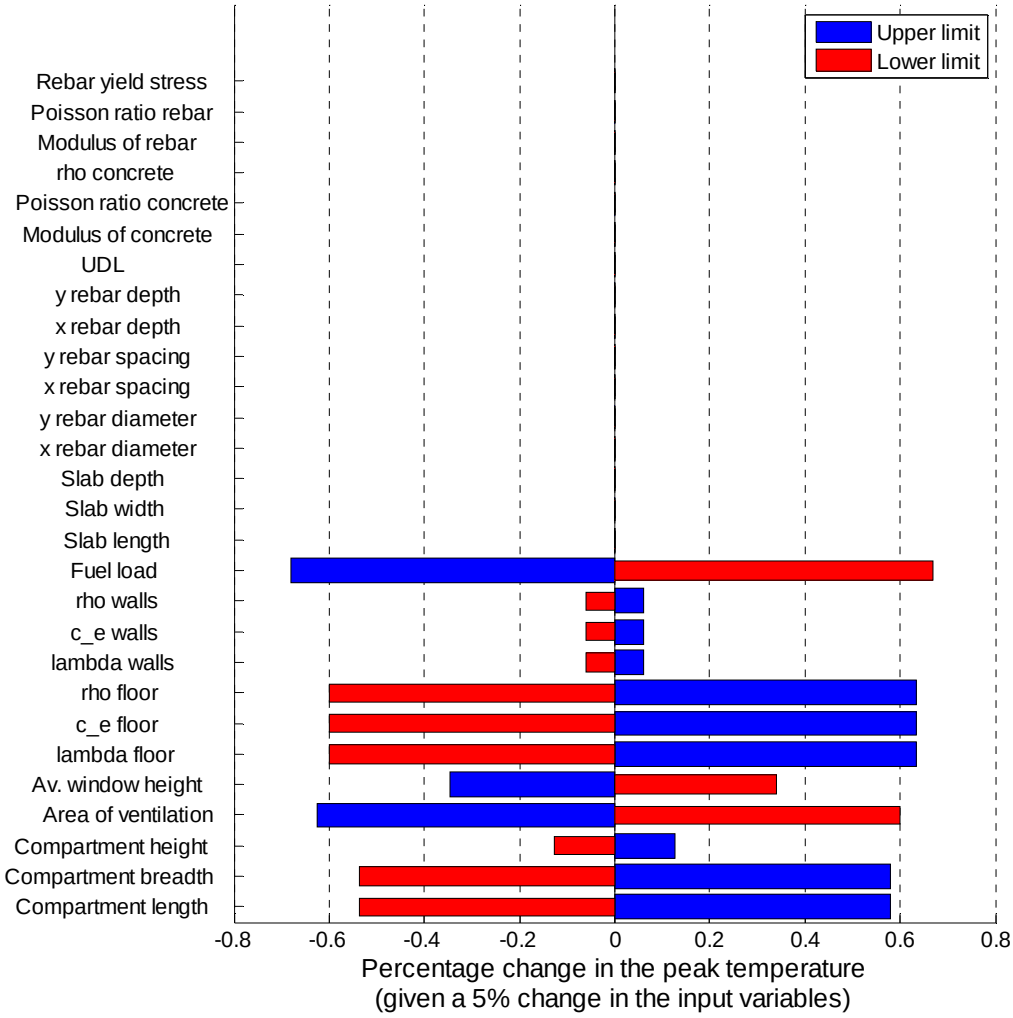

Figure 4.5: Sensitivity analysis of the inputs that affect the peak temperature in the compartment.

Figure 4.5 above confirms that the fuel load and the area of ventilation are important sources of uncertainty in the fire load. The compartment dimensions and the material properties of the compartment lining also contribute to the uncertainty in the problem, but these parameters have little variability in practice.

The temperature distribution within the slab was calculated using a one dimensional finite difference heat transfer process. The structural response of the slab was calculated using the Cameron method, as described in section 2.4.2. The slab is 7.5m long, 3.75m wide and 70mm deep. Figure 4.6 below shows the sensitivity of the midspan deflection of the slab to a five percent change in each of the input variables.

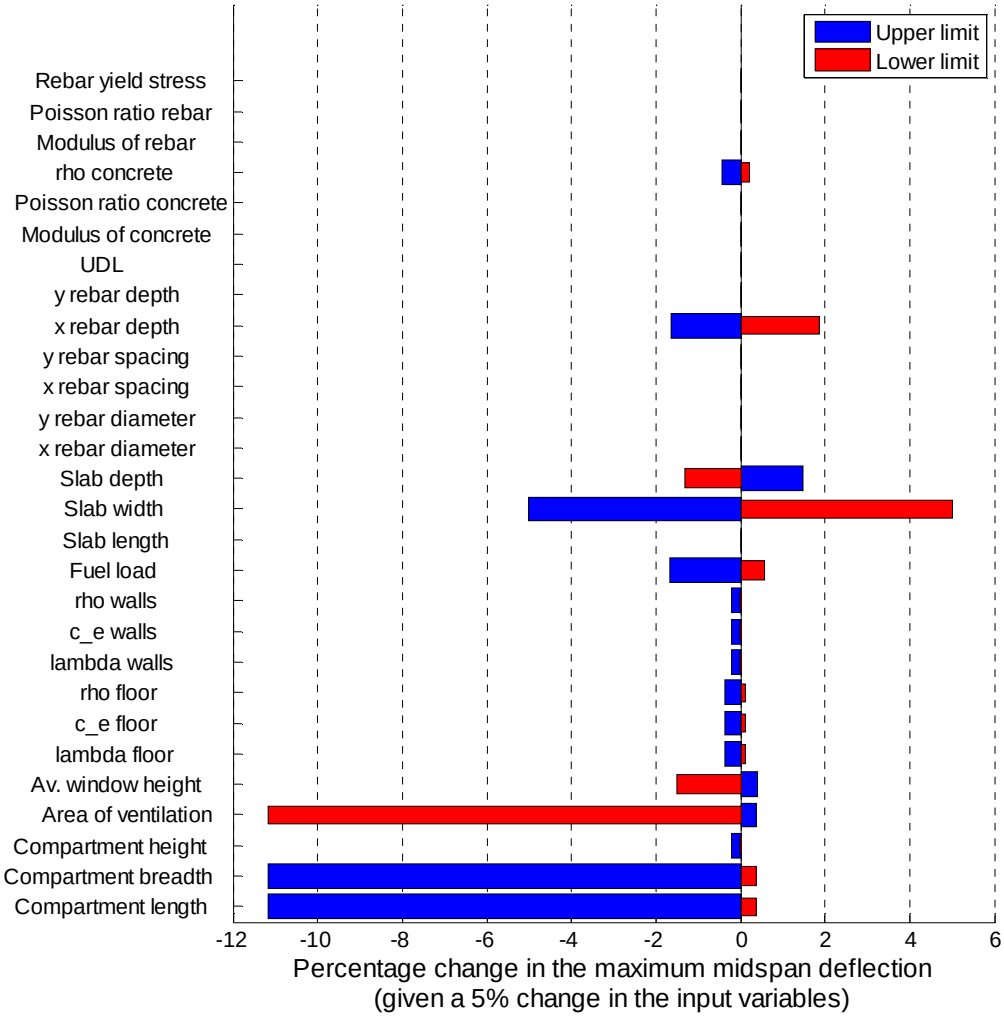

Figure 4.6: Sensitivity analysis of the inputs that affect the maximum midspan deflection of a composite slab.

It can be seen that the response of the slab is sensitive to variations in the fire. The area of ventilation in particular has a large effect on the structural response. Of the structural

parameters, the width of the slab, the depth of the slab and the depth of the reinforcing steel are all important sources of uncertainty.

4.2.5 Examples of Monte Carlo simulations

This section is concerned with the probabilistic analysis of structural elements. It is shown that the previously presented methods may be combined to easily evaluate the probabilistic performance of structures in fire. Through the use of rigorous probabilistic analysis it is possible for a designer to optimise a structure to meet the performance objectives.

The reliability of a steel-concrete beam with various levels of fire protection is evaluated through the use of a Monte Carlo simulation. The beam is taken from Building B of the SCI document, “Comparative Structure Cost of Modern Commercial Buildings” [165]. The dimensions (shown in Figure 4.7) and material properties of the beam are similar to those used in the sensitivity analysis above. The beam is assumed to have pinned supports at either end. The first case assumes that the steel beam is left unprotected. Then, the beam is analysed assuming one, two and three layers of 12.5mm thick plasterboard protection. These design cases are chosen to illustrate how probabilistic analysis may be used to optimise the level of fire protection provided. Each design case is analysed using a 10000 run Monte Carlo simulation.

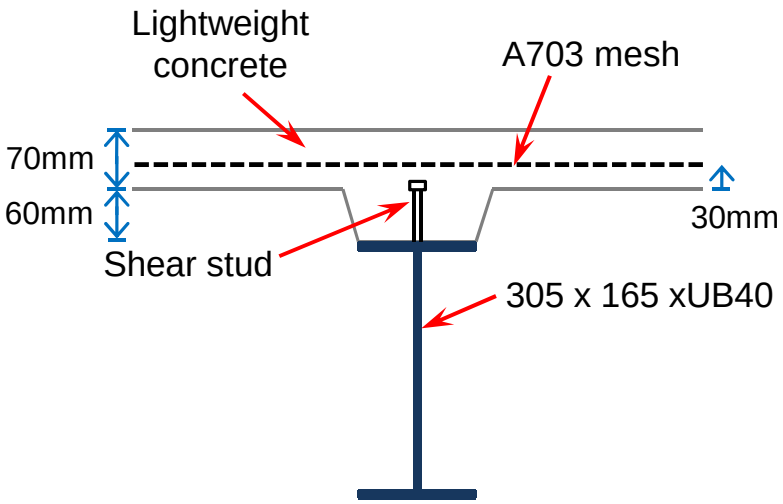

Figure 4.7: Cross-section of the composite beam.

The key input parameters identified in the sensitivity analysis were taken as independent and identically distributed random inputs. The definition of these stochastic variables is given below in Table 4.1.

Table 4.1: Stochastic variables for the Monte Carlo analysis of a composite beam.

Variable	Units	Distribution type	Distribution parameter 1	Distribution parameter 2
Fuel load	MJ/m^2	Gumbel	363.29 (mode)	98.24 (scale)
Area of ventilation	m^2	Truncated log-normal	60 (upper limit)	0.25 (standard deviation)
U.D.L.	N/m	Gumbel	5054.9 (mode)	1637.4 (scale)
Length of beam	m	Log-normal	7.500 (mean)	0.005 (C.o.V.)
Depth to the rebar	m	Gaussian	0.04 (mean)	0.02 (C.o.V.)
Young's modulus of steel	kN/mm^2	Log-normal	210 (mean)	0.03 (C.o.V.)
Young's modulus of concrete	kN/mm^2	Log-normal	35 (mean)	0.15 (C.o.V.)
Yield stress of the rebar	N/mm^2	Log-normal	562.3 (mean)	0.07 (C.o.V.)

The midspan deflection of the composite beam was chosen as the performance measure. The failure limit is difficult to define for structures in the case of fire as large deflections commonly occur due to thermal expansion. One commonly used approach is to use span/30 as the failure limit [154]; however in this case the limiting deflection is specified based on the ultimate strain in the composite beam [3].

$$w_{lim} = \frac{L}{\pi}\sqrt{4\varepsilon_{lim}} \tag{4.7}$$

where ε_{lim} is equal to $min(\varepsilon_{ult,r}, \varepsilon_{ult,s})$, where $\varepsilon_{ult,r}$ is the ultimate strain of the steel reinforcement, $\varepsilon_{ult,s}$ is ultimate strain of the structural steel, L is the length of the beam and w_{lim} is the limiting deflection. The ultimate mechanical strain of reinforcing steel is given in Eurocode 2 as 2.5% for normal ductility bars and 5% for high ductility bars [64]. The ultimate strain of structural steel is defined by Eurocode 3 as $15\varepsilon_y$ [55]. Therefore, it can be calculated that the limiting strain for s275 steel is 1.95% and the limiting strain for s355 steel is 2.55%. This limit is a conservative estimate of failure as it does not include the effects of thermal expansion. The limiting deflection is calculated as 0.667m, based on a beam length of 7.5m and a limiting steel strain of 0.0195. This limit is based on structural failure of the beam and does not measure the reusability or reparability of the beam after the fire. The deflection exceedance curves for each of the design cases are shown below in Figure 4.8. Each design case shows large deflections as the perfect translational restraints lead to buckling induced deflections at very low temperatures. It can be seen that even minimal amounts of fire protection can lead to a large reductions in the magnitude of the deflections. It can be seen from Figure 4.8 that 37.5mm of fire protection yields a substantial reduction in the deflection, when compared with the results from the 25mm and 12.5mm design cases. This is likely due to the nonlinear relationship between material temperature and midspan deflection. The calculated nominal probability of failure for all cases is approximately 0.00%, however it should be noted that this is based on 10000 runs and the accuracy of the solution is therefore limited to roughly two decimal places. The variance of the nominal probability of failure for all cases is zero, which indicates a high level of accuracy in the results.

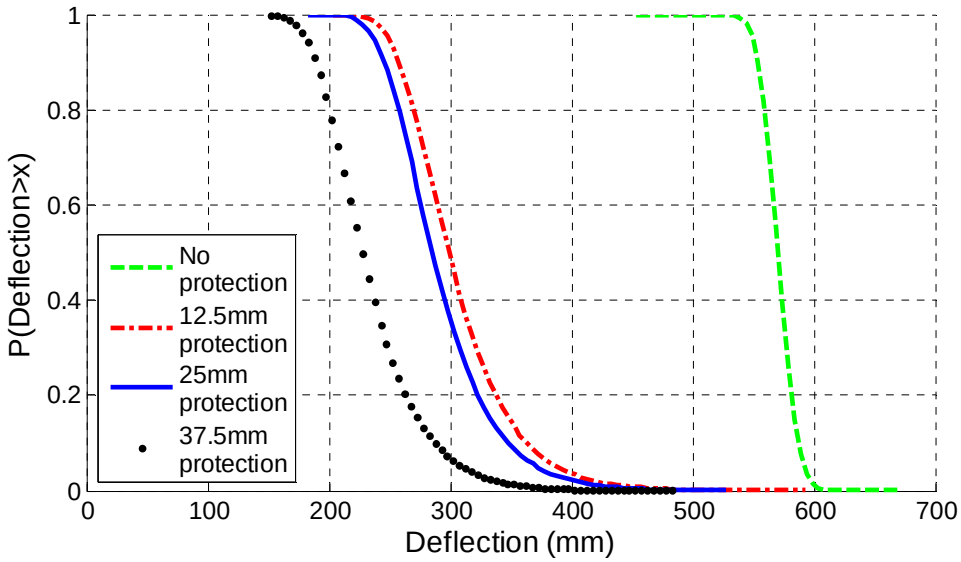

Figure 4.8: Deflection exceedance curves for each of the design options.

The reliability of a composite slab is evaluated in a similar method using Monte Carlo simulation. The slab dimensions and material properties are taken from Building B, as per the sensitivity analysis [165]. Two different design cases are examined; one where the secondary steel is assumed to be well protected giving an effective slab width of 3.75m and one where the secondary steel is assumed to be unprotected giving an effective slab width of 7.5m. The Monte Carlo simulation consists of 10000 runs for each design case. The distribution parameters for the key inputs identified in the sensitivity analysis are given below in Table 4.2. The rebar strain exceedance curves for both cases are shown below in Figure 4.9. Rebar strain is examined as it provides an accurate measure of the performance of concrete slabs and the occurrence of collapse.

Table 4.2: Stochastic variables for the Monte Carlo analysis of a composite slab.

Variable	Units	Distribution type	Distribution parameter 1	Distribution parameter 2
Fuel load	MJ/m^2	Gumbel	363.29 (mode)	98.24 (scale)
Area of ventilation	m^2	Truncated log-normal	60 (upper limit)	0.25 (standard deviation)
U.D.L.	kN/m^2	Gumbel	3.7912 (mode)	1.2280 (scale)
Length of slab	m	Log-normal	7.50 (mean)	0.005 (C.o.V.)
Width of slab	m	Log-normal	3.75 or 7.50 (mean)	0.005 (C.o.V.)
Depth of slab	m	Log-normal	0.07 (mean)	0.005 (C.o.V.)
Depth to the rebar	m	Gaussian	0.04 (mean)	0.02 (C.o.V.)
Young's modulus of concrete	kN/mm^2	Log-normal	35 (mean)	0.15 (C.o.V.)

The strain results shown below have been assigned a lognormal distribution. The strain limit is based on the rebar ultimate strain and is equal to 0.025. The probability of failure for the rectangular slab is zero (using LHS) and 0.03% (using random sampling). The probability of failure for the square slab is 6.92% (from LHS) and 6.65% (from random sampling). The highest variance for the results of the rectangular slab analyses is 2.99×10^{-8}. The results from the random sampling analysis and the Latin hypercube analysis fall within the expected. The results of the square slab analyses yield a variance of 6.44×10^{-6} and therefore can be said to differ by a small margin. The excellent

agreement between the analyses using Latin hypercube sampling and the analyses using random sampling indicate that both methods have been implemented correctly.

The square slab has an unacceptably high probability of failure. In this case, the secondary beam requires fire protection in order to reduce the probability of failure to an acceptable level.

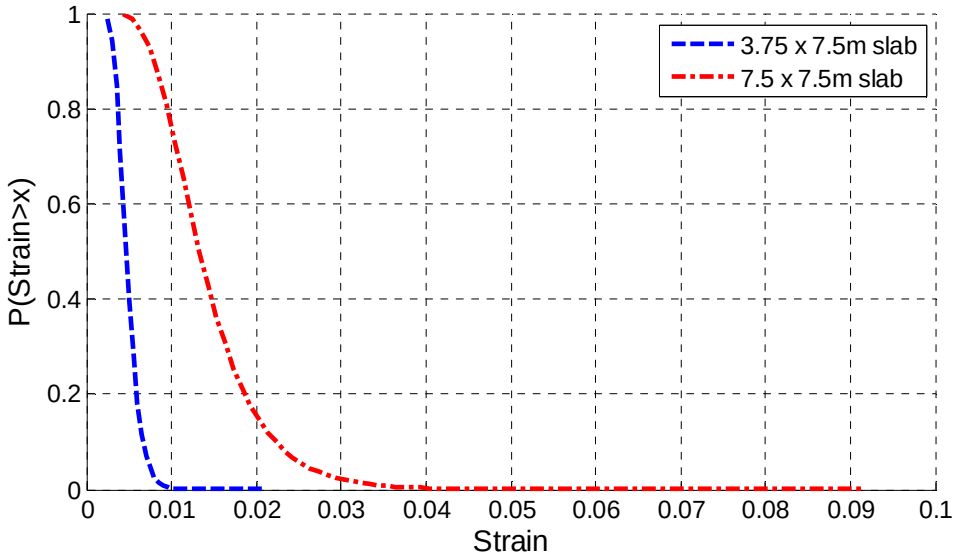

Figure 4.9: Comparison of strain exceedance curves for both slabs.

4.3 First-Order Reliability Method

The First-Order Reliability Method (FORM) is a procedure for calculating the reliability of a system based on the reliability (or 'safety') index β [151], [166]. FORM is a commonly used alternative to Monte Carlo simulation that is much less computationally intensive [167]. FORM is particularly useful for examining problems with a very low probability of failure, e.g. $<10^{-5}$. In such a case, the Monte Carlo method becomes impractical as it would potential require millions of runs. In comparison, FORM can solve an equivalent problem with several thousand runs. The disadvantages of FORM are that the accuracy of the solution is not known and the method is not suited to the analysis of nonlinear limit state surfaces. In a simple case where the response of the system can be represented using a normal distribution, then β represents the number of standard deviations from the mean to the failure limit. β can calculated from μ_z/σ_z, where

μ_z is the mean of the response and σ_z is the standard deviation of the response. In a complex analysis, the failure limit may be defined as a surface over several dimensions. In this case β is defined as the shortest distance from the origin to the failure surface, in standard normal space. A disadvantage associated with the use of β as an indicator of reliability is that it considers only the worst case, i.e. it does not consider the shape of the failure surface, only the distance from the origin to the closest point. It is possible to have several different failure surfaces each with the same β value, but a different nominal probability of failure. The reliability index assumes a linear limit state. It underestimates the probability of failure if the limit surface is concave towards the origin and overestimates the probability of failure if the limit surface is convex towards the origin. An example of a convex failure limit state, $G(\boldsymbol{x})=0$, and a linearized failure limit state, $G_L(x)=0$, subject to two variables is shown in Figure 4.10.

The nominal probability of failure is calculated from β using:

$$p_f = \Phi(-\beta) \tag{4.8}$$

where p_f is the nominal probability of failure and $\Phi(\ )$ is the standard normal cumulative distribution function.

FORM is an advanced version of the First-Order Second-Moment (FOSM) method. FOSM uses the first two moments of the stochastic variables to determine the behaviour of the system and it uses a linear (first-order) limit state to define the failure region. The first stage of a FOSM analysis is to transform the variables into standard normal space.

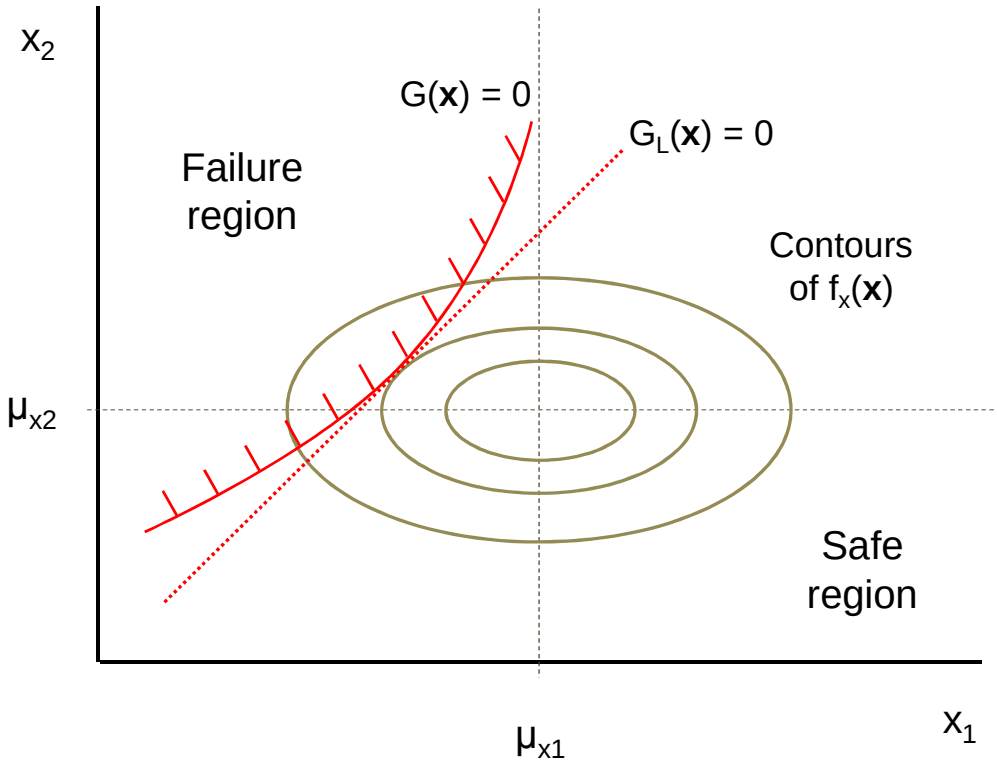

Figure 4.10: Probability density function contours and the original and linearized limit state lines in variable space.

This is done using the simple transformation:

$$U_i = \frac{X_i - \mu_{Xi}}{\sigma_{Xi}} \tag{4.9}$$

where U_i is the standardised form of the variable with $\mu_{Ui} = 0$ and $\sigma_{Ui} = 1$, X_i is the value of the variable, μ_{Xi} is the mean of the variable and σ_{Xi} is the standard deviation of the variable. This method assumes that all of the variables have a normal distribution prior to the transformation and that the variables are independent of each other. The Hasofer-Lind transformation allows for the joint probability density function of the system response to be represented by a standardized multivariate normal distribution, as shown by $f_u(\boldsymbol{u})$ in Figure 4.11. This simplifies the solution of the reliability problem. The point which is the shortest distance from the origin is known as the design point and is given by:

$$\beta = min\left(\sum_{i=1}^{n} y_i^2\right)^{1/2} = \min(\boldsymbol{y}^T.\boldsymbol{y})^{1/2} \quad (4.10)$$

subject to $g(y) = 0$

where y_i are the coordinates of any point on the limit state surface.

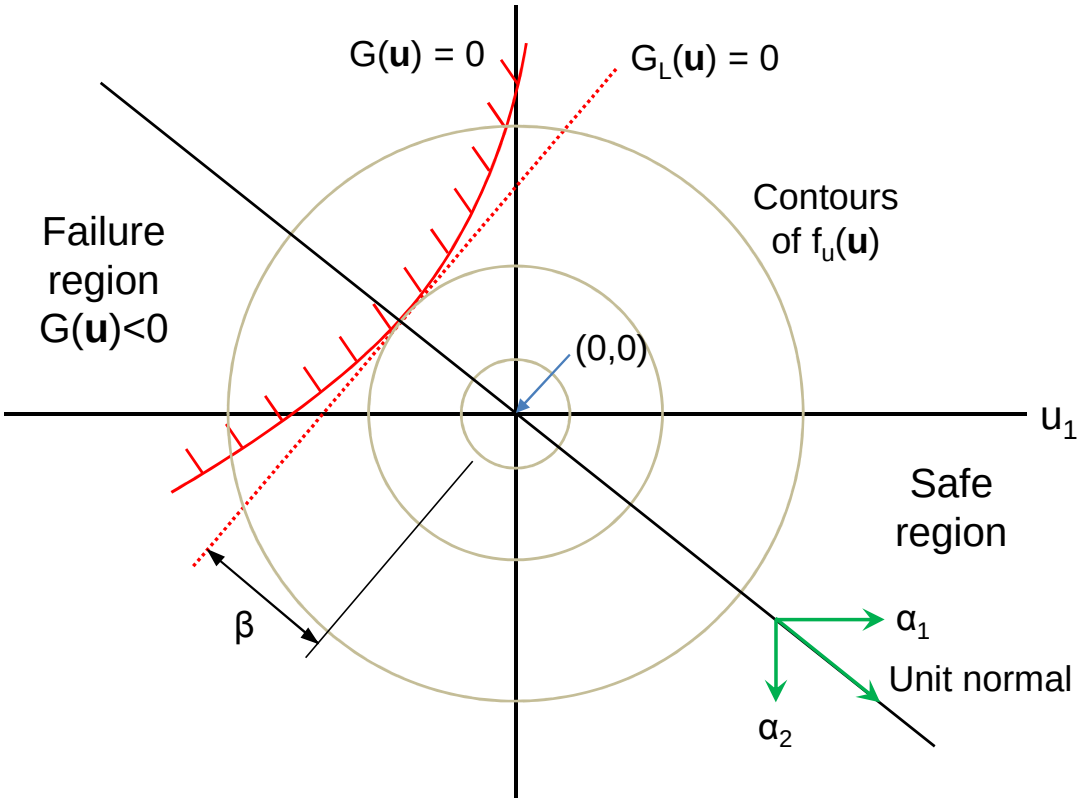

Figure 4.11: Probability density function contours, the original limit state and the linearized limit state lines in standard normal space.

The following algorithm was presented by Melchers [151] for the implementation of the FOSM method:

1. standardise the basic random variables to the independent standardized normal variables using the simple transformation given above in Equation (4.9)
2. transform the limit state function
3. select an initial checking point
4. calculate $\beta^{(1)}$ at the checking point from $[\mathbf{y}^{(1)T}.\mathbf{y}^{(1)}]^{1/2}$, let $m = 1$

5. calculate the direction cosines $\alpha^{(m)}$
6. calculate $G(\mathbf{y}^{(m)})$
7. calculate $\mathbf{y}^{(m+1)}$
8. calculate $\beta^{(m+1)} = [\mathbf{y}^{(m+1)T}.\mathbf{y}^{(m+1)}]^{1/2}$
9. repeat steps 5 – 8 until $y^{(m+1)}$ and/or $\beta^{(m+1)}$ have stabilized

FORM is similar in principle to FOSM, however FORM accounts for the distribution type of the variables and for correlation between the variables. FORM uses transformation procedures to transform any non-normal variables into standard normal variables. Commonly used transformation procedures include the normal tail transformation, the Rosenblatt transformation and the Nataf transformation [151]. A simple transformation may be defined as:

$$\Phi(y_i) = F_i(x_i), \quad i = 1, \dots, n \tag{4.11}$$

Where Φ is the standardized normal cumulative distribution function, x is value of the variable and F_1, …, F_n are continuous and increasing distribution functions. This process is shown below in Figure 4.12.

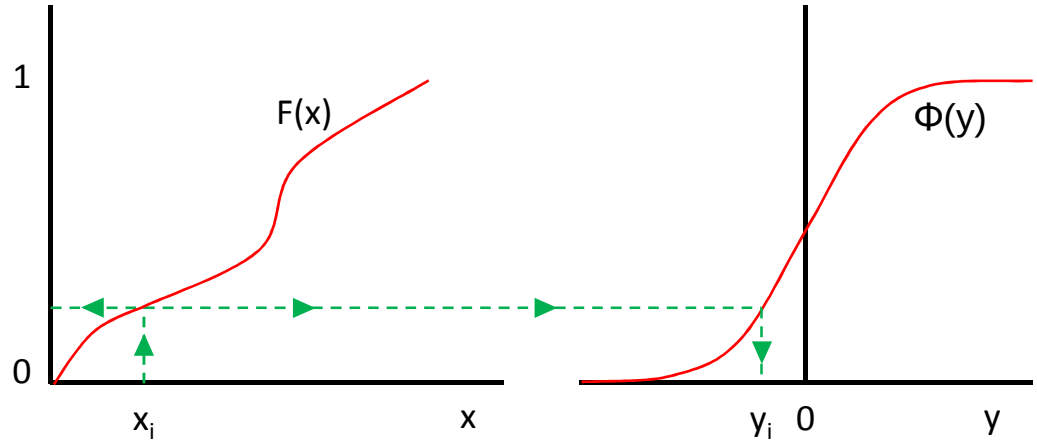

Figure 4.12: Transformation of a variable to a standardized normal distribution.

This work uses the Nataf transformation. The Nataf transformation requires the marginal cumulative distribution function of each variable and the correlation matrix $\boldsymbol{P}_{corr} = \{\rho_{ij}\}$. The correlation matrix must be positive definite. The Nataf approximation also requires

that the cumulative distribution function of the variables be strictly increasing. The Nataf approximation of the joint probability density function $f_X(\ )$ for the variables is given by [168]:

$$f_X(\boldsymbol{x}) = \phi_n(\boldsymbol{y}, \boldsymbol{P'}_{\boldsymbol{corr}}).|\boldsymbol{J}| \tag{4.12}$$

where

$$|\boldsymbol{J}| = \frac{\partial(y_1, \dots, y_n)}{\partial(x_1, \dots, x_n)} = \frac{f_{X1}(x_1) \times \dots \times f_{Xn}(x_n)}{\varphi(y_1) \times \dots \times \varphi(y_n)}$$

and

$$\phi_n(\boldsymbol{y}, \boldsymbol{P'}_{\boldsymbol{corr}}) = \frac{1}{\sqrt{(2\pi)^n det \boldsymbol{P'}_{\boldsymbol{corr}}}} exp\left(-\frac{1}{2}\boldsymbol{y^T P'}_{\boldsymbol{corr}}{}^{-1}\boldsymbol{y}\right)$$

where $\varphi_n(\boldsymbol{y},\boldsymbol{P'}_{\boldsymbol{corr}})$ is the n-dimensional normal density function with mean values of zero, unit standard deviations and the correlation matrix $\boldsymbol{P'}_{\boldsymbol{corr}}$, and $\boldsymbol{J}$ is the Jacobian.

The correlation between any two random variables can be represented as:

$$\rho_{ij} = \frac{cov[X_i X_j]}{\sigma_{Xi}\sigma_{Xj}} = E[Z_i Z_j] = \int_{-\infty}^{\infty}\int_{-\infty}^{\infty} z_i z_j \varphi_2(y_i, y_j; \rho'_{ij}) dy_i dy_j \tag{4.13}$$

where z_i and z_j are normalized random variables and φ_2 is the bivariate normal distribution. Given the correlation between the variables and the marginal distributions of each of the variables it is possible to determine the correlation matrix $\boldsymbol{P'}_{\boldsymbol{corr}} = \{\rho'_{ij}\}$ from the above equation.

The following algorithm was presented by Melchers [151] for the implementation of the FORM method:

1. select an initial check point vector $\boldsymbol{x^*} = \boldsymbol{x}^{(1)}$ (e.g. $\boldsymbol{x}^{(1)} = \mu_X$)
2. use a suitable transformation such as the Nataf transformation as described above to obtain $\boldsymbol{y}^{(1)}$
3. calculate the Jacobian $\boldsymbol{J}$ and its inverse $\boldsymbol{J^{-1}}$
4. calculate the direction cosines α_i
5. calculate the current value of $g(\boldsymbol{y}^{(1)})$
6. calculate the current estimate of β according to $\beta = -\boldsymbol{y}^{*T}.\alpha$

7. calculate the updated co-ordinates of the checking point in $\boldsymbol{y}$ space using the current β value
8. calculate the co-ordinates in $\boldsymbol{x}$ space of the current estimate of the checking point using the reverse transformation
9. repeat steps (2) to (8) until the co-ordinates of the checking point or β stabilize in value.

A modified version of this algorithm has been implemented in Matlab for the analysis of structural elements subject to fire. In the Matlab scripts, the Nataf transformation is carried out once in order to generate the n-dimensional normal distribution. The process then continues as outlined above until the design point has been identified and then the co-ordinates of the design point are found in **x** space and the nominal probability of failure is calculated. An advanced version of FORM exists (known as the Second-Order Reliability Method or SORM) which uses a second order approximation of the limit state surface. SORM has not been implemented in this work.

The FORM procedure was first implemented for the analytical composite beam problem with ten stochastic variables. The results of this implementation were poor and highly dependent on the method of calculating the slope of the limit state surface in u-space. This is due to the non-linearity of the limit state surface. The accuracy of the procedure was also highly dependent on the value of the failure limit. In order to simplify the problem the number of stochastic variables was reduced to two. This produced more accurate results and reduced the level of dependence on the slope of the limit state surface.

4.3.1 Application of FORM

FORM has been implemented in Matlab for two types of structural analysis models: an analytical model of a composite beam and an Abaqus model of a composite beam. A composite beam, similar to the beam described above in section 4.2, is analysed using FORM. A variety of stochastic variables and limit states are examined. The accuracy of the results is checked by comparison with the results of Monte Carlo simulations.

The first example uses the analytical solution to the composite beam described in section 2.4.2. The area of ventilation and the fuel load were taken as the two stochastic variables.

The deflection limit was firstly set at 400mm. The nominal probability of failure calculated using FORM is 43.6%. This compares well with the nominal probability of failure of 42.5% derived from a 10000 run Monte Carlo simulation. The corresponding variance and standard deviation for the Monte Carlo simulation result are 2.44×10^{-5} and 4.94×10^{-3}, respectively. The FORM result is approximately two standard deviations from the Monte Carlo simulation result.

The same example was then examined while treating the length of the beam and the uniformly distributed load as the stochastic variables. The Monte Carlo simulations used to check the accuracy of the FORM analyses consisted of 10000 runs each. The results of these analyses are presented in Table 4.3 below. The variance of the results of the Monte Carlo simulation with the deflection limit set at 370mm is 2.48×10^{-5}. From this value the standard deviation is calculated as 4.98×10^{-3}. The FORM result is over six standard deviations from the result of the Monte Carlo simulation which shows that the FORM result has a relatively poor accuracy. The results of the second Monte Carlo simulation with the deflection limit set to 400mm have a variance 4.188×10^{-6}. This yields a standard deviation of 2.05×10^{-3} and from this it can be seen that the results of the FORM analysis are within three standard deviations of the Monte Carlo simulation result. This is more accurate than the previous example, but it is not sufficiently accurate to be considered reliable.

Table 4.3: Comparison of analysis results for different deflection limits.

Deflection Limit (mm)	$p_{f,N}$ from FORM	$p_{f,N}$ from Monte Carlo simulation
370	49.1%	45.9%
400	4.9%	4.4%

A similar procedure was employed to analyse the accuracy of FORM when used with an Abaqus finite element model of the composite beam. The two stochastic variables were taken as the length of the beam and the uniformly distributed load. The deflection limit was set at 10mm. The nominal probability of failure calculated using FORM is 13.4%, compared to a nominal probability of failure of 12.2% derived from a Monte Carlo simulation. The variance of the Monte Carlo result is 2.14×10^{-4} and the resulting

standard deviation is 0.015. The FORM results therefore fall within one standard deviation of the results of the Monte Carlo simulation. In this case, the FORM result can therefore be judged as accurate.

These results show that FORM is capable of predicting the probability of failure of highly simplified structural fire engineering problems, albeit with limited accuracy. However, the engineering problems encountered in practice typically exhibit a much greater level of uncertainty than that considered in the examples above. As noted previously, the procedure is not as accurate when further uncertainty is introduced to the problem. Also, FORM lacks a method for the easy verification of the accuracy of the calculated probability of failure. These two drawbacks of FORM mean that it is not a suitable method for the analysis of practical structural fire engineering problems.

4.4 Summary

In this chapter, a variety of methods for conducting probabilistic analysis have been examined. These methods form the basis of reliability analysis and quantitative risk analysis. The crude Monte Carlo method has been identified as an accurate and robust method that is well suited to the analysis of structural fire engineering problems. The main disadvantage of the Monte Carlo method is that it is computationally demanding, particularly when large models are used (e.g. finite element models for thermomechanical analysis). The computation cost can be greatly reduced through the use of simple, analytical models. Latin hypercube sampling is proposed as a suitable sampling method for increasing the rate of convergence of the Monte Carlo method. Importance sampling has also been examined as a means of improving the rate of convergence of Monte Carlo simulations, however it is not suited to problems with a large number of stochastic variables. Subset simulation is a promising method for improving the rate of convergence of Monte Carlo simulations and is an excellent topic for further research.

One-at-a-time sensitivity analyses were carried out on composite beams and composite slabs in order to identify the important variables that require a stochastic definition. The results of Monte Carlo simulations of composite beams and slabs are presented. The

inputs to these simulations are based on the results of the sensitivity analyses and were sampled using Latin hypercube sampling.

The First-Order Reliability Method (FORM) is examined as an alternative to the Monte Carlo methods. FORM is a first-order method as it uses a linear approximation of the limit state surface. FORM defines the nominal probability of failure based on the safety index β, where β is the shortest distance from the origin to the limit state surface in u-space. The main advantage of FORM is that it is less computationally demanding than the Monte Carlo method. Disadvantages of the FORM method are that it cannot cope with a large number of variables, it is not always accurate and the accuracy of the final answer is unknown. Due to these drawbacks, FORM is of limited use to structural fire engineers. An example of FORM applied to the analysis of a composite beam subject to fire is shown.

Chapter 5: The PEER-PBEE Framework and its Application to Structural Fire Engineering

5.1 Preamble

This chapter looks at the development of a probabilistic framework for the performance-based design of structures in fire. This framework is based on an existing framework developed by the Pacific Earthquake Engineering Research center (PEER) for undertaking performance-based earthquake engineering (PBEE). The framework provides the design team with information on the various costs associated with different design options. The PEER framework follows a four stage linear process from hazard analysis to structural analysis to damage analysis and on to loss analysis. Each of the stages is represented by a single parameter.

The framework has been applied to performance-based structural fire design. The hazard analysis stage considers the occurrence and magnitude of potential fires in the structure. A suitable intensity measure (IM) is identified to represent the magnitude of the hazard in the next stage of the analysis. A range of structural models are presented for use in the structural system domain. Engineering demand parameters (EDPs) are presented for different structural members that capture the effect of the fire on the structure. Damage measures (DMs) are chosen to represent the level of damage done to the structure by the EDPs and fragility functions are developed to enable to estimation of the damage state the structure is in. Finally decision variables (DVs) are presented for estimating the fire related costs associated with the structure. The decision variables considered are the monetary cost of repair and the downtime due to repair.

An example office building is presented and two structural elements from the building are analysed under the proposed framework. A second example building is analysed to illustrate the application of the developed framework to a structural sub-assembly.

5.2 Background to the PEER Method

The Pacific Earthquake Engineering Research center (PEER) framework has been developed as a performance-based earthquake engineering (PBEE) methodology for buildings and bridges [125], [169]–[171]. The framework relates the earthquake hazard to a range of performance metrics. Traditionally engineers have used parameters such as stress, strain or deformation in order to classify the performance of a structure. These parameters are useful in deciding if a design is safe under a set of design loads, but they tell us little about the level of safety of a design and they tell us less about the likely performance of the structure over its design life. The PEER framework uses a linear four stage process to predict the likely level of performance metrics based on the earthquake hazard, as shown in Figure 5.1. This process is expressed mathematically as follows [125]:

$$\lambda_{DV}(DV > dv) = \int\int\int P(DV > dv|DM = dm)|dP(DM > dm|EDP = edp)| \\ |dP(EDP > edp|IM = im)||d\lambda(IM > im)| \tag{5.1}$$

where $\lambda_{DV}(DV > dv)$ is the mean annual frequency of exceedance of a decision variable, DV is a decision variable, $P(DV > dv|DM = dm)$ is the probability of exceedance of the decision variable conditioned on the damage measure, DM is a damage measure, $P(DM > dm|EDP = edp)$ is the probability of exceedance of a damage measure conditioned on the engineering demand parameter, EDP is an engineering demand parameter, $P(EDP > edp|IM=im)$ is the probability of exceedance of an EDP conditioned on the intensity measure, IM is an intensity measure and $\lambda(IM > im)$ is the mean annual frequency of exceedance of an intensity measure.

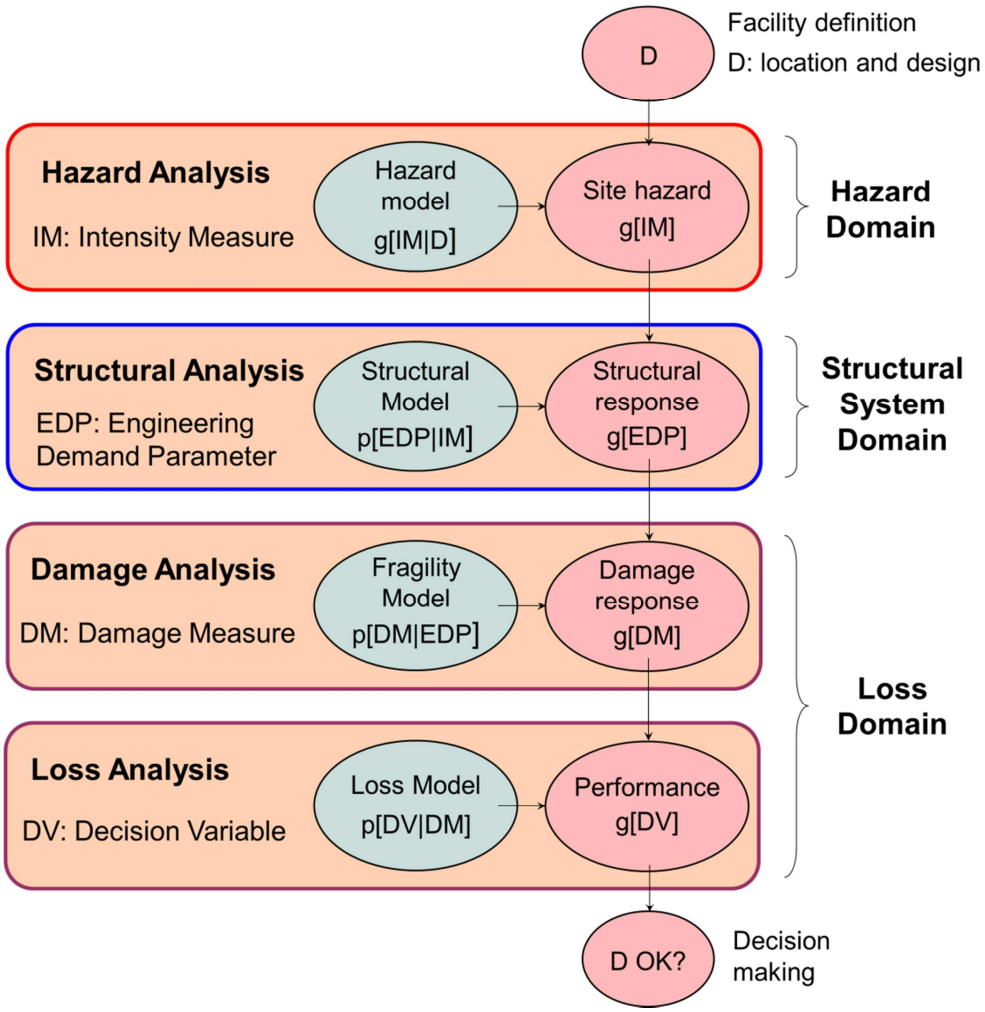

Figure 5.1: Flowchart of the PEER framework (adapted from [8]).

The first stage of the analysis lies within the hazard domain. Hazard analysis involves calculating the range of earthquake magnitudes and their associated likelihood of occurrence for a given structure. Other performance-based design frameworks, such as AB-083 from the Structural Engineers Association of Northern California or the Tall Buildings Initiative from the PEER center, require that a structure is checked under three performance-based criteria: immediate occupancy, life safety and collapse prevention [119], [121]. The immediate occupancy criterion requires that a structure be undamaged and suitable for re-use immediately subsequent to minor, relatively frequent earthquakes. The life safety criterion states that the structure should be able to withstand a larger earthquake (typically of an intensity equal to two thirds of the maximum considered earthquake) without posing a significant risk to life. Collapse prevention requires that the

building be designed to withstand a large infrequent earthquake, referred to as the maximum considered earthquake. These types of limits constitute an approximate relationship between structural response and the performance of the structure. The PEER framework, in contrast, considers the full range of earthquake loads that may occur. The seismic demand placed on a structure is a highly variable parameter. The seismic demand is dependent on the magnitude of the earthquake, the frequency of occurrence, the type of fault rupture mechanism, the path from the focus to the site of the structure and the soil conditions at the site [115], [172]. The random occurrence of an earthquake may be defined using the homogeneous Poisson process. The seismic demand can therefore be evaluated based on a combination of historical records and modelling work. Intensity measures are the output of a hazard analysis and they are presented as hazard curves. The hazard curve shows the probability of exceedance of a given value of intensity measure from the range of possible intensity measures [173], [174].

The annual rate of exceeding a given intensity is given by:

$$R(IM > im_i) = \sum_{n=1}^{N} r_n P_n(IM > im_i) \tag{5.2}$$

where N is the number of earthquake scenarios under consideration, r_n is the annual rate of occurrence and $P_n(\mathrm{IM}>\mathrm{im_i})$ is the probability of exceeding a given intensity were the scenario to occur. $P_n(\mathrm{IM}>\mathrm{im_i})$ is also known as the complementary cumulative distribution curve for IM. Using the Poisson distribution, the probability of exceeding a level of intensity over the design life of the building given the annual rate is then given as:

$$\lambda(IM > im_i) = 1 - e^{-R(IM>im_i)T_D} \tag{5.3}$$

where T_D is the design life of the building in years.

The intensity measures represent the link between geologists and structural engineers. Typical parameters used for earthquake intensity measures are peak ground acceleration/velocity, spectral acceleration/velocity or some other normalised parameter [175]. The chosen IM should satisfy two conditions, “efficiency” and “sufficiency”. An efficient IM is defined as an IM that produces little variability in the resulting damage measure given the IM. This has the effect of reducing the number of simulated hazards required to accurately estimate $P[DM|IM]$. A sufficient IM is defined as one that renders

the damage measure conditionally independent of the earthquake scenario, given IM. An insufficient IM will therefore result in dependence between the DM results and the earthquake scenarios chosen as input.

The second domain in the analysis framework is the structural system domain. In this domain the effects of the hazards identified in the hazard analysis are applied to a structural model in order to evaluate the response of the structure. Geometrically and materially nonlinear time-dependent finite element models are frequently used to model the structure due to the complex geometry of typical structures, the occurrence of large deformations, the cyclic loading and the significant stiffness degradation that can occur in the structural elements [176], [177]. The output of the structural analysis model is characterised by a single parameter, the engineering demand parameter (EDP). The nature of the EDP depends on the type of analysis, the type of structure, the failure mechanism under consideration and on the chosen performance metric [178]. The chosen structural analysis method must be capable of accurately calculating the EDPs. Also, the EDPs must be a suitable predictor of the damage caused by the response of the structure to the hazard. Typical EDPs for building structures include storey drift, floor accelerations or plastic deformation. Bridge structures on the other hand may consider parameters such as peak lateral pier drift (as a measure of the likelihood of flexural failure of the pier) or shear key deformation (as a measure of the likelihood of shear key failure) [179]. The uncertainties in the hazard model and the variability in the IM to EDP response are captured by integration of the hazard curve over the conditional probabilities of $P(EDP|IM)$ for the relevant range of IMs. This process yields the following equation for the mean annual probability of the EDP exceeding a given EDP value [125].

$$\lambda(EDP > edp_i) = \int P[EDP > edp_i | IM = im_i] | d\lambda(IM > im_i) | \tag{5.4}$$

The third domain of the framework is the loss domain which covers both damage analysis and loss analysis. The level of damage inflicted on a structure is calculated from the EDP records. The damage is then expressed using damage measures (DMs). Damage measures are generated for all of the elements (either structural or non-structural) under consideration. A common example is that of a stud wall with plasterboard facing. A set of fragility curves for this example is shown in Figure 5.2.

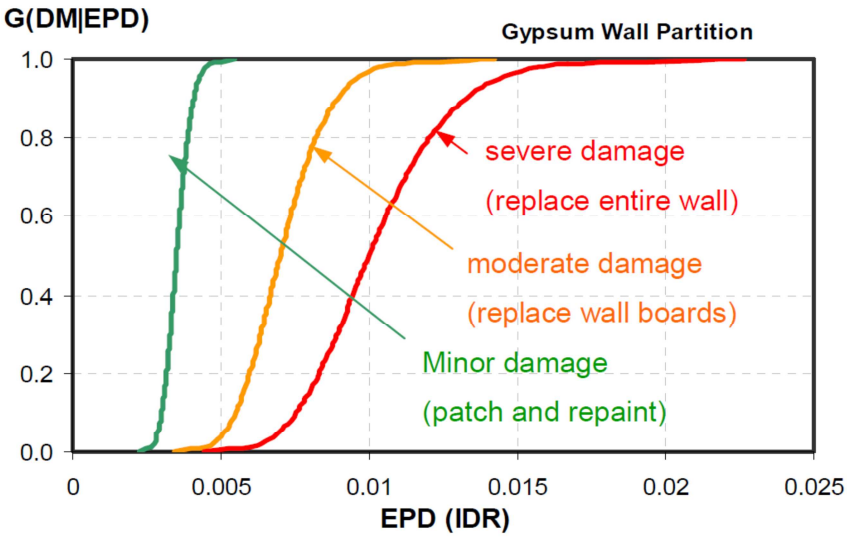

Figure 5.2: Example of EDP to DM fragility curves for gypsum wall (taken from [125]).

Figure 5.2 shows the four damage states that are considered; no damage, minor damage, moderate damage and severe damage. Each damage state corresponds to an expected level of damage and repair procedure, e.g. minor damage is described as cracking at the joints, cracking around openings and connector damage. The repair of minor damage typically consists of taping, applying filler to cracks and re-painting the partition. Fragility functions such as these are typically derived from the statistical analysis of experiments on specific building components under simulated earthquake loading.

Once the level of damage to the structure and the method of repair are determined a loss analysis is conducted. Typical loss parameters considered under the framework are casualties/fatalities, financial loss and repair time. The evaluation of the risk of casualties or fatalities is a complicated process that requires considering both the probable occupancy of the structure at the time of the earthquake and the level of damage done by the earthquake. The monetary loss due to earthquake loads may be evaluated by several different procedures. The component-based loss estimation method is the most common methodology and is fully described in Ramirez and Miranda [180]. Under the component-based method the structure is divided into components and the total loss is taken as the sum of all of the components [181]. A probability distribution is assigned to each component to capture the variation in the level of losses. The mean monetary cost of a component is calculated using construction cost estimating. The distribution type

and variance of the monetary loss are determined based on statistical data collected from construction companies [182]. The distributions for downtime are likewise calculated from a combination of construction scheduling methods and statistical data. The variance of the loss parameters is difficult to calculate accurately due to the scarcity of available cost data. Typical component groups are beams, columns, connections, partitions, finishes, glazing, sprinklers, etc. The level of refinement in the component groups is based on the level of detail available from both the cost data and the structural response model. Once distribution parameters have been assigned to each component, the cumulative distribution function for each component may be plotted, otherwise known as cost consequence function.

The expected losses conditioned on the intensity measure can then be described as the sum of the expected losses due to collapse multiplied by the probability of collapse and the expected losses due to non-collapse/repair multiplied by the probability of non-collapse [180].

$$E[L_e|IM] = E[L_e|NC, IM]P(NC|IM) + E[L_e|Coll]P(Coll|IM) \quad (5.5)$$

where $E[L_e|NC,IM]$ is the expected loss given collapse does not occur at an intensity level of IM, $P(NC|IM)$ is the probability of non-collapse at an intensity level of IM, $E[L_e|Coll]$ is the expected loss given collapse and $P(Coll|IM)$ is the probability of collapse conditioned on the intensity measure.

The loss outputs may be presented in different formats, depending on the interests of the designer. The costs may be shown as an exceedance curve which specifies the probability of the earthquake losses exceeding a specific cost, either per annum or over the design life of the structure. Alternatively the costs may be presented as an expected annual loss or the expected loss given a specific earthquake scenario occurs [183].

The PEER framework is now well established within the earthquake engineering community. A comprehensive set of guidelines outlining the framework has been published by FEMA in order to help engineers implement the framework, help researchers identify areas for improvement and to help code developers incorporate ideas from the framework into future codes [184], [185]. The application of the framework has also spread beyond earthquake engineering [186]. Ciampoli, Petrini and Augusti have adapted the framework to performance-based wind engineering and have presented examples of the framework applied both buildings and bridges [187], [188]. The

framework has also been applied to tall buildings subject to wind loading by Clannachan [189].

5.3 Application of the PEER Method to Structural Fire Engineering

The PEER framework was firstly applied to individual structural elements during the course of this work. The structural elements chosen for analysis were a composite beam and a composite slab. The hazard was taken to be a fully developed compartment fire and the possibility of fire spread outside of the compartment was not considered. Adapting the framework required identifying and investigating potential intensity measures that would accurately capture the intensity of a compartment fire. Engineering demand parameters for both types of structural element were then chosen based on the information required for estimating damage and the capabilities of the structural model. Fragility functions were developed as part of this work which allows the estimation of the level of damage done to the structure given a specific demand has been placed on the structural element. The decision variables that are examined in this work are monetary cost and downtime due to repair work. The occurrence of injuries or fatalities is a common and important decision variable that is frequently examined in the course of performance-based earthquake engineering however it is not considered in this work. The estimation of the likelihood of fatalities or injuries would require a coupled model to evaluate the production of toxic species, the movement of smoke, the likely occupancy level in the building at the time of a fire and the egress paths and egress times for the occupants. The estimation of fatalities or injuries is therefore outside the scope of this work.

5.3.1 Hazard domain

The hazard considered in this work is a fully developed compartment fire. Localised fires or smouldering fires may also occur in buildings and may result in substantial damage but they are unlikely to lead to large scale collapse of the structure. The Eurocode parametric fire, as described in section 2.2.2, is used as the fire model in this work as it is capable of accounting for variation in the compartment geometry, enclosure boundary materials, fuel load and ventilation. The parametric fire is therefore capable of

capturing a wide range of fires that could potentially occur within the fire compartment. The parametric fire is computationally light and because of this a large number of fires may be easily simulated when conducting an analysis.

In order to describe the hazard in a suitable manner for probabilistic assessment it is necessary to define two separate parameters, namely the frequency of occurrence and the magnitude or intensity of the hazard. The rate of occurrence of a structurally significant fire may be calculated using the event tree analysis method described in the Natural Fire Safety Concept and shown in Figure 5.3 [190].

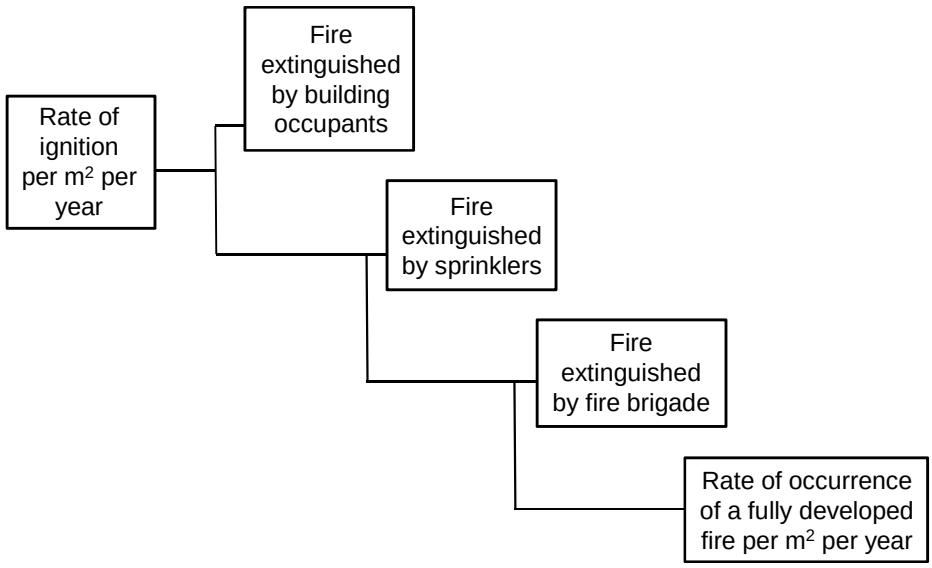

Figure 5.3: Event tree analysis of fire development in a typical building.

The event tree process may be expressed mathematically as:

$$r_{fi} = A_{fi} \times p_1 \times p_2 \times p_3 \times p_4 \quad (5.6)$$

where r_{fi} is the mean annual rate of occurrence of a structurally significant fire, A_{fi} is the area of the fire compartment, p_1 is the probability of a severe fire (accounting for the actions of occupants and the standard fire brigade) per m^2 of floor area and per year, p_2 is the probability of the fire brigade failing to stop the fire, p_3 is a reduction factor to account for the effect of automatic fire detection and alarm transmission and $p4$ is a reduction factor to account for the effect of a sprinkler system. The factors p_1 to p_4 are derived from historical data. p_1 provides the probability of a sever fire occurring. p_2 to p_4 are reduction factors which reduce the overall probability of a fire occurring. For

example, a better fire detection system would lead to earlier detection of a fire and a swifter response from the fire brigade. This would reduce the likelihood of a fire growing into a fully developed fire. This is reflected in the p_3 values. A building with no active fire detection measure would have a p_3 factor of 1 whereas a building with smoke detectors would have a p_3 value of 0.0625. Using this method the mean annual rate of occurrence of a structurally significant fire may be calculated for compartments of any size and various occupancy types.

The intensity of a fire which occurs in the compartment is the second parameter required in the analysis. There are a number of factors which may be considered for use as the intensity measure of a fire, such as peak compartment temperature, time to peak temperature, rate of temperature increase within the compartment, equivalent time of fire exposure or temperature of a structural element. A variety of intensity measures have been considered in this work as the choice of intensity measure is a key part of the PEER process. If the intensity of the hazard cannot be accurately quantified, the magnitude and rate of occurrence of structural responses cannot be quantified and the inaccuracy is carried through to the end of the process.

One of the earliest attempts at quantifying the severity of a fire was introduced by Ingberg's equal area concept [11]. Under Ingberg's procedure the area under a temperature-time curve is related to the area under the standard temperature-time curve in order to define an equivalent length of exposure to the standard curve. This method is a crude approximation of severity that ignores the temperature dependent nature of construction materials, the nonlinear variation of the radiative heat flux with temperature and the distribution of thermal forces within a structural element. Due to these shortcomings the equivalent time of fire exposure is not seen as a suitable intensity measure.

The use of the maximum steel temperature has previously been suggested as a potential intensity measure by Hamilton and others [5], [186], [191]. The maximum steel temperature is a suitable intensity measure where the steel members are the dominant load carrying elements. However the temperature of the steel is clearly dependent on the nature of the structure and as such may be considered as a structural response parameter rather than a hazard intensity measure. Using the steel temperature as intensity measure creates difficulty in a structure composed of steel columns, primary beams and

secondary beams, each of which may have a different level of fire protection. For example the secondary beams may be unprotected and therefore very hot, but the consequences of failure of a secondary beam are minor relative to failure of a column or even a primary beam.

The rate of temperature increase within a compartment directly affects the distribution of temperatures within a structural member and therefore it affects the distribution of thermal forces within a member. However the rate of temperature increase does not provide any information on the peak temperature of a fire or on the duration of a fire, both of which may be expected to have a greater impact on the structural response.

The peak compartment gas temperature has been chosen as the intensity measure for use in this work. The peak gas temperature is a suitable intensity measure for non-insulated or lightly insulated structures. It is also a useful intensity measure for practicing engineers as performance based design is often used in practice to justify the omission of fire protection on secondary beams in order to produce a more economical design. Figure 5.4 below shows the efficiency of peak compartment temperature as an intensity measure in predicting the response of a structure. Figure 5.4 show a negligible level of variability in the structural response given a specified level of intensity measure. Figure 5.5 shows the efficiency of the time taken to reach the peak compartment temperature as a predictor of the structural response. It is clear that the time to peak compartment temperature is not a useful intensity measure for un-insulated structures.

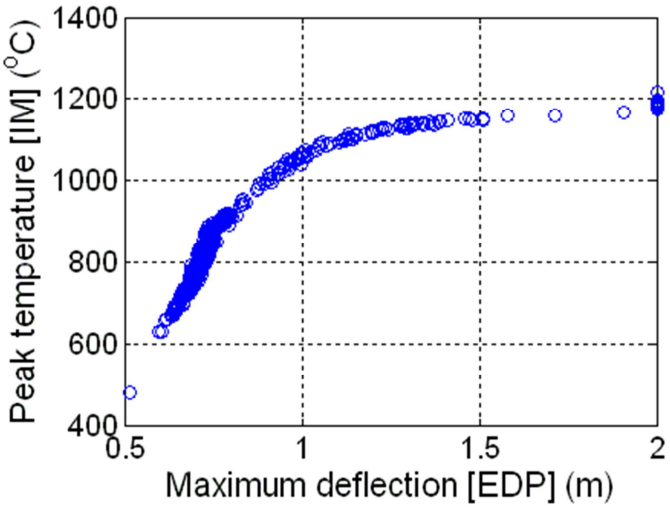

Figure 5.4: Peak compartment temperature as a predictor of EDP, for an un-insulated composite beam.

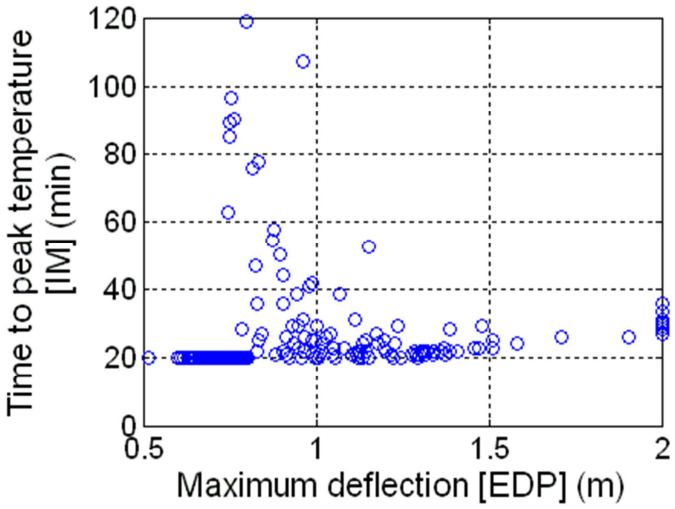

Figure 5.5: Time to peak compartment temperature as a predictor of EDP, for an un-insulated composite beam.

The peak compartment temperature is not an ideal intensity measure for well-insulated structures as they are more resilient to the large, brief temperature increases that are associated with short-hot fires. In the case of a well-insulated structure it is reasonable to assume that a long-cool fire will have a much greater effect than a short-hot fire. Figure 5.6 and Figure 5.7 below show the efficiency of peak compartment temperature and the time to peak compartment temperature in predicting the structural response. It can be seen that the time to peak compartment temperature provides a more efficient intensity measure for the well-insulated beam. An alternative approach to capturing the intensity of the hazard would be to use a vector of intensity measures. In this way both the peak temperature and the time taken to reach the peak temperature could be considered when evaluating the intensity of the hazard.

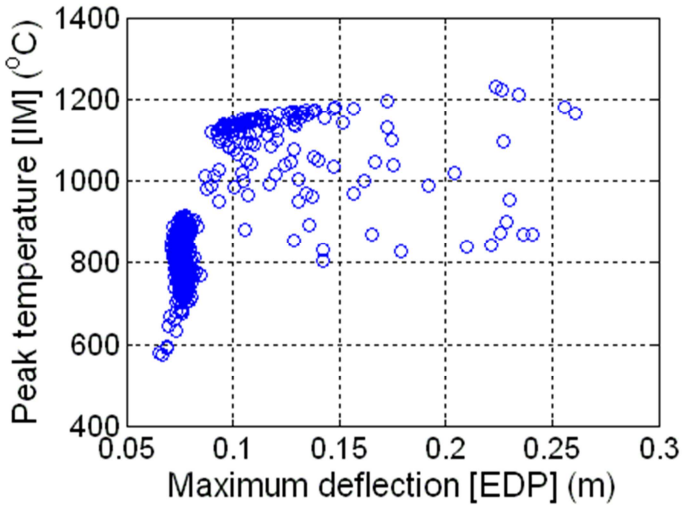

Figure 5.6: Peak compartment temperature as a predictor of EDP, for a well-insulated composite beam.

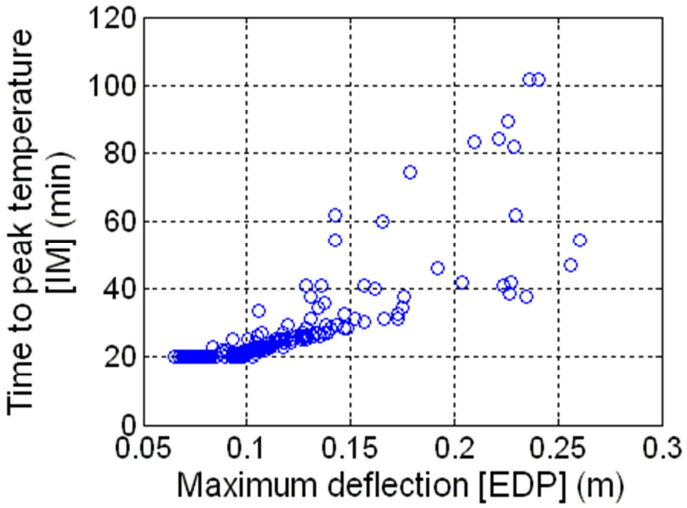

Figure 5.7: Time to peak compartment temperature as a predictor of EDP, for a well-insulated composite beam.

In order to generate the intensity measure hazard curve a large number of simulations of the hazard are required in order to get a realistic range of intensity measure results. The range of hazards is examined through the use of a crude Monte Carlo simulation, using the stochastic input definitions described in section 2.2.1. The peak temperature is taken from each run in the Monte Carlo simulation and a probability mass function is

generated, as shown in Figure 5.8. The probability mass function of the intensity measures will vary in shape depending on the type of distributions and the distribution parameters chosen for the inputs.

Figure 5.8 shows a bimodal distribution of the peak temperature results. The bimodality occurs in part due to the nature of the parametric temperature-time curve. The parametric temperature-time curve sets the length of time until the peak temperature occurs based on whether the fire is assumed to be fuel controlled or ventilation controlled. This leads to two separate types of fire. The bimodal distribution of peak temperatures will not occur if the mean of the inputs heavily favours either burning regime.

A range of probability density functions, such as the normal, Weibull or Gumbel distributions, are fitted to the probability mass function using maximum likelihood estimation. The best fitting distribution is then chosen to represent the distribution of peak temperatures based on a chi-squared goodness-of-fit test.

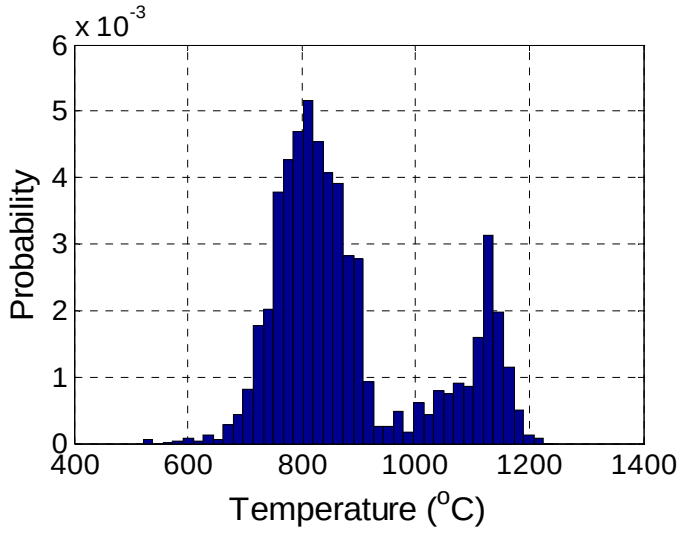

Figure 5.8: Probability mass function of the intensity measure results.

The probability of the temperature being less than or equal to a given temperature can be found by integrating the probability density function to yield the cumulative distribution function of the peak temperatures. The probability of a given temperature being exceeded is found from the complementary cumulative distribution function which is taken as one minus the cumulative distribution function. The total probability theorem is then used to construct the intensity measure hazard curve:

$$\lambda(IM > im_i) = r_{fi} \times P\left(T_{peak} > T_{peak,i} | F.O.\right) \quad (5.7)$$

where $\lambda(IM \geq im_i)$ is the mean annual rate of exceedance of a given intensity measure, r_{fi} is the mean annual rate of a structurally significant fire occurring, T_{peak} is the peak temperature of a fire, *F.O.* denotes the occurrence of a fire and therefore $P(T_{peak} \geq T_{peak,i} | F.O.)$ is the probability of the peak temperature being greater than a specific value given that a fire occurs.

5.3.2 Structural system domain

The level of structural response induced by the hazard is a critical feature in determining the level of damage done to the structure. The structural response must be accurately calculated in order to estimate the level of damage. Simple structural analysis methods that predict only the occurrence of structural failure are not suitable for predicting the wide range of damage that may occur. Conversely, the structural analysis method should not be overly complicated as this can lead to very long simulation run-times and impedes the use of the PEER framework in practice. The analysis of a structure subject to fire requires the use of two separate types of model, a heat transfer model and a structural analysis model. The heat transfer models used in this work are lumped capacitance models for both protected and un-protected steelwork and a one-dimensional finite difference model for concrete slabs, described in detail in section 2.3. Temperature dependent material parameters are used where required. The results of the sensitivity analysis in section 4.2.4 show the importance of the heat transfer process in the analysis of structures subject to fire. It is important that the varying effect of the fire on the structure is accurately captured by the structural model.

A number of structural analysis models have been examined as part of this work, including various analytical models and finite element models. Analytical models, such as the method of slices and Cameron's method, are quick to run and do not suffer from convergency problems when the input parameters are varied. The method of slices was chosen as the model for protected composite beams as it is suited to low levels of deflection and Cameron's method was chosen for unprotected beams as it is more suited to large deflections. The engineering demand parameter (EDP) chosen for composite beams is the vertical deflection at the midspan of the beam. The midspan deflection provides information on the level of damage done to the structure and on the likelihood

of collapse. Other parameters examined as potential EDPs include strain in the steel beam and strain in the reinforcement mesh in the concrete slab. The strain in the steel beam was rejected as an EDP for two reasons:

- A beam in a composite structure subject to fire may exhibit large strains due to restrained thermal expansion long before the beam reaches failure.
- It is not possible to quantify localised strains with the implemented analytical models.

The strain in the reinforcement mesh was rejected as an EDP as:

- The reinforcement mesh does not control the behaviour of a composite beam if the steel beam is relatively stiff and/or well insulated with fire protection.

The engineering demand parameter chosen to represent the demand placed on a concrete slab in a composite structure is the strain in the reinforcing mesh. The rebar strain was chosen as the EDP as:

- Concrete slabs in fire suffer from large deflections and are therefore dependent on tensile membrane action as the primary load carrying mechanism. Tensile membrane forces are carried through the reinforcement mesh as concrete is very weak in tension.
- The strain in the reinforcement mesh provides a clear indication of the level of damage done to the slab and the possible occurrence of failure.

In order to quantify the demand placed on the structure, the structural response to each individual realisation of the hazard identified in the hazard domain is calculated. The EDP exceedance curve may be derived from the following expression, where the complementary cumulative distribution function associated with each step of intensity measure is integrated with respect to the probability of exceedance of the intensity measure

$$\lambda(\delta > \delta_i) = \int P\left(\delta > \delta_i | T_{peak}\right) | d\lambda_{IM} | \tag{5.8}$$

where $\lambda(\delta>\delta_i)$ is the mean annual rate of exceedance of a given engineering demand parameter, $P(\delta>\delta_i|T_{peak})$ is the mean annual rate of exceedance of a given engineering

demand parameter conditioned on the intensity measure and $d\lambda_{IM}$ is the change in the intensity measure hazard curve.

5.3.3 Loss domain

The loss domain may be divided into damage analysis and loss analysis. Damage analysis is the calculation of the extent of the damage caused to the structure and its contents given that a specific value of the engineering demand parameter has occurred. Loss analysis is the calculation of the loss in terms of monetary loss, downtime or injuries given that a certain level of damage has occurred. In this work the damage and resulting losses associated with the non-structural elements of the structure and the contents of a structure are not evaluated, though it would be reasonable to assume that any contents in a room subject to a fully developed fire will be either completely destroyed or damaged beyond repair. The damage done to the structure is categorised through the use of fragility functions.

Fragility functions express the conditional probability of incurring a damage state of an element given a specific value of the engineering demand parameter (Figure 5.9). Fragility functions may be constructed for both structural and non-structural elements. There is a lack of experimental or field measurements required for the construction of detailed fragility functions. Fragility functions for a composite beam in fire have been developed as part of this work by considering the likely levels of repair of the beam [192], [193]. If the beam is relatively undamaged by the fire then it is conceivable that no structural repair work will be required, in this case the beam may be considered to be in damage state 0. If the composite beam has suffered minor damage, then the repair work may involve removing the steel deck and replacing any damaged concrete as well as applying self-levelling screed to the upper-side of the slab. Major damage to the composite beam will require the demolition of the damaged element and re-construction of the beam. A similar set of repair works was considered in the construction of the fragility function for composite slabs. Due to the lack of experimental results defining the level of variation in the damage done to a beam in fire, it was decided to utilise discrete damage states defined by specific values of engineering demand parameter. *DS1* and *DS2* in Figure 5.9 below are defined as Damage State 1 and Damage State 2, where *DS1* corresponds to minor damage and *DS2* corresponds to major damage. *P[DM|EDP]*

is the probability of a damage measure (*DM*), given a specific *EDP* value. The damage measure may be defined as the probability of a damage state being incurred.

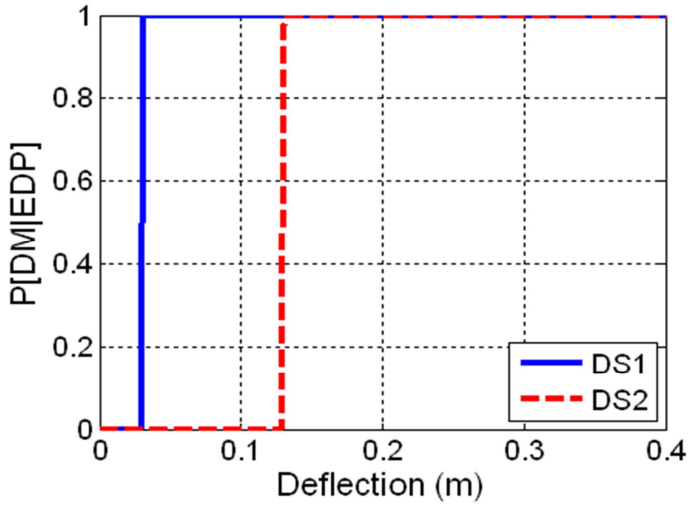

Figure 5.9: Fragility functions based on the deflection of a composite beam.

Cost consequence functions were defined for each possible damage state, as shown in Figure 5.10. The monetary cost consequence functions are based on construction cost estimates for the work required to repair each damage state. Cost data was taken from Spon's price book [194]. Information of the variability of construction costs was taken from Touran and Suphot [182]. The downtime cost consequence functions are based on the use of construction scheduling methods.

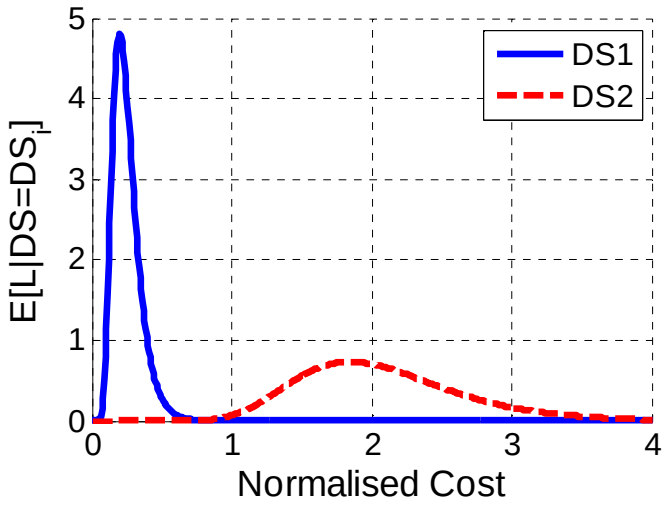

Figure 5.10: Monetary cost consequence functions for a composite beam.

5.4 Example Application of the PEER Framework to a Composite Beam

The adapted PEER framework for performance-based structural fire engineering has been applied to a sub-assembly within a typical office building, Figure 5.11. The building chosen for analysis is taken from the SCI report "Comparative Structure Cost of Modern Commercial Buildings" [165]. The SCI report presents the results of a study into the costs of various construction forms. It provides information on the design brief, the structural layout and the estimated construction costs. The building is rectangular in plan, with a central covered atrium and is eight storeys high. The structure is composed of steel-concrete composite construction with a regular column grid at 7.5 m spacings.

Figure 5.11: Artist's impression of Building B [165].

A partial floor plan of the building is shown in Figure 5.12, with the area of the fire compartment highlighted. The composite beam to be analysed is shown in red. It is a 305 x 165 UB40 section. Two separate design cases are considered in this example, one where the secondary steel beam in the sub-assembly is protected with fire protection and one where no fire protection is used. The fire protection applied to the steel beam consists of two layers of 12mm plasterboard.

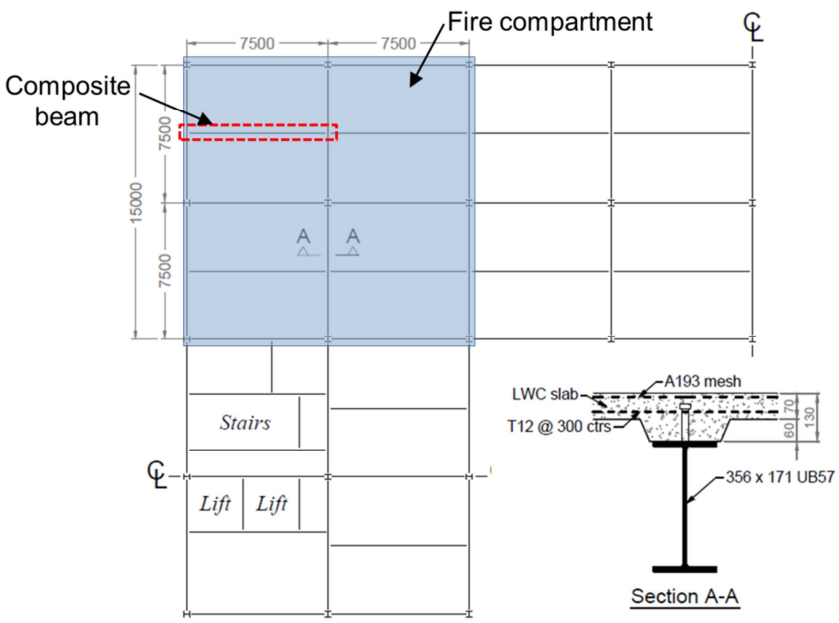

Figure 5.12: Partial building floor plan and typical beam cross section.

The hazard is modelled using the parametric temperature-time curve from Eurocode 1, with both the fuel load and area of ventilation taken as stochastic variables as shown in Table 5.1. The resulting library of design fires from 5000 runs is shown in Figure 5.13.

Table 5.1: Stochastic models for variables used in the fire model.

Variable	**Distribution type**	**Units**	**Distribution parameter 1**	**Distribution parameter 2**
Fuel load	Gumbel	MJ/m^2	363.29 (mode)	98.24 (scale)
Area of ventilation	Truncated log-normal	m^2	60 (upper limit)	0.25 (standard deviation)

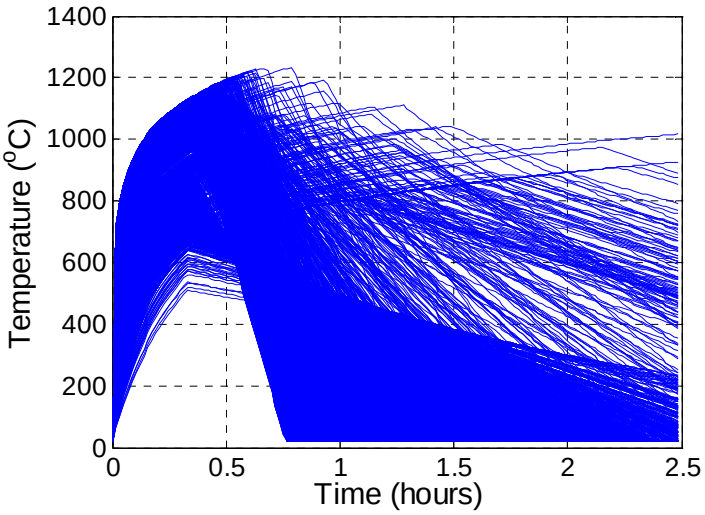

Figure 5.13: Library of possible fires.

The annual probability of occurrence of a structurally significant fire was calculated, according to the procedure outlined in section 5.3.1, to be 4.22 x 10^{-6}. The distribution of peak temperatures from the library of fires is then used, along with the probability of occurrence of a structurally significant fire, to produce the intensity measure hazard curve, shown in Figure 5.14. For this example, the normal distribution is the best fit distribution for the peak temperature results.

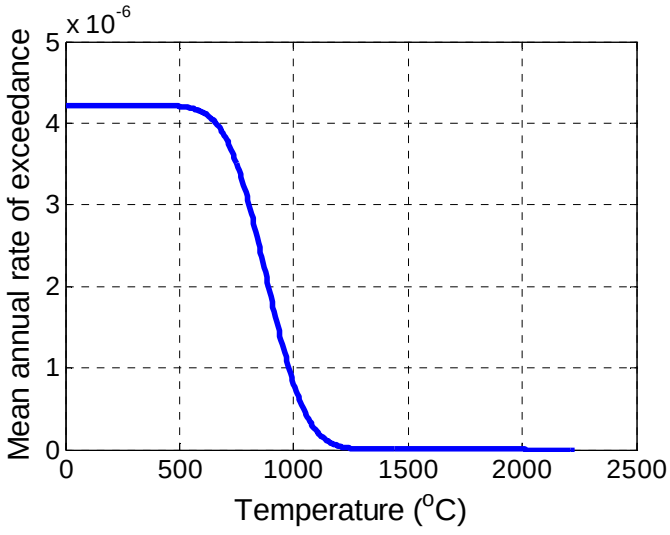

Figure 5.14: Intensity measure hazard curve.

The response of the composite beam was then analysed for each of the temperature-time histories. A number of geometrical and material parameters were taken as stochastic variables. These variables are described in Table 5.2. All other geometrical and material parameters were treated as deterministic variables. The parameters with the greatest associated level of uncertainty are the ones that are taken as stochastic variables. The level of uncertainty associated with each variable was determined based on the results of the sensitivity analyses carried out in Chapter 4 and the variance of each variable. The sensitivity analysis identified which variables produce a large change in the response of the beam with only a small change in the value of the variable. However, the variance of each variable must also be considered as some variables are unlikely to vary even by a small amount, whereas other variables may vary by relatively large amounts. An example of a variable that can produce a large change in the behaviour of the composite beam with only a small change in the value of the variable is the web height of the steel beam. This variable is not treated as stochastic as the dimensions of a steel beam are tightly controlled during manufacture and therefore the variance of the web height is so small as to render the uncertainty associated with the web height negligible.

Table 5.2: Stochastic models for variables used in the heat transfer analysis and structural analysis.

Variable	Distribution type	Units	Distribution parameter 1	Distribution parameter 2
U.D.L.	Gumbel	N/m	5054.9 (mode)	1637.4 (scale)
Length of beam	Log-normal	m	7.500 (mean)	0.005 (C.o.V.)
Depth to the rebar	Gaussian	m	0.04 (mean)	0.02 (C.o.V.)
Young's modulus of steel	Log-normal	kN/mm^2	210 (mean)	0.03 (C.o.V.)
Young's modulus of concrete	Log-normal	kN/mm^2	35 (mean)	0.15 (C.o.V.)
Yield stress of the rebar	Log-normal	N/mm^2	562.3 (mean)	0.07 (C.o.V.)

The heat transfer analysis is carried out using the methods described in section 2.3. The composite beam with fire protection is modelled using the method of slices and the unprotected composite beam is modelled using Cameron's method, as described in section 2.4.2. The deflection results for the protected beam are shown in Figure 5.15. The recovery of deflection as the fire cools has been prevented.

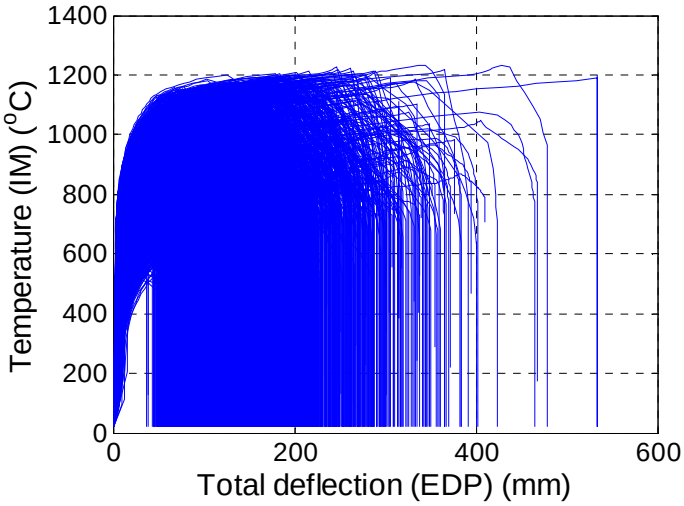

Figure 5.15: Library of deflection records for the protected beam.

The EDP exceedance curves for the protected and unprotected beams are shown below in Figure 5.16. It clearly shows that greater deflections are much more likely to occur when the section is left unprotected.

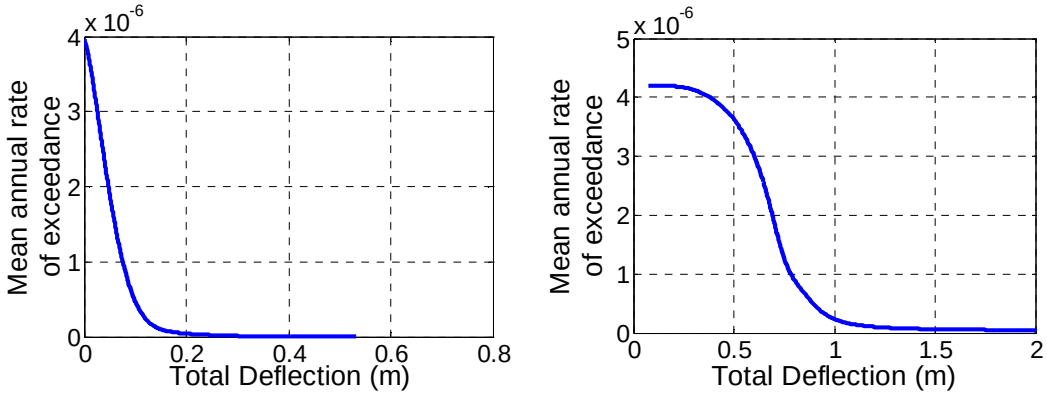

Figure 5.16: EDP exceedance curves for the protected and unprotected sections.

The damage states are based on limiting deflections and are defined in Table 5.3. Major damage is assumed to occur if the deflection exceeds 130mm, which is the overall depth of the concrete slab. Minor damage is assumed to occur when the deflection exceeds

30mm, which is the deflection limit from Eurocode 2 [64]. The generated fragility functions are shown in Figure 5.17.

Table 5.3: Parameters for the fragility functions.

	Distribution type	Units	Mean	Coefficient of Variation
Damage State 1	Gaussian	m	0.03	0.0001
Damage State 2	Gaussian	m	0.13	0.0001

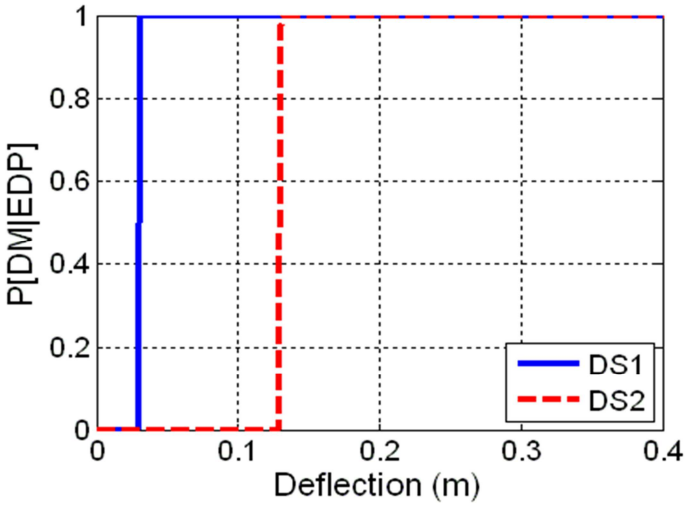

Figure 5.17: Deflection based fragility functions for a composite beam.

Costs for the repair work have been estimated based on the information given in the SCI document and Spon's price book [165], [194]. These costs were then normalised using the initial cost of construction. The distribution parameters for the cost consequence functions are given in Table 5.4 and are shown graphically in Figure 5.18.

Table 5.4: Normalised parameters for the cost consequence functions.

	Distribution type	Mean	Coefficient of Variation
Monetary repair cost of DS1	Log-normal	0.25	1.2
Monetary repair cost of DS2	Log-normal	1.54	0.2
Downtime due to repair for DS1	Log-normal	2.8	0.1
Downtime due to repair for DS2	Log-normal	10.1	0.03

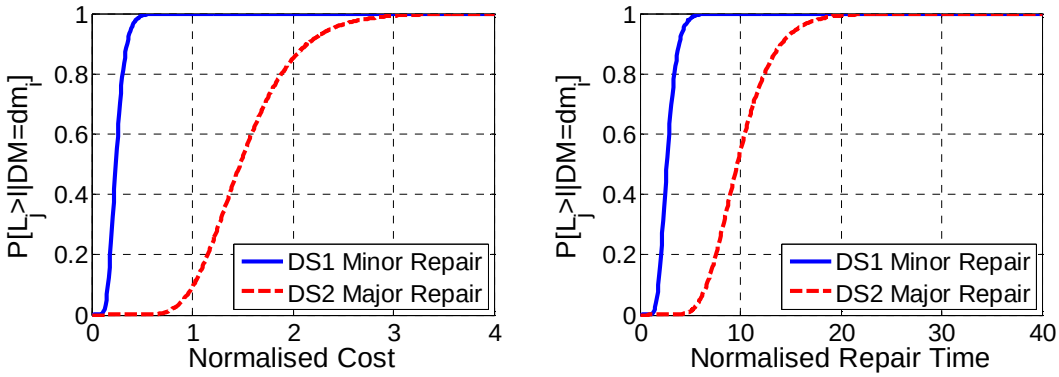

Figure 5.18: Cost consequence functions for a composite beam.

The information from the EDP exceedance curves is then combined with the fragility functions and the cost consequence functions to calculate the annual frequency of exceedance of the decision variables, shown in Figure 5.19 and Figure 5.20. The expected annual loss can be calculated by integrating the mean annual rate of exceedance curve. The normalised expected annual loss is 1.677×10^{-7} and 3.854×10^{-6} for the protected and unprotected beams, respectively.

These results show that the application of fire protection to the beam greatly reduces the likely losses due to fire. The normalised expected annual loss is reduced by a factor of

approximately 23. The improved performance not only affects the repair costs, the downtime due to repair is also significantly reduced by the use of fire protection. An informed choice on whether or not to apply fire protection to the secondary steel beams can now be made by comparing the expected annual monetary loss and the expected losses due to downtime against the fire protection costs.

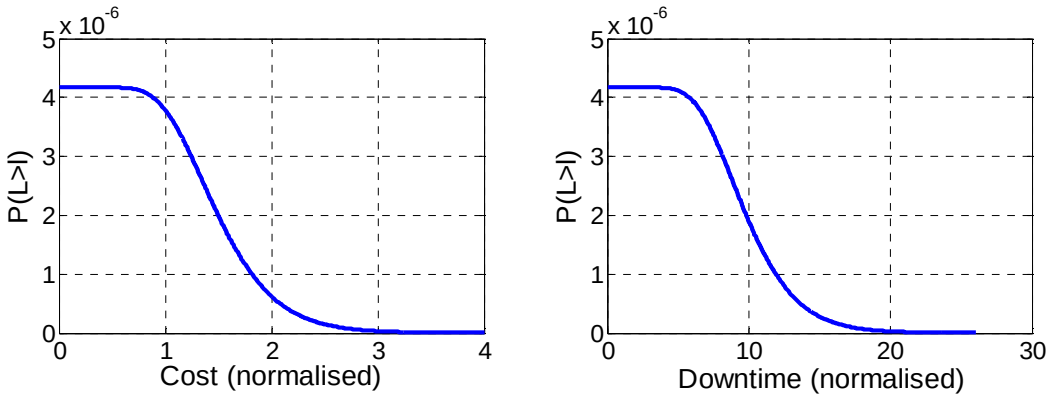

Figure 5.19: Mean annual rate of exceedance curves of monetary cost and downtime for an unprotected beam.

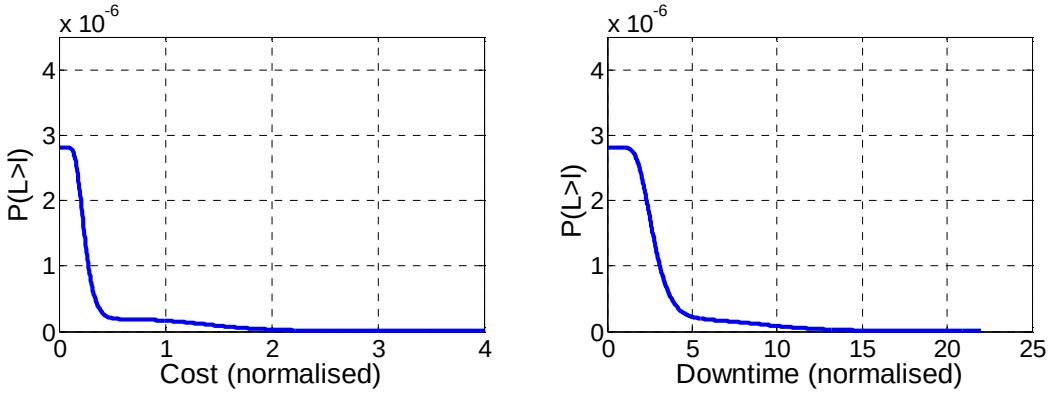

Figure 5.20: Mean annual rate of exceedance curves of monetary cost and downtime for a protected beam.

5.5 Example Application of the PEER Framework to a Composite Slab

The adapted PEER framework has been applied to the analysis of a composite slab sub-assembly. A composite slab from Building B, described in section 5.4, was chosen as the example case. The same design cases were considered, one where the secondary beams

are given fire protection and one where the secondary beams are left unprotected. The location and size of both composite slabs is highlighted in Figure 5.21. The hazard is identical to that outlined in section 5.4 and the parametric fire curve is used to model temperature development. The values used for the stochastic inputs to the fire model are given in Table 5.5.

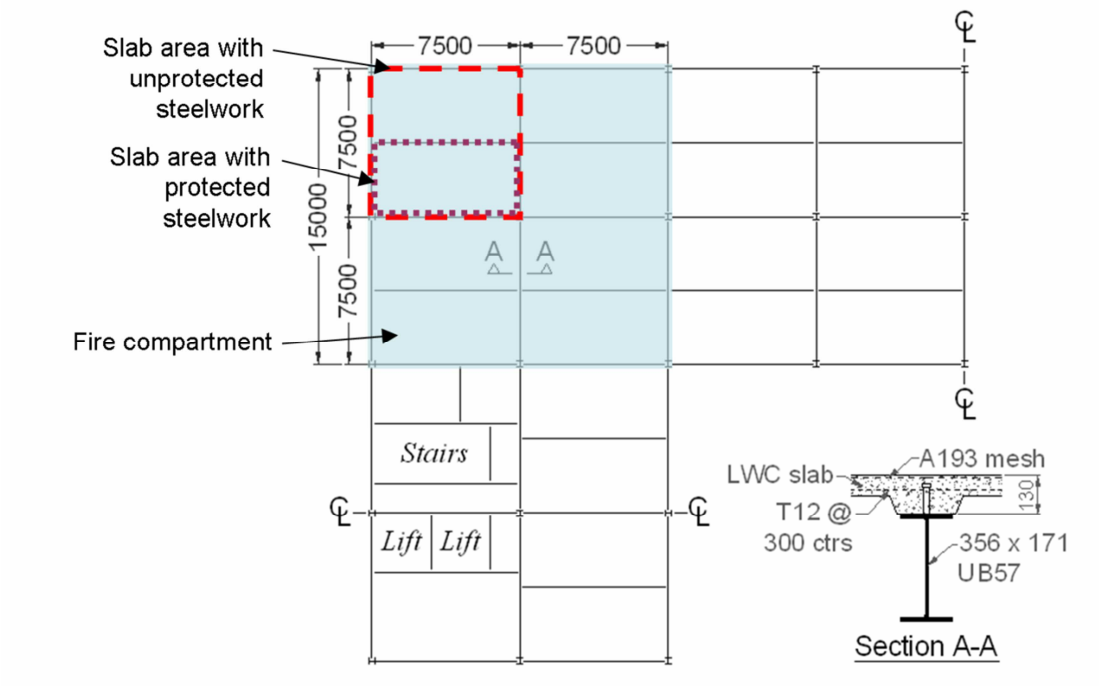

Figure 5.21: Partial building layout and cross-section of the composite slab (adapted from [165]).

Table 5.5: Stochastic models for variables used in the fire model.

Variable	Distribution type	Units	Distribution parameter 1	Distribution parameter 2
Fuel load	Gumbel	MJ/m^2	363.29 (mode)	98.24 (scale)
Area of ventilation	Truncated log-normal	m^2	60 (upper limit)	0.25 (standard deviation)

The resulting library of fires, developed from 5000 runs, is shown in Figure 5.22. It can be seen that the uncertainty of the fire is captured by the stochastic inputs and the fire model. Figure 5.22 shows a wide spread in the range of peak temperatures, times to peak temperature and cooling rates. The calculation of the intensity measure hazard curve is carried out as before using Equation (5.7) and the result is shown in Figure 5.23. The average peak temperature in this example is 850°C.

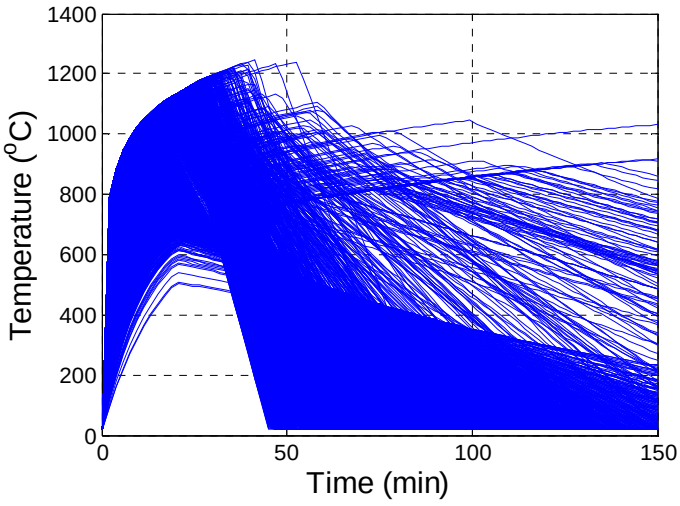

Figure 5.22: Library of temperature-time curves.

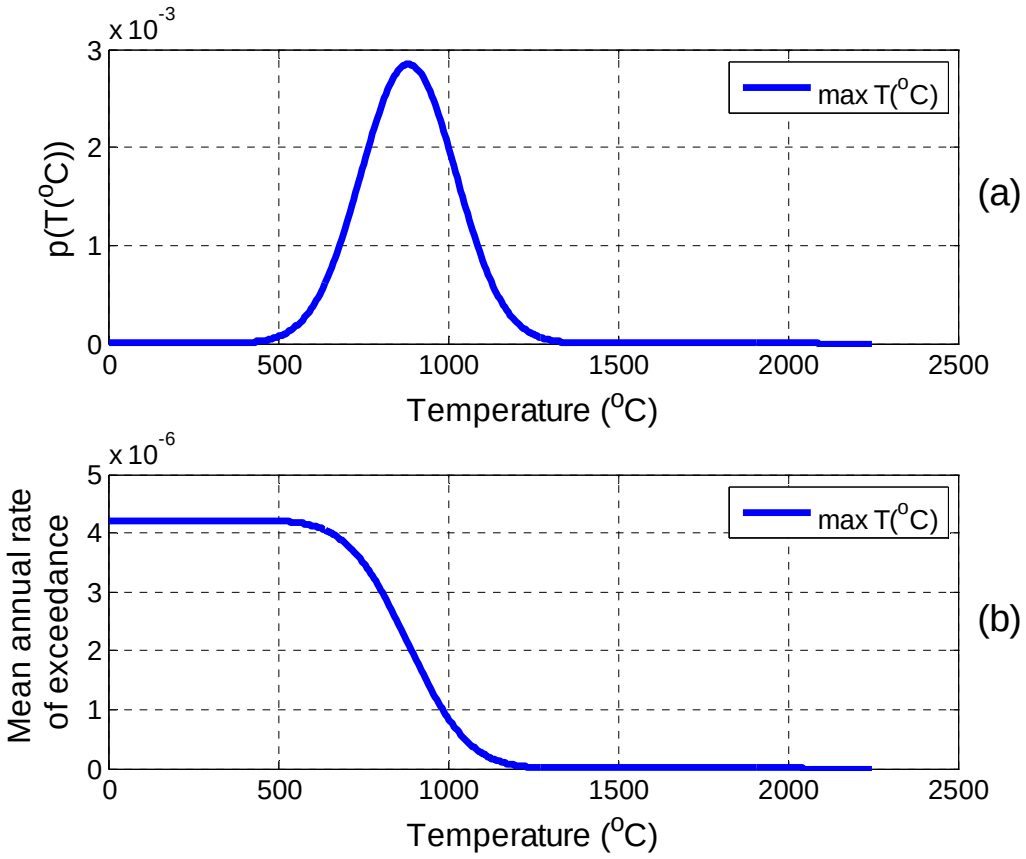

Figure 5.23: (a) Probability of peak temperatures as intensity measure, (b) Intensity measure hazard curve.

The values of the stochastic inputs to the heat transfer and structural analyses are given below in Table 5.6. The heat transfer analysis through the depth of the slab is carried out using the finite difference method described in section 2.3. The structural response of the composite slab is modelled using Cameron's method, as described in section 2.4.2.

Table 5.6: Stochastic models for variables used in the heat transfer analysis and structural analysis.

Variable	Distribution type	Units	Distribution parameter 1	Distribution parameter 2
U.D.L.	Gumbel	kN/m^2	3.7912 (mode)	1.2280 (scale)
Length of slab	Log-normal	m	7.50 (mean)	0.005 (C.o.V.)
Width of slab	Log-normal	m	3.75 or 7.50 (mean)	0.005 (C.o.V.)
Depth to slab	Log-normal	m	0.07 (mean)	0.005 (C.o.V.)
Young's modulus of concrete	Log-normal	kN/mm^2	35 (mean)	0.15 (C.o.V.)

The EDP exceedance curves for both design cases are shown below in Figure 5.24. It can be seen that leaving the secondary beam unprotected leads to higher levels of strain within the steel reinforcement.

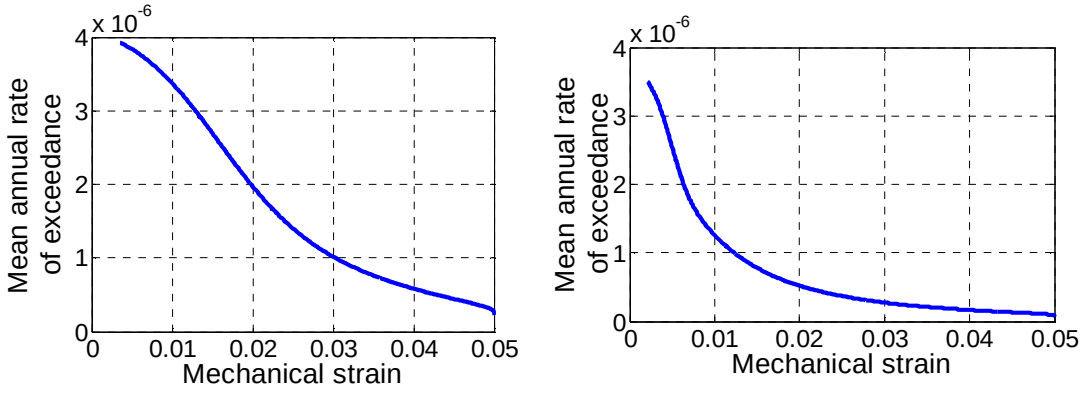

(a) (b)

Figure 5.24: EDP exceedance curves of the strain in the rebar for (a) the slab with unprotected secondary beams and (b) the slab with protected secondary beams.

Two damage measures were developed for composite slabs. The lowest damage measure is based on the strain in the steel reinforcement exceeding the strain which corresponds to the deflection reaching span/250. This deflection limit is taken from the Eurocodes. It is assumed that a slab in damage state one will require minimal repair, such as levelling screed to correct the residual deflection and new fire protection for the steel beams. The upper damage measure is set at the yield strain of the steel reinforcement. It is assumed that if the strain in the rebar exceeds the yield strain, then the slab is beyond repair and will require demolition and replacement. The fragility function parameters developed for the example composite slab are given in Table 5.7 below and the fragility functions shown in Figure 5.25. Figure 5.25 shows that damage state 1 occurs at very relatively low levels of strain and therefore it is unlikely that a concrete slab will remain undamaged if a fully developed fire occurs.

Table 5.7: Parameters for the fragility functions.

	Distribution type	**Units**	**Mean**	**Coefficient of Variation**
Damage State 1	Log-normal	/	3.95E-5	1.0E-6
Damage State 2	Log-normal	/	0.0029	1.0E-6

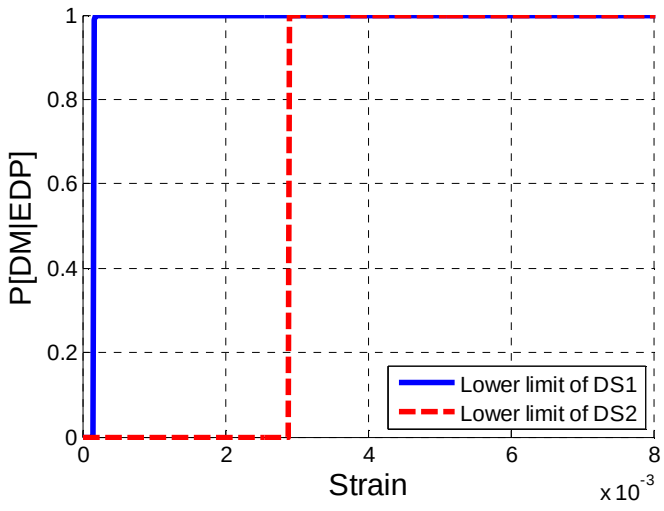

Figure 5.25: Fragility functions for the composite slab with protected secondary beams.

Monetary cost consequence functions and downtime cost consequence functions were developed for both of the damage states associated with the composite slab. The monetary cost consequence functions were developed by firstly estimating the mean costs of repairing the structural damage associated with each damage state. The mean costs were then divided into five categories: Sitework, Concrete, Metals, Finishes and Other. The work of Touran and Suphot presents data on the variance for the first four categories, based on a survey of construction costs in the United States [182]. The "Other" category contains items not covered in the survey and it was assigned a variance equal to the mean variance of all of the other categories. A series of 100,000 run Monte Carlo simulations was then conducted to calculate the mean cost of repair and the variance of the cost of repair for each damage state, shown below in Table 5.8. The costs are assumed to be log-normally distributed.

In order to evaluate the downtime cost consequence function, the mean repair time for each damage state was estimated through the use of construction scheduling. In the absence of survey data, the repair time is assumed to be log-normally distributed with a coefficient of variation of 0.2. The cost consequence functions for the composite slab are shown below in Figure 5.26.

Table 5.8: Normalised parameters for the cost consequence functions associated with the slab with unprotected secondary beams.

	Distribution type	**Mean**	**Coefficient of Variation**
Monetary repair cost of DS1	Log-normal	0.1072	0.5653
Monetary repair cost of DS2	Log-normal	1.1802	0.8233
Downtime due to repair for DS1	Log-normal	2.6	0.2
Downtime due to repair for DS2	Log-normal	7.3	0.2

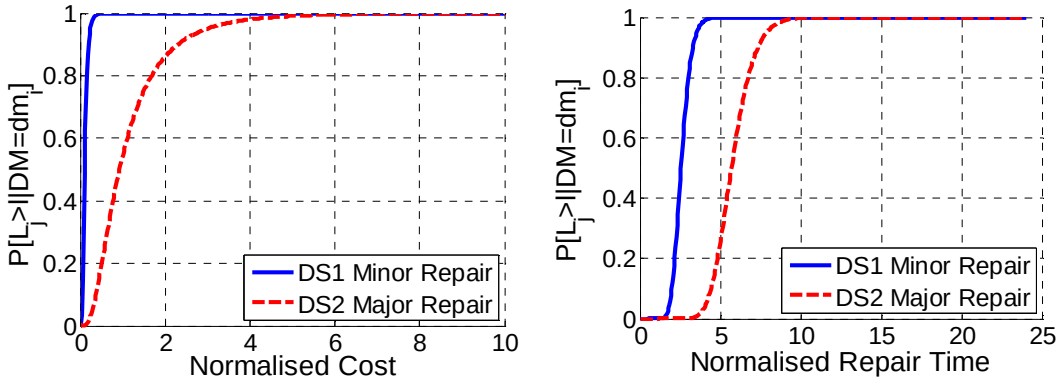

Figure 5.26: Monetary and Downtime Cost Consequence Functions for the composite slab.

The DV exceedance curves are shown in Figure 5.27 and Figure 5.28, where *P(L>l)* is the probability of the losses exceeding a given value of loss. The expected annual monetary loss can be calculated by integrating the mean annual rate of exceedance curve. The normalised expected annual loss is 3.91 x 10^{-7} and 4.36 x 10^{-6} for the composite slabs with protected and unprotected secondary beams, respectively. In this example, the omission of fire protection increases the normalised expected annual loss by a factor of 11, approximately. The cost effectiveness of applying fire protection can be estimated by comparing the increase in repair costs and the increased revenue losses due to downtime with the application costs of the fire protection. Comparing the downtime exceedance curves in Figures 5.27 and 5.28 below, it can be seen that there is relatively little benefit to the application of fire protection. This is due to the fact that the repair process for both design cases are broadly similar and involve many of the same processes.

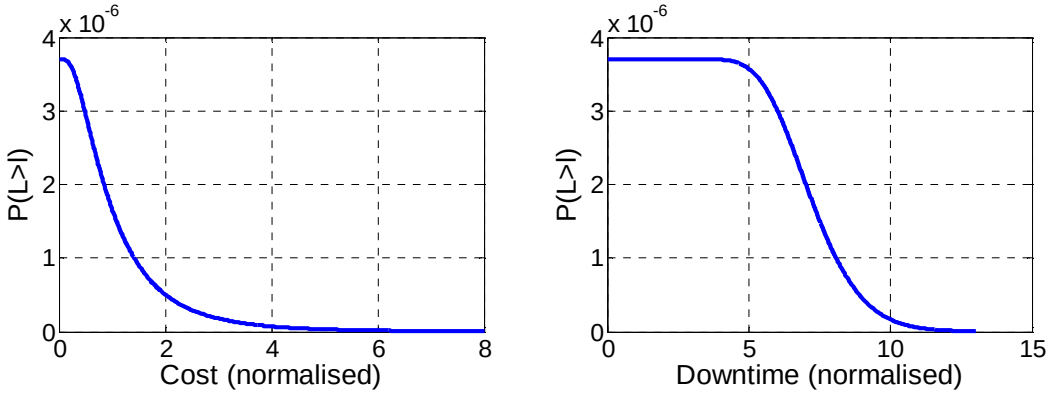

Figure 5.27: Mean annual rate of exceedance curves of monetary cost and downtime for the composite slab with an unprotected secondary beam.

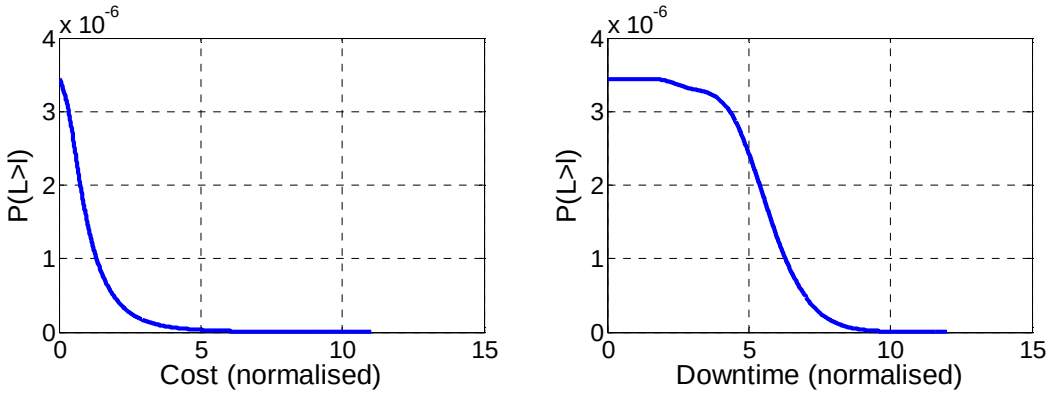

Figure 5.28: Mean annual rate of exceedance curves of monetary cost and downtime for the composite slab with a protected secondary beam.

5.6 Adaptation of the PEER Method to the Structural Fire Engineering Analysis of a Structure Sub-Section

The previous sections have discussed the application of the PEER PBEE methodology to the analysis of single structural members under fire loading. This section expands upon that work to apply the methodology to a sub-section of the structure which includes a multi-storey column and the adjoining internal primary beams. The EC parametric fire curve is again chosen as the hazard model and it is combined with a probabilistic fire spread model to account for the occurrence of vertical fire spread within the structure. New engineering demand parameters and damage measures are defined in order to account for both the possibility and the effects of column collapse. The direct stiffness

method described in section 2.4.2 is used as the structural model. In the case of no column collapse, the costs associated with the fire affected composite beams are analysed as previously described. The decision variables are taken as monetary cost of repair and downtime due to repair works.

5.6.1 Hazard domain

The temperature development within a compartment is defined by the EC parametric fire curve. It is assumed that the initial fire occurs on a random floor within the structure, in a compartment on the external perimeter of the structure. Internal compartments are not considered in this work due to the additional support available to internal columns from the encompassing floor slab and beams. Horizontal fire spread is not considered for similar reasons.

The vertical fire spread is defined based on the probability of spread and the speed of spread. The probability of vertical fire spread from the initial fire floor is defined as the sum of the probability of upward fire spread and the probability of downward fire spread. These probabilities may be estimated, based on published fire statistics [103]. These probabilities may then be used to define further fire spread through the building. As a result of using a probabilistic definition of fire spread, the number of fire floors will vary from one analysis to the next. In order to avoid excessively onerous conditions, an upper limit may be set for the number of fire floors. In practice, the delay in fire spread from one floor to the next places a limit on the number of floors simultaneously exposed to fire loading.

The rate of fire spread is determined from a uniform distribution with the upper and lower limits based on the start and finish of the fire which is causing the spread.

The peak temperature in the compartments is taken as the intensity measure for all three EDPs. An intensity measure hazard curve is created as before. However in this case the rate of occurrence of a structurally significant fire is calculated based on the floor area of all of the compartments considered:

$$r_{fi} = n_{ff,max} \times A_{fi} \times p_1 \times p_2 \times p_3 \times p_4 \tag{5.9}$$

where $n_{ff,max}$ is the maximum potential number of fire floors considered, r_{fi} is the mean annual rate of occurrence of a structurally significant fire, A_{fi} is the area of the fire compartment, p_1 is the probability of a severe fire (accounting for the actions of occupants and the standard fire brigade) per m^2 of floor area and per year, p_2 is the probability of the fire brigade failing to stop the fire, p_3 is a reduction factor to account for the effect of automatic fire detection and alarm transmission and p_4 is a reduction factor to account for the effect of a sprinkler system.

The intensity measures for the analysis of the beam are taken from the records which result in no collapse of the column. In this case, the procedure for calculating the intensity measure hazard curve for the beam is modified in two ways. Firstly, the probability of non-collapse of the column is considered and secondly, the probability of a fire affecting a composite beam is used instead of the probability of a fire starting. The difference occurs as when the fire spreads it will affect a separate beam on each floor. The probability of fire affecting a beam, $r_{fi,ff}$, is therefore based maximum number of fire floors considered and the probability of spread from the initial floor. A section of Matlab script is given below to illustrate the procedure for calculating the probability of fire affecting a beam, given that a fire has occurred. This procedure was developed as part of this work and the portion of code given below has been included in this thesis in order to accurately represent the implemented approach.

```
%% Calculation of the probability of fire affecting a
%%  composite beam

% P_xff: probability of x no. of fire floors, given a fire
%        has occurred on one floor
% max_no_fire_floors: upper limit on the number of fire
%        floors
% P_upward_spread: probability of upward fire spread
% P_downward_spread: probability of downward fire spread

   for ii = 1:max_no_fire_floors
        no_ff = ii;
     k = no_ff-1;
     l = 0;
      for j = 1:no_ff
        P_xff(ii,1)                  =                  ...
((P_upward_spread^k)*(P_downward_spread^l)) + P_xff(ii,1);
           k = k-1;
           l = l+1;
      end
   end
```

The modified procedure for calculation of the intensity measure hazard curve for a beam is:

$$\lambda(IM > im_i, NC) = r_{fi,ff} \times P(NC|F.O.) \times P\left(T_{peak} > T_{peak,i}, NC|F.O.\right) \quad (5.10)$$

where *P(NC|F.O.)* is the probability of no collapse given that a fire occurs.

5.6.2 Structural system domain

The structural system domain is split across three parts; modelling the primary composite beams under fire loading, modelling the continuous column and modelling the composite beam under axial compression. The primary composite beams subjected to fire determine the horizontal pull-in force affecting the column. In the case of non-collapse of the column, the beam response is used to determine the level of damage done

to the beam and surrounding slab. Common construction practice requires fire protection to be applied to primary beams. This means that primary beams can be expected to retain a large proportion of their bending capacity during a fire. For this reason, the "method of slices", as described in section 2.4.2, has been chosen to model the response of the beam. The primary beam is modelled as simply supported, with an axial spring restraining the free end. The midspan deflection of the beam is again used as the engineering demand parameter for this case.

The responses of the column under strong floor collapse and the composite beam under weak floor collapse are modelled using the direct stiffness approach described in section 2.4.2. The utilisation factor, $\frac{P}{P_{Re,T}} + \frac{M}{M_{Re,T}}$, is taken as the engineering demand parameter for both the steel column and the composite beam; where P is the applied axial load, M is the applied moment, $P_{Re,T}$ is the temperature-dependent axial resistance of the member and $M_{Re,T}$ is the temperature-dependent moment resistance of the member. The capacity of the sections are determined based on the Eurocode rules [55], [108]. Using the utilisation factor, the state of the members can be determined. If the utilisation factor exceeds 1, then the element is treated as collapsed. By adopting this approach, separate fragility functions are not required to assess the probability of either strong floor collapse or weak floor collapse.

$$P(Coll) = P(Coll|F.O.)P(F.O.) \tag{5.11}$$

where

$$P(Coll|F.O.) = \frac{\sum_{i=0}^{N} No.\,of\ Collapses}{N} \tag{5.12}$$

where *P(Coll)* is the probability of collapse, *P(Coll|F.O.)* is the probability of collapse given that a fire has occurred, *P(F.O.)* is the probability of a fire occurring and *N* is the number of runs undertaken in the analysis.

The engineering demand parameter exceedance curve for the beams subjected to fire is calculated as described in section 5.3.2, though only the non-collapse results are considered, Equation (5.13).

$$\lambda(EDP > edp_i, NC) = \int P[EDP > edp_i, NC|IM = im_i]|d\lambda(IM > im_i, NC)| \tag{5.13}$$

5.6.3 Loss domain

The losses due to fire are calculated based on two conditions; collapse of the column, either through the strong floor or weak floor mechanism, and damage to the composite beam. The probable losses due to collapse of the column may be calculated by:

$$\lambda(L_f > l_f, Coll) = r_{fi} \times P(Coll|F.O.) \times (1 - F(cost)) \tag{5.14}$$

where $\lambda(L_f>l_f,Coll)$ is the mean annual rate of exceedance of cost due to collapse and $F(cost)$ is the cumulative distribution function of the cost consequence function.

The losses associated with non-collapse are due to damage to the beam and adjacent slabs. As before, the three damage states are identified; undamaged, lightly damaged requiring minor repair work and major damage requiring demolition and replacement of the section. Fragility functions and cost consequence functions are derived for the composite beam, as described in section 5.3.3.

$$\lambda(L_f > l_f, NC) = \int P(L_f > l_f, NC|EDP)|d\lambda_{EDP}| \tag{5.15}$$

where

$$\begin{aligned} P(L_f > l_f, NC|EDP) \\ &= P(L_f > l_f|DM1)P(DM1|\overline{DM2}, EDP) \\ &+ P(L_f > l_f|DM2)P(DM2|EDP) \end{aligned} \tag{5.16}$$

where $\lambda(L_f>l_f,NC)$ is the loss exceedance curve due to non-collapse of the structure, $P(L_f>l_f|DM)$ is the complementary cumulative distribution function for the cost consequence function of the relevant damage state, $P(DM2|EDP)$ is the probability of being in damage state 2 given a specific value of EDP and $P(DM1|\overline{DM2},EDP)$ is the probability of being in damage state 1 given that the member is not in damage state 2 and given a specific value of EDP.

The total mean annual rate of exceedance of a cost is then calculated as:

$$\lambda(L_f > l_f) = \lambda(L_f > l_f, Coll) + \lambda(L_f > l_f, NC) \tag{5.17}$$

5.7 Multi-Storey Stability Example

The PEER-PBSFE analysis developed in the previous section is applied here to a typical UK office building. The building description is taken from a study done by Vlassis et al. into progressive collapse of multi-storey buildings [195]. The building is a 7 storey office with a steel framed composite structure. The building is rectangular in plan, with a central atrium. Lateral stability is provided by two identical braced cores within the building. A plan view of the column and surrounding structure is shown in Figure 5.29, with the column and beam considered in the analysis highlighted in red.

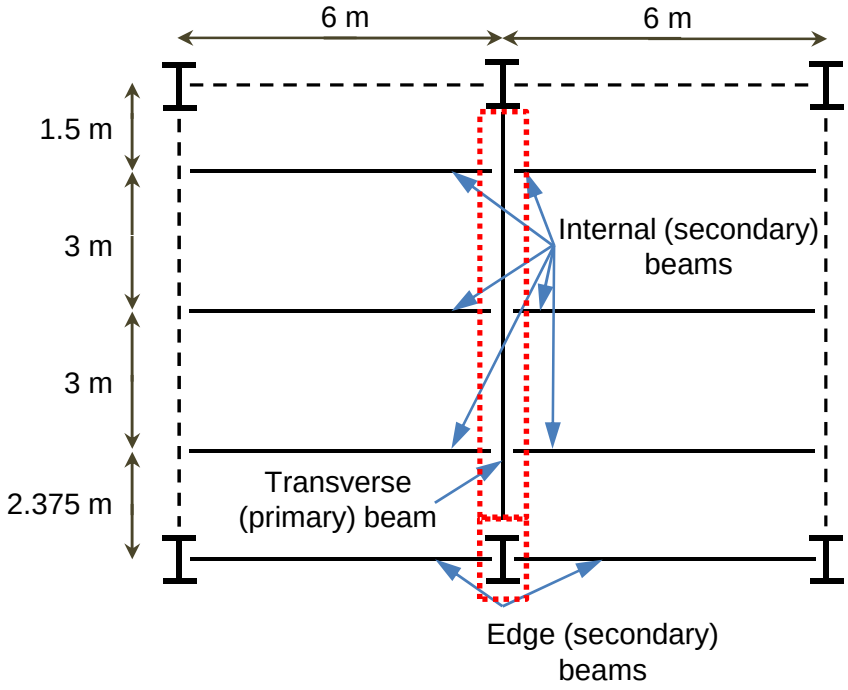

Figure 5.29: Plan view of the floor area surrounding the column (adapted from Vlassis et al. [195]).

A description of the geometry of the steel and concrete structure, including the stochastic definition, is given in Table 5.9 and Table 5.10. The material properties are then described in Table 5.11 and Table 5.12.

Table 5.9: Geometry of the steel members.

Member	Section Designation	Length	Distribution	Distribution parameter 1	Distribution parameter 2
Column	UC 305 x 305 x 118	3.6 m	Log-normal	3.6 (mean)	0.005 (C.o.V.)
Primary beam	UC 356 x 368 x 153	9.875 m	Log-normal	9.875 (mean)	0.005 (C.o.V.)
Internal secondary beam	UB 305 x 102 x 25	6 m	/	/	/
Perimeter secondary beam	UB 406 x 140 x 39	6 m	/	/	/

Table 5.10: Geometry of the concrete slab.

Length	Width	Depth	Depth of rib
9.875 m	2.1 m	0.07 m	0.06 m

Table 5.11: Material properties.

Material	Grade	Elastic Modulus (GPa)	Strength (MPa)
Structural steel	s355	210	355
Concrete	C30 (L.W.)	27.3	30
Rebar	Type 2	200	460

Table 5.12: Stochastic definition of the material properties and loading conditions.

Material property	Units	Distribution	Distribution parameter 1	Distribution parameter 2
$\mathbf{E_{steel}}$	kN/mm^2	Log-normal	210 (mean)	0.03 (C.o.V.)
$\mathbf{E_{concrete}}$	kN/mm^2	Log-normal	27.3 (mean)	0.15 (C.o.V.)
$\mathbf{E_{rebar}}$	kN/mm^2	Log-normal	200 (mean)	0.03 (C.o.V.)
$\boldsymbol{\sigma_{y,steel}}$	N/mm^2	Log-normal	399.2 (mean)	0.07 (C.o.V.)
Area of ventilation	m^2	Truncated log-normal	21.2 (Upper limit)	0.25 (standard deviation)
Fuel load	MJ/m^2	Gumbel	363.29 (mode)	98.24 (scale)
U.D.L.	kN/m	Gumbel	15.165 (mode)	4.912 (scale)

A PEER analysis of 5000 runs was conducted for this example. Each run consisted of the generation of a temperature-time curve, heat transfer analysis to the affected beams, slabs and columns and analysis of the structural response of the structure sub-assembly. Once all of the runs were completed, the instances which suffered collapse of the sub-assembly were identified and the mean annual rate of exceedance of the decision variables due to collapse was evaluated. The probability of exceeding these costs is based on the frequency of fire occurring, the probability of collapse given a fire occurs and the probable costs due to collapse, as described by the cost consequence functions for collapse. The parameters of the cost consequence functions for collapse are listed

below in Table 5.13 and the mean annual rate of exceedance curves for both monetary repair cost and downtime due to repair are shown in Figure 5.30 below.

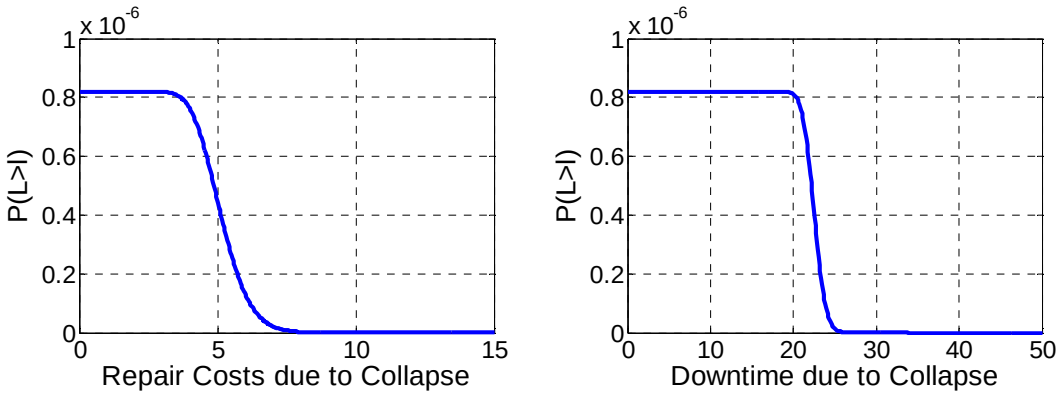

Figure 5.30: Mean annual rate of exceedance curves of losses due to collapse.

The next stage of the analysis is to define the mean annual rate of exceedance of the decision variables due to the non-collapse instances. Firstly, the intensity measure hazard curve is defined based on the recorded peak temperatures from the instances of non-collapse. Then a probability density function is fitted to the results and the probability of occurrence of a fire is determined, as described in section 5.3.1. The intensity measure hazard curve is then created using Equation (5.10), as shown in Figure 5.31.

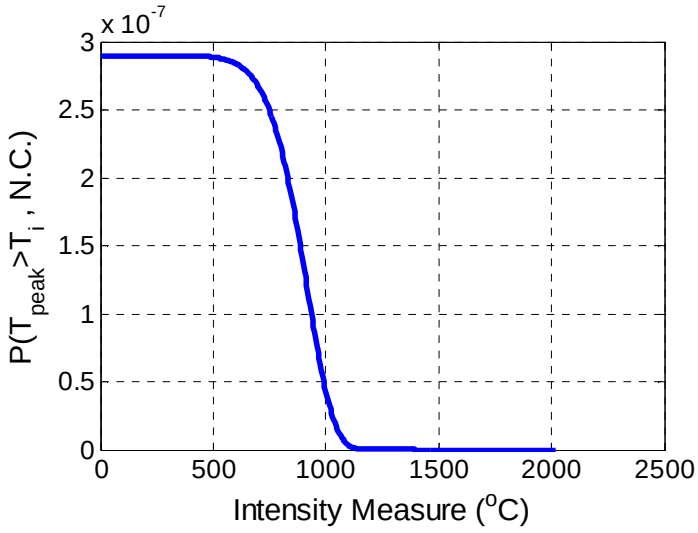

Figure 5.31: Intensity measure hazard curve, considering only the non-collapse instances.

Following on from the previous step, the engineering demand parameter exceedance curve is then defined. This is done in accordance with the procedure outline previously in section 5.3.2 for PEER-PBSFE analysis of a composite beam. The EDP exceedance curve for this example, showing the likelihood of one of the primary beams exceeding a specific midspan deflection, is presented in Figure 5.32.

Once the likelihood of exceedance of the EDP is found, then the damage to the structure and the resulting costs can be estimated. The parameters of the fragility functions defining the likelihood of damage to the beam given an EDP are listed in Table 5.13. Also listed are the parameters of the cost consequence functions for the primary beams.

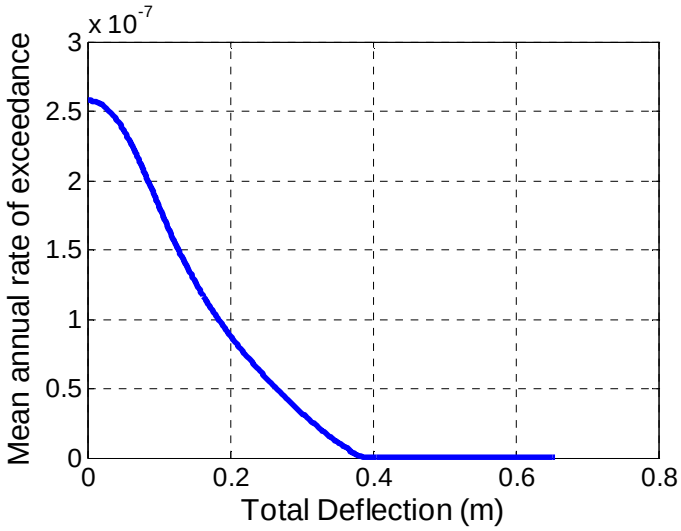

Figure 5.32: Engineering demand parameter exceedance curve, for the non-collapse instances.

Table 5.13: Definition of the fragility and cost consequence functions.

	Distribution	Distribution parameter 1	Distribution parameter 2
Fragility function, DS1 beam	Gaussian	1.069×10^{-4} (mean)	0.009 (C.o.V.)
Fragility function, DS2 beam	Gaussian	0.0022 (mean)	0.0046 (C.o.V.)
Monetary cost consequence function, DS1 beam	Log-normal	0.0764 (mean)	0.414 (C.o.V.)
Monetary cost consequence function, DS2 beam	Log-normal	1.2338 (mean)	0.694 (C.o.V.)
Monetary cost consequence function, Column collapse	Log-normal	1.2918 (mean)	0.661 (C.o.V.)
Downtime cost consequence function, DS1 beam	Log-normal	1.44 (mean)	0.2 (C.o.V.)
Downtime cost consequence function, DS2 beam	Log-normal	4.63 (mean)	0.2 (C.o.V.)
Downtime cost consequence function, Column collapse	Log-normal	5.63 (mean)	0.2 (C.o.V.)

Using the fragility functions and cost consequence functions, the mean annual rate of exceeding a given cost is evaluated, as per section 5.3.3. This yields the cost exceedance curves for the non-collapse instances shown below in Figure 5.33. A clear step can be seen in both curves, approximately corresponding to a probability of exceedance of 1.5×10^{-7}. This step is a result of the sudden jump in costs if the fire spreads beyond the initial fire floor. The cost exceedance curves for all instances are then found as the sum of the collapse and non-collapse instances. These total cost exceedance curves are shown in Figure 5.34.

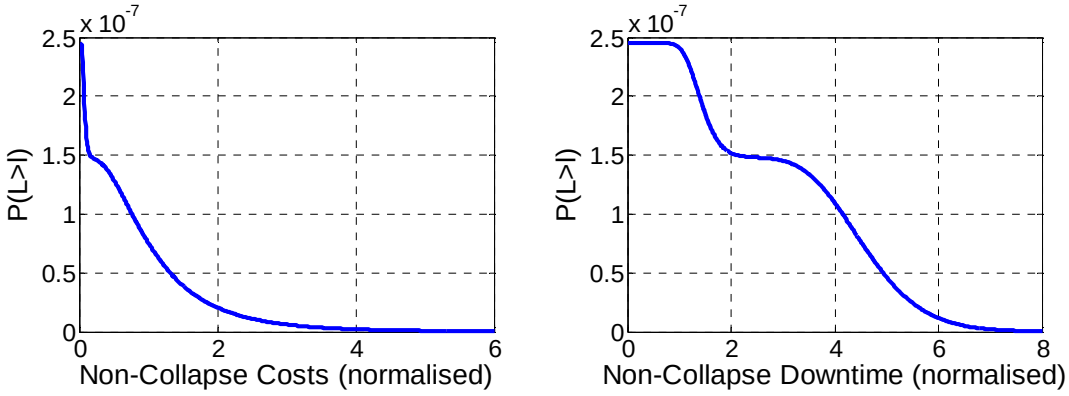

Figure 5.33: Mean annual rate of exceedance curves for non-collapse induced losses.

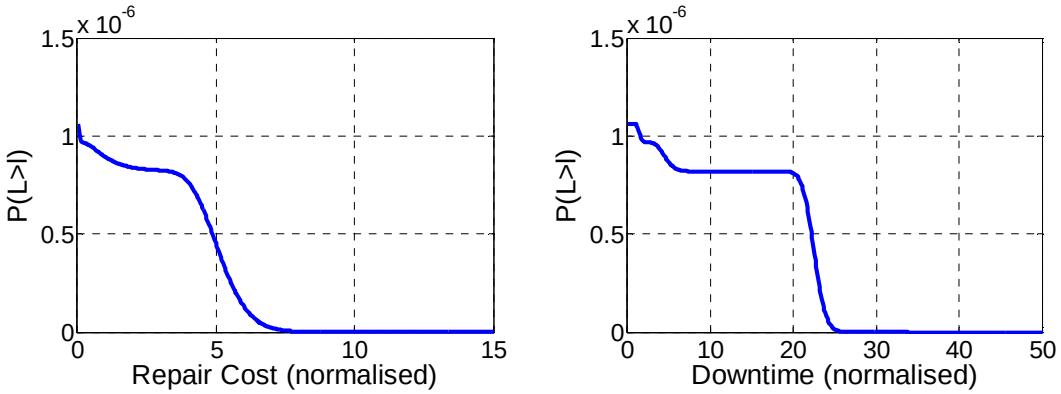

Figure 5.34: Mean annual rate of exceedance curves for all losses.

The difference in the costs due to collapse and the costs due to non-collapse can be seen in Figure 5.34 above. The upper left hand end of both the repair cost and downtime curves show an increased likelihood of incurring a cost. This increase stems from the non-collapse instances and because of this, the increased likelihood only extends over the lower range of probable costs. The collapse induced costs, in contrast, are of a greater magnitude and a lower likelihood of occurrence.

5.8 Summary

In this chapter an overview of the Pacific Earthquake Engineering Research (PEER) center's Performance-Based Earthquake Engineering (PBEE) methodology is presented. The PEER method is a four stage process covering hazard analysis, structural system analysis, damage analysis and loss analysis. Each stage of the process is defined by a single parameter. Hazard analysis concerns the evaluation of the likelihood of an earthquake affecting the structure and the probable range of magnitudes of such an earthquake. The hazard analysis is defined by an intensity measure, typically taken as the spectral acceleration. The structural system analysis evaluates the effect of the hazard on the structure. It is commonly performed using a nonlinear finite element program. The structural analysis is defined by an engineering demand parameter, such as interstorey drift. Damage analysis is carried out to evaluate the level of damage caused by the engineering demand parameter. A range of damage states are assigned to each component in the structure and a repair cost is associated with each damage state. The final stage is loss analysis which evaluates the likely annual loss due to an earthquake. The loss may be taken as monetary loss, fatalities or downtime due to repair works.

The PEER methodology has been adapted to structural fire engineering. The parametric temperature-time curve has been presented as a suitable hazard model. The suitability of the peak fire temperature as an intensity measure has been examined and a procedure for calculating the hazard exceedance curve with peak fire temperature as the intensity measure has been presented. Analytical structural models have been presented for calculating the engineering demand parameters. Midspan deflection and rebar strain are presented as suitable engineering demand parameters for composite beams and slabs, respectively. Fragility functions have been developed to classify the level of damage done to the structure. Cost consequence functions have been developed in order to quantify the costs associated with the damage states. Example applications of the framework to the analysis of a composite beam and a composite slab in a typical office building have been presented. The likelihood of exceeding a given cost, either monetary cost or downtime, has been calculated in each case for two different design options.

The PEER methodology has also been extended to the analysis of a multi-storey sub-assembly from a multi-storey building. An example of the methodology applied to the

analysis of four floors from a generic steel framed composite office building has been presented and likelihood of exceeding various decision variables has been evaluated.

Chapter 6: Development of Software FireLab for the Probabilistic Design of Structures Subjected to Fire

6.1 Preamble

This chapter presents a software tool (*FireLab*) that allows engineers to apply performance-based engineering methods to the fire resistance design of regular steel framed composite buildings while also accounting for uncertainties in key design parameters. The aim of the software tool is to simplify the process of applying performance-based engineering methods in order to encourage the spread of performance-based design. FireLab may be used in a deterministic manner to check if a structural element can withstand specific load combinations or it may be used in a stochastic manner to quantify the probability of failure of an element. The range of fire models, heat transfer models and structural models incorporated into the tool are discussed in this chapter. The ability of the software to call external programs is discussed and examples are given. FireLab features a parallel option for reducing the runtime of computationally intensive Monte Carlo simulations. The software is available as a standalone executable; however it was initially developed as a suite of Matlab scripts and functions [107].

The nature of the output of the software tool is described in this chapter. The output varies depending on the type of analysis chosen. Deterministic analyses output deformations or stresses and strains. Probabilistic analyses output information on the mean deformations or stresses and strains, as well as the probability of failure.

Existing fire design software is examined and compared with FireLab. Examples of the use of FireLab are given.

6.2 Overview of FireLab

FireLab is a software tool that allows engineers to apply performance-based engineering methods to the fire resistance design of regular steel framed composite buildings while also accounting for uncertainties in key design parameters. The aim of the software tool

is to simplify the process of applying performance-based engineering methods in order to encourage the spread of performance-based design. To this end, simple analytical models are used where possible. Also, all of the models required to conduct a structural fire engineering analysis are included in the software tool. This removes the difficulty of having to extract results from one software tool and format them to produce a suitable set of inputs for the next stage of the analysis. A graphical overview of the program procedure is given below in Figure 6.1.

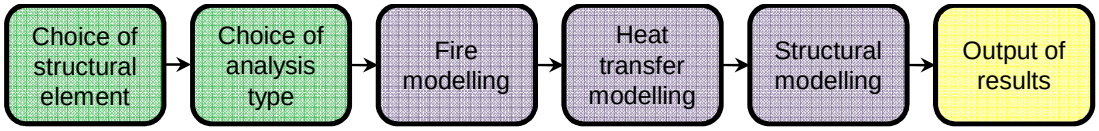

Figure 6.1: Outline of the program procedure.

FireLab may be used to conduct deterministic analyses to evaluate the response of a structural element under specific load combinations. This option may be used to examine the structural response under a set of identified loads, for example when following the short-hot/long-cool methodology [146], [196]. Alternatively, FireLab may be used to conduct a variety of different stochastic analyses in order to determine either the nominal probability of failure or the full range of likely responses of the structural element.

6.2.1 Analysis models in FireLab

Deterministic analysis: Deterministic analysis allows for the evaluation of a single set of inputs and is available for all of the physical models in FireLab.

Monte Carlo simulation: Monte Carlo simulation is described in detail in section 4.2. The Monte Carlo method is available with either random sampling or Latin hypercube sampling for all of the physical models in FireLab.

First-Order Reliability Method: FORM is described in detail in section 4.3. It is available for any of the fire models and heat transfer models, but the choice of structural

model restricted to either the analytical composite beam solution or the Abaqus composite beam solution.

PEER method: The PEER method is fully described in Chapter 5. It is available for any of the fire models and heat transfer models, but the choice of structural element is limited to either a composite beam or composite slab. If a slab is chosen, then the Cameron method will be used as the structural model. If a beam is chosen, then the user may decide from any of the available beam models.

6.2.2 Physical models in FireLab

Fire models: FireLab features several temperature-time curves; the EC parametric temperature-time curve, the EC standard temperature-time curve, the EC hydrocarbon temperature-time curve and the JCSS temperature-time curve [12], [17]. Each of these methods is described in detail in Chapter 2. The user is free to choose any of the fire curves, but only the parametric curve is capable of representing the variability associated with a real fire.

Heat transfer models: FireLab features four heat transfer procedures. Two different lumped capacitance methods are included in the program, one for uninsulated steel members and one for insulated steel members [38]. The third option is a one-dimensional finite difference solution for calculating the temperature distribution through the depth of a concrete slab [9]. The final heat transfer option uses an interface procedure in FireLab to call the external finite element program, Abaqus [75]. This heat transfer option may only be used when analysing a composite beam using Abaqus. The details of these methods are given in section 2.3.

Structural models: FireLab features a large variety of models for evaluating the response of structures to fire. These models can be divided into three categories; composite beam models, composite slab models and models for analysing the vertical stability of tall steel framed buildings.

The user may choose from a range of models within FireLab when analysing a composite beam. Analytical solutions include the method of slices [67], [71] or the Cameron method [68]. Alternatively the user may use the interface option in FireLab to

call an external finite element solver, such as Abaqus or OpenSees [73]. The ability to utilize an external finite element solver allows for the possibility to tackle problems that are much larger or more complex than can be solved using analytical solutions. It also provides a greater level of accuracy to the results.

Options for the analysis of a composite slab include the Cameron method [3], the Bailey method [76] and the method presented by Omer, Izzuddin and Elghazouli [80]. The Cameron method has been implemented for deterministic analysis, Monte Carlo analysis and PEER analysis. The Bailey method has been implemented for both the deterministic analysis and the Monte Carlo analysis. The method by Omer et al. has been implemented for deterministic analysis only [80].

A direct stiffness based solver has been implemented for evaluating the effects of multi-floor fires on the stability of tall, steel-framed buildings. This analysis method is fully described in section 2.4.2. This method is available for deterministic, Monte Carlo and PEER analyses.

The structural analysis procedures in FireLab follow previously published analysis methods. The suitability of these methods for the analysis of structural elements in fire has been thoroughly examined. In order to ensure that the models are correctly implemented within FireLab a number of test cases were examined. The FireLab models were compared against published results where possible. Any models lacking published example results were compared against the results of a separate analysis program. These test cases are presented in Appendices F – H.

6.2.3 Input/Output

A series of spreadsheet forms have been developed as an interface for FireLab. These spreadsheets list the inputs required for each analysis, the possible options for each input and they define the required units. Examples of the spreadsheet forms are provided in Appendices C-E. The spreadsheet forms feature macros for interacting with FireLab. The first stage of the macro creates and saves a set of tab delimited text files. These files are the input files that are used by FireLab. The set consists of four to five files, depending on the type of analysis chosen. The first file defines the type of analysis. The second file contains information on the problem definition such as element dimensions, material

properties and loads. Any of the variables in this file may be treated either as deterministic or stochastic. The options for probability distribution are Gaussian, uniform, lognormal, Gumbel or truncated lognormal. The third file contains inputs which consist of absolute values, such as the ambient temperature. The fourth text file contains text inputs and a fifth file is created for the correlation matrix if a stochastic analysis is chosen. Alternatively, if the user wishes the input files may be written directly in a text editor. The second stage of the macro calls the FireLab executable and begins the analysis.

The output from the FireLab executable consists of a text file and graphs. The text file contains a list of the inputs describing the problem along with outputs from the analysis. In the case of deterministic analyses, information such as compartment temperature, member temperature, thermal forces and deflections are written to the output file. Graphs are used to illustrate temperature-time curves, stress/strain distributions and bending moment distributions, as shown in Figure 6.2. In the case of stochastic analyses, information such as the mean and standard deviation of the structural response and the nominal probability of failure are written to the output file.

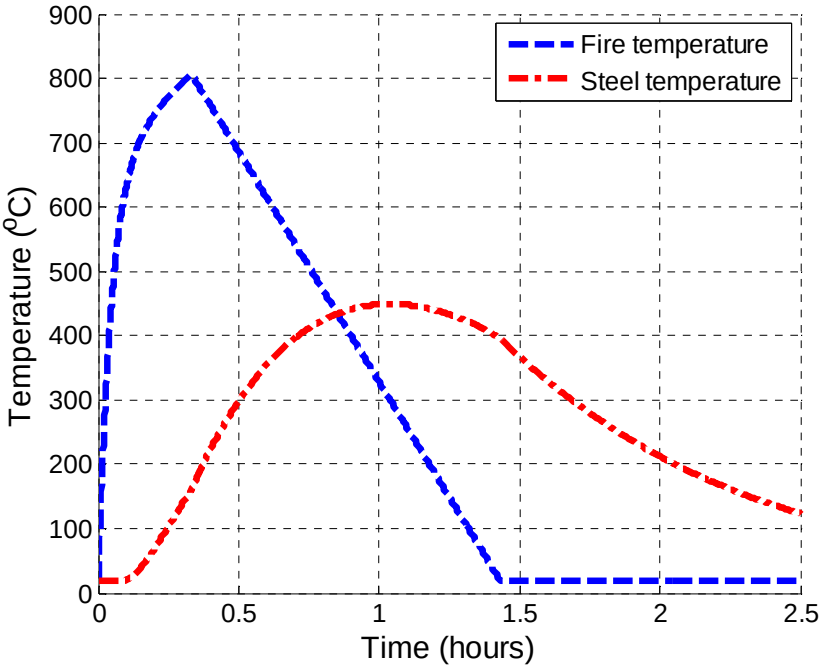

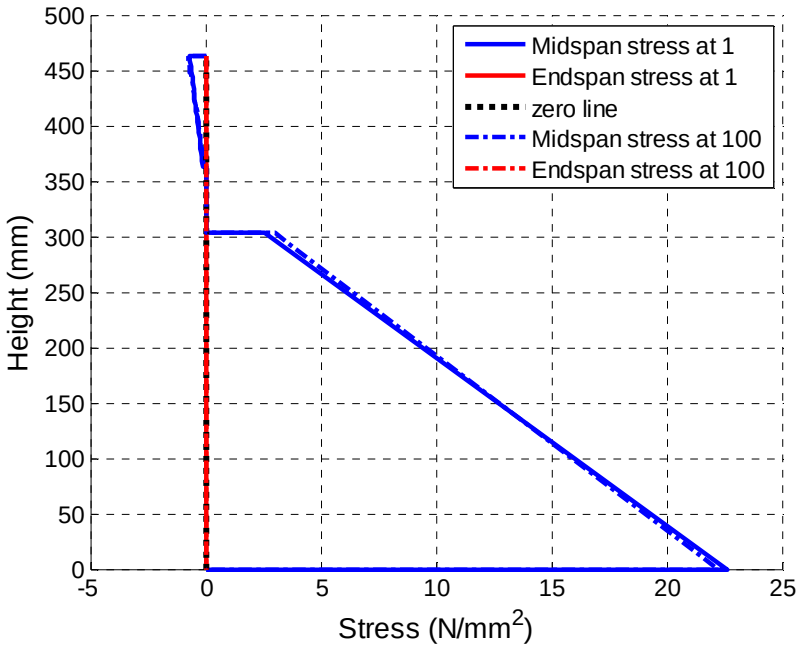

Figure 6.2: Typical output graphs from FireLab.

6.2.4 Parallelism in FireLab

Parallel computing techniques have been incorporated in FireLab in order to increase the performance of the program. Parallel computing is the process of dividing the workload, or a portion of the workload, into a number of smaller pieces and solving these pieces concurrently using multiple processors or processor cores. Parallel techniques have been incorporated into the Monte Carlo simulation options in FireLab. Parallel computing is particularly effective for this workload as Monte Carlo simulations are considered to be 'embarrassingly parallel'. This is because a large proportion of the workload in a Monte Carlo simulation can be parallelised and there is no communication required between the separate threads. There are two opposing advantages to parallelism; either the analysis can be parallelised in order to reduce the runtime or the level of complexity of the analysis can be increased with a minimal increase in runtime.

Parallelism was introduced for the Monte Carlo simulation option in FireLab through the use of the Parallel Computing Toolbox from Mathworks. There are four stages to a Monte Carlo simulation; collecting the inputs, creating a sufficient number of samples, analysis of the problem for each sample set and analysis of the results. The bulk of the workload is due to the third step, the analysis of the problem. In the serial solution a *for* loop is used to analyse the problem a specific number of times. In the parallel solution a computation pool, consisting of a number of processor cores, is firstly opened. Then a *parfor* loop is used to distribute the required number of analysis runs between each core in the computation pool.

The act of splitting the workload into smaller pieces, distributing the pieces and then collecting the solutions creates extra computational work. Therefore, the *parfor* loop is best used in cases where the solution to the problem is significantly more time consuming than the act of parallelising the workload, e.g. when using large models, such as complex finite element models.

A Monte Carlo simulation of a composite beam was examined in order to evaluate the possible reductions in runtime due to the use of parallel computing techniques. The simulation consisted of 20 runs and used Abaqus finite element models for both heat transfer analysis and thermomechanical analysis. The simulation was run on an AMD Opteron 8-core processor. The results of the analysis are shown below in Figure 6.3. It can be seen that the runtime can be reduced by over 50% by using four cores instead of

one. The reduction in elapsed time is not linear for a number of reasons. Firstly, the work involved in generating the inputs and collating the results cannot be reduced as it cannot be parallelised. Secondly, the Abaqus program uses parallelisation techniques. These techniques are not particularly efficient as there is more overhead involved in splitting a finite element analysis across multiple threads than there is in splitting a number of Monte Carlo runs. However, using parallelisation techniques within the Matlab script prevents Abaqus from using the same techniques as each core is running at full capacity. This reduces the efficiency gain that can be achieved through parallelisation.

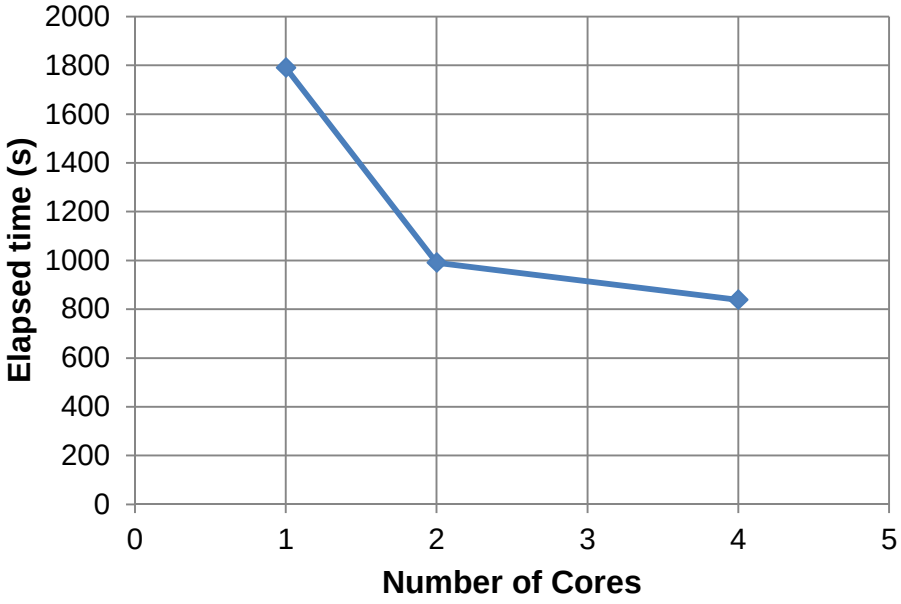

Figure 6.3: Variation of simulation runtime with increasing levels of parallelism.

6.3 Comparison Against Existing Fire Design Software

There exists a large library of design and analysis software for use in the field of fire engineering. Morente, de la Quintana and Wald conducted a survey of available fire engineering computer models and catalogued a total 177 different programs relating to fire engineering [197]. These field of application of these programs covered structural fire resistance, fire development, egress, detector response and other miscellaneous fields.

Table 6.1 shows a selection of well-known structural fire engineering software packages and their capabilities. It shows that there is a wide range of fire modelling software, ranging from simple zone models to complex field models. Table 6.1 also shows that a range of structural response software exists which are capable of modelling the development of a fire, the corresponding temperature distribution in a member and the resulting structural response. However, it also shows the lack of probabilistic analysis and loss assessment options in software for evaluating structural response. CRISP [198] and FiRECAM [199] both include probabilistic methods but these programs are aimed at fire safety engineering rather than structural engineering. Loss assessment is incorporated in the FiRECAM software, though the cost is determined from statistics based on the calculated size of the fire. This is a different approach to the PEER method where the cost is based on an estimate of the damage caused by the fire.

Table 6.1: Capability comparison of a selection of available fire engineering software packages.

	Fire modelling	Heat transfer modelling	Code based structural response	Structural response modelling	Loss assessment modelling	Probabilistic analysis	Egress modelling
FireLab	✓	✓		✓	✓	✓	
CFAST	✓						
JASMINE	✓						
FDS	✓						✓
OZONE	✓	✓	✓				
DIFISEK	✓	✓	✓				
Elefir-EN	✓	✓	✓				
OpenSees-Thermal		✓		✓			
Abaqus		✓		✓			
Vulcan				✓			
CRISP	✓					✓	✓
FiRECAM	✓				✓	✓	✓

6.4 Example Application of FireLab

Current day practice in structural fire engineering involves the evaluation of the performance of a structural sub-system against a small selection of design fires. Typically, four to five fires are chosen to represent the various different types of fire. The response of the structure is then examined to see if the three basic requirements of integrity, insulation and load-bearing capacity are maintained [147], [200]. In this example, FireLab is used to evaluate the performance of three separate elements against a wide range of possible design fires.

Firstly, the 8-storey steel framed composite building which has previously been examined in Chapters 4 and 5 is again used here to illustrate the analysis of the slab and beam elements [165]. This building is used as it represents a typical UK office building. The methods implemented in FireLab are based on a set of requirements:

- The loads are assumed to be transferred from the slab to the beams and onto the columns. Therefore, the capacity of each part of this load path must be checked.
- The floor slab must be divided into rectilinear panels which are supported on all sides by protected beams.
- All edge beams and beams connected to columns are assumed to be protected, to prevent disproportionate collapse.
- The slab panels are assumed to be restrained against lateral translation along the boundaries, but free to rotate.
- The structure should meet the reliability requirements set out in the Eurocodes. The maximum failure probability of an office type building with a 55 year design life is 7.23×10^{-5} [126], [201].

The building features a regular column grid laid out on 7.5m by 7.5m spacings, as shown in Figure 6.4. The maximum size of each of the individual slab panels is illustrated with red broken lines and further possible sub divisions of the slab are shown with a yellow broken line. The size of the panel defines the area considered in the slab analysis and is defined by the presence of supporting beams. Shown in Figure 6.4 are the slab area to be analysed and the beam area to be analysed.

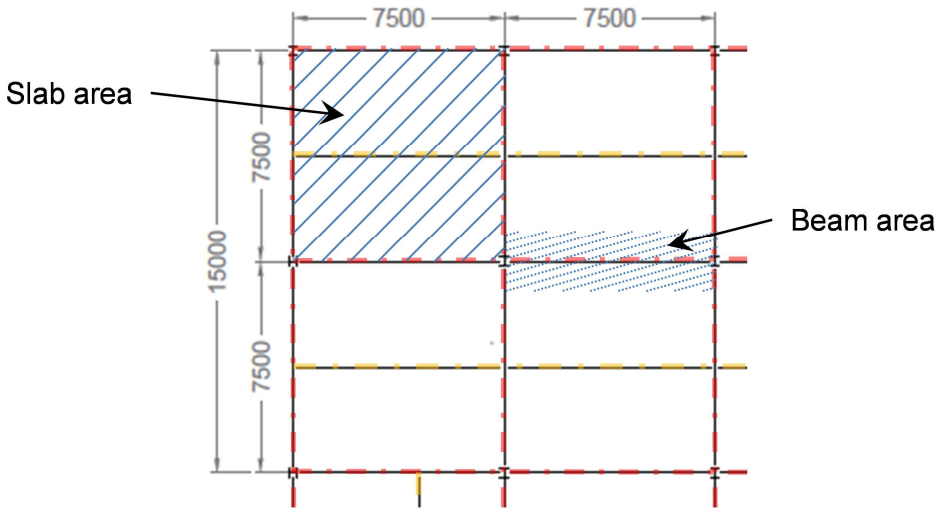

Figure 6.4: Partial floor plan showing the required slab boundaries marked by broken red lines and possible additional boundaries marked by broken yellow lines.

The multi-storey stability analysis is illustrated using the building designed by Vlassis et al. [195], presented previously in section 5.7. The reliability of the multi-storey sub-structure is evaluated against the same Eurocode reliability limits as the other elements.

The analysis presented here considers three separate elements from a typical steel framed office building, however it does not represent the full design process. Structural elements, such as connections, are subject to very high compressive, tensile and rotational demands during a fire and the effects of these factors should be evaluated during the design process.

6.4.1 Example of a slab analysis

Two different design options are considered for the slab panel indicated in Figure 6.4. The first option assumes that the secondary beam spanning across the middle of the slab panel is left unprotected and therefore it does not offer any additional load carrying capacity during a fire. The second option assumes that the secondary beam is protected and that it is capable of supporting the beam during the fire. Each of these design cases was examined with a 10000 run Monte Carlo simulation in Chapter 4, and the results of

the simulation are shown in Figure 4.9. In order to judge the performance of the slab panel, a performance limit must be specified. The ultimate strain of the reinforcing steel is taken as the performance limit as it is a good indicator of collapse of the slab. The Monte Carlo simulations discussed in Chapter 4 give a probability of failure of 6.9% for the slab with an unprotected secondary steel beam and 0.0% for the slab with a protected secondary steel beam. Clearly the slab with the unprotected secondary beam does meet the Eurocode reliability requirements and cannot be used. The slab with a protected secondary beam meets the Eurocode reliability requirements; however the estimated probability of failure is not accurate enough. Therefore a second Monte Carlo simulation consisting of 500000 runs was conducted in order to calculate an accurate estimate of the probability of failure for the rectangular slab. The results of this simulation are shown below in Figure 6.5. The probability of failure from this simulation was found to be 7 x 10^{-5}, which meets the Eurocode reliability requirements. Therefore the slab panel with a protected secondary beam represents a safe design option.

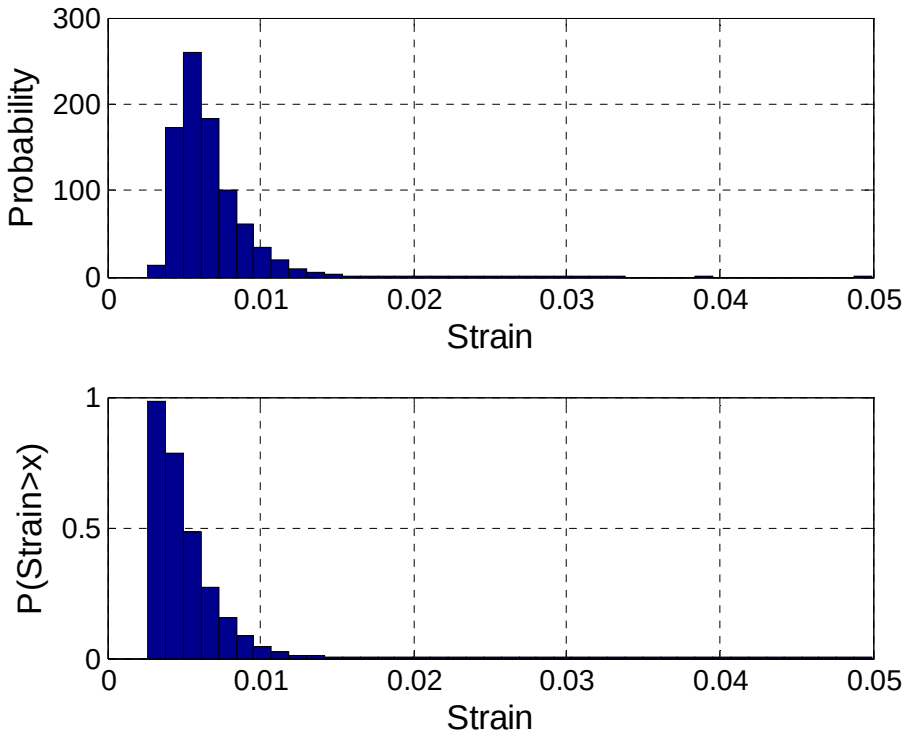

Figure 6.5: (a) Probability of a given strain occurring and (b) Probability of a given strain being exceeded.

6.4.2 Example of a composite beam analysis

The composite beam chosen for the design example is also taken from the SCI document "Comparative Structure Cost of Modern Commercial Structures" [165] and has been previously analysed in Chapter 4. Four design options were analysed for the composite beam; no fire protection to the steel beam, 12.5mm of fire protection to the steel beam, 25mm of fire protection to the steel beam and 37.5mm of fire protection to the steel beam. The probability of failure was found for each of these design options, based on a limiting midspan deflection of the beam. The results of these studies, shown in Figure 4.8, showed that the steel beam with no protection applied suffers from very high deflections, therefore the steel beam with 12.5mm was chosen as the preferred design option for further analysis. A Monte Carlo simulation of 500000 runs was conducted in order to obtain an accurate prediction of the probability of failure for this design option, the results of which are shown below in Figure 6.6. The probability of failure for the steel beam with 12.5mm of fire protection was found to be 1.6×10^{-5}, which is within the limits set out by the Eurocodes. The steel beam with 12.5mm of fire protection may therefore be taken as a safe design option.

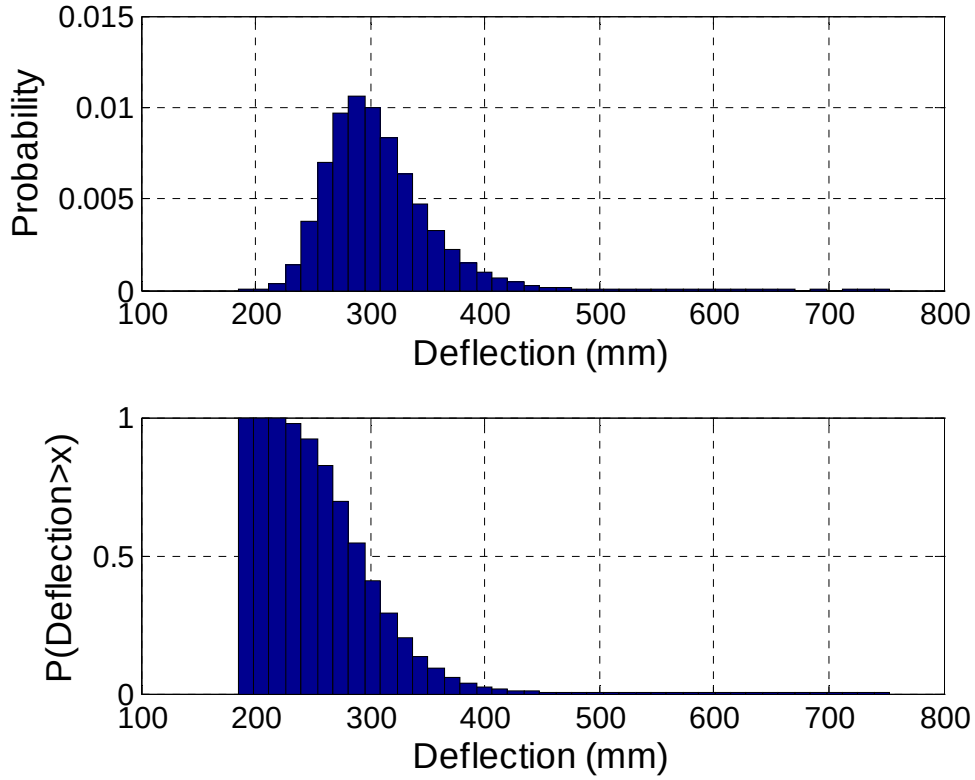

Figure 6.6: (a) Probability of a given deflection occurring and (b) Probability of a given deflection being exceeded.

6.4.3 Example of the analysis of multi-storey stability

This example analyses the stability of a multi-storey steel-framed composite building, using the analysis procedure set out in section 2.4.2. The analysis procedure is applied within a Monte Carlo simulation with Latin hypercube sampling in order to determine the probability of failure of the structure. The building chosen for this example is taken from a study conducted by Vlassis et al. and has previously been described in section 5.7 [195]. The building is a seven storey office structure, as shown in Figure 6.7 below. Figure 6.7 shows a partial front elevation of the structure. Highlighted in the figure is the area affected by a fire that has spread over three storeys. Also shown are the members that must be analysed as a result of the fire. The structure geometry, material properties and loadings are given in tables 5.9 -5.12.

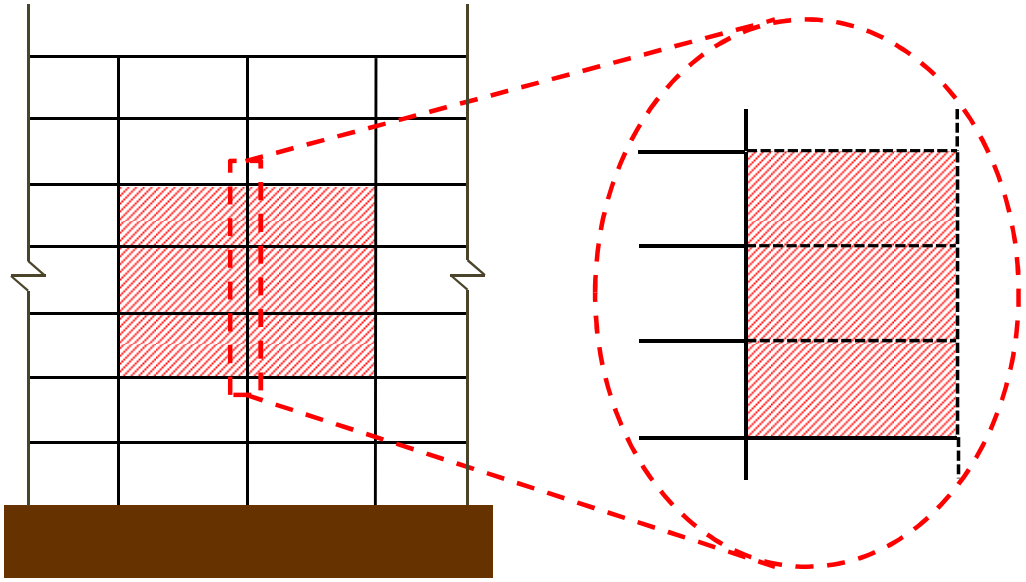

(a) (b)

Figure 6.7: (a) Partial elevation of the building showing three potential fire floors with red hatching, (b) Partial cross section with the structural members to be analysed shown with broken lines.

Structural failure is defined as the occurrence of either weak floor collapse or strong floor collapse. As previously discussed in section 2.4.2, weak floor collapse occurs when the beam beneath the lowest fire floor is insufficient to resist the axial forces and bending moments generated by the sagging of the beams above. Strong floor collapse occurs when the column is unable to resist the large horizontal forces generated by the sagging of the fire affected beams. The strong floor collapse limit is evaluated according to the combined axial and bending capacity of the column based on Eurocode 3 limits, shown in Figure 2.23.

The overall probability of failure was found from a 100000 run Monte Carlo simulation as 64.46%. The probability of failure due solely to weak floor collapse was found to be 0% and the probability of failure due solely to strong floor collapse was found to be 64.46%. From these results it is clear that the weak floor collapse mechanism does not present a threat to this design. However, the strong floor results show that this design does not meet the Eurocode requirements for reliability and would require further improvement, such as the addition of additional fire protection or a stronger column

section. The full results of the Monte Carlo simulations are shown below in Figures 6.8 and 6.9.

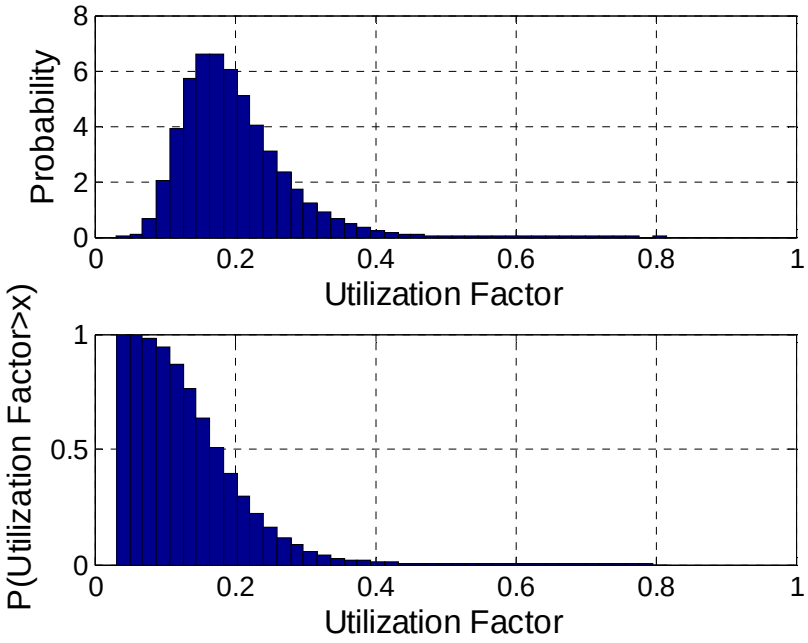

Figure 6.8: (a) Probability of a weak floor utilization factor occurring and (b) Probability of a given weak floor utilization factor being exceeded.

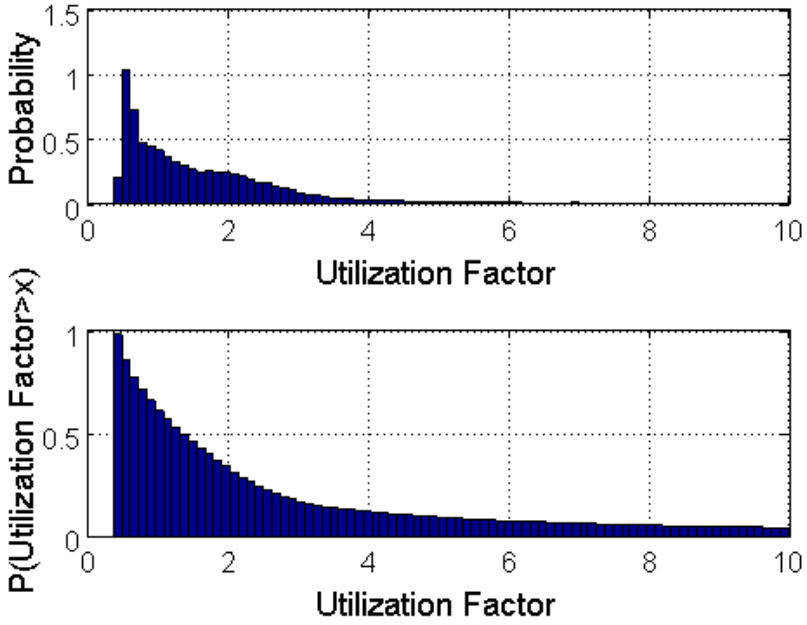

Figure 6.9: (a) Probability of a strong floor utilization factor occurring and (b) Probability of a given strong floor utilization factor being exceeded.

6.5 Summary

In this chapter the software tool FireLab is presented for the performance-based design of steel framed structures in fire. One of the main aims of FireLab is to promote the wider use of performance-based engineering methods in structural fire engineering. In order to achieve this aim the analysis process has been simplified by incorporating all of the models necessary to analyse a structural fire engineering problem within FireLab. FireLab includes a number of fire models, heat transfer models and structural response models. The structural analysis options include composite beam analysis, composite slab analysis and a method for analysing the stability of a tall steel building subject to multi-floor fires. FireLab also includes an interface to external finite element solvers for problems that require a greater level of accuracy or complexity.

FireLab also provides a number of stochastic analysis options, in addition to deterministic analysis. These options are Monte Carlo simulation, the First-Order Reliability Method and the PEER method. The stochastic analysis options allow the user to consider the range of conditions that could occur and to calculate a probability of failure for the structure. The PEER method also allows the user to estimate probable costs due to fire over the lifetime of the structure.

The form of the inputs and outputs to the program are described in this chapter. The incorporation of parallelism in the program for Monte Carlo simulations and its associated advantages are discussed. The capabilities of FireLab are presented and compared to other available fire design software packages. Finally, example applications of the program to various structural elements are given.

Chapter 7: Conclusions and Further Work

7.1 Preamble

This research has examined the use of performance-based design in the field of structural fire engineering. A range of existing analysis models has been examined and their suitability for use in performance-based design has been judged. The important sources of uncertainty have been identified and suitable probability distributions have been assigned to them. A framework for structural fire engineering has been developed, based on the PEER earthquake engineering framework. This framework has been implemented in a software tool, FireLab. This chapter summarises the work presented in this thesis and provides an overview of areas suitable for further research.

7.2 Summary and Conclusions

This thesis has investigated the application of a range of probabilistic analysis methods in the field of structural fire engineering. The advantages of performance-based design over prescriptive design, such as improved economy and structural efficiency, have been discussed. The need for performance-based design to incorporate probability theory in order to quantify the level of safety associated with a structure has been discussed. The PEER-PBEE framework was chosen as the basis for much of the work in this thesis as it is a well-known, well-developed framework with previous application across fields such as earthquake engineering, blast engineering and wind engineering.

- The process of structural fire engineering is discussed and the required inputs and types of analysis model are defined.
- The uncertainty associated with the loading conditions, member geometry and material properties as used in structural fire engineering has been identified. Stochastic definitions have been provided for the relevant input variables.
- A set of physical, analytical models suitable for the probabilistic analysis of structures in fire has been collected. This includes fire models, heat transfer models for both steel and concrete members and structural analysis models for composite beams, composite slabs and multi-storey stability.

- Performance-based engineering is based on the idea of designing to a set of identified performance objectives using engineering methods that are based on scientific principles. The development of performance-based engineering has been covered and a discussion is given of the merits of the performance-based approach over the prescriptive approach. Suitable performance objectives for performance-based design are outlined in this thesis. The importance of defining the risks to the structure and the reliability of the structure for performance-based design are discussed. The application of performance-based design to structural fire engineering is also discussed.
- The practicality of applying the Monte Carlo method to structural fire engineering problems is investigated. The Monte Carlo method is a robust analysis method that can be used either to determine the range of behaviour of a system or to evaluate the probability of failure of a system. The main disadvantage of the Monte Carlo method is that it is computationally expensive, often prohibitively so. In order to reduce the computational work load a number of different approaches were adopted. Analytical solutions were used wherever possible as they are typically much simpler to solve, in comparison with numerical methods. Latin hypercube sampling was used to improve the spread of the chosen samples, thus reducing the total number of samples required to reach a given level of accuracy. Parallelism was employed in the solution of the analysis. By taking advantage of the multiple cores available on modern computers, the run time of an analysis can be significantly reduced.
- In addition to the Monte Carlo method, the practicality of applying the first-order reliability method (FORM) to structural fire engineering was also investigated. The first-order reliability method lacks the robustness of the Monte Carlo method when dealing with highly non-linear problems. This problem is compounded by the fact that the accuracy of the FORM results can vary and this variation is not measured by the analysis.
- One-at-a-time sensitivity analysis was used to identify the input variables with the greatest amount of uncertainty in the analysis of composite beams and slabs under fire loading. The fuel load and area of ventilation were identified as the main sources of uncertainty, as they can dramatically change the nature of the fire load. It was noticed that the uncertainty in the fire development stemming from one of these variables always tends to outweigh the uncertainty from the

other, depending on whether the fire is fuel controlled or ventilation controlled. Other important sources of uncertainty include the loading on the member, the Young's modulus of the construction materials and the strength of the construction members.

- The Pacific Earthquake Engineering Research (PEER) center's framework for performance-based earthquake engineering (PBEE) has been adapted and applied to performance-based structural fire engineering. The PEER framework covers hazard analysis, structural analysis, damage analysis and loss analysis. Suitable models have been identified for use in each stage of the framework. Each stage of the framework is represented by a "pinch variable"; i.e. intensity measures, engineering demand parameters, damage measures and decision variables.
- Peak compartment temperatures were identified as part of this work as a suitable intensity measure. Peak compartment temperatures are particularly suitable for thermally thin members such as exposed structural steel sections. The time taken to reach the peak temperature was found in some cases be a more suitable intensity measure, particularly for heavily insulated members. However, performance based structural fire engineering is often concerned with the performance of beams with little to no fire protection therefore the peak compartment temperature was chosen as the optimal intensity measure.
- Suitable engineering demand parameters (EDPs) have been identified for beams, slabs and columns within a steel-frame composite building. Reinforcement strain was chosen as the EDP for composite slabs. Midspan deflection was chosen as the EDP for composite beams. Strain is not a useful EDP for composite beams as the relative importance of the steel section and the slab reinforcement can vary depending on the design. The utilisation factor was chosen as the EDP for columns to allow for a simple estimate of collapse.
- Fragility functions and cost consequence functions have been developed as part of this work to allow for the calculation of the mean annual rate of exceedance of the decision variables, based on the chosen EDPs. The fragility functions define the likely damage state of the structure based on the demand the structure has been exposed to. The cost consequence functions are then used to calculate the likely cost associated with a given damage state. The decision variables considered in this work are repair cost and downtime due to repair works.

- Examples are given of the PEER framework applied to the analysis of a composite beam under fire loading and a composite slab under fire loading. Relevant stochastic inputs are defined and two different design cases are examined for each member to illustrate the use of the PEER method to compare different designs.
- A further example of the PEER framework applied to a structural sub-assembly is given. This example required the development of a probabilistic model for the rate and extent of vertical fire spread. An elastic, second-order direct stiffness solver was developed to analyse the response of a multi-storey steel column to multiple floor fires and to analyse an unheated composite beam under axial load. In addition to calculating the total mean annual rate of exceedance of the decision variables, this example also provides the mean annual rate of exceedance of the decisions variables due to both collapse induced damage and non-collapse induced damage.
- A software tool, FireLab, was developed as part of this work. FireLab allows engineers to systematically use performance-based engineering methods for the fire resistance design of typical steel-framed composite structures whilst including the effects of uncertainty arising from key input parameters. FireLab features the physical and probabilistic models discussed throughout this thesis.
    - Fire models built into FireLab include:
        - The EC standard temperature-time curve
        - The EC hydrocarbon temperature-time curve
        - The EC parametric temperature-time curve
        - The JCSS temperature-time curve
    - Heat transfer models in FireLab include:
        - Lumped capacitance methods for protected and unprotected steel sections
        - 1 dimensional finite difference method for concrete slabs
        - The finite element program Abaqus may be called to carry out the heat transfer analysis
    - Structural models in FireLab include:
        - Composite beam models, both analytical and numerical
        - Composite slab models
        - Multi-storey stability models

    - Probabilistic analysis options include:
        - Monte Carlo simulation, using either random or Latin hypercube sampling
        - First-order reliability method
        - The PEER method
- FireLab has been developed in order to help spread the adoption of PBSFE. It also helps to spread the use of reliability theory in PBSFE.
- The Firelab program has been validated against a selection of test cases, presented in the appendices.
- FireLab was developed through Matlab as a collection of scripts and functions. This modular approach allows for new models to be easily incorporated as new functions. The development of FireLab in Matlab also allows it to be compiled and distributed as a standalone executable program.

7.3 Further Work

This thesis has been primarily concerned with the development of a performance-based structural fire engineering framework centred on reliability theory. This thesis has also identified suitable models for use in probabilistic analysis and in the PEER framework and these methods have been incorporated into the software tool FireLab. There is scope for improvement to both the physical models and the probabilistic methods presented in this thesis.

In the area of probabilistic analysis:

- Subset simulation could be investigated as an alternative to Monte Carlo simulation for calculating the nominal probability of failure of a structure or structural element.
- Updated fire statistics would improve the accuracy of the analyses and the applicability of the results to modern structures.
- There is a high level of uncertainty associated with the heat transfer process, particularly in judging the coefficients of heat transfer. The accuracy of the predictions could be improved through quantification of the uncertainty surrounding the heat transfer process.

In the area of physical models:

- A two-zone fire model would improve the range of applicability of the FireLab software. It would also allow for the possibility of capturing the effects of window breakage during the fire.
- Analytical solutions to structural response problems provide a simple and quick method of analysing structural elements. However it is difficult to account for nonlinearities within these methods. Nonlinear analytical solutions for composite beams and composite slabs, such as those currently under investigation at the University of Edinburgh, would provide an increased level of accuracy whilst maintaining a short computation time.
- Performance-based engineering requires the assessment of all possible modes of failure and because of this further work is required to incorporate cooling stresses and connection behaviour into the software.

In the area of the PEER-PBSFE framework:

- The incorporation of a vector intensity measure would allow for the more accurate estimation of the probability of damage resulting from fire. A suitable vector of intensity measures would include both peak temperature and time taken to reach the peak temperature.
- Further work is required to accurately estimate damage levels, given the magnitude of the response of the structure to a fire. Work is also required to improve the estimates of the likely repair costs and downtime costs from the level of damage to the structure.
- In the long term, the inclusion of improved fire models, smoke spread models and egress models would lead to the ability to predict the likelihood of fatalities due to fire. The use of improved fire models would also allow for better estimation of the impact of fire on a structure.
- The development of a more detailed fire spread model would allow for a complete structure to be analysed under the PEER-PBSFE framework.

Chapter 8: Bibliography

[1] M. Gillie, “Analysis of Heated Structures: Nature and Modelling Benchmarks,” *Fire Saf. J.*, vol. 44, no. 5, pp. 673–680, Jul. 2009.

[2] A. S. Usmani, J. M. Rotter, S. Lamont, A. M. Sanad, and M. Gillie, “Fundamental Principles of Structural Behaviour under Thermal Effects,” *Fire Saf. J.*, vol. 36, no. 8, pp. 721–744, 2001.

[3] A. S. Usmani and N. J. K. Cameron, “Limit Capacity of Laterally Restrained Reinforced Concrete Floor Slabs in Fire,” *Cem. Concr. Compos.*, vol. 26, no. 2, pp. 127–140, Feb. 2004.

[4] C. G. Bailey, “Membrane Action of Unrestrained Lightly Reinforced Concrete Slabs at Large Displacements,” *Eng. Struct.*, vol. 23, no. 5, pp. 470–483, May 2001.

[5] G. G. Deierlein and S. Hamilton, “Framework for Structural Fire Engineering and Design Methods,” in *NIST-SFPE Workshop for Development of a National R&D Roadmap for Structural Fire Safety Design and Retrofit of Structures: Proceedings*, 2004, pp. 75–99.

[6] The University of Edinburgh, “Behaviour of Steel Framed Structures under Fire Conditions - Main Report,” 2000.

[7] E. Omer, B. A. Izzuddin, and A. Y. Elghazouli, “Failure of Unrestrained Lightly Reinforced Concrete Slabs Under Fire, Part I: Analytical Models,” *Eng. Struct.*, vol. 32, no. 9, pp. 2631–2646, Sep. 2010.

[8] K. A. Porter, “An Overview of PEER’s Performance-Based Earthquake Engineering Methodology,” in *Ninth International Conference on Applications of Statistics and Probability in Civil Engineering (ICASP9)*, 2003, no. 1995.

[9] D. Drysdale, *An Introduction to Fire Dynamics*, Third Ed. John Wiley & Sons, Ltd., 2011.

[10] I. Thomas and I. Bennetts, “Fires in Enclosures with Single Ventilation Openings - Comparison of Long and Wide Enclosures,” in *Fire Safety Science - Proceedings of the Sixth International Symposium*, 1999, pp. 941–952.

[11] S. H. Ingberg, “Tests of the Severity of Building Fires,” *Q. J. Natl. Fire Prot. Assoc.*, vol. 22, pp. 43–61, 1928.

[12] “BS EN 1991-1-2:2002. Eurocode 1: Actions on structures - Part 1-2: General actions-Actions on structures exposed to fire.” BSI, 2002.

[13] Leonardo Da Vinci Pilot Project, “Implementation of Eurocodes - Handbook 5 - Design of Buildings for the Fire Situation,” 2005.

[14] P. Thomas, “Design Guide: Structural Fire Safety CIB W14 Workshop,” *Fire Saf. J.*, vol. 10, no. 2, pp. 77–137, Mar. 1986.

[15] A. H.-S. Ang and W. H. Tang, *Probability Concepts in Engineering - Emphasis on Application to Civil and Environmental Engineering*, 2nd ed. John Wiley & Sons, 2007, p. 406.

[16] M. Law, “A Relationship Between Fire Grading and Building Design and Contents,” in *Fire Research Note No 877*, 1971, no. 877, p. 47.

[17] “JCSS Probabilistic Model Code - Part 2: Load Models.” The Joint Committee on Structural Safety, p. 73, 2001.

[18] “E 119 - Standard Test Methods for Fire Tests of Building Construction and Materials.” ASTM International, p. 21.

[19] “BS 476: Part 20: 1987 Fire tests on building materials and structures - Method for determination of the fire resistance of elements of construction (general principles).” BSI, p. 44, 1987.

[20] C. R. Barnett, “BFD Curve: A New Empirical Model for Fire Compartment Temperatures,” *Fire Saf. J.*, vol. 37, no. 5, pp. 437–463, Jul. 2002.

[21] O. Pettersson, S.-E. Magnusson, and J. Thor, *Fire Engineering Design of Steel Structures*. Swedish Institute of Steel Construction, 1976, p. 234.

[22] “UK National Annex to Eurocode 1: Actions on structures – Part 1-2: General actions – Actions on structures exposed to fire.” BSI, 2002.

[23] “PD 6688-1-2:2007 Background paper to the UK National Annex to BS EN 1991-1-2,” no. 1. BSI, p. 22, 2007.

[24] C. R. Barnett, “Erratum to ‘BFD Curve: A New Empirical Model for Compartment Fire Temperatures’ [Fire Saf J 37(5) (2002) 437-463],” *Fire Saf. J.*, vol. 37, no. 7, p. 719, Oct. 2002.

[25] C. Barnett, “Replacing International Temperature–Time Curves with BFD Curve,” *Fire Saf. J.*, vol. 42, no. 4, pp. 321–327, Jun. 2007.

[26] P. J. DiNenno, D. Drysdale, C. Beyler, W. D. Walton, R. L. P. Custer, J. R. Hall, and J. M. Watts, Eds., *SFPE Handbook of Fire Protection Engineering*, Third., vol. 17, no. 3. National Fire Protection Association, 2002, p. 1604.

[27] O. Pettersson, “Structural Fire Behaviour - Development Trends,” in *Fire Safety Science - Proceedings of the First International Symposium*, 1986, pp. 229–247.

[28] W. W. Jones, R. D. Peacock, G. P. Forney, and P. A. Reneke, “NIST Special Publication 1030 CFAST – Consolidated Model of Fire Growth and Smoke Transport (Version 5) Technical Reference Guide.” National Institute of Standards and Technology, p. 158, 2004.

[29] J.-F. Cadorin and J.-M. Franssen, “A Tool to Design Steel Elements Submitted to Compartment Fires—OZone V2. Part 1: Pre- and Post-Flashover Compartment Fire Model,” *Fire Saf. J.*, vol. 38, no. 5, pp. 395–427, Sep. 2003.

[30] J.-F. Cadorin, D. Pintea, J.-C. Dotreppe, and J.-M. Franssen, “A Tool to Design Steel Elements Submitted to Compartment Fires—OZone V2. Part 2: Methodology and Application,” *Fire Saf. J.*, vol. 38, no. 5, pp. 429–451, Sep. 2003.

[31] K. McGrattan, S. Hostikka, R. McDermott, J. Floyd, C. Weischenk, and K. Overholt, “Fire Dynamics Simulator (FDS) User’s Guide - NIST Special Publication 1019, Sixth Edition,” NIST, 6.1.2, 2013.

[32] FM Global, “FireFOAM.” FM Global, 2014.

[33] G. Rein, X. Zhang, P. Williams, B. Hume, A. Heise, A. Jowsey, B. Lane, and J. L. Torero, “Multi-Storey Fire Analysis for High-Rise Buildings,” in *Proceedings of the 11th International Interflam Conference*, 2007, no. September, pp. 605–616.

[34] J. Stern-Gottfried and G. Rein, “Travelling Fires for Structural Design-Part II: Design Methodology,” *Fire Saf. J.*, vol. 54, no. 11, pp. 96–112, Nov. 2012.

[35] R. L. Alpert, “Calculation of Response Time of Ceiling-Mounted Fire Detectors,” *Fire Technol.*, vol. 8, no. 3, pp. 181–195, 1972.

[36] R. L. Alpert, “The Fire-Induced Ceiling-Jet Revisited,” in *Fireseat*, 2011, pp. 1–22.

[37] J. Stern-Gottfried, G. Rein, B. Lane, and J. L. Torero, “An Innovative Approach to Design Fires for Structural Analysis of Non-Conventional Buildings, a Case Study,” in *Proceeding of International Conference on Appplications of Structural Fire Engineering*, 2009.

[38] A. Buchanan, *Structural Design for Fire Safety*. Wiley-Blackwell, 2001, p. 444.

[39] Y. C. Wang, *Steel and Composite Structures: Behaviour and Design for Fire Safety*. Taylor and Francis, 2002, p. 352.

[40] B. Davison and G. W. Owens, Eds., *Steel Designers' Manual*, Seventh Ed. Wiley-Blackwell, 2013, p. 1400.

[41] Steel Construction Industry Forum, "Investigation of Broadgate Phase 8 Fire." Ascot, UK, p. 88, 1991.

[42] G. M. Newman, J. T. Robinson, and C. G. Bailey, *Fire Safe Design: A New Approach to Multi-Storey Steel-Framed Buildings*, Second. Ascot, Berkshire: The Steel Construction Institute, 2006, p. 116.

[43] S. Lamont, "The Behaviour of Multi-storey Composite Steel Framed Structures in Response to Compartment Fires," PhD Thesis, The University of Edinburgh, 2001.

[44] "BS EN 1993-1-2:2005. Eurocode 3: Design of steel structures - Part 1-2: General rules - Structural fire design." BSI, Sep-2005.

[45] "BS EN 1992-1-2:2004. Eurocode 2: Design of concrete structures — Part 1-2: General rules - Structural fire design." BSI, 2004.

[46] Leonardo Da Vinci Pilot Project, "Implementation of Eurocodes - Handbook 3 - Action Effects for Buildings," Leonardo da Vinci Pilot Project, Aachen, 2005.

[47] "BS EN 1991-1-1:2002. Eurocode 1: Actions on structures — Part 1-1: General actions - Densities, self-weight, imposed loads for buildings," vol. 3. BSI, p. 50, 2002.

[48] "BS EN 1993-1-1:2005. Eurocode 3: Design of steel structures - Part 1-1: General rules and rules for buildings." BSI, Sep-2005.

[49] L. Twilt, "Strength and Deformation Properties of Steel at Elevated Temperatures: Some Practical Implications," *Fire Saf. J.*, vol. 13, no. 1, pp. 9–15, 1988.

[50] Y. Anderberg, "Modelling Steel Behaviour," *Fire Saf. J.*, vol. 13, no. 1, pp. 17–26, 1988.

[51] V. Kodur, M. Dwaikat, and R. Fike, "High-Temperature Properties of Steel for Fire Resistance Modeling of Structures," *J. Mater. Civ. Eng.*, vol. 22, no. 5, pp. 423–434, 2010.

[52] B. R. Kirby and R. R. Preston, "High Temperature Properties of Hot-rolled, Structural Steels for Use in Fire Engineering Design Studies," *Fire Saf. J.*, vol. 13, no. 1, pp. 27–37, 1988.

[53] M. P. Byfield and D. A. Nethercot, “Material and Geometric Properties of Structural Steel for Use in Design,” *Struct. Eng.*, vol. 75, no. 21, pp. 363–367, 1997.

[54] M. Byfield and D. Nethercot, “Safety Variations in Steel Designed Using Eurocode 3,” in *Workshop on Reliability Based Code Calibration*, 2002, pp. 1–7.

[55] *BS EN 1993-1-1:2005: Eurocode 3: Design of steel structures - Part 1-1: General rules and rules for buildings*, vol. 1, no. 1. BSI, 2005, p. 96.

[56] “JCSS Probabilistic Model Code - Part 3: Material Properties.” Joint Committee on Structural Safety, p. 41, Nov-2001.

[57] *Interactive “blue book,”* Version 4. Tata Steel, 2013.

[58] A. M. Neville, *Properties of Concrete*, 4th ed. Pearson-Prentice Hall, 2009.

[59] V. K. R. Kodur, “Properties of Concrete at Elevated Temperatures,” *ISRN Civ. Eng.*, vol. 2014, pp. 1–15, 2014.

[60] U. Schneider, “Concrete at High Temperature - A General Review,” *Fire Saf. J.*, vol. 13, no. 1, pp. 55–68, 1988.

[61] A. W. Beeby and R. S. Narayanan, *Designers’ guide to Eurocode 2: Design of concrete structures Designers' Guide to EN1992-1-1 and EN1992-1-2 Eurocode 2: Design of concrete structures. General rules and rules for buildings and structural fire design*. Thomas Telford, 2010, p. 230.

[62] R. Van Coile, E. Annerel, R. Caspeele, and L. Taerwe, “Probabilistic Analysis of Concrete Beams During Fire,” in *Proceedings of International Conference Applications of Structural Fire Engineering*, 2011, pp. 127–132.

[63] M. Holický, “Verification of Load Factors for Concrete Components by Reliability and Optimization Analysis : Background Documents for Implementing Eurocodes,” *Prog. Struct. Eng. Mater.*, vol. 2, no. 4, pp. 502–507, 2000.

[64] “BS EN 1992-1-1:2004. Eurocode 2: Design of concrete structures - Part 1-1: General rules and rules for buildings.” BSI, 2004.

[65] A. Y. Elghazouli, K. A. Cashell, and B. A. Izzuddin, “Experimental Evaluation of the Mechanical Properties of Steel Reinforcement at Elevated Temperature,” *Fire Saf. J.*, vol. 44, no. 6, pp. 909–919, Aug. 2009.

[66] “Fire Resistance of Steel-Framed Buildings.” Corus, p. 40, Aug-2006.

[67] A. S. Usmani, “Understanding the Response of Composite Structures to Fire,” *Eng. J.*, vol. 42, pp. 83–98, 2005.

[68] N. J. K. Cameron, “The Behaviour and Design of Composite Floor Systems in Fire,” PhD Thesis, The University of Edinburgh, 2003.

[69] A. Heidarpour and M. A. Bradford, “Nonlinear Analysis of Composite Beams with Partial Interaction in Steel Frame Structures at Elevated Temperature,” *J. Struct. Eng.*, vol. 136, no. 8, pp. 968–977, 2010.

[70] B. A. Izzuddin and A. Y. Elghazouli, “Failure of Lightly Reinforced Concrete Members under Fire. I: Analytical Modeling,” *J. Struct. Eng.*, vol. 130, no. 1, pp. 3–17, 2004.

[71] R. P. Johnson and R. J. Buckby, *Composite Structures of Steel and Concrete - Volume 2: Bridges*. London: Collins, 1986.

[72] L. H. Donnell, *Beams, Plates and Shells*. McGraw-Hill Book Company, 1976.

[73] F. McKenna, “Object-Oriented finite element programming: frameworks for analysis, algorithms and parallel computing,” PhD Thesis, University of California, Berkeley, 1997.

[74] A. Usmani, J. Zhang, J. Jiang, Y. Jiang, and I. May, “Using Opensees for Structures in Fire,” *J. Struct. Fire Eng.*, vol. 3, no. 1, pp. 57–70, Mar. 2012.

[75] Abaqus, “Abaqus analysis user’s manual.” Dassault Systemes, Simulia Corp., Providence, 2008.

[76] C. G. Bailey, D. S. White, and D. B. Moore, “The Tensile Membrane Action of Unrestrained Composite Slabs Simulated Under Fire Conditions,” *Eng. Struct.*, vol. 22, no. 12, pp. 1583–1595, Dec. 2000.

[77] S. J. Foster, C. G. Bailey, I. W. Burgess, and R. J. Plank, “Experimental Behaviour of Concrete Floor Slabs at Large Displacements,” *Eng. Struct.*, vol. 26, no. 9, pp. 1231–1247, Jul. 2004.

[78] G. Kennedy and C. Goodchild, *Practical Yield Line Design*. British Cement Association, 2003, p. 175.

[79] C. G. Bailey and D. B. Moore, “The Structural Behaviour of Steel Frames with Composite Floorslabs Subject to Fire : Part 1: Theory,” *Struct. Eng.*, vol. 78, no. 7, pp. 19–27, 2000.

[80] E. Omer, B. A. Izzuddin, and A. Y. Elghazouli, “Failure of Lightly Reinforced Concrete Floor Slabs with Planar Edge Restraints under Fire,” *J. Struct. Eng.*, vol. 135, no. 9, pp. 1068–1080, 2009.

[81] N. J. K. Cameron and A. S. Usmani, “New Design Method to Determine the Membrane Capacity of Laterally Restrained Composite Floor Slabs in Fire Part 1: Theory and Method,” *Struct. Eng.*, vol. 83, no. 10, pp. 28–33, 2005.

[82] N. J. K. Cameron and A. S. Usmani, “A New Design Method to Determine the Membrane Capacity of Laterally Restrained Composite Floor Slabs in Fire Part 2: Validation,” *Struct. Eng.*, vol. 83, no. 10, pp. 34–39, 2005.

[83] F. Graeme, U. Asif, L. Susan, L. Barbara, and T. Jose, “Structural Response of Tall Buildings to Multiple Floor Fires,” *J. Struct. Eng.*, vol. 133, no. 12, pp. 1719–1732, 2007.

[84] A. S. Usmani, C. Roben, and A. Al-Remal, “A Very Simple Method for Assessing Tall Building Safety in Major Fires,” *Steel Struct.*, vol. 9, pp. 17–28, 2009.

[85] D. J. Lange, C. Röben, and A. S. Usmani, “Tall Building Collapse Mechanisms Initiated by Fire: Mechanisms and Design Methodology,” *Eng. Struct.*, vol. 36, no. 3, pp. 90–103, Mar. 2012.

[86] *Yellow Book - Fire Protection for Structural Steel in Buildings - Volume 1*, Fourth Ed., vol. 1. Association for Specialist Fire Protection, 2010, p. 92.

[87] F. A. Ali, P. Shepherd, M. Randall, I. Simms, D. J. O. Connor, and I. Burgess, “The Effect Of Axial Restraint On The Fire Resistance Of Steel Columns,” *J. Constr. Steel Res.*, vol. 46, pp. 305–315, 1998.

[88] A. J. P. M. Correia and J. P. C. Rodrigues, “Fire Resistance of Steel Columns with Restrained Thermal Elongation,” *Fire Saf. J.*, vol. 50, no. 5, pp. 1–11, May 2012.

[89] K. W. Poh and I. D. Bennetts, “Behavor of Steel Columns at Elevated Temperatures,” *J. Struct. Eng.*, vol. 121, no. 4, pp. 676–684, 1995.

[90] J. M. Franssen, D. Talamona, J. Kruppa, and L. G. Cajot, “Stability of Steel Columns in Case of Fire: Experimental Evaluation,” *J. Struct. Eng.*, vol. 124, no. 2, pp. 158–163, Feb. 1998.

[91] Y. Wang and J. Davies, “An Experimental Study of Non-Sway Loaded and Rotationally Restrained Steel Column Assemblies under Fire Conditions: Analysis of Test Results and Design Calculations,” *J. Constr. Steel Res.*, vol. 59, no. 3, pp. 291–313, Mar. 2003.

[92] C. Zhang, G. Li, and Y. Wang, “Probabilistic analysis of steel columns protected by intumescent coatings subjected to natural fires,” *Struct. Saf.*, vol. 50, no. 9, pp. 16–26, 2014.

[93] E. Nigro, A. Bilotta, D. Asprone, F. Jalayer, A. Prota, and G. Manfredi, “Probabilistic approach for failure assessment of steel structures in fire by means of plastic limit analysis,” *Fire Saf. J.*, vol. 68, no. 8, pp. 16–29, 2014.

[94] J.-M. Franssen, “Failure Temperature of a System Comprising a Restrained Column Submitted to Fire,” *Fire Saf. J.*, vol. 34, no. 2, pp. 191–207, 2000.

[95] C. G. Bailey, “The Influence of the Thermal Expansion of Beams on the Structural Behaviour of Columns in Steel-Framed Structures During a Fire,” *Eng. Struct.*, vol. 22, no. 7, pp. 755–768, Jul. 2000.

[96] I. Fletcher, A. Borg, N. Hitchen, and S. Welch, “Performance of Concrete in Fire: A Review of the State of the Art, with a Case Study of the Windsor Tower Fire,” in *6th International Conference Structures in Fire (SiF ’10)*, 2010.

[97] J. G. Routley, “Interstate Bank Building Fire - USFA-TR-022,” no. May. U.S. Fire Administration, p. 41, 1988.

[98] R. Hamburger, W. Baker, J. Barnett, C. Marrion, J. Milke, and H. Nelson, “World Trade Center Building Performance Study - Chapter 2.” FEMA, 2002.

[99] A. Jowsey, J. L. Torero, A. Usmani, B. Lane, and S. Lamont, “Determination of Fire Induced Collapse Mechanisms of Multi-Storey Steel Framed Structures,” in *4th European Conference on Steel and Composite Structures*, 2005, no. June, p. 8.

[100] C. Röben, M. Gillie, and J. Torero, “Structural Behaviour During a Vertically Travelling Fire,” *J. Constr. Steel Res.*, vol. 66, no. 2, pp. 191–197, Feb. 2010.

[101] P. Kotsovinos and A. Usmani, “The World Trade Center 9/11 Disaster and Progressive Collapse of Tall Buildings,” *Fire Technol.*, vol. 49, no. 3, pp. 741–765, Jul. 2012.

[102] A. S. Usmani, Y. C. Chung, and J. L. Torero, “How did the WTC Towers Collapse: A New Theory,” *Fire Saf. J.*, vol. 38, no. 6, pp. 501–533, Oct. 2003.

[103] “Fire Statistics United Kingdom 1988.” Home Office, 1990.

[104] “Fire Statistics Great Britain, 2011 to 2012,” Department for Communities and Local Government, 2012.

[105] W. McGuire, R. Gallagher, and R. Ziemian, *Matrix Structural Analysis*, Second. John Wiley & Sons, Ltd., 2000, p. 459.

[106] W. Weaver and J. M. Gere, *Matrix Analysis of Framed Structures*, Second. D. Van Nostrand, 1980, p. 492.

[107] “MATLAB®.” The Mathworks Inc., Natick, Massachusetts, 2011.

[108] “BS EN 1994-1-1:2004. Eurocode 4: Design of composite steel and concrete structures — Part 1-1: General rules and rules for buildings.” BSI, p. 122, 2004.

[109] R. M. Lawson and K. F. Chung, “Composite Beam Design to Eurocode 4,” vol. 30, no. 1, p. 148, 1994.

[110] E. J. Gibson, “Working with the Performance Approach in Building,” in *CIB State of the Art Report no. 64*, 1982.

[111] IRCC, “Performance-Based Building Regulatory Systems - Principles and Experiences,” 2010.

[112] Applied Technology Council, “ATC-3-06: Tentative Provisions for the Development of Seismic Regulations for Buildings.” Redwood City, 1978.

[113] D. S. Haviland, “Toward a Performance Approach to Life Safety from Fire in Building Codes and Regulations.” Center for Fire Research, National Bureau of Standards, US Department of Commerce, 1978.

[114] Y. Anderberg, “Fire Safety Design practices in Scandinavia,” in *Conference on Fire Safety Design in the 21st Century*, 1991, pp. 30–44.

[115] C. A. Cornell, “Engineering Seismic Risk Analysis,” *Bull. Seismol. Soc. Am.*, vol. 58, no. 5, pp. 1583–1606, 1968.

[116] Structural Engineers Association of California, “Vision 2000 - A framework for performance-based design.” California Office of Emergency Services, 1995.

[117] R. O. Hamburger, “Performance-Based Seismic Engineering: The Next Generation of Structural Engineering Practice,” *Property Risk*, 2001.

[118] “An Alternative Procedure for Seismic Analysis and Design of Tall Buildings Located in the Los Angeles Region.” Los Angeles Tall Buildings Structural Design Council, p. 48, 2011.

[119] AB-083, “Recommended Administrative Bulletin on the seismic Design and review of Tall Buildings Using Non-Prescriptive Procedures.” Structural Engineers Association of Northern California (SEAONC), p. 16, 2007.

[120] M. Willford, A. Whittaker, and R. Klemencic, “Recommendations for the Seismic Design of High-Rise Buildings - Draft.” Council on Tall Buildings and Urban Habitat, p. 28, 2008.

[121] “Tall Buildings Initiative - Guidelines for Performance-Based Seismic Design of Tall Buildings.” Pacific Earthquake Engineering Research Center, 2010.

[122] R. R. Gerges, K. Benuska, and C. Kumabe, “Performance-Based Seismic Design of Tall Buildings,” *Struct. Mag.*, no. 6, pp. 11–18, 2012.

[123] A. Whittaker, R. Hamburger, and M. Mahoney, “Performance-Based Engineering of Buildings for Extreme Events,” in *AISC-SINY Symposium on Resisting Blast and Progressive Collapse*, 2003, pp. 55–66.

[124] C. A. Cornell and H. Krawinkler, “Progress and Challenges in Seismic Performance Assessment,” *PEER News*, 2000.

[125] G. G. Deierlein, H. Krawinkler, and C. A. Cornell, “A Framework for Performance-Based Earthquake Engineering,” in *2003 Pacific Conference on Earthquake Engineering*, 2003, pp. 1–8.

[126] “BS EN 1990: 2002. Eurocode - Basis of structural design.” BSI, 2002.

[127] T. Bedford and R. Cooke, *Probabilistic Risk Analysis: Foundations and Methods*. Cambridge Univ Press, 2001, p. 393.

[128] F. R. Farmer, “Siting Criteria - a New Approach,” *Atom*, vol. 128, pp. 152–170, 1967.

[129] M. F. Versteeg, “External Safety Policy in the Netherlands: An Approach to Risk Management,” *J. Hazard. Mater.*, vol. 17, pp. 215–222, 1988.

[130] Health & Safety Executive, “The Tolerability of Risk from Nuclear Power Stations,” 1992.

[131] M. Law, “Fire Safety Design Practices in the United Kingdom - New Building Regulations,” in *Conference on Fire Safety Design in the 21st Century*, 1991, pp. 259–268.

[132] *The Building Regulations 1985*. England and Wales, 1985.

[133] S. E. Magnusson and O. Pettersson, “Rational Design Methodology for Fire Exposed Load Bearing Structures,” *Fire Saf. J.*, vol. 3, no. 4, pp. 227–241, Mar. 1981.

[134] G. V. Hadjisophocleous, N. Benichou, and a. S. Tamim, “Literature Review of Performance-Based Fire Codes and Design Environment,” *J. Fire Prot. Eng.*, vol. 9, no. 1, pp. 12–40, Jan. 1998.

[135] A. Buchanan, “Fire Engineering for a Performance Based Code,” *Fire Saf. J.*, vol. 23, no. 1, pp. 1–16, 1994.

[136] T. Wakamatsu, “Development of Design System for Building Fire Safety,” in *Fire Safety Science - Proceedings of the Second International Symposium*, 1988, pp. 881–895.

[137] V. Beck, “Fire Research Lecture 1993: Performance Based Fire Safety Design—Recent Developments in Australia,” *Fire Saf. J.*, vol. 23, no. 2, pp. 133–158, 1994.

[138] M. Law, “The New Code of Practice (Part 1) - The Philosophy and Understanding,” in *Seminar at AEA Technology*, 1995, pp. 347–352.

[139] G. Deakin, “Future Codes for Fire Safety Design,” *Fire Saf. J.*, vol. 23, no. 2, pp. 193–218, 1994.

[140] A. Buchanan, “Implementation of Performance-Based Fire Codes,” *Fire Saf. J.*, vol. 32, no. 4, pp. 377–383, Jun. 1999.

[141] The Institution of Structural Engineers, “Guide to the Advanced Fire Safety Engineering of Structures,” London, 2007.

[142] Y. Wang, I. Burgess, F. Wald, and M. Gillie, *Performance-Based Fire Engineering of Structures*. CRC Press, 2013, p. 369.

[143] M. A. Johann, L. D. Albano, R. W. Fitzgerald, and B. J. Meacham, “Performance-Based Structural Fire Safety,” *J. Perform. Constr. Facil.*, vol. 20, no. 1, pp. 45–53, 2006.

[144] D. J. Lange, “Risk and Performance Based Fire Safety Design of Steel and Composite Structures,” PhD Thesis, The University of Edinburgh, 2009.

[145] “BS 7974:2001 Application of Fire Safety Engineering Principles to the Design of Buildings — Code of Practice.” BSI, 2001.

[146] S. Lamont, B. Lane, G. Flint, and A. Usmani, “Behavior of Structures in Fire and Real Design - A Case Study,” *J. Fire Prot. Eng.*, vol. 16, no. 1, pp. 5–35, Feb. 2006.

[147] F. M. Block, C. Yu, and N. A. Butterworth, “The Practical Application of Structural Fire Engineering on a Retail Development in the UK,” *J. Struct. Fire Eng.*, vol. 1, no. 4, pp. 205–218, 2010.

[148] CIB, “Rational Fire Safety Engineering Approach to Fire Resistance of Buildings,” 2001.

[149] *The Building Regulations 2000*, no. 2531. England and Wales, 2001.

[150] N. Metropolis and S. Ulam, “The Monte Carlo Method,” *J. Am. Stat. Assoc.*, vol. 44, no. 247, pp. 335–341, 1949.

[151] R. E. Melchers, *Structural Reliability Analysis and Prediction*, Second Edi. John Wiley & Sons, 1999.

[152] G. I. Schuëller, H. J. Pradlwarter, and P. S. Koutsourelakis, "A Critical Appraisal of Reliability Estimation Procedures for High Dimensions," *Probabilistic Eng. Mech.*, vol. 19, no. 4, pp. 463–474, Oct. 2004.

[153] W. C. Broding, F. W. Diederich, and P. S. Parker, "Structural Optimization and Design Based on a Reliability Design Criterion," *J. Spacecr. Rockets*, vol. 1, no. 1, pp. 56–61, 1964.

[154] K. Shi, Q. Guo, and A. E. Jeffers, "Stochastic Analysis of Structures in Fire by Monte Carlo Simulation," *J. Struct. Fire Eng.*, vol. 4, no. 1, pp. 37–46, Mar. 2013.

[155] M. Matsumoto and T. Nishimura, "Mersenne Twister: A 623-Dimensionally Equidistributed Uniform Pseudorandom Number Generator," *ACM Trans. Model. Comput. Simul.*, vol. 8, no. 1, pp. 3–30, 1998.

[156] D. Kurowicka and R. Cooke, *Uncertainty Analysis with High Dimensional Dependence Modelling*. John Wiley & Sons, Ltd., 2006, p. 284.

[157] M. D. McKay, R. J. Beckman, and W. J. Conover, "A Comparison of Three Methods for Selecting Values of Input Variables in the Analysis of Output from a Computer Code," *Technometrics*, vol. 21, no. 2, pp. 239–245, 1979.

[158] S. Engelund and R. Rackwitz, "A Benchmark Study on Importance Sampling Techniques in Structural Reliability," *Struct. Saf.*, vol. 12, no. 4, pp. 255–276, Jul. 1993.

[159] R. Y. Rubinstein, *Simulation and the Monte Carlo Method*. John Wiley & Sons, 1981, p. 278.

[160] S. Au, "Important Sampling in High Dimensions," *Struct. Saf.*, vol. 25, no. 2, pp. 139–163, Apr. 2003.

[161] S.-K. Au and J. L. Beck, "Estimation of Small Failure Probabilities in High Dimensions by Subset Simulation," *Probabilistic Eng. Mech.*, vol. 16, no. 4, pp. 263–277, 2001.

[162] G. I. Schuëller and H. J. J. Pradlwarter, "Benchmark Study on Reliability Estimation in Higher Dimensions of Structural Systems - An Overview," *Struct. Saf.*, vol. 29, no. 3, pp. 167–182, Jul. 2007.

[163] S. Au, J. Ching, and J. Beck, "Application of Subset Simulation Methods to Reliability Benchmark Problems," *Struct. Saf.*, vol. 29, no. 3, pp. 183–193, Jul. 2007.

[164] S. Au, Z. Wang, and S. Lo, “Compartment Fire Risk Analysis by Advanced Monte Carlo Simulation,” *Eng. Struct.*, vol. 29, no. 9, pp. 2381–2390, Sep. 2007.

[165] S. J. J. Hicks, R. M. M. Lawson, J. W. W. Rackham, and P. Fordham, *Comparative Structure Cost of Modern Commercial Buildings*, Second edi. Ascot, Berkshire: The Steel Construction Institute, 2004, p. 96.

[166] O. Ditlevsen and H. O. Madsen, *Structural Reliability Methods*, 2nd ed. John Wiley & Sons, Ltd., 2005, p. 363.

[167] V. Verderaime, “Illustrated Structural Application of Universal First-Order Reliability Method,” Alabama, 1994.

[168] A. Nataf, “Determination des Distribution Dont les Marges Sont Données,” *Comptes Redus l’Academie des Sci.*, vol. 225, pp. 42–43, 1962.

[169] “Seismic Waves - The Pacific Earthquake Engineering Research Center: A Decade of Achievement,” 2008.

[170] G. G. Deierlein, “Overview of a Comprehensive Framework for Earthquake Performance Assessment,” in *Performance-Based Seismic Design Concepts and Implementation*, 2004, pp. 15–26.

[171] “Pacific Earthquake Engineering Research Center,” 2011. [Online]. Available: http://peer.berkeley.edu/. [Accessed: 25-Nov-2011].

[172] J. P. Conte and Y. Zhang, “Performance Based Earthquake Engineering : Application to an Actual Bridge-Foundation-Ground System,” in *12th Italian National Conference on Earthquake Engineering*, 2007.

[173] E. (Ned) H. Field, “Probabilistic Seismic Hazard Analysis (PSHA) - A Primer.” USGS, p. 8.

[174] J. W. Baker, “An Introduction to Probabilistic Seismic Hazard Analysis (PSHA),” 2008.

[175] N. Luco and C. A. Cornell, “Structure-Specific Scalar Intensity Measures for Near-Source and Ordinary Earthquake Ground Motions,” *Earthq. Spectra*, vol. 23, no. 2, p. 357, 2007.

[176] T. Haukaas, “Finite Element Reliability and Sensitivity Methods for Performance-Based Engineering,” University of California, Berkeley, 2003.

[177] M. Mahsuli and T. Haukaas, “Seismic Risk Analysis with Reliability Methods, Part I: Models,” *Struct. Saf.*, vol. 42, pp. 54–62, May 2013.

[178] R. Medina and H. Krawinkler, “Seismic Demands for Nondeteriorating Frame Structures and Their Dependence on Ground Motions,” 2004.

[179] J. Moehle, B. Stojadinovic, A. Der Kiureghian, and T. Y. Yang, “An Application of PEER Performance-Based Earthquake Engineering Methodology,” 2005.

[180] C. M. Ramirez and E. Miranda, “Building-Specific Loss Estimation Methods & Tools for Simplified Performance-Based Earthquake Engineering,” *Report No. 171*, no. 171. The John A. Blume Earthquake Engineering Center, Stanford University, p. 370, 2009.

[181] C. A. Goulet, C. B. Haselton, J. Mitrani-Reiser, J. L. Beck, G. G. Deierlein, K. A. Porter, and J. P. Stewart, “Evaluation of the Seismic Performance of a Code-Conforming Reinforced-Concrete Frame Building — from Seismic Hazard to Collapse Safety and Economic Losses,” *Earthq. Eng. Struct. Dyn.*, vol. 36, no. 6, pp. 1973–1997, 2007.

[182] A. Touran and L. Suphot, “Rank Correlations in Simulating Construction Costs,” *J. Constr. Eng. Manag.*, vol. 123, no. 9, pp. 297–301, 1997.

[183] R. P. Dhakal and J. B. Mander, “Financial Risk Assessment Methodology for Natural Hazards,” *Bull. New Zeal. Soc. Earthq. Eng.*, vol. 39, no. 2, pp. 91–105, 2006.

[184] Applied Technology Council, “Seismic Performance Assessment of Buildings Volume 1 - Methodology - P-58-1,” FEMA, 2012.

[185] Applied Technology Council, “Seismic Performance Assessment of Buildings Volume 2 - Implementation Guide - P-58-2,” FEMA, 2012.

[186] H. Krawinkler, “Generalising PEER PBEE Methodology to PBSE,” 2009.

[187] G. Augusti and M. Ciampoli, “Performance-Based Design in Risk Assessment and Reduction,” *Probabilistic Eng. Mech.*, vol. 23, no. 4, pp. 496–508, Oct. 2008.

[188] M. Ciampoli, F. Petrini, and G. Augusti, “Performance-Based Wind Engineering: Towards a General Procedure,” *Struct. Saf.*, vol. 33, no. 6, pp. 1–12, Aug. 2011.

[189] G. H. Clannachan, “Modelling and Simulation Aspects of Performance-Based Wind Engineering of Tall Buildings,” PhD Thesis, University of Strathclyde, 2012.

[190] J. B. Schleich, “Valorisation Project: Natural Fire Safety Concept,” Report, ProfilARBED-Recherches, 2001.

[191] S. R. Hamilton, “Performance-Based Fire Engineering for Steel Framed Structures: A Probabilistic Methodology,” PhD Thesis, Stanford University, 2011.

[192] R. H. R. Tide, “Integrity of Structural Steel after Exposure to Fire,” *AISC Eng. J.*, no. 1, pp. 26–38, 1998.

[193] *Technical Report No. 68: Assessment, Design and Repair of Fire-damaged Concrete Structures*. The Concrete Society, 2008, p. 93.

[194] D. Langdon, Ed., *Spon’s Architects' and Builders' Price Book*, 133rd ed. Taylor and Francis, 2008.

[195] A. G. Vlassis, B. A. Izzuddin, A. Y. Elghazouli, and D. A. Nethercot, “Progressive Collapse of Multi-Storey Buildings due to Sudden Column Loss—Part II: Application,” *Eng. Struct.*, vol. 30, no. 5, pp. 1424–1438, May 2008.

[196] S. Lamont, A. S. Usmani, and M. Gillie, “Behaviour of a Small Composite Steel Frame Structure in a ‘Long-Cool’ and a ‘Short-Hot’ Fire,” *Fire Saf. J.*, vol. 39, no. 5, pp. 327–357, Jul. 2004.

[197] F. Morente, J. de la Quintana, and F. Wald, “PART 4 : Software for Fire Design.” pp. 1–43.

[198] J. Fraser-Mitchell, “An Object-Oriented Simulation (CRISP 2) for Fire Risk Assessment,” in *Fire Safety Science - Proceedings of the Fourth International Symposium*, 1994, p. 793.

[199] N. Benichou and D. Yung, “FiRECAM^{TM} : An Equivalency and Performance-Compliance Tool for Cost-Effective Fire Safety Design,” in *International Conference on Engineered Fire Protection Design*, 2001, pp. 11–15.

[200] D. Rini and S. Lamont, “Performance Based Structural Fire Engineering for Modern Building Design,” in *Structures Congress*, 2008, pp. 1–12.

[201] Leonardo Da Vinci Pilot Project, “Implementation of Eurocodes - Handbook 2 - Reliability Backgrounds,” Leonardo Da Vinci Pilot Project, Prague, 2005.

Appendix A Sample Monte Carlo Simulation of a Composite Beam

List of the deterministic inputs (contained in input_det.txt)

Variable Value
amb_temp 20
no_conc_layers 20
no_steel_layers 3
no_void_layers 1
boundary_type 3
allowabledeflection 667
fire_curve_type 1
concrete_type 1
n_analyses 1000
Annual_return 0.02
rebar_type 2

List of text inputs (contained in input_text.txt)

fgr m
steel_protection y
analysistype blank
SamplingMethod random
occupancytype dwelling
firebrigadetype professional
responsetime underten
activemeasures smokedetection
autoalarm y
sprinklertype normalstandard

List of probabilistic inputs (contained in input_prob.txt)

Variable	itype	mu	ccov	
compartment_length		0	15	0.01
compartment_breadth		0	15	0.01
compartment_height		0	3.2	0.01
Av	11	60	0.25	
h_eq	0	1.5	0.01	
L_beam		5	7.5	0.0014
L_slab	0	7.5	0.0001	
hw_mm		0	283	300
tw_mm	0	6	0.08	
tf_mm	0	10.2	0.01	
b_beam_mm		0	165	0.01
d_slab_mm		0	70	0.05
w_slab_mm		0	800	0.1
d_rib_mm		0	60	0.01
lambda_conc		0	0.988	0.01
c_conc	0	840	0.01	
rho_conc		0	1800	0.01
lambda_floors		0	0.988	0.01
c_e_floors		0	840	0.01
rho_e_floors		0	1800	0.01
lambda_walls		0	0.16	0.01
c_e_walls		0	840	0.01
rho_e_walls		0	950	0.01
qfd	8	363.29	98.24	
c_protection		0	837	0.01
lambda_protection		0	0.48	0.01
rho_protection		0	1442	0.01
depth_of_protection		0	0.0125	0.2
trans_spring_1		0	999.9	0.01

udl	8	5054.9	1637.4	
rho_steel	0	7850	0.001	
v_steel	0	0.3	0.001	
sigma_y_steel	0	309300000	0.001	
E_steel	5	2.10E+11	3.969E+19	
alpha_steel	0	999.9	0.001	
E_conc	5	3.5E+10	2.7563E+19	
alpha_conc	0	999.9	0.01	
v_conc	0	999.9	0.01	
sigma_y_c_conc	0	37.5E+06	0.01	
sigma_y_rebar	5	562.3E+06	1.5493E+15	
E_rebar	0	2.10E+11	0.01	
v_rebar	0	999.9	0.01	
alpha_rebar	0	999.9	0.01	
epsilon_p_rebar	0	999.9	0.01	
phi_rebar	0	0.012	0.01	
s_rebar	0	0.3	0.01	
d_rebar	1	0.040	0.02	
w_rib_max_mm	0	999.9	0.01	
w_rib_min_mm	0	999.9	0.01	
lambda_steel	0	999.9	0.001	
c_steel	0	999.9	0.001	
epsilon_c_conc	0	999.9	0.01	
sigma_y_t_conc	0	999.9	0.01	
epsilon_t_conc	0	999.9	0.01	
epsilon_p_steel	0	999.9	0.01	
ds_limit_1	0	999.9	0.001	
ds_limit_2	0	999.9	0.0001	
cc_cost_1	0	999.9	1.2	
cc_cost_2	0	999.9	0.2	
cc_time_1	0	999.9	0.1	
cc_time_2	0	999.9	0.03	

Results from the above analysis

Probability of failure: 2.6%

Mean of the maximum deflections: 303mm

Standard deviation of the maximum deflections: 42.6mm

Mean of the peak temperatures: 831°C

Standard deviation of the peak temperatures: 132°C

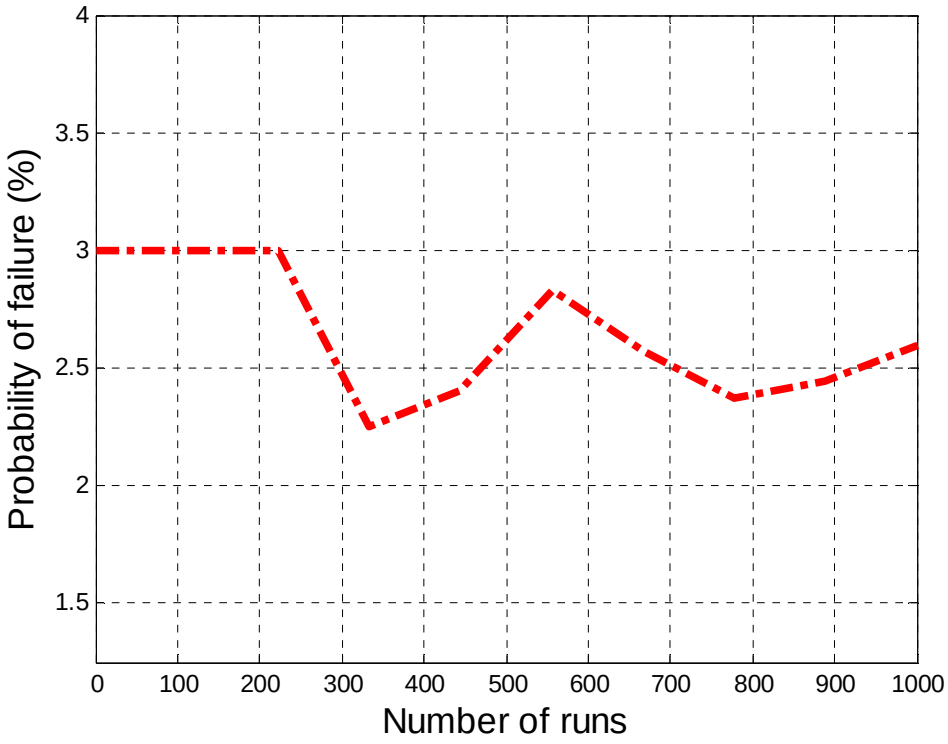

The above graph shows the convergence of the probability of failure during the Monte Carlo simulation. As the number of runs increases, the variance of the estimator decreases and the red line (which represents the estimate of the probability of failure) begins to approach the exact probability of failure.

Appendix B Sample PEER Analysis of a Composite Slab

List of deterministic inputs (contained in input_det_slab_C.txt)

Variable	Value
amb_temp	20
no_conc_layers	4
allowabledeflection	640
fire_curve_type	1
concrete_type	1
rebar_type	2
n_analyses	1000
no_tsteps	801

List of text inputs (contained in input_text_slab_C.txt)

fgr	m
analysistype	cameron
SamplingMethod	latinhypercube
occupancytype	office
firebrigadetype	professional
responsetime	overthirty
activemeasures	smokedetection
autoalarm	n
sprinklertype	none

List of probabilistic inputs (contained in input_prob_slab_C.txt)

Variable	itype	mu	ccov
compartment_length	0	15	0.01
compartment_breadth	0	15	0.01

compartment_height	0	2.7	0.01	
Av	11	60	0.25	
h_eq	0	1.5	0.01	
lambda_floors	0	0.988	0.001	
c_e_floors	0	840	0.1	
rho_e_floors	0	1800	0.1	
lambda_walls	0	0.16	0.001	
c_e_walls	0	840	0.1	
rho_e_walls	0	950	0.1	
qfd	8	363.29	98.24	
L_slab	5	7.5	0.0014	
B_slab	5	7.5	0.0014	
h_slab	5	0.07	1.225E-7	
rebar_dia_xx	0	7	0.01	
rebar_dia_yy	0	7	0.01	
rebar_spacing_x	0	200	0.01	
rebar_spacing_y	0	200	0.005	
d_rebar_xx	0	55	0.01	
d_rebar_yy	0	55	0.01	
udl	8	3.7912	1.2280	
additional_dead_load	0	0.7	0.03	
E_conc	5	3.50E+10	2.7563E+19	
v_conc	0	2.00E-01	0.1	
rho_conc	0	1800	0.1	
alpha_conc	0	8.00E-06	0.000001	
sigma_y_c_conc	0	8.96E+06	0.1	
E_steel	0	2.10E+11	0.1	
v_steel	0	0.3	0.001	
rho_steel	0	7850	0.1	
alpha_steel	0	1.20E-05	0.00001	
sigma_y_steel	0	2.75E+08	0.1	
E_rebar	0	2.1E+11	0.01	
v_rebar	0	3.00E-01	0.001	

rho_rebar	0	7850	0.1
alpha_rebar	0	1.20E-05	0.02
sigma_y_rebar	0	6.00E+08	0.067
ds_limit_1	5	3.948E-5	1.0E-12
ds_limit_2	5	0.0029	1.0E-12
cc_cost_1	5	0.1072	0.004
cc_cost_2	5	1.1802	0.944
cc_time_1	5	2.60	0.270
cc_time_2	5	7.30	2.132

Results from the above analysis

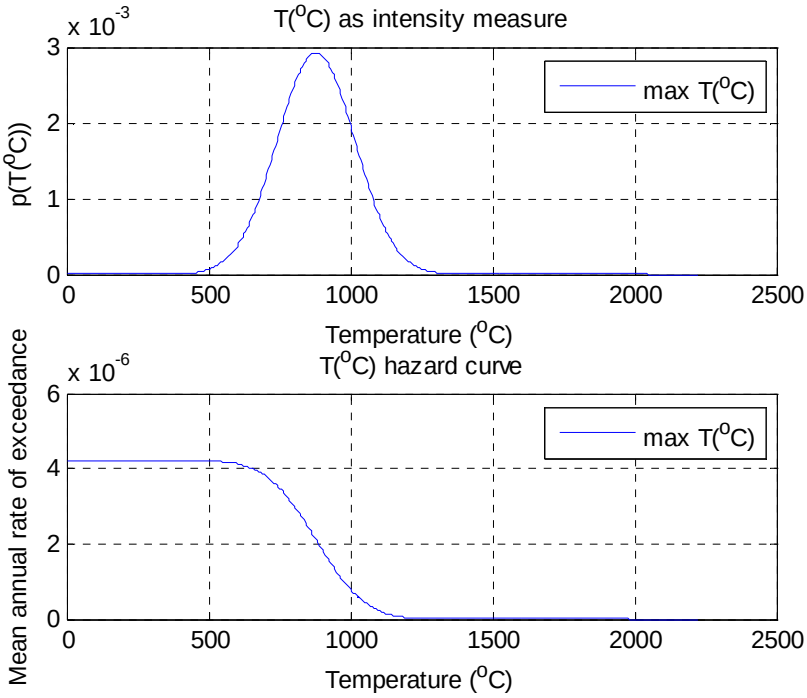

Figure B1: Intensity measure hazard curve.

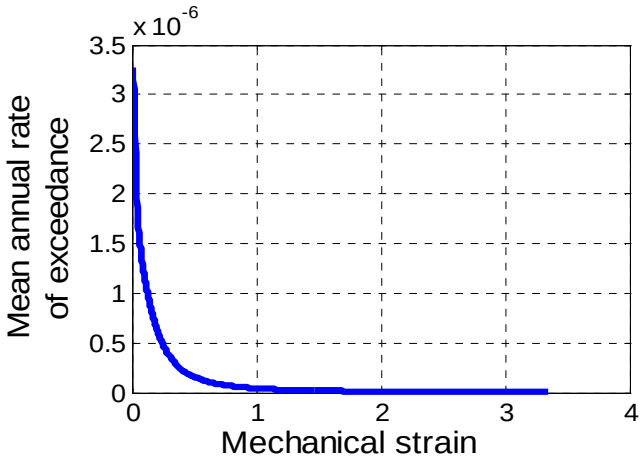

Figure B2: Engineering demand parameter exceedance curve.

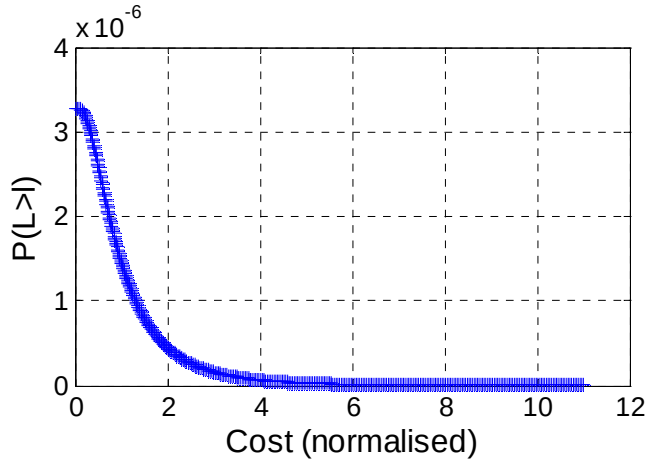

Figure B3: Mean annual exceedance curve for monetary cost.

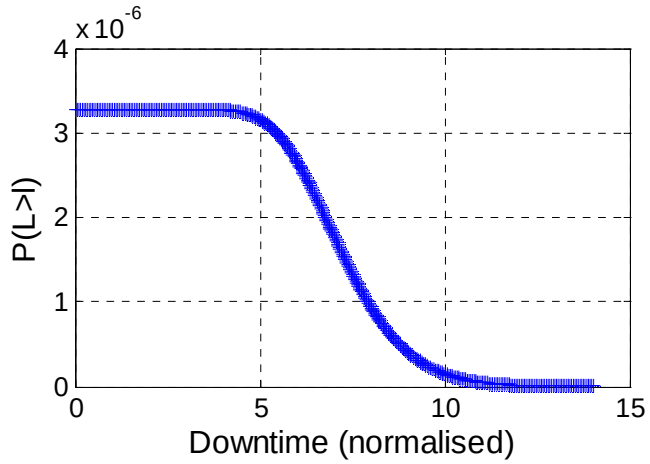

Figure B4: Mean annual exceedance curve for downtime.

Appendix C Spreadsheet Input Form for Composite Beam Analysis

Composite Beam Analysis

Type of analysis:	Deterministic			
Fire Curve Definition				
Fire curve type:	Parametric Eurocode			
	Distribution Parameter 1	**units**	**Distribution Parameter 2**	**Distribution Type**
Length of compartment:	10	m		Deterministic
Breadth of compartment:	10	m		
Height of compartment:	3	m		
Area of ventilation	30	m^2		
Averaged height of the openings:	1	m		
Conductivity of the compartment floor:	0.988	W/mK		
Specific heat capacity of the compartment floor:	840	J/kgK		
Density of the compartment floor:	1400	kg/m^3		
Conductivity of the compartment walls	0.16	W/mK		
Specific heat capacity of the compartment walls:	840	J/kgK		
Density of the compartment walls:	1100	kg/m^3		
Fire load density	370	MJ/m^2		
Fire growth rate	m			
Structural Geometry Definition				
Length of the beam	8	m		
Height of the web	273	mm		
Thickness of the web	8	mm		
Thickness of the flange	10	mm		
Breadth of the beam	220	mm		
Length of the slab	8	m		
Depth of the slab	100	mm		
Width of the slab	1200	mm		
Depth of the rib	40	mm		
Depth to the steel reinforcement	0.06	m		
Diameter of the steel reinforcement	0.008	m		
Spacing of the steel reinforcement	0.2	m		
Material Definition				
Density of the steel	7850	kg/m^3		
Poisson's ratio of steel	0.3			
Young's modulus of steel	2.10E+11	N/m^2		
Yield stress of steel	2.75E+08	N/m^2		
Coefficient of thermal expansion of steel	1.20E-05	/°C		
Type of concrete in the slab	NWC			
Conductivity of concrete	0.988	W/mK		
Specific heat capacity of concrete	840	J/kgK		
Density of concrete	1400	kg/m^3		
Young's modulus of concrete	1.79E+10	N/m^2		
Coefficient of thermal expansion of concrete	1.00E-06	/°C		
Poisson's ratio of concrete	0.2			
Compressive strength of concrete	27	MPa		
Type of steel reinforcement	Hot worked			
Yield stress of the steel reinforcement	6.00E+08	N/m^2		
Young's modulus of the steel reinforcement	2.10E+11	N/m^2		

Steel Protection Definition				
Does the steel have protection applied	Yes			
Specific heat capacity of the steel protection	837	J/kgK		
Conductivity of the steel protection	0.48	W/mK		Deterministic
Density of the steel protection	1442	kg/m^3		
Depth of the steel protection	0.04	m		
Total load on the beam	4000	N/m		
Other inputs				
Ambient temperature	20	°C		
Number of concrete layers	20			
Number of steel layers	3			
Number of void layers	1			
Boundary Type	3			
Alllowable deflection	400	mm		
Number of analysis runs	20			
Annual return	0.02			
Sampling method for Monte Carlo Simulation	random			
	Save the input files:		Save Btn	
	Run the program:		Run Btn	

Appendix D Spreadsheet Input Form for Composite Slab Analysis

Composite Slab Analysis (Bailey Method)

Type of analysis:	Deterministic			
Fire Curve Definition				
Fire curve type:	Parametric Eurocode			
	Distribution Parameter	**units**	**istribution Parameter**	**Distribution Type**
Length of compartment:	10	m		Deterministic
Breadth of compartment:	10	m		
Height of compartment:	3	m		
Area of ventilation	30	m^2		
Averaged height of the openings:	1	m		
Conductivity of the compartment floor:	0.988	W/mK		
Specific heat capacity of the compartment floor:	840	J/kgK		
Density of the compartment floor:	1400	kg/m^3		
Conductivity of the compartment walls	0.16	W/mK		
Specific heat capacity of the compartment walls:	840	J/kgK		
Density of the compartment walls:	1100	kg/m^3		
Fire load density	370	MJ/m^2		
Fire growth rate	m			
Structural Geometry Definition				
Primary beam definition				
Length of the primary beams	8	m		
Height of the web	273	mm		
Thickness of the web	8	mm		
Thickness of the flange	10	mm		
Breadth of the beam	220	mm		
Secondary beam definition				
Number of secondary beams	3			
Spacing of the secondary beams	3	m		
Level of beam utilisation	0.9			
Length of the beam	8	m		
Height of the web	273	mm		
Thickness of the web	8	mm		
Thickness of the flange	10	mm		
Breadth of the beam	220	mm		
Section mass per m	40	kg/m		
Concrete slab definition				
Length of the slab	7.5	m		
Breadth of the slab	7.5	m		
Depth of the slab	100	mm		
Depth of the rib	40	mm		
Thickness of the steel decking	1.2	mm		
Cover to steel reinforcement	40	mm		
Diameter of the steel reinforcement	7	mm		
Spacing of the steel reinforcement (along x and y axes)	200	mm		
Steel decking definition				
Type of steel decking	ComFlor_46			
Orthogonality	Not isotropic			
Material Definition				
Density of the steel	7850	kg/m^3		
Poisson's ratio of steel	0.3			
Young's modulus of steel	2.10E+11	N/m^2		
Yield stress of steel	2.75E+08	N/m^2		
Coefficient of thermal expansion of steel	1.20E-05	/°C		
Type of concrete in the slab	NWC			
Density of concrete	1400	kg/m^3		
Young's modulus of concrete	1.79E+10	N/m^2		
Coefficient of thermal expansion of concrete	1.00E-06	/°C		
Poisson's ratio of concrete	0.2			
Compressive strength of concrete	27	MPa		
Type of steel reinforcement	Cold rolled			
Yield stress of the steel reinforcement	5.00E+08	N/m^2		
Young's modulus of the steel reinforcement	2.10E+11	N/m^2		
Poisson's ratio of the steel reinforcement	0.3			
Density of the steel reinforcement	7850	kg/m^3		
Coefficient of thermal expansion of steel reinforcement	1.20E-05	/°C		

Steel Protection Definition				
Does the steel have protection applied	Yes			
Specific heat capacity of the steel protection	837	J/kgK		
Conductivity of the steel protection	0.48	W/mK		
Density of the steel protection	1442	kg/m³		
Depth of the steel protection	0.04	m		
Imposed load	4	kN/m²		
Additional dead load	0.5	kN/m²		
Other inputs				
Ambient temperature	20	°C		
Alllowable deflection	0.46	m		
Number of analysis runs	20			
Sampling method for Monte Carlo Simulation	random			
Save the input files:	Need to fix the script so that it calls the det and text input files.			
Run FireLab:				

Appendix E Spreadsheet Input Form for Multi-Storey Stability Analysis

Analysis of Multi-Storey Steel Framed Structures under Multiple Fires					
Type of analysis:	Deterministic				
Fire Curve Definition					
Fire curve type:	Parametric Eurocode				
	Distribution Parameter 1	**units**	**Distribution Parameter 2**	**Distribution Type**	
Length of compartment:	10	m			
Breadth of compartment:	10	m			
Height of compartment:	3.6	m			
Area of ventilation	50	m^2			
Averaged height of the openings:	1.4	m			
Conductivity of the compartment floor:	0.988	W/mK			
Specific heat capacity of the compartment floor	840	J/kgK			
Density of the compartment floor:	1400	kg/m^3			
Conductivity of the compartment walls	0.16	W/mK			
Specific heat capacity of the compartment walls	840	J/kgK			
Density of the compartment walls:	950	kg/m^3			
Fire load density	450	MJ/m^2			
Fire growth rate	Medium				
Fire Spread Definition					
Deterministic or probabilistic fire spread	Probabilistic				
Deterministic					
Number of fire floors	2				
Time to fire spread	0.0,0.5	hours			
Probabilistic					
Maximum number of fire floors considered	3				
Probability of upward fire spread	0.4				
Probability of downward fire spread	0.2				
Fault Tree Analysis of Fire Occurrence					
Occupancy/Activity type:	office				
Local fire brigade type:	professional				
Anticipated response time between alarm activation and action of the firemen:	10 to 20 minutes				
Type of active measures:	Smoke detectors				
Automatic transmission to fire brigade:	No				
Sprinkler type:	None				
Structural Geometry Definition					
Beam geometry					
Length of the beam	7	m			
Height of the beam web	350	mm			
Thickness of the beam web	8	mm			
Thickness of the beam flange	12	mm			
Breadth of the beam flange	280	mm			
Width of the slab	6	m			
Depth of the slab	0.08	m			
Depth of the rib	0.03	m			
Stiffness of the axial spring restraining the bea	10000000	N/m			

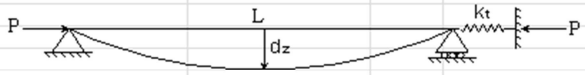

Column geometry				
Height of the column	3.6	m		
Height of the column web	225	mm		
Thickness of the column web	9	mm		
Thickness of the column flange	10	mm		
Breadth of the column flange	220	mm		
Radius of the column	6	mm		
Second moment of area of the column	6.00E+07	mm^4		
Cross-sectional area of the column	4.00E+03	mm^2		
Axis of bending	yy			
Material Definition				
Yield stress of steel	275	N/mm^2		
Young's modulus of steel	200	kN/mm^2		
Coefficient of thermal expansion of steel	1.60E-06	/°C		
Density of the steel	7850	kg/m^3		
Type of concrete in the slab	NWC			
Compressive strength of concrete	30	N/mm^2		
Tensile strength of concrete	0	N/mm^2		
Density of concrete	1800	kg/m^3		
Young's modulus of concrete	1.79E+10	kN/mm^2		
Steel Protection Definition				
Steel beam protection				
Specific heat capacity of the steel protection	837	J/kgK		
Conductivity of the steel protection	0.48	W/mK		
Density of the steel protection	1442	kg/m^3		
Depth of the steel protection	0.04	m		
Steel column protection				
Specific heat capacity of the steel protection	837	J/kgK		
Conductivity of the steel protection	0.48	W/mk		
Density of the steel protection	1442	kg/m^3		
Depth of the steel protection	0.05	m		
Load Definition				
Vertical load on top of the column	300	kN		
Uniformly distributed load on the beam	5	kN/m		
Damage Definition				
Fragility functions for the composite beam				
Damage State 1	0.1			
Damage State 2	1			
Decision Variables				
Monetary cost consequence functions				
Column collapse	2			
Beam DS1	0.25			
Beam DS2	1.54			
Downtime cost consequence functions				
Column collapse	10			
Beam DS1	2.8			
Beam DS2	10.1			
Miscellaneous Input Definition				
Ambient temperature	20	°C		
Number of analysis runs	30			
Sampling method for Monte Carlo Simulation	random			
Save the input files:	Save Button			
Run FireLab:	Run FireLab Analysis			

Appendix F Validation of the Beam Analysis Methods

There are four methods of beam analysis considered in this thesis; the method of slices, the Cameron method, OpenSees finite element analysis and Abaqus finite element analysis. The two methods implemented in Matlab by the author (the method of slices and the Cameron method) are examined in this appendix. The methods are validated by comparison against OpenSees models. OpenSees is well regarded finite element package that is widely used in structural fire engineering.

Method of Slices for the Analysis of Composite Beams

The method of slices is discussed in detail in section 2.4.2 of this thesis. The accuracy of the method, as implemented in Matlab, is examined here by comparison of the analysis of the results with an OpenSees model. The method of slices is an approximate analytical method. It is uses assumptions to simplify the load transfer mechanism and the material behaviour.

The example beam is a 6m steel-concrete composite beam under fire load and a transverse uniformly distributed load. The beam is taken as simply supported. The steel beam has fire protection applied to it. The full details of the beam are given below.

Deterministic Inputs

amb_temp 20

no_conc_layers 20

no_steel_layers 3

no_void_layers 1

boundary_type 1

fire_curve_type 1

concrete_type 1

Potentially Probabilistic Inputs

compartment_length	15
compartment_breadth	15
compartment_height	3.9
Av	20
h_eq	1
L_beam	6
L_slab	6
hw_mm	283
tw_mm	6
tf_mm	10.2
b_beam_mm	165
d_slab_mm	100
w_slab_mm	800
d_rib_mm	60
lambda_lwc	0.988
c_lwc	840
rho_lwc	1800
lambda_floors	0.988
c_e_floors	840
rho_e_floors	1800
lambda_walls	0.16
c_e_walls	840
rho_e_walls	950
qfd	200
c_protection	837
lambda_protection	0.48
rho_protection	1442
depth_of_protection	0.05

trans_spring_1 1000

udl 2000.0

rho_steel 7850

v_steel 0.3

sigma_y_steel 275000000

E_steel 2.10E+11

alpha_steel 1.20E-05

E_lwc 1.79E+10

alpha_lwc 8.00E-06

v_lwc 2.00E-01

sigma_y_c_lwc 8.96E+06

sigma_y_rebar 6.00E+08

E_rebar 2.10E+11

v_rebar 0.3

alpha_rebar 1.22E-05

epsilon_p_rebar 0

phi_rebar 0.016

s_rebar 0.2

d_rebar 0.045

w_rib_max_mm 120

w_rib_min_mm 60

lambda_steel 53.33

c_steel 439.802

epsilon_c_conc 0

sigma_y_t_conc 1500000

epsilon_t_conc 0

epsilon_p_steel 0

Text Inputs

fgr m

steel_protection y

The nature of the analysis results vary depending on the chosen method. The method of slices procedure calculates the deflection of the beam for each time step, but only at the midspan of the beam. The OpenSees model calculates the deflection at a number of points along the beam, but it does not calculate the deflection at every time step due to the amount of calculation required. Therefore, the midspan deflections corresponding to the peak fire temperature are used to compare the models. The method of slices predicts a midspan deflection of 23mm and the OpenSees model predicts 20.3mm of deflection. This is an acceptable level of accuracy as the two approaches are based on very different assumptions.

Cameron's method for the Analysis of Composite Beams

Cameron's method is discussed in detail in section 2.4.2 of this thesis. The accuracy of the method, as implemented in Matlab, is examined here by comparison of the analysis of the results with an OpenSees beam model.

The example beam is a 9m steel-concrete composite beam under fire load and a transverse uniformly distributed load. The steel beam does not have fire protection applied to it. The full details of the beam are given below.

<u>Deterministic Inputs</u>

Variable Value

amb_temp 20

no_conc_layers 20

no_steel_layers 3

no_void_layers 1

boundary_type 1

allowabledeflection 800

fire_curve_type 1

concrete_type 1

n_analyses 50

Annual_return 0.02

rebar_type 2

Potentially Probabilistic Inputs

Variable	itype	mu	ccov
compartment_length	0	15	0.01
compartment_breadth	0	15	0.01
compartment_height	0	3.9	0.01
Av	0	20	0.2
h_eq	0	1	0.01
L_beam	1	9	0.01
L_slab	0	9	0.0001
hw_mm	0	283	300
tw_mm	0	6	0.08
tf_mm	0	10.2	0.01
b_beam_mm	0	165	0.01
d_slab_mm	0	100	0.05
w_slab_mm	0	600	0.1
d_rib_mm	0	60	0.01
lambda_lwc	0	0.988	0.01
c_lwc	0	840	0.01
rho_lwc	0	1800	0.01
lambda_floors	0	0.988	0.01
c_e_floors	0	840	0.01
rho_e_floors	0	1800	0.01
lambda_walls	0	0.16	0.01

c_e_walls	0	840	0.01		
rho_e_walls	0	950	0.01		
qfd	8	170	98.24		
c_protection	0	837	0.01		
lambda_protection	0	0.48	0.01		
rho_protection	0	1442	0.01		
depth_of_protection	0	0.05	0.2		
trans_spring_1	0	1000	0.01		
udl	1	7500.0	0.1		
rho_steel	0	7850	0.001		
v_steel	0	0.3	0.001		
sigma_y_steel	0	275000000	0.001		
E_steel	0	2.10E+11	0.001		
alpha_steel	0	1.20E-05	0.001		
E_lwc	0	1.79E+10	0.01		
alpha_lwc	0	8.00E-06	0.01		
v_lwc	0	2.00E-01	0.01		
sigma_y_c_lwc	0	8.96E+06	0.01		
sigma_y_rebar	0	6.00E+08	0.01		
E_rebar	0	2.10E+11	0.01		
v_rebar	0	0.3	0.01		
alpha_rebar	0	1.22E-05	0.01		
epsilon_p_rebar	0	0	0.01		
phi_rebar	0	0.016	0.01		
s_rebar	0	0.2	0.01		
d_rebar	0	0.045	0.02		
w_rib_max_mm	0	120	0.01		

w_rib_min_mm	0	60	0.01	
lambda_steel	0	53.33	0.001	
c_steel	0	439.802	0.001	
epsilon_c_conc	0	0	0.01	
sigma_y_t_conc	0	1500000	0.01	
epsilon_t_conc	0	0	0.01	
epsilon_p_steel	0	0	0.01	
ds_limit_1	1	0.1	0.001	
ds_limit_2	1	1.0	0.0001	
cc_cost_1	5	0.25	1.2	
cc_cost_2	5	1.54	0.2	
cc_time_1	5	2.80	0.1	
cc_time_2	5	10.10	0.03	

Text Inputs

fgr	m
steel_protection	n
analysistype	blank
SamplingMethod	latinhypercube
occupancytype	dwelling
firebrigadetype	professional
responsetime	underten
activemeasures	smokedetection
autoalarm	y
sprinklertype	normalstandard

The OpenSees analysis predicts a peak midspan displacement of 658mm. This compares well with the peak midspan displacement of 612mm. The differences in the two results

are due to the number of assumptions inherent in the Cameron method and in the differences between the material models used by each method.

Appendix G Validation of the Slab Analysis Methods

There are three methods of slab analysis considered in this thesis; the Cameron method, the Bailey method and the Izzuddin method. The suitability of each of these methods for the analysis of concrete slabs and their implementation in Matlab is examined in this appendix.

Cameron Method for the Analysis of Composite Slabs

The Cameron method for the analysis of composite slabs is discussed in detail in section 2.4.2 of this thesis. The accuracy of the method, as implemented in Matlab, is examined here by comparison with published results from Cameron and Usmani (Cameron and Usmani, 2005, A new design method to determine the membrane capacity of laterally restrained composite floor slabs in fire – Part 2, The Structural Engineer, 10, pp. 34-39). Cameron and Usmani examined a 6m x 9m slab under fire conditions. They calculated that the slab would require a deflection of 336mm to carry the imposed load through membrane action. The Matlab scripts calculate that the slab would need to deflect by 334mm to carry the imposed load. This is an excellent match with the results of Cameron and Usmani. The input files used with the Matlab scripts are presented below.

Deterministic Inputs

Variable	Value
amb_temp	20
no_conc_layers	4
allowabledeflection	640
fire_curve_type	1
concrete_type	1
rebar_type	2
n_analyses	40
no_tsteps	801

Potentially Probabilistic Inputs

Variable	itype	mu	ccov

compartment_length	1	15	0.01	
compartment_breadth	1	15	0.01	
compartment_height	1	2.7	0.01	
Av	1	60	0.025	
h_eq	1	1.5	0.01	
lambda_floors	1	0.988	0.001	
c_e_floors	1	840	0.1	
rho_e_floors	1	1800	0.1	
lambda_walls	1	0.16	0.001	
c_e_walls	1	840	0.1	
rho_e_walls	1	950	0.1	
qfd	1	363.29	0.01	
L_slab	1	9	0.001	
B_slab	1	6	0.001	
h_slab	1	0.07	0.0063	
rebar_dia_xx	1	7	0.01	
rebar_dia_yy	1	7	0.01	
rebar_spacing_x	1	200	0.01	
rebar_spacing_y	1	200	0.005	
d_rebar_xx	1	55	0.01	
d_rebar_yy	1	55	0.01	
udl	1	4.9	0.05	
additional_dead_load	1	0.0	0.03	
E_conc	1	4.00E+10	0.1	
v_conc	1	2.00E-01	0.1	
rho_conc	1	1800	0.1	
alpha_conc	1	8.00E-06	0.000001	

sigma_y_c_conc	1	44E+06	0.1
E_steel	1	2.10E+11	0.1
v_steel	1	0.3	0.001
rho_steel	1	7850	0.1
alpha_steel	1	1.20E-05	0.00001
sigma_y_steel	1	2.75E+08	0.1
E_rebar	1	2.1E+11	0.01
v_rebar	1	3.00E-01	0.001
rho_rebar	1	7850	0.1
alpha_rebar	1	1.20E-05	0.02
sigma_y_rebar	1	6.00E+08	0.067
ds_limit_1	1	0.0250	0.0040
ds_limit_2	5	0.2000	0.0600
cc_cost_1	5	-0.7991	-0.0626
cc_cost_2	5	0.9059	0.2208
cc_time_1	5	1.5711	0.0318
cc_time_2	5	2.4379	0.0820

Text Inputs

fgr	m
analysistype	cameron
SamplingMethod	latinhypercube
occupancytype	office
firebrigadetype	amateur
responsetime	twentytothirty
activemeasures	none
autoalarm	n
sprinklertype	none

Bailey Method for the Analysis of Composite Slabs

The Bailey method for the analysis of composite slabs is discussed in detail in section 2.4.2 of this thesis. The accuracy of the method, as implemented in Matlab, is examined here by comparison with published results from Annex B of the FRACOF report by Bailey et al.

The slab is a re-entrant composite deck. A single panel of the deck is 9m by 12m with 3 unprotected secondary beams, spaced at regular intervals, spanning the breadth of the slab. The fire load is not specified in the published example. Only the member temperatures are given, therefore these temperatures are used in the Matlab example as well. The primary steelwork is assumed to be protected. The input files for the example are given below.

Deterministic Inputs

Variable	Value
amb_temp	20
allowabledeflection	0.46
fire_curve_type	1
No_sec_beams	3
sec_beam_spacing	3
beam_utilisation	0.9
concrete_type	1
rebar_type	2
n_analyses	100
no_tsteps	150

Potentially Probabilistic Inputs

Variable	itype	mu	ccov
compartment_length	1	12	0.1
compartment_breadth	1	9	0.1
compartment_height	1	3	0.1

Av	1	40	0.1	
h_eq	1	1	0.05	
L_slab	1	12	0.1	
B_slab	1	9	0.1	
deck_thickness	1	1.2	0.05	
h_slab	1	0.12	0.01	
L_beam_pri	1	12	0.1	
tw_pri_mm	1	8.5	0.1	
tf_pri_mm	1	12.7	0.1	
hw_pri_mm	1	428	0.1	
b_beam_pri_mm	1	189.9	0.1	
L_beam_sec	1	9	0.1	
tw_sec_mm	1	6.4	0.1	
tf_sec_mm	1	8.6	0.1	
hw_sec_mm	1	380.8	0.1	
b_beam_sec_mm	1	141.8	0.1	
sec_mass_per_m	1	39	0.1	
rebar_dia_xx	1	6	0.1	
rebar_dia_yy	1	6	0.1	
rebar_spacing_x	1	200	0.1	
rebar_spacing_y	1	200	0.1	
mesh_area_xx	1	142	0.1	
mesh_area_yy	1	142	0.1	
cover	1	30	0.1	
E_conc	1	1.79E+10	0.1	
v_conc	1	0.2	0.01	
rho_conc	1	2300	0.1	
alpha_conc	1	12.00E-06	0.000001	
sigma_y_c_conc	1	25000000	0.1	

E_steel	1	2.10E+11	0.1	
v_steel	1	0.3	0.1	
rho_steel	1	7850	0.1	
alpha_steel	1	1.20E-05	0.1	
sigma_y_steel	1	2.75E+08	0.1	
E_rebar	1	2.10E+11	0.1	
v_rebar	1	0.3	0.01	
rho_rebar	1	7850	0.1	
alpha_rebar	1	1.20E-05	0.1	
sigma_y_rebar	1	5.00E+08	0.1	
c_protection	1	1200	0.1	
lambda_protection	1	0.12	0.1	
rho_protection	1	300	0.1	
depth_of_protection	1	0.015	0.1	
lambda_floors	1	0.988	0.01	
c_e_floors	1	840	0.1	
rho_e_floors	1	1800	0.1	
lambda_walls	1	0.16	0.01	
c_e_walls	1	840	0.1	
rho_e_walls	1	950	0.1	
qfd	8	363.29	98.24	
imposed_load	1	4.5	0.1	
additional_dead_load	1	0.5	0.01	

Text Inputs

fgr	m
analysistype	Bailey
SamplingMethod	random
ComFlor_type	ComFlor_51
orthogonality_check	isotropic

The maximum predicted deflection from the published example is 552mm and the deflection calculated in Matlab is 556mm. This is judged to be an acceptable level of accuracy. The slight variation in response is due to the difference in the material models used.

Izzuddin Method for the Analysis of Composite Slabs

The Izzuddin method for the analysis of composite slabs is discussed in detail in section 2.4.2 of this thesis. The accuracy of the method, as implemented in Matlab, is examined here by comparison with published results from Cashell et al. (Cashell, Elghazouli and Izzuddin, 2011, Failure Assessment of Lightly Reinforced Floor Slabs. I: Experimental Investigation, Journal of Structural Engineering, 137, 9, pp. 977-988; Cashell, Elghazouli and Izzuddin, 2011, Failure Assessment of Lightly Reinforced Floor Slabs. II: Analytical Studies, Journal of Structural Engineering, 137, 9, pp. 989-1001).

The slab is 2.25m long by 1.5m wide and 0.06m thick. The reinforcement is specified as 6mm diameter bars at 200mm spacings. The deflection calculated in Matlab is 64.3mm. This compares well with both the deflection of 67.7mm calculated by Cashell et al. (using the Izzuddin method) and the experimental deflection of 69mm measured by Cashell et al. The three millimetre discrepancy in the calculated is likely due to differences in the material models used. The input files used with the Matlab scripts are given below.

<u>Deterministic Inputs</u>

Variable	Value
amb_temp	20
no_conc_layers	20
allowabledeflection	130
fire_curve_type	2
concrete_type	1

rebar_type	2			
n_analyses	1000			

Potentially Probabilistic Inputs

Variable	itype	mu	ccov	
compartment_length		1	10	0.1
compartment_breadth		1	10	0.1
compartment_height		1	3	0.1
Av	5	30	0.3	
h_eq	0	1	0	
lambda_floors	0	0.988	0	
c_e_floors	0	840	0	
rho_e_floors	0	1400	0	
lambda_walls	0	0.16	0	
c_e_walls	0	840	0	
rho_e_walls	0	1100	0	
qfd	8	370	100	
L_slab	1	2.25	0.2	
B_slab	1	1.5	0.2	
h_slab	1	0.060	0.01	
rebar_dia	0	6	0	
rebar_spacing	0	200	0	
d_rebar	5	50	0.05	
udl	0	21244	0	
rho_conc	0	1400	0	
E_conc	0	1.79E+10	0	
sigma_y_steel	0	5.00E+08	0	
sigma_u_steel	0	6.00E+08	0	
E_2	0	1.02E+09	0	
sigma_bond	0	1.50E+05	0	

Text Inputs

fgr	m
analysistype	izzuddin
SamplingMethod	random
occupancytype	office
firebrigadetype	professional
responsetime	10 to 20 minutes
activemeasures	smokedetection
autoalarm	y
sprinklertype	none

Appendix H Validation of the Multi-Storey Analysis Method

A direct stiffness based method, implemented in Matlab, is used in this thesis to examine the structural behaviour of multi-storey steel frames subject to multiple floor fires. This method, as implemented in Matlab, is validated in this appendix against Mastan2. Mastan2 is a well-known direct stiffness based solver. It is an ideal tool for examining the capabilities of the solver used in this thesis as it is based on the same analysis methods.

Two separate direct stiffness models are used in this thesis; one of a composite beam at room temperature subject to both transverse and axial loads and one of a heated multi-storey column subject to axial and horizontal loads. Both of these models will be examined separately in this appendix.

Description of the Composite Beam

The beam is a 7.5m long steel-concrete composite beam. There is no fire protection applied to the steel beam. The beam is subject to both an axial force and a transverse uniformly distributed load. One end of the beam is assumed to be fully fixed and the other end is assumed to be simply supported. The analysis model is described in detail in section 2.4.2.

Input for the Analysis of the Composite Beam

The input values are listed below, as input into the Matlab program.

Deterministic Inputs

amb_temp = 20;

fire_curve_type = 5;

concrete_type = 1;

no_fire_floors = 3;

t_FireSpread = [0/60,5/60,10/60];

Text Inputs

fgr = 'm';

steel_protection = 'y';

steel_protection_beam = 'n';

Potentially Probabilistic Inputs

compartment_length = 10;

compartment_breadth = 10;

compartment_height = 4;

Av = 50;

h_eq = 1.4;

lambda_floors = 0.988;

c_e_floors = 840;

rho_e_floors = 1400;

lambda_walls = 0.16;

c_e_walls = 840;

rho_e_walls = 950;

qfd = 450;

c_protection = 837;

lambda_protection = 0.48;

rho_protection = 1442;

depth_of_protection = 0.028;

c_protection_beam = 837;

lambda_protection_beam = 0.48;

rho_protection_beam = 1442;

depth_of_protection_beam = 0.04;

Col_load = 6000;

udl = 5.2;

```
Load_Ratio = 0.6;
L_beam = 7.5;
hw_mm_beam = 265.2+(2*8.9);
tw_mm_beam = 6.0;
tf_mm_beam = 10.2;
b_beam_mm = 165.0;
axis_of_bending = 'yy';
h_col = [4; 4; 4; 4; 4; 4];
xx_h = 246.7+(2*15.2);
hw_mm_col = [xx_h; xx_h; xx_h; xx_h; xx_h; xx_h];
tw_mm_col = [19.1;19.1;19.1;19.1;19.1;19.1];
tf_mm_col = [31.4;31.4;31.4;31.4;31.4;31.4];
b_mm_col = [314.5;314.5;314.5;314.5;314.5;314.5];
A_mm_col = [25200;25200;25200;25200;25200;25200];
B_slab = 7.5; % 7.6;
h_slab = 0.13;
sigma_y_c_conc = 30;
sigma_y_t_conc = 0;
rho_conc = 1800;
E_conc = 14;
sigma_y_steel = 275; % in N/mm^2
E_steel = 210;
alpha_steel = 1.6*10^-6;
rho_steel = 7850;
```

Output from the Analysis of the Composite Beam

As can be seen from Figure H.1 below, the maximum sagging bending moment is 20.68kNm and the maximum hogging bending moment is 36.79kNm. The maximum axial force in the beam is calculated as 306.04kN.

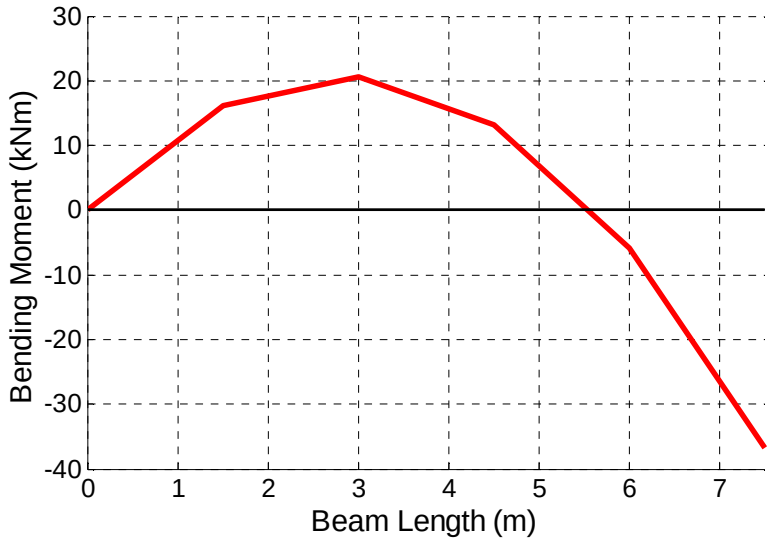

Figure H.1: Bending Moment Diagram for the Composite Beam.

Output from the Mastan2 Analysis of the Composite Beam

Mastan2 predicts a maximum axial force of 306kN and a maximum moment of 36.79kNm, as shown below in Figures H.2 and H.3.

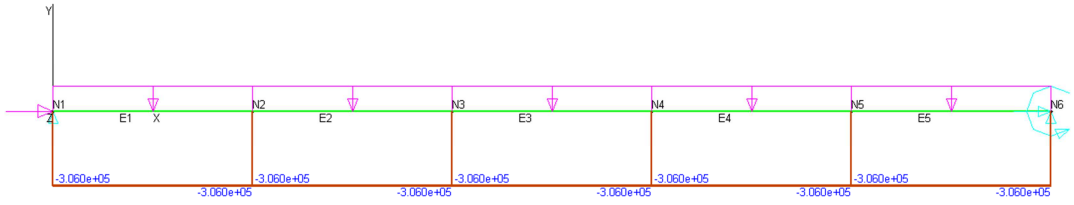

Figure H.2: Axial Force Diagram for the Composite Beam from Mastan2.

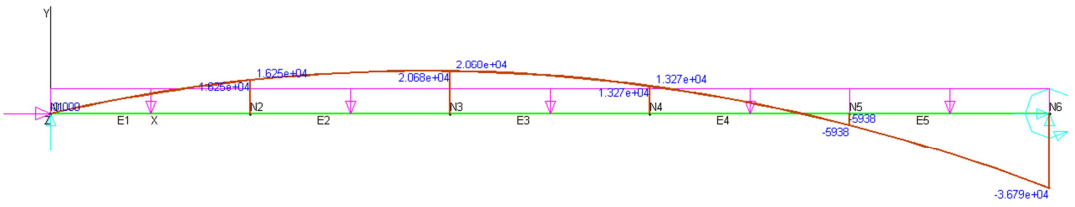

Figure H.3: Bending Moment Diagram for the Composite Beam from Mastan2.

Comparison of the Composite Beam Results

The results from Mastan2 are in excellent agreement with the results from the Matlab based analysis, with both methods predicting the same values of axial force and bending moment. This level of agreement is to be expected as both methods are based on similar principles.

Description of the Multi-Storey Column

A four storey column is analysed in this appendix. The height of each storey is 3.6m. There is a fire applied to a single storey. The column model is subject to both an axial compressive force and a horizontal force. The analysis model is covered in further detail in section 2.4.2.

Inputs for the Analysis of the Multi-Storey Column

Deterministic Inputs

amb_temp	20	
fire_curve_type	1	

Text Inputs

fgr	m	
steel_protection	y	
steel_protection_beam	y	
fire_spread_def	prob	
axis_of_bending	yy	

Potentially Probabilistic Inputs

compartment_length	0	12
compartment_breadth	0	12
compartment_height	0	3.6

Av	0	21.2		
h_eq	0	1.6		
lambda_floors	0	0.988		
c_e_floors	0	840		
rho_e_floors	0	1400		
lambda_walls	0	0.16		
c_e_walls	0	840		
rho_e_walls	0	950		
qfd	0	363.29		
c_protection	0	837		
lambda_protection	0	0.48		
rho_protection	0	1442		
depth_of_protection	0	0.05		
c_protection_beam	0	837		
lambda_protection_beam	0	0.48		
rho_protection_beam	0	1442		
depth_of_protection_beam	0	0.04		
Col_load	0	1090.2		
udl	0	15.165		
L_beam	0	9.875		
hw_mm_beam	0	320.6		
tw_mm_beam	0	12.3		
tf_mm_beam	0	20.7		
b_beam_mm	0	307.4		
h_col	0	3.6		
hw_mm_col	0	277.1		
tw_mm_col	0	12		
tf_mm_col	0	18.7		
b_mm_col	0	307.4		

r_mm_col	0	15.2
I_mm_col	0	2.767E+08
A_mm_col	0	1.500E+04
B_slab	0	2.1
sigma_y_steel	0	399.2
E_steel	0	210
alpha_steel	0	0.0000016

Output from the Analysis of the Multi-Storey Column

The vertical displacements recorded at each node are: 0mm, -1.2mm, -2.5mm, -3.7mm and -5mm.

Output from the Mastan2 Analysis of the Multi-Storey Column

The vertical displacements calculated by Mastan2 at each node are: 0mm, -1.246mm, -2.492, -3.738mm and -4.984mm.

Comparison of the Multi-Storey Column Results

It can be seen from the above results that both methods are in excellent agreement, though it is noted that Mastan2 provides more precise results.